

**UC Irvine**

**UC Irvine Electronic Theses and Dissertations**

**Title**

Sustainable Polymer Designs via Dynamic Covalent Chemistries

**Permalink**

<https://escholarship.org/uc/item/7p6267xb>

**Author**

Tretbar, Chase

**Publication Date**

2021

Peer reviewed|Thesis/dissertation

UNIVERSITY OF CALIFORNIA,  
IRVINE

Sustainable Polymer Designs via Dynamic Covalent Chemistries

DISSERTATION

submitted in partial satisfaction of the requirements  
for the degree of

DOCTOR OF PHILOSOPHY

in Chemistry

by

Chase Tretbar

Dissertation Committee:  
Professor Zhibin Guan, Chair  
Professor Ken Shea  
Professor Shane Ardo

2021



## **DEDICATION**

To

Leda Tretbar

*by my side forever and always*



# TABLE OF CONTENTS

<b>LIST OF FIGURES &amp; TABLES .....</b>	<b>vi</b>
<b>ACKNOWLEDGEMENTS .....</b>	<b>viii</b>
<b>CIRRICULUM VITAE .....</b>	<b>x</b>
<b>ABSTRACT .....</b>	<b>xii</b>
<b>Chapter 1: Exchangeable Chemical Bonds in Polymer Networks .....</b>	<b>1</b>
1.1 The Background of Dynamic Covalent Chemistry in Polymers.....	1
1.2 Dissociative Exchange .....	4
1.3 Associative Exchange in Covalent Adaptive Networks .....	12
<b>Chapter 2: Combining Supramolecular &amp; Dynamic Covalent Interactions for Advanced Self-Healing Polymers.....</b>	<b>39</b>
2.1 Introduction.....	39
2.1.1 Designs for extrinsic and intrinsic self-healing materials .....	39
2.1.2 Our design for hydrolytically stable intrinsically self-healing polymers.....	40
2.2 Results and Discussion.....	43
2.2.1 Small molecule synthesis .....	43
2.2.3 Polymer synthesis and characterization.....	47
2.3 Conclusion and Future Work .....	50
2.4 References .....	52

2.5 Supporting Information.....	55
<b>Chapter 3: Direct Silyl Ether Metathesis for Vitrimers with Exceptional Thermal Stability .....</b>	<b>97</b>
3.1 Introduction.....	97
3.2 Results and Discussion.....	99
3.2.1 Small molecule synthesis and kinetic studies.....	99
3.2.2 Synthesis of PE-OTMS and vitrimer preparation .....	101
3.2.3 Mechanical and thermal testing.....	103
3.3 Conclusion .....	108
3.4 References .....	109
3.5 Experimental .....	112
<b>Chapter 4: Siloxane Exchange Chemistry for High-Stability Vitrimer Designs .....</b>	<b>138</b>
4.1 Introduction.....	138
4.2 Results and Discussion.....	140
4.3 Conclusion .....	151
4.4 References .....	152
4.5 Experimental .....	156
4.6 References .....	178
<b>Chapter 5: Progress Towards a General Strategy for Polymer Compatibilization ....</b>	<b>179</b>
5.1 Introduction and current state of compatibilizers .....	179

5.2 Our design for a general polymer compatibilizer .....	180
5.3 Results and Discussion.....	181
5.3.1 Initial efforts with furan and maleimide DA adducts .....	181
5.3.2 Current efforts towards anthracene-maleimide DA adducts.....	186
5.4 Troubleshooting and future directions.....	190
5.5 References .....	191
5.6 Experimental .....	193
5.7 Spectra .....	202
5.8 References .....	209

## LIST OF FIGURES & TABLES

	Page	
Figure 1.1	Dissociative and associative exchange	4
Figure 1.2	Diels-Alder dissociative exchange networks	6
Figure 1.3	Bulky urea self-healing polymer	8
Figure 1.4	Alkoxyamine-based self-healing polymer	10
Figure 1.5	Diarylbenzofuranone-based self-healing polymer	11
Figure 1.6	Radical addition-fragmentation chain transfer	14
Figure 1.7	Metathesis in polybutadiene networks	16
Figure 1.8	Transesterification in epoxy networks	17
Figure 1.9	Vinylogous urethane exchange	21
Figure 1.10	Catalytic control over vinylogous urethane exchange	22
Figure 1.11	Boronic ester exchange	24
Figure 1.12	Boroxine exchange in polymer networks	26
Figure 1.13	Siloxane anionic exchange	27
Figure 1.14	Silyl ether transesterification	29
Figure 2.1	Formation of sterically hindered urea	40
Figure 2.2	Urea hydrogen bonding	41
Figure 2.3	Sterically hindered thiourea in equilibrium	44
Figure 2.4	Equilibrium studies of sterically hindered thiourea	46

Figure 2.5	GPC chromatograms of polythiourea	47
Figure 2.6	Self-healing studies on polythiourea	50
Figure 3.1	Silyl ether hydroxyl exchange vs silyl ether metathesis	99
Figure 3.2	GC chromatograms of silyl ether exchange	100
Figure 3.3	Mechanical analysis of PE-OTMS vitrimer	103
Figure 3.4	Stress relaxation of PE-OTMS vitrimer	105
Figure 3.5	Reprocessability testing for PE-OTMS vitrimer	107
Figure 4.1	Reversible siloxane exchange	139
Figure 4.2	GC chromatograms of catalyzed siloxane exchange	142
Figure 4.3	PDMS elastomer with embedded fluoride catalyst	143
Figure 4.4	Preparation of siloxane-bearing vitrimers	145
Table 4.1	PMMA-v crosslinking conditions	146
Figure 4.5	Physical testing of PMMA-v and HDPE-v	148
Figure 4.6	Creep and rheological testing of HDPE-v and PMMA-v	149
Figure 5.1	Design concept for generalized compatibilizer	181
Figure 5.2	Representative SEM micrographs of immiscible polymer blends	184
Figure 5.3	Model reactions of substituted anthracene and maleimides	188
Figure 5.4	DSC thermograms of DA adduct	189

## ACKNOWLEDGEMENTS

I would like to thank Professor Zhibin Guan for the opportunity to work in his lab and his support throughout my endeavors. He has pushed me to be an excellent scientist and his innate curiosity and work ethic are goals that I hope to achieve. I find his most admirable trait to be how he strives to tackle the most challenging scientific problems that can make a meaningful contribution to the world. I would like to thank my committee members Professor Ken Shea and Professor Shane Ardo. I would also like to thank Dr. Felix Grun and Ben Katz for the abundance of assistance with mass spectrometry. I would like to thank Phil Dennison for his help with NMR analysis and training. I would also like to thank Dr. Xiaofeng Liu for his help with material characterizations using the well maintained TEMPR facility under IMRI. The funding for my research was provided in part by the National Science Foundation, Division of Materials Research and the U. S. Department of Energy, Basic Energy Science, Division of Materials Sciences. Without their financial support, I wouldn't have been able to accomplish what I set out to achieve.

I was incredibly fortunate to have joined a research group that not only fostered scientific exploration, but also fostered deep friendships. I would like to thank the members before me: Dr. Nate Oldenhuis, Dr. James Neal, Dr. Dong-chu Yang, Billy Ogden, Dr. Alex Eldridge, and Dr. Hurik Muradyan. James was one of the best mentors I could have asked for and I strive to provide as much guidance to the younger generation as he gave to me. I would like to thank Dr. Dong-chu Yang and Billy Ogden for their interesting conversations. I would like to thank Alex for being a top-notch spotter and his constant uplifting of group morale. Hurik, you did an excellent job of keeping the wheels on when it all wanted to fly apart. You

were always there to lend an ear and every group member was incredibly appreciative for it. To the younger students, I wish you the best. I tried to leave the lab in a better spot than when I arrived. Collin, I am glad that I was able to meet you when you were fresh and excited – otherwise we would not have been as good of friends. I hope you continue your mycology ventures and become the mushroom master. Jordan, I hope you are able to keep up the positive attitude and good spirits for the rest of your career. Your cheerful attitude is a severely underrated skill and I hope that whatever guidance I could provide will lead you down the best path.

Saving the best for last, I am entirely thankful to my wife, Leda Tretbar, for she is the most supportive and compassionate person that I could ever ask for. She has been by my side for years and has been a steady rock in the murky waters. Without her encouragement and company, graduate school would have been even more of a challenge. You deserve an honorary doctorate for all the effort you put into helping me get mine. I'm thankful for my dogs, Jack and Myla, who cheer me up at the end of each day. I'm wholly grateful to my parents, Teresa and Lee, who have unwaveringly supported my endeavors regardless of how far away I move from home. Their constant encouragement and weekly phone calls have kept me going when things were rough. I would like to thank the rest of my family and friends for the love and friendship throughout the process. I could write a page to each of you for all the support, unconditional love, and fun times you have provided.

## CURRICULUM VITAE

**Chase A. Tretbar** Ph. D., Chemistry  
University of California, Irvine, Irvine, CA 92697

### Objective & Profile of Skills

I am a **Scientist with a Ph. D. in Organic Chemistry** specializing in the synthesis and testing of polymers and am enthusiastic to apply my skills towards the process development of impactful materials. I am:

- Skilled in the **synthesis, processing, and testing of materials** for a broad variety of applications
- Experienced with the **development of functional prototypes** and production practices
- **Collaborative** with both scientific and non-scientific peers
- An **effective communicator** of scientific ideas in both written and oral formats to diverse audiences
- **Effective at creative problem solving** as shown by my diverse R&D experience

### Relevant Experience

#### Doctor of Philosophy, Chemistry

*Dec. 2016 – Present*

The University of California, Irvine, CA

- Designed, synthesized, evaluated, and characterized polymeric materials leading to a peer-reviewed first-author publication in a premier organic chemistry journal.
- Worked with material vendors to optimize polymer blends for targeted extrusion profiles.
- Devised multi-component formulations for polymer extrusion enhancement resulting in suppressed oxidation, targeted tensile properties, and lowered melt flow rate.
- Developed new chemistries imparting the highest recorded thermal stability in vitrimer networks.
- Characterized substrates through NMR spectroscopy, FT-IR, Mass Spectrometry, GC-MS, HPLC-MS, GPC, DSC, DMA, TGA, and rheology.
- Supervised undergraduate students and planned projects for their growth as researchers.
- Negotiated multiple purchases of large equipment, resulting in savings of over \$25,000.

#### 3D Printing and Testing Specialist

*May 2015 – Aug. 2016*

The Mississippi Polymer Institute, Hattiesburg, MS

- Worked closely with grassroots inventors and businesses through early stages of product design to translate prototypes into manufacturable products.
- Consulted for, designed, and 3D printed prototypes with high volume manufacturing in mind.
- Performed ASTM industrial polymer processing and testing: compound extrusion, injection molding, tensile testing, Izod impact, melt flow index and other forms of polymer physical testing.
- Collaborated with recycling companies to improve extrusion melt flow properties of raw feed stock.
- Worked with engineering firms for initial production runs of injection molded parts.

#### Teaching Assistant

*Sept. 2016 – Present*

The University of California, Irvine, CA

- Developed course loads, testing methods, and teaching materials for classes of 300 students.
- Instructed the safe usage of dangerous and air-sensitive reagents to classes of undergraduate chemistry students.
- Received the *Departmental Service Team Award* as well as the *Division for Teaching Excellence & Innovation Fellowship* awards for my impact on student learning and successful outcomes.



## Researcher

The University of Southern Mississippi, Hattiesburg, MS

- Prepared brush polymers on the surface of silicon wafers for highly sensitive chemical sensors.
- Developed new chemical methods for tuning the thermal properties of poly(benzoxazine) films.
- Functionalized medical device surfaces with bacteriophages to impart anti-microbial properties.

## Education

### Doctor of Philosophy, Chemistry

University of California, Irvine, CA; *Advisor: Dr. Zhibin Guan*

- **Dissertation:** Sustainable Polymer Designs via Dynamic Covalent Chemistries
- Division for Teaching Excellence & Innovation Fellowship (\$5,000)
- Chemistry Graduate Dissertation Fellowship (\$9,000)
- LaVerne Noyes Award (\$6,000)

### B.S., Polymer Science with Biological Sciences Minor

**Magna Cum Laude** GPA 3.5/4.0

The University of Southern Mississippi, Hattiesburg, MS; *Advisor: Dr. Derek Patton*

- **Thesis:** Polymerization of Blocked Isocyanate Functional Polymer Surfaces and Post-Polymerization Modification by Thiol-Isocyanate Reactions.
- Honors College Graduate
- University Scholar (\$24,000)
- Mississippi Eminent Scholar (\$10,000)

## Publications and Selected Public Presentations

**Tretbar, C.,** Neal, J., Guan, Z. "Direct Silyl Ether Metathesis for Vitrimers with Exceptional Thermal Stability" *J. Am. Chem. Soc.* 2019, *141*, 16995.

Howitz, W., Thane, T., Frey, T., Wang, X., Gonzales, J., **Tretbar, C.,** Seith, D., Saluga, S., Lam, S., Nguyen, M., Tieu, P., Link, R., Edwards, K. "Online in No Time: Design and Implementation of a Remote Learning First Quarter General Chemistry Laboratory and Second Quarter Organic Chemistry Laboratory" *J. of Chemical Education* 2020, *97*(9), 2624.

**Tretbar, C.,** Neal, J., Guan, Z. (2019) Direct Silyl Ether Metathesis for Vitrimers with Exceptional Thermal Stability. National Convention of the American Chemical Society (ACS).

**Tretbar, C.,** Hoff, E., Patton, D. (2015) Synthesis of Hydrazide Functional Polymers by RAFT Polymerization. National Waterborne Symposium. [Poster Presentation, 2<sup>nd</sup> Place]

Hoff, E., Abel, B., **Tretbar, C.,** McCormick, C., Patton, D. "Aqueous RAFT at pH zero: enabling controlled polymerization of unprotected acyl hydrazide methacrylamides" *Polym. Chem.* 2017, *34*, 4978.

Hoff, E., Abel, B., **Tretbar, C.,** McCormick, C., Patton, D. "RAFT polymerization of splitters and cryptos: Exploiting azole-N-carboxamides as blocked isocyanates for ambient temperature postpolymerization modification" *Macromolecules* 2016, *49*, 554.

Baranek, A., Kendrick, L., **Tretbar, C.,** Patton, D. "Solvent-free copolymerization of rigid and flexible bis-1,3-benzoxazines: Tunability of polybenzoxazine network properties" *Polymer* 2013, *54*, 5553.

# **ABSTRACT OF THE DISSERTATION**

## **Sustainable Polymer Designs via Dynamic Covalent Chemistries**

By

Chase Tretbar

Doctor of Philosophy in Chemistry

University of California, Irvine, 2021

Professor Zhibin Guan, Chair

Polymers have become a ubiquitous part of our lives, filling diverse applications ranging from aerospace to children's toys. With over three hundred million tons of plastics being produced annually, it's crucial to increase their usable lifespan and reduce their relegation to waste. As such, it is necessary to move away from traditional commodity polymers and steer towards new structural designs that make the polymers more recyclable and more resistant toward deterioration and failure. For wider adoption, these new structural designs should be thermally stable, resistant to additives, and can resist/repair damage. The incorporation of dynamic covalent chemistries into polymers offer an attractive route towards our dream of limitless recyclability. Dynamic covalent bonds allow for the shuffling of crosslink points between disparate polymer backbones, allowing for benefits such as self-healing, moldability, and malleability within static materials. The incorporation of dynamic covalent chemistries provides a platform for the next generation of green materials by imparting recyclability in traditionally un-recyclable materials. Chapter 1 of this

thesis will provide the reader with an overview of the field for understanding the most meaningful contributions to the field of dynamic covalent chemistries in polymer networks.

Chapter 2 describes my work towards developing a robust self-healing polymer by incorporating both dynamic covalent chemistry and supramolecular interactions via sterically hindered thiourea linkages. In model compounds studies I found that tuning the bulkiness of the thiourea linkage led to the tunability of the association and dissociation equilibrium. When transferred to polymers, these findings led to the generation of both high molecular weight polymers and efficient self-healing at ambient temperatures.

In Chapter 3 we report our discovery of a new silyl ether metathesis reaction and its application in vitrimer design. The incorporation of silyl ether crosslinks led to enhanced mechanical properties and significant creep resistance over unmodified polymers. Our silyl ether-based vitrimer represents the most thermally stable vitrimer reported to date, owing to the high thermal and oxidative stability of the Si-O bond.

In Chapter 4 we describe our developments towards a new fluoride catalyst for selective and rapid exchange of siloxanes, thereby expanding the scope of Si-O vitrimer chemistry. The field of vitrimers has largely focused on niche polymers with little attention into the expansion of vitrimer chemistry into commodity plastics. Here, I work on developing industrially relevant methods for preparing vitrimers from commodity polymers.

Chapter 5 summarizes our work towards the development of a generalized polymer compatibilizer using thermally reversible Diels-Alder chemistry. This compatibilizer uses thermally reversible mechanical interlocks to stabilize the phase separation of immiscible

polymer blends. If successful, this work would provide both a new recycling method and a technique to produce novel polymer blends.

# **CHAPTER 1: Exchangeable Chemical Bonds in Polymer Networks**

## **1.1 The Background of Dynamic Covalent Chemistry in Polymers**

Humans have long used naturally occurring polymeric materials such as cellulose, natural fibers, and leather in a variety of applications such as tools, clothing, and shelter. Their applications were often rudimentary due to the limited sophistication of these natural polymers. Until Hermann Staudinger's seminal proposition that polymers were small molecules covalently linked together,<sup>1</sup> there was much debate on the molecular basis for these ubiquitous materials. Staudinger's proposition led to the development of modern macromolecular chemistry and was awarded the Nobel Prize in Chemistry in 1953 for his pioneering contributions in polymer science.<sup>2</sup> Despite misunderstanding the molecular basis for polymerization, the first commercial synthetic polymer was widely recognized as the phenolic resin Bakelite from Leo Baekeland in 1909.<sup>3</sup> Bakelite was a densely crosslinked polymer that offered significant manufacturing possibilities over traditional materials such as high rigidity, solvent resistance, ease of processing, and resistance to melting. The significance of this synthetic polymer was quickly realized, ushering in a new era of synthetic materials. The new synthetic polymers offered a lightweight alternative to metal and could be easily molded into intricate shapes. Modern polymers have extremely diverse mechanical properties, ranging from soft rubbers to high modulus fibers. Despite these advances, there are no single polymer systems that offer physical traits to meet all applications. Some physical behaviors are complementary, while others are diametrically opposed. Depending on the application, we are required to choose a specific family of polymer to meet the required criteria.

There are two broad categories of synthetic polymers: thermoplastics and thermosets. Thermoplastics are linear polymer chains that derive their strength from covalent bonds in the backbone as well as chain entanglement and non-covalent intermolecular interactions.<sup>4</sup> Thermoplastics are the most widely used family of polymers and include the common polymers such as polyethylene, polypropylene, polymethyl methacrylate, polyvinyl chloride, and polystyrene. The benefit of using thermoplastics is that they are easy to process and can often be reprocessed several times.<sup>5</sup> This makes them an ideal candidate for commodity materials such as shopping bags, clothing textiles, and food packaging. However, there exists significant drawbacks to using thermoplastics such as poor dimensional stability at high temperatures, poor solvent resistance, and creep under load.<sup>6</sup> In contrast to thermoplastics, thermosets are polymer networks where polymer chains are covalently bonded to each other, preventing slippage between polymer chains. This limited mobility provides enhanced thermal stability, creep resistance, and solvent resistance.<sup>7,8</sup> However, unlike thermoplastics, thermosets cannot be reprocessed without breaking covalent bonds.<sup>5</sup> In the following work, I will discuss recent efforts on combining the best attributes of thermoplastics and thermosets to prepare a reprocessable material for high-performance applications.

To increase the reprocessability of thermosets, research focus has turned towards replacing the permanent covalent bonds in between chains with dynamic covalent chemistries (DCCs).<sup>9-11</sup> DCCs are a family of diverse chemical functionalities that offer covalent bonds that are reversible under relevant/mild conditions. DCCs are thermodynamically controlled processes where the equilibrium can be shifted towards the

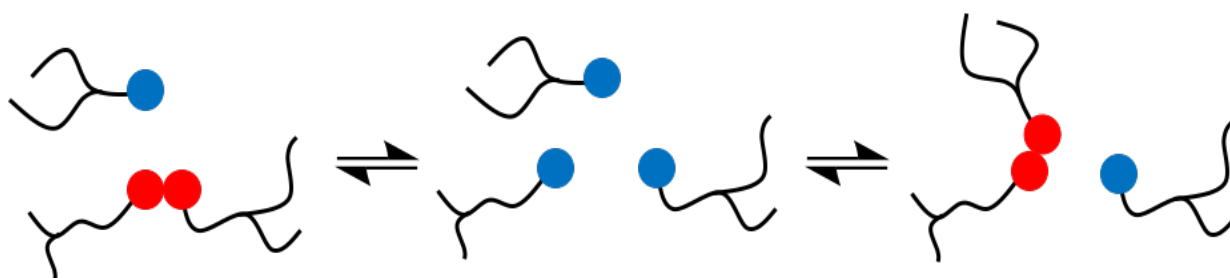
products or reactants depending on the stimuli exerted on the material.<sup>12</sup> Many types of DCCs have been reported such as Diels-Alder cycloadditions,<sup>13,14</sup> alkene and alkyne metathesis,<sup>15-19</sup> transesterification,<sup>20-22</sup> imine exchange,<sup>23</sup> aminal and hemiaminal exchange,<sup>24,25</sup> disulfide exchange,<sup>26</sup> boronic acid and boroxine exchange,<sup>27,28</sup> silyl ether exchange,<sup>29</sup> reversible addition fragmentation radical chemistry,<sup>30-33</sup> and several others.<sup>12</sup> In material applications, dynamic covalent crosslinkers allow for polymer networks to have the strength, solvent resistance, and creep resistance of traditional thermosets at working conditions, while offering reprocessability and malleability at elevated temperatures.

To be relevant for use in polymers, DCCs must meet two main requirements. The first is that the reaction needs to be truly reversible. In principle, all chemical reactions are reversible, yet in reality many reactions are not reversible due to kinetic traps or unfavorable thermodynamics.<sup>34</sup> Often, catalysts are required to lower the energy of activation to induce reversibility in some reactions.<sup>35</sup> Secondly, the DCCs must be stable at *working* conditions and can be shifted to favor either the reactants or products under *processing* conditions. This change in equilibrium can be modulated through different stimuli to perturb the equilibria and change the reactivity. An example is in the case of self-healing materials.<sup>36</sup> In the event of a damage, applying a targeted stimulus would modify the local chemical environment, shifting and rearranging the dynamic bonds and inducing repair of the damaged spot. After the stimuli is removed, the material would revert to its stable state. In the case of the aforementioned dynamic thermosets, heat is commonly used to shift the dynamic chemical bonds and cause malleability in traditionally non-malleable materials. While under working conditions, exchange would be suppressed to allow for a stable material.

## 1.2 Dissociative Exchange

DCCs used in polymer systems are generally divided into two categories: dissociative exchange and associative exchange.<sup>37</sup> Dissociative exchange requires the dynamic linkage to at first dissociate before finding a new chemical handle to exchange with, while associative exchange requires the new chemical functionality to form a covalent bond to the dynamic linker, thereby forming a 3-membered intermediate before expelling the original linker. Both exchange methods have their merits depending on the application. As such, a spectrum of material properties ranging from materials with emphasized malleability/reprocessability on one end to materials with increased toughness on the other can be obtained from the

### a) Dissociative exchange pathway



### b) Associative exchange pathway

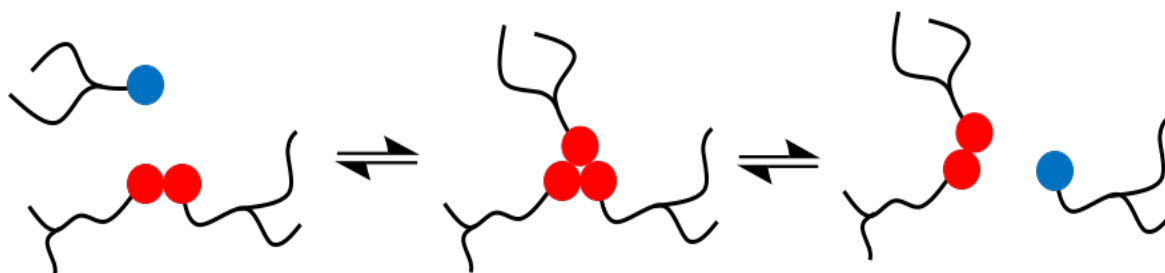


**Figure 1.1.** Pathways for the dynamic covalent chemical linker exchange using an a) dissociative exchange mechanism and b) associative exchange mechanism.



judicious selection of dynamic linkages.<sup>38</sup> On the most reprocessible side of the spectrum, the dissociative pathways are preferred when large scale topographical changes are required such as in self-healing applications. Because the dissociative pathway decreases the crosslink density due to the breaking of covalent bonds, dissociative exchange is more beneficial when reprocessability is more important than structural integrity. When heated at sufficiently high temperatures, the equilibrium of the dynamic covalent chemistries will shift towards the reactants and the system will flow like molten liquid. The following literature is intended to show how several chemical motifs have been studied to tune the behavior, compatibility, and thermal sensitivity of these dissociative exchange pathways.

One of the earliest and most well-studied forms of dissociative dynamic covalent chemistry uses the Diels-Alder (DA) reaction. Otto Diels and Kurt Alder received the 1950 Nobel Prize in Chemistry for their work on [4 + 2] cycloaddition of an electron-rich diene to an electron-deficient dienophile.<sup>13</sup> Their ground-breaking discovery has been applied to numerous chemical and polymeric systems such as reversible crosslinking<sup>39</sup> and reversible chain extension.<sup>40</sup> The [4 + 2] cycloaddition of substituted furan and maleimide was utilized by Wudl and coworkers in 2002 to prepare one of the first widely recognized self-healing polymers.<sup>41</sup> The material was a densely crosslinked transparent polymer network that could re-mend itself upon heating. The resin was prepared by blending a 4-functional furan and 3-functional maleimide in a stoichiometric ratio. For this particular Diels-Alder adduct, equilibrium shifts towards the reactants above 120 °C as dissociation becomes more favorable. Below 80 °C, the formation of the adduct begins to dominate and the resin begins to harden. The furan-maleimide curing occurred rapidly at 75 °C, reaching 95% conversion

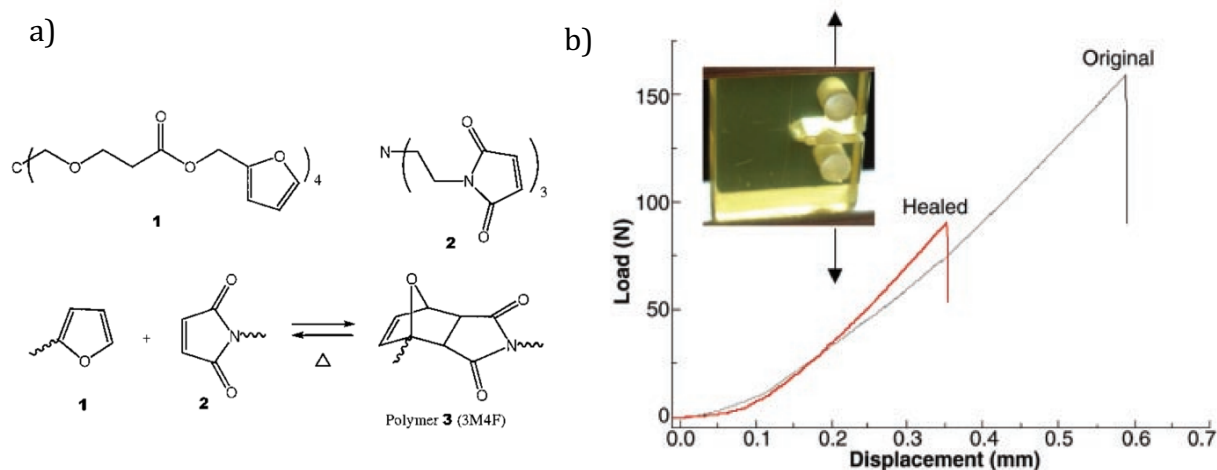


**Figure 1.2.** Formation and dissociation of the Diels-Alder adduct (a) Addition of a multifunctional furan, **1**, and maleimide, **2**, to prepare the densely crosslinked reversible network. (b) Mechanical tensile testing of the cured thermoset before and after healing. Adapted and reprinted from Wudl, F., *et al. Science* **2002**.

within just 3 hours. When cured at room temperature, the conversion was much slower, reaching 60-70% in 5 days indicating the material could be used in ambient-healing applications, but would be best suited for applications at elevated temperatures. The resin was shown to be reprocessable and could be broken and reformed several times while recovering much of the original mechanical properties (Figure 1.2b).

The furan-maleimide Diels-Alder pair have been used extensively for gel-sol transitions due to their stability and low temperature for addition.<sup>42</sup> First, both furan and maleimide motifs are relatively heat stable, which is an important attribute for processing polymer networks. Secondly, the furan-maleimide pair allows for the forward Diels-Alder reaction to occur at room temperature (or slightly elevated temperatures) as evidenced by several works on furan-maleimide self-healing.<sup>43-45</sup> The DA cycloaddition must reach a temperature threshold to overcome the energy barrier for dimerization. For comparison, the

$\Delta G^\ddagger$  of the cycloaddition of furan-maleimide is calculated to be only 25.0 kJ/mol while anthracene-maleimide cycloaddition is 132 kJ/mol.<sup>46</sup> Once formed, however the anthracene-maleimide retro Diels-Alder  $\Delta G^\ddagger$  is 325 kJ/mol, rendering the retro Diels-Alder reaction impractical without destroying other parts of the network.

One unfortunate side effect of the furan-maleimide DA system is that the furan group can become oxidized in the presence of light.<sup>43,47</sup> Another important consideration is the maleimide's tendency towards Michael addition in the presence of nucleophiles such as thiol<sup>48</sup> or benzamine.<sup>49</sup> Along with the other problems mentioned, the maleimide is sensitive to radicals and has been shown to homopolymerize,<sup>50</sup> rendering the effective maleimide concentration lower than anticipated and decreasing the expected material properties. Beyond thermally reversible Diels-Alder crosslinkers,<sup>51</sup> several other dynamic networks have leveraged other cycloadditions such as [2+2] and [4+4] photocycloadditions of coumarin,<sup>52</sup> anthracene,<sup>53</sup> cinnamoyl,<sup>54</sup> thymine,<sup>55</sup> and stilbene.<sup>56</sup>

In the pursuit of alternative methods for self-healing, Cheng and coworkers developed a clever dynamic system using the ubiquitous urea linkage prepared from isocyanates and amines.<sup>57</sup> The key modification was to add a bulky substituent to the N-position on the amine, forcing unfavorable sterics in the urea product and reducing the strength of the C-N bond adjacent to the bulky group. Due to the weakened C-N bond, the urea could spontaneously revert back to the starting isocyanate and amine. By carefully

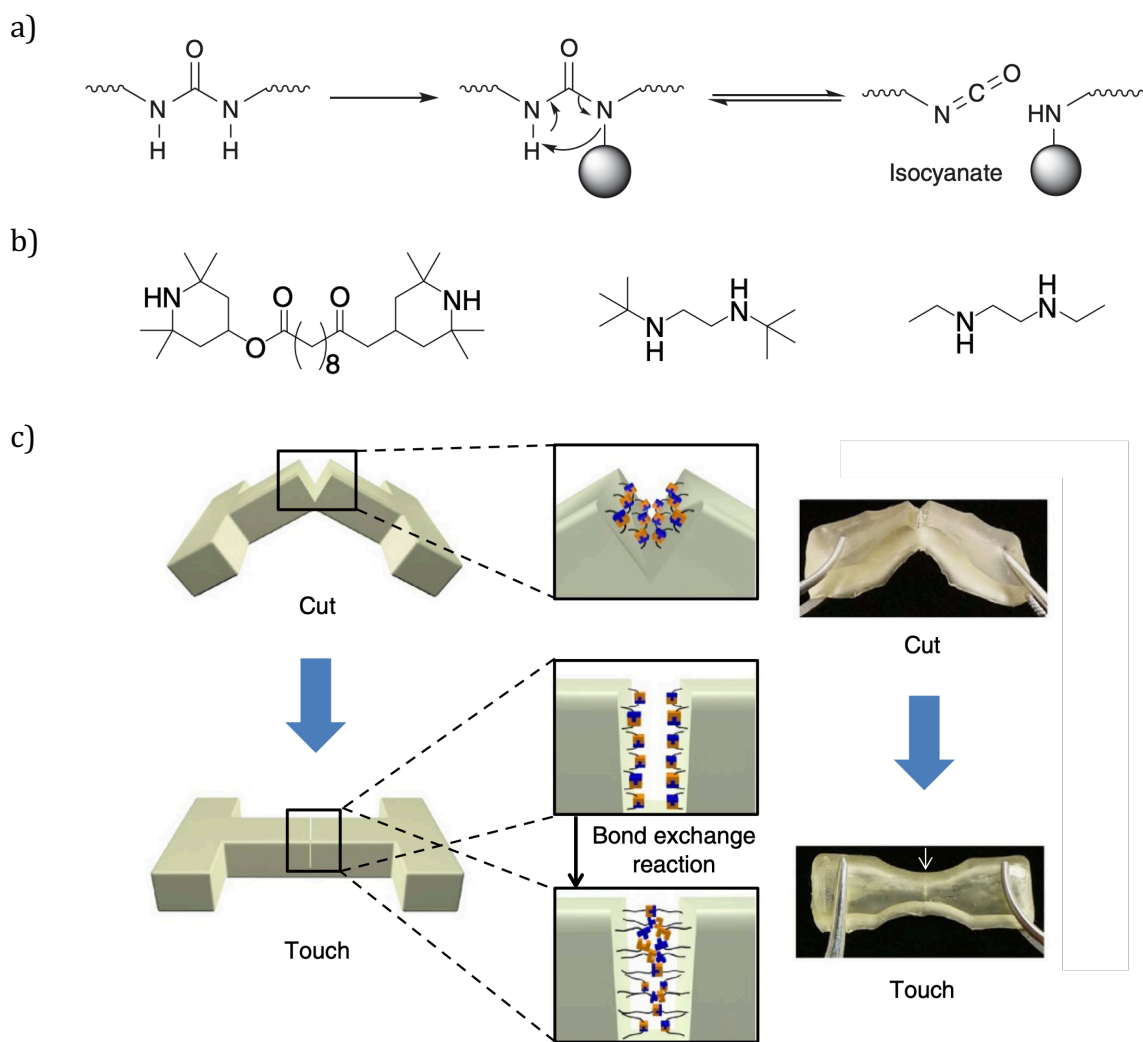


**Figure 1.3.** Dissociative exchange reaction between an isocyanate and a secondary amine. (a) Adding steric groups to the urea impart reversibility to an otherwise stable linkage. (b) Three diamine crosslinkers with varying steric hinderance. (c) Depiction of the exchange between functional groups at the interface of a damaged material. Adapted from Cheng *et al. Nature Comm.* **2014**.

choosing the bulkiness of the substituent, the equilibrium could be adjusted to increase the amount of starting material at any given time. The bulky urea linkages were incorporated into a polymer backbone to produce a self-healing material at room temperatures. When the material was cut and pushed back together, the *N*-substituted urea linkages throughout the backbone dissociate, diffuse across the cut interface, and find new corresponding functional

groups to associate with. The polymer network exists in a constant state of flux with dissociation and association occurring throughout the backbone at any given time.

One of the major drawbacks to this system is its inherent sensitivity towards moisture. While the urea linkage itself is very stable, the isocyanate starting material rapidly reacts with water to form a primary amine and carbon dioxide.<sup>58</sup> Since the dynamic polymer network exists in equilibria with secondary amine and isocyanate, moisture uptake will constantly be degrading the crosslink density and molecular weight of the polymers, ultimately reducing the effectiveness of the self-healing network. One method for slowing this process would be to reduce the effective concentration of isocyanates by reducing the steric bulk on the *N*-substituted urea, however that would result in reduced self-healing capability. We proposed a new way to address this issue by replacing the isocyanate with an isothiocyanate, which is significantly more hydrolytically stable than the isocyanate analogue. The details of my efforts towards this chemistry will be found in Chapter 2 of this thesis.

Thus far we have discussed dissociative DCCs in the context of elimination and cycloreversion reactions, however an unusual but effective method is the use homolytic bond cleavage and radical recombination. Otsuka *et al.* were pioneers in the use of alkoxyamine radical cleavage and recombination to scramble linear polymers,<sup>59</sup> however their initial work was focused on linear polymer chains. One of the first instances of incorporating this chemistry into bulk networks was done by Yuan and coworkers in 2011 where they used the dynamically reversible C-ON bond of an alkoxyamine group to relieve stress in a crosslinked polystyrene network (Figure 1.4).<sup>60</sup> Upon heating, crosslinks

containing alkoxyamine groups homolytically cleave into both carbon-centered radicals and persistent nitroxide radicals. Because the dissociation and reassociation occur at extremely high frequency ( $2.5 \times 10^{14}$  Hz)<sup>61</sup> the crosslink density is marginally reduced up on heating, preventing substantial creep above the glass transition temperature,  $T_g$ . At low temperatures, free radical generation is suppressed as seen in Figure 1.4b, where the electron spin resonance (ESR) spectroscopy measurements indicate the decreased abundance of free radicals at lower temperatures.

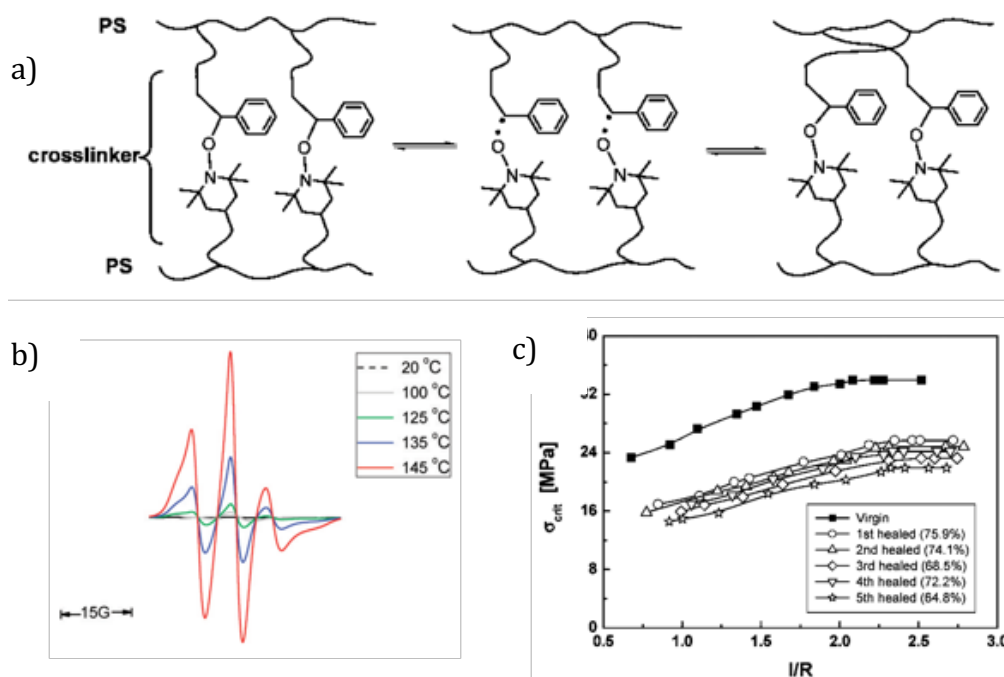


**Figure 1.4.** Dynamic alkoxyamine crosslinkers are used to generate dissociative crosslinks based on stabilized radical formation. (a) Polystyrene backbone crosslinked with the alkoxyamine linkages. Upon heating, the C-ON bond homolytically cleaves, allowing for the shuffling of crosslinks, and upon cooling the radical generation is suppressed. (b) electron spin resonance (ESR) spectrogram shows an increased abundance of radicals at higher temperatures. (c) Critical stress vs fracture length of virgin and healed samples as tested by double cleavage drilled compression test. Adapted from Yuan, C., *et al. Chem. Mater.* **2011**.

Only one month after Yuan and coworker's publication on nitroxide crosslinkers, a similar radical chemistry motif was published by Otsuka *et al.*<sup>62</sup> Instead of using TEMPO for the crosslinker, they used diarylbibenzofuranone (DABBF) which can homolytically cleave to form stable C-centered radicals (Figure 1.5).<sup>63-65</sup> In their case, the backbone polymer was polypropylene glycol which allowed for a soft matrix that would have good contact upon rejoining. As evidence the DABBF dimer existed in equilibrium with the radical monomer, excess DABBF was added to a solution of the gelled network, and linear polymer were produced. This proved that autonomous rearrangement at room temperature was occurring.

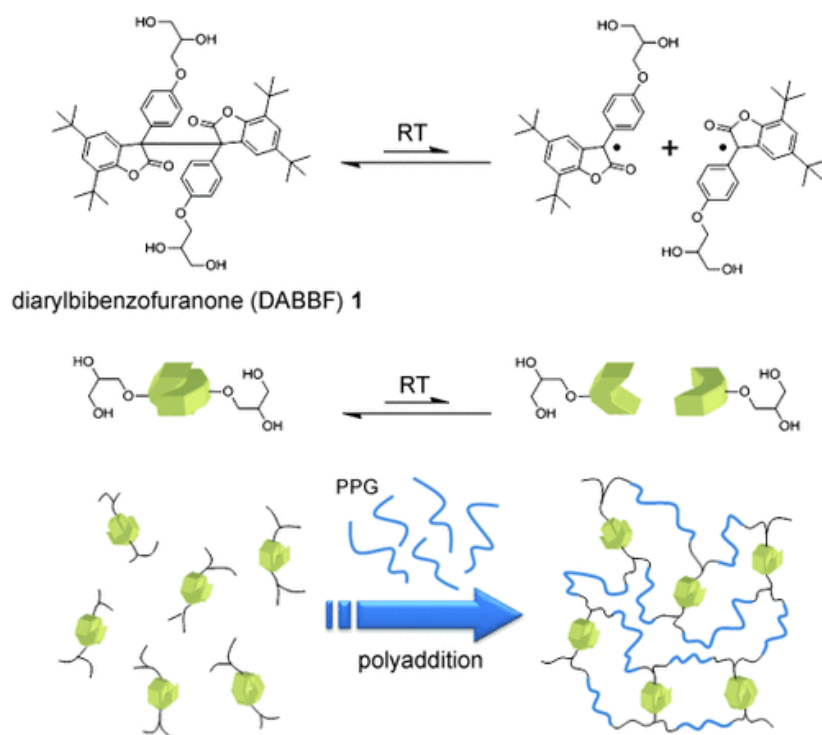


**Figure 1.5.** Diarylbibenzofuranone (DABBF) has a labile C-C bond that is prone to homolytic dissociation at room temperature. Once the radical species are formed, they quickly rejoin and the dimer is formed again. When used as a tetrafunctional crosslinker, DABBF allows for shuffling of crosslinks in the network due to constant dissociation/recombination of DABBF. Adapted from Imato, K., *et al. Angew. Chem. Int. Ed.* **2012**.

However, when the temperature was lowered to 0 °C all exchange ceased, and the network could no longer reorganize or self-heal.

Using radical generation for self-healing materials provides a unique platform for self-healing materials, however it does have some drawbacks. Primarily, radicals generated for healing can be quenched on exposure to oxygen.<sup>4</sup> This is obviously detrimental to their real-world applications since gasses can easily diffuse into the fractured substrates eliminating the healing. The molecular structure can be modified to further stabilize the radicals against oxidation; however, this will have the inherent side effect of reducing the healing efficacy.<sup>66,67</sup> Another challenge with radical sources is their proclivity towards H-abstraction and/or disproportionation at high temperatures which in living polymerizations leads to dead chain ends.<sup>68</sup> Also, at sufficiently high temperatures the radical species will undergo permanent decomposition.<sup>31</sup>

### **1.3 Associative Exchange in Covalent Adaptive Networks**

Thus far I have given examples of dissociative exchange mechanisms, which are useful where processing conditions allow the network to flow freely above the dissociation temperature. An example would be when the molten polymer is physically contained in a mold and there is no concern about liquid flow. However, the dissociative exchange sol-gel transition is a binary behavior such that dynamic network is either reprocessable or not reprocessable. Many applications benefit from a more gradual decrease in viscosity where fine control of processing parameters is necessary. In such instances, network integrity should be retained at high temperatures as opposed to strict melting. Instead of using



dissociative exchange to cause sol-gel transition, associative exchange can be used to provide a more gradual viscosity change.

Associative exchange mechanisms are an interesting exchange route that maintains a high degree of crosslinking despite their dynamic nature. Associative exchange occurs when a free chemical motif reacts with a dynamic linker, forming a multi-functional intermediate that collapses back into its lower energy state.<sup>69</sup> The newly freed motif can continue to exchange with other dynamic linkages (Figure 1.1b). The associative nature of these reactions ensures the network does not melt at increased temperature yet is still malleable under external forces. The rate of the exchange is often governed by temperature, and as such the dynamic exchange follows an Arrhenius-type temperature dependence. This behavior is similar to that of molten glass (vitreous silica) whereby the term “vitriimer” was coined for dynamic crosslinked networks that exhibit a gradual decrease in modulus above the processing conditions.<sup>70</sup> This is in contrast to the sudden drop in modulus often observed in linear polymers or dissociative DCC networks. Over the last 10 years, many new vitriimer motifs have been discovered that follow an associative exchange pathway allowing for the gradual drop in viscosity. The scope of vitrimers has broadened to include many unique functional groups that have differing strengths and weaknesses.

One of the first dynamic materials utilizing associative exchange Bowman *et al.*, where they used addition fragmentation chain transfer for the rearrangement of the polymer topology.<sup>30</sup> They prepared a traditional thiol-ene network using the photopolymerization of pentaerythritol tetra(3-mercaptopropionate) (PETMP) and triethyleneglycol divinyl ether (Figure 1.6). When the cyclic ring opening monomer 2-methyl-7-methylene-1,5-

dithiacyclooctane (MDTO) was incorporated as a co-monomer, allyl sulfide functional groups were positioned in the backbone. The authors found that under UV light, residual photoinitiator would decompose and produce sulfur-centered radicals that would add to the in-chain allyl sulfide  $\pi$ -bond. The resulting C-centered radical would quickly combine with an adjacent sulfide which would then fragment producing a new sulfur-centered radical that could further propagate.

The degree of malleability could be fine-tuned by the amount of MDTO incorporation, where more MDTO allowed for more addition fragmentation chain transfer into the backbone. In Figure 1.6c,d, we see that upon the exposure of stress the sample crept

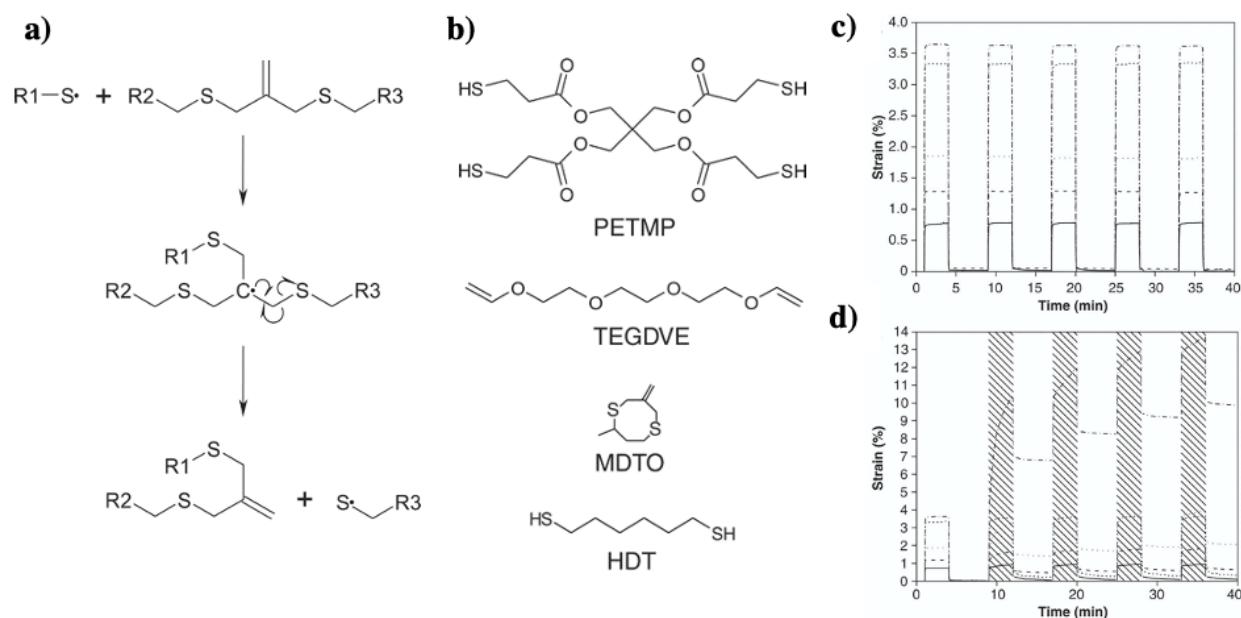


**Figure 1.6.** Thiyl radical addition-fragmentation chain transfer in polymer networks. (a) Thiyl radicals transfer to allyl sulfide groups in the network backbone. Homolytic fragmentation of the C-S bond generates another thiyl radical for further propagation. (b) Monomers used in the synthesis of dynamic thiol-ene networks. MDTO is used to introduce cleavable allyl sulfide groups along the backbone. Strain-recovery profiles of dynamic thiol-ene network (c) without irradiation and (d) with  $30 \text{ mW}\cdot\text{cm}^2$  UV light. Reproduced from Scott, T., *et al. Science*. **2005**.

substantially during the five-minute intervals of UV light exposure, such that it did not return to the previous strain prior to irradiation. At this point in time, chain transfer from thiyl to alkene was the major reaction in the widely used thiol-ene photopolymerization, however the second step of chain transfer fragmentation had only been recently discovered in reversible addition fragmentation chain transfer (RAFT) polymerization.<sup>33</sup> RAFT polymerization is a living polymerization used to prepare low dispersity polymers, however Bowman's work was the first instance of the fragmentation step being used as a stimuli-responsive motif in bulk polymers.

Despite radical chain transfer fragmentation motifs ushering in a new era of malleable thermosets, it should be noted that there are several limitations to this chemistry. First, the radical generation requires latent photoinitiator, which will be both incompatible with many systems and also be depleted upon repeated uses. Second, radical chemistry is more sensitive to a wide variety of unsaturated bonds, thereby eliminating its use in many commodity polymers. Third, the use of UV light poses challenges as polymers may be inaccessible during molding or not transparent to UV light. In such instances the malleability of the resin would be limited to open air applications. Finally, a high loading of MDTO was required for malleability to proceed, indicating the low efficiency of the fragmentation reaction. Despite these drawbacks, this work opened a door to an untapped field of material chemistry that would prove to be rich with opportunity.

One such opportunity was found in the area of polyolefin exchange. Polyolefins are the largest family of commercially produced plastics, but they are often overlooked as backbones for dynamic exchange due to their stability and inert nature. One of the first

efforts towards olefin dynamic exchange was reported in our lab through use of ruthenium-catalyzed olefin metathesis (Figure 1.7).<sup>71</sup> Olefin metathesis offers an interesting approach as an associative exchange mechanism due to its autonomous exchange over a wide temperature range, high efficiency, and high tolerance to functional groups.<sup>17,72</sup> To generate the malleable network, linear polybutadiene (PBD) was first radically crosslinked to form an insoluble rubber followed by the diffusion of Grubbs 2<sup>nd</sup> generation catalyst by solvent swelling. After addition of the catalyst into the PBD rubber, residual double bonds along the backbone would continuously undergo metathesis and dissipate stress in the network. While originally used to show malleability in thermosets, this work was subsequently shown to provide a platform for efficient self-healing cut materials by simply sprinkling catalyst at the interface.<sup>73</sup> This updated method using the sprinkled Grubb's catalyst would offer similar self-healing capabilities without the requirement for solvent swelling, dramatically reducing the processing steps to produce a self-healing rubber.

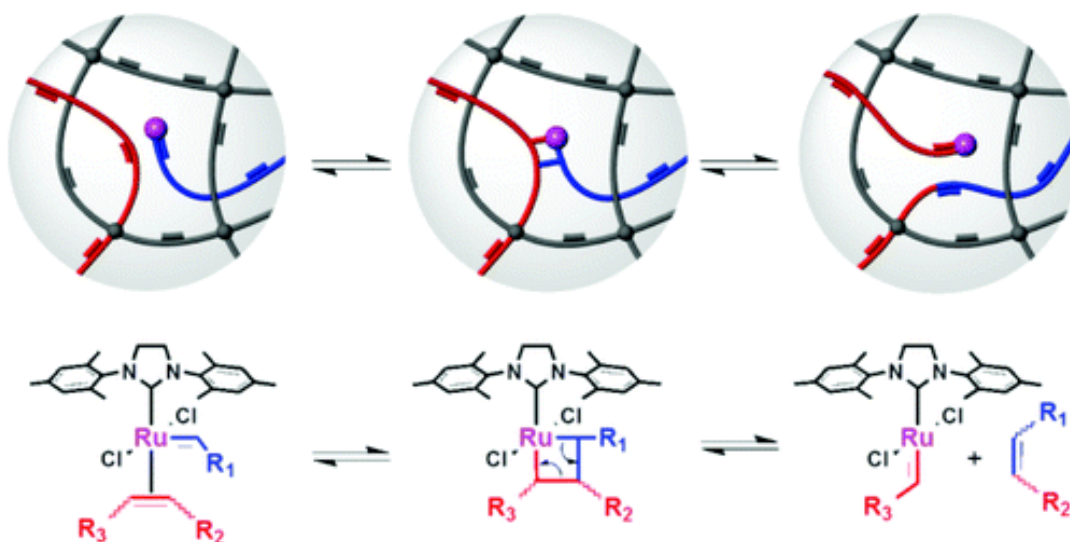


**Figure 1.7.** Polybutadiene rubber was blended with 0.0050, 0.0075, and 0.0100 Grubbs 2<sup>nd</sup> Generation Ru catalyst to produce a dynamic network from olefin metathesis reactions. Reproduced from Lu, Y., *et al. J. Am. Chem. Soc.* **2012**.

One of the most popular chemistries to exploit this new field is transition metal-catalyzed transesterification in crosslinked polyester networks. Leibler *et al.* were the first to incorporate zinc in epoxy networks where they noted that the malleability followed an Arrhenius-type temperature dependence.<sup>70</sup> The epoxy thermoset was prepared between a mixture of diglycidyl ether of bisphenol A (DGEBA) and multifunctional fatty carboxylic acids in a 1:1 stoichiometric ratio (Figure 1.8). Zinc acetate was blended into the mixture before curing, which provided the catalysts for the exchange mechanism. The  $Zn^{2+}$  ions coordinate to the lone pair electrons on the carbonyl, increasing the susceptibility for nucleophilic addition into the  $\pi^*_{C-O}$  bond.<sup>74,75</sup> After curing, the epoxy thermoset was insoluble in solvent

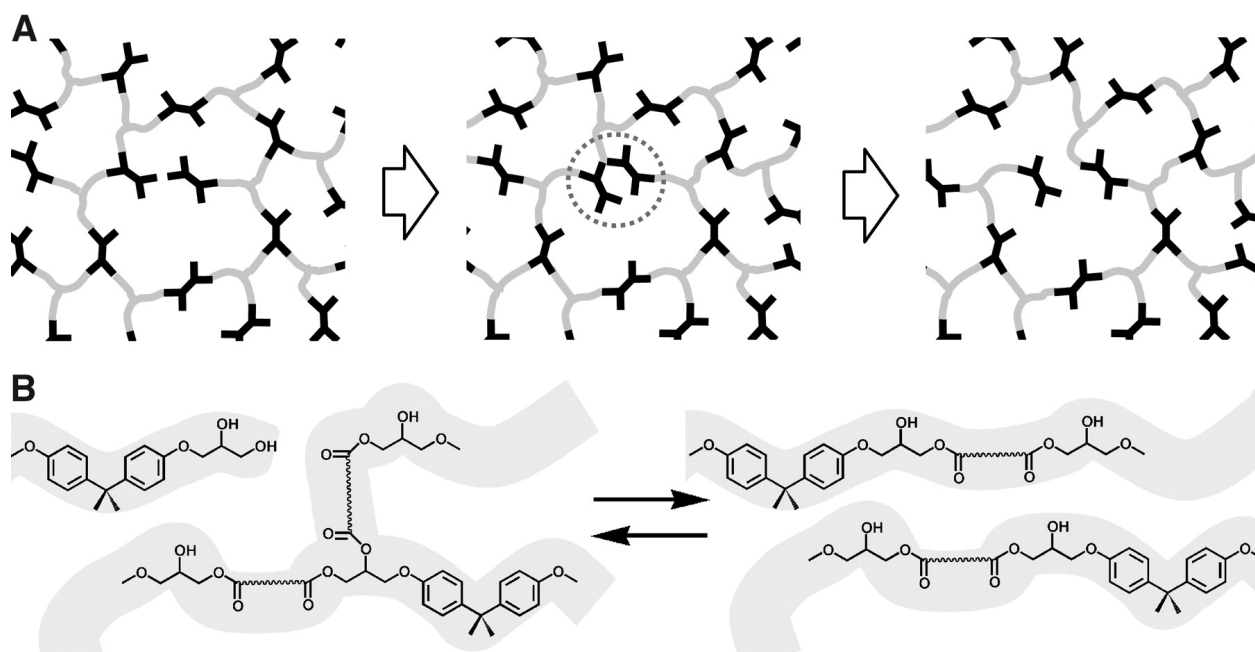


**Figure 1.8.** Epoxy networks containing excess hydroxyl groups undergo exchange at sufficiently high temperatures in the presence of transition metal catalysts. The exchange reaction occurs via associative exchange, allowing for fixed crosslink density during the exchange process. Reproduced from Montarnal, D. *et al. Science* **2011**.

signaling that the network was fully crosslinked. When heated, free alcohol groups from the epoxy ring-opening could associatively exchange with the ester groups forming the crosslinking points, thus alleviating stress in the material. Without the catalyst, the transesterification reaction energy barrier was too high to occur at reasonable processing temperatures and times. In the catalyzed system at room temperature, the transesterification reactions were almost entirely suppressed, however at temperatures above 150 °C the network topology would rearrange to flow and dissipate stress. This work was unique in that it relied solely on associative exchange reactions, whereas many dynamic materials before had utilized depolymerization-polymerization equilibria to maintain reprocessability.

Further work on transition metal catalyzed transesterification<sup>76,77</sup> found that the exchange rate was dictated by three major factors: catalyst concentration, free alcohol concentration, and temperature. The exchange rate can be experimentally tested by stress relaxation experiments whereby a constant strain is applied to the sample and the relaxation time is measured. The exchange rate should follow an Arrhenius-type temperature dependence, therefore we can use the Maxwell model for relaxation to find the time required to reach 37% (1/e) of the original stress (Equation 1)<sup>76,78</sup>:

$$\tau^* = \tau_0 \exp\left(\frac{E_a}{R * T}\right) \quad (1)$$

By running the relaxation experiment at different temperatures, an Arrhenius plot can be tabulated to find the energy of activation ( $E_A$ ) for that particular system. The derived energy of activation is an apparent value and does not reflect the true  $E_A$  for the exchange mechanism. This is because any physical property that significantly increases the melt

viscosity (*i.e.*, strong intermolecular forces, polymer branching, chain extension, irreversible crosslinks, etc.) cannot be delineated from the dynamic exchange when performing physical tests such as stress relaxation. In Leibler's work on Zn-catalyzed transesterification, the activation energy was found to be  $\sim 88$  kJ/mol $\cdot$ K when loaded with 10 mol% catalyst. When Brønsted Acid catalyst such as triflic acid, bis(trifluoromethane)sulfonimide, benzene sulfonic acid, methanesulfonic acid, and trifluoroacetic acid were used as transesterification catalysts, the  $E_A$  was found to be 66.7, 60.2, 56.4, 49.7 and 49.6 kJ/mol, respectively.<sup>77</sup>

Regardless of the  $E_A$  for the dynamic motif, there is a lower temperature threshold at which the network rearrangement is effectively frozen. That freezing point is generally considered when the viscosity ( $\eta$ ) is equal to  $10^{12}$  Pa $\cdot$ s. This value is often used in calculations because the value is sufficiently high that the material is considered a solid for the purposes of practical use. Using a derivation of Maxwell's equation (Equation 2),

$$\eta = G \cdot \tau^* = \frac{E'}{2(1 + \nu)} \cdot \tau^* \quad (2)$$

we can find the extrapolated relaxation time that the associated viscosity occurs. The storage modulus,  $E'$ , is determined from the modulus plateau above the  $T_g$  and/or  $T_m$  in a dynamic mechanical analysis (DMA) temperature sweep. At that point, the modulus reflects the covalent bonds holding the network together which would otherwise melt at such high temperatures. By inputting the derived  $\tau^*$  back into Equation 1, we can calculate the theoretical temperature at which the network no longer exchanges. This temperature is called the vitrimer exchange temperature ( $T_v$ ) and is useful for gauging what vitrimer system is useful in a certain application. In most cases, the  $T_v$  should be above the working temperature of the material, only being exceeded when reprocessing is needed.

In a similar vein to the above-mentioned transesterification reactions, transamidation offers an interesting method for stable linkages that can also undergo 3-membered intermediates. In fact, the amide bond is more thermodynamically favored than an ester group and significantly more resistant to hydrolysis at processing temperatures. Unfortunately, the amide bond is so inert that strong transition metal catalysts are required to observe transamidation at reasonable temperatures.<sup>79</sup> In 2015, Du Prez and coworkers attempted to circumvent the low reactivity of amides by utilizing vinylogous urethanes, a conjugated analogue to amides, as a dynamic motif (Figure 1.9).<sup>80</sup> Vinylogous urethanes act as a catalyst-free Michael acceptor for the conjugate addition of a primary amine. Above 140 °C, this exchange begins to occur in reasonable timeframes for most applications. The  $E_A$  was found to be ~60 kJ/mol, which is in line with many of the other previously listed vitrimer chemistries and agreed with the model compound studies in their work. Interestingly, the  $T_v$  of 29 °C was below the  $T_g$  of 87 °C, meaning the network rearrangement could be arrested above the  $T_v$  as long as vitrimer was also below the  $T_g$ .

Further work on vinylogous urethane vitrimers showed that additives could accelerate the exchange process through different mechanisms.<sup>81</sup> As the exchange reaction occurs between primary amines and vinylogous urethanes through a proposed imidinium intermediate (Figure 1.10), catalysts were chosen to either facilitate or hinder the proton transfer. Among the chosen catalysts were the Brønsted acids *p*-toluene sulphonic acid (*p*TsOH) and sulfuric acid (H<sub>2</sub>SO<sub>4</sub>), strong bases triazabicyclodecene (TBD) and 1,5-



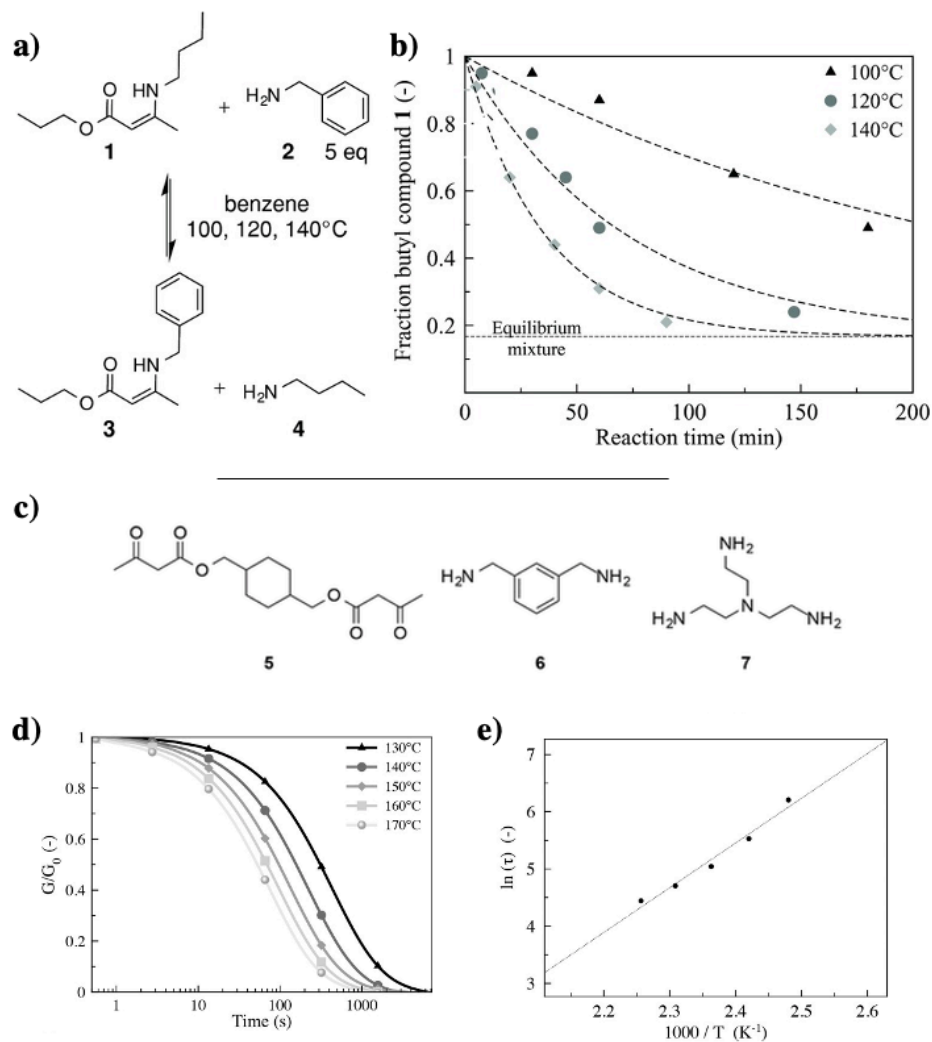


**Figure 1.9.** Vinylogous urethane exchange. (a) Upon heating, a free primary amine will undergo conjugate addition to the Michael acceptor on the vinylogous urethane, displacing the covalently bound secondary amine. (b) At temperatures above 100 °C, the reaction is spontaneous at reasonable time scales. (c) An addition reaction between acetoacetate and a primary amine will produce the vinylogous urethane linkages, and a trifunctional amine can be used as a crosslinker. (d, e) Associative addition of the primary amine dissipates stress with Arrhenius temperature-dependance. Reproduced from Denissen, W. *et al. Adv. Func. Mater.* **2015**.

Diazabicyclo[4.3.0]non-5-ene (DBN), and the commonly used Lewis acid transesterification catalyst, dibutyltindilaurate (DBTL). In model compound studies (Figure 1.10a,b) it was found the inclusion of acid catalysts to greatly increase the rate of the reaction with *p*TsOH

having the largest effect and  $\text{H}_2\text{SO}_4$  having the least effect with the conclusion that solubility of the organic catalyst having a significant impact on reaction rates.

Interestingly, the measured  $E_a$  for both uncatalyzed and *p*TsOH-catalyzed reactions were  $\sim 74$  kJ/mol, indicating the reaction proceeded through the same iminium intermediate pathway despite the faster rate. The increased rate was attributed to a higher concentration of active iminium species due to the acid catalyst. The DBTDL-catalyzed exchange had a significantly lower  $E_a$  of 45 kJ/mol indicating the reaction proceeded through a different mechanism, likely through activation of the carbonyl and stabilization of the zwitterion. Conversely, the addition of the strong bases like TBD and DBU significantly retarded the

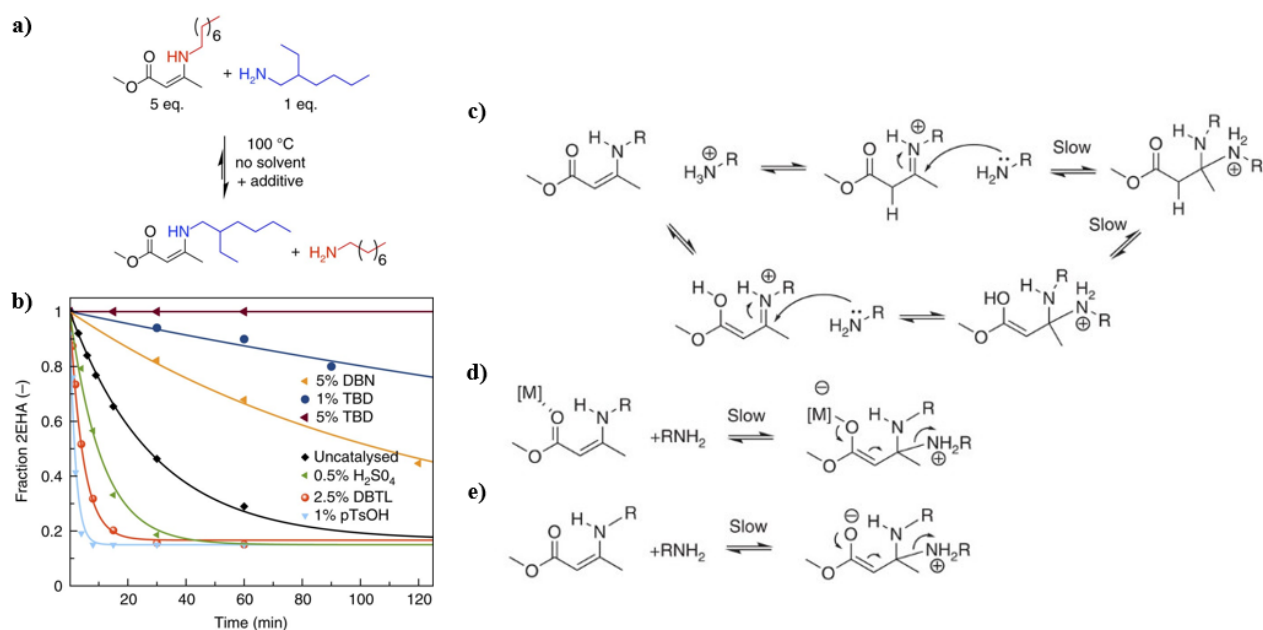


**Figure 1.10.** Catalytic control over vinylogous urethane exchange. (a) Model compounds used in exchange study. (b) Concentration of 2-ethylhexylamine with respect to time in the model compound exchange study. (c) Proposed mechanism for neutral and acidic conditions proceeding through an iminium intermediate. (d) Proposed mechanism in the presence of transition metal catalyst via activation of the carbonyl. (e) Proposed mechanism in basic conditions such as DBN and TBD where the zwitterion is unstabilized due to proton trapping. Reproduced from reference Denissen, W., *et al. Nat. Chem.* **2017**.

exchange rate by increasing the  $E_a$  to 102 kJ/mol. Under 5% TBD the exchange was arrested, indicating that bases were solely proton scavengers thereby eliminating any of the required proton exchange. When incorporated into the vitrimer network, the catalytic trends were the same as observed in small molecule studies. This work signified that additives could not only be used to speed up the exchange reaction within vitrimer networks, but under judicious consideration can also slow the exchange to better match the required application.

Vinylogous urethanes have become a popular vitrimer motif due to their stability towards a wide variety of functionalities, however there are some drawbacks. The requirement of excess primary amines does pose a challenge to electrophilic functional groups such as carbonyls and aldehydes due to imide formation at elevated temperatures.<sup>82</sup> Another drawback is the requirement for acetoacetate functional groups for the preparation of the vinylogous urethane moiety. Acetoacetates are uncommon in commodity materials; therefore, custom polymers will have to be made which limits the broad adoption of vinylogous urethanes as associative exchange motifs.

An alternative dynamic exchange uses boronic esters and boroxines to relax stress in crosslinked networks. Exchange between B-O bonds occur when a nucleophile adds to the boron's empty p-orbital producing a 4-membered intermediate.<sup>83</sup> As such, the crosslink density during exchange remains high and network integrity is preserved. Boronic ester and boroxine exchange are prominent methods of dynamic exchange and have taken several avenues during their implementation. Some of the first uses of boroxine and/or boronic acid as a polymer dynamic motif were in solution to form gels,<sup>84</sup> block-copolymers,<sup>85</sup> and self-repairing linear polymers.<sup>86</sup> The Summerlin group was the first to incorporate boronic ester

exchange into bulk networks where they observed self-healing properties.<sup>87</sup> They used thiol-ene photopolymerization to prepare a soft network, wherein autonomic boronic ester exchange occurred at the interface between cut pieces. One drawback to their design was the requirement for the cut faces to be wet with water. The addition of water shifted equilibrium from boronic ester to boronic acid, thereby increasing the reactivity and bridge-forming ability.

Simultaneously and independently to the Summerlin's work, our lab was pursuing boronic ester exchange for self-healing applications without the need for special treatment.

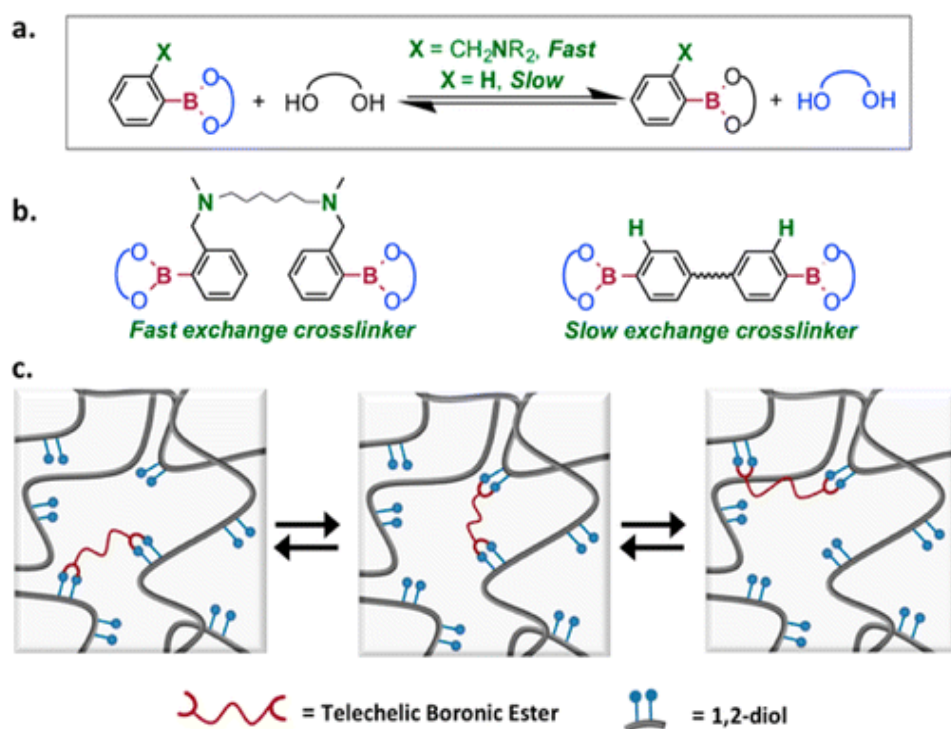


**Figure 1.11.** Boronic ester exchange. (a) Incorporation of internal amine catalysts accelerates the exchange reaction. (b) Two crosslinkers were prepared. The ‘fast exchange crosslinker’ contained a tertiary amine to facilitate proton transfer, while the ‘slow exchange crosslinker’ had an aliphatic bridge. The amine-containing monomer increased the rate of exchange by five orders of magnitude. (c) Diagram of the boronic ester exchange in the polymer network. Reproduced from Cromwell, O., *et al. J. Am. Chem. Soc.* **2015**.

The key advancement was the use of internal amine-based catalysts to promote rapid exchange of boronic esters and boroxines in bulk polymers.<sup>88</sup> It was found that by modifying the monomer to contain a neighboring amine, boronic ester exchange was accelerated by five orders of magnitude (Figure 1.11). This work pioneered the concept of internal catalysts in dynamic networks and has since been expanded to many different systems.<sup>89-92</sup> In the work of Cromwell *et al.*, it was presumed that the amine acted as a proximal base for proton transfer during the boronic acid transesterification. As such, the exchange kinetics are dependent on the concentration of free boronic acid to initiate exchange. When incorporated into bulk polymers, the crosslinked network retained malleability and was able to self-heal at relatively low temperatures of 50 °C.

Advancing on the platform of boronic ester exchange in bulk, it was found that when boronic acid is dehydrated to form 6-membered boroxine rings, those rings can also participate in dynamic exchange.<sup>93</sup> Previous literature had shown that boroxine dynamic networks underwent dissociative exchange through hydrolysis, rearrangement, and subsequent dehydration to re-form the network.<sup>84,94,95</sup> However, recently it was shown in our lab<sup>93</sup> that boroxine rings may directly exchange through an associative mechanism (Figure 1.12). Unlike boronic ester exchange, the addition of an amine catalyst such as pyridine showed no influence on the exchange kinetics. It was concluded that residual boronic acid facilitated exchange in the boroxine network. The added benefit of using boroxine rings is their ability to be placed at the crosslinking point due to their tri-functionality. Without the reliance on pendent boronic acids from the backbone of a polymer,

shorter molecular weight linkers with varying physical properties can be used to tune the system.

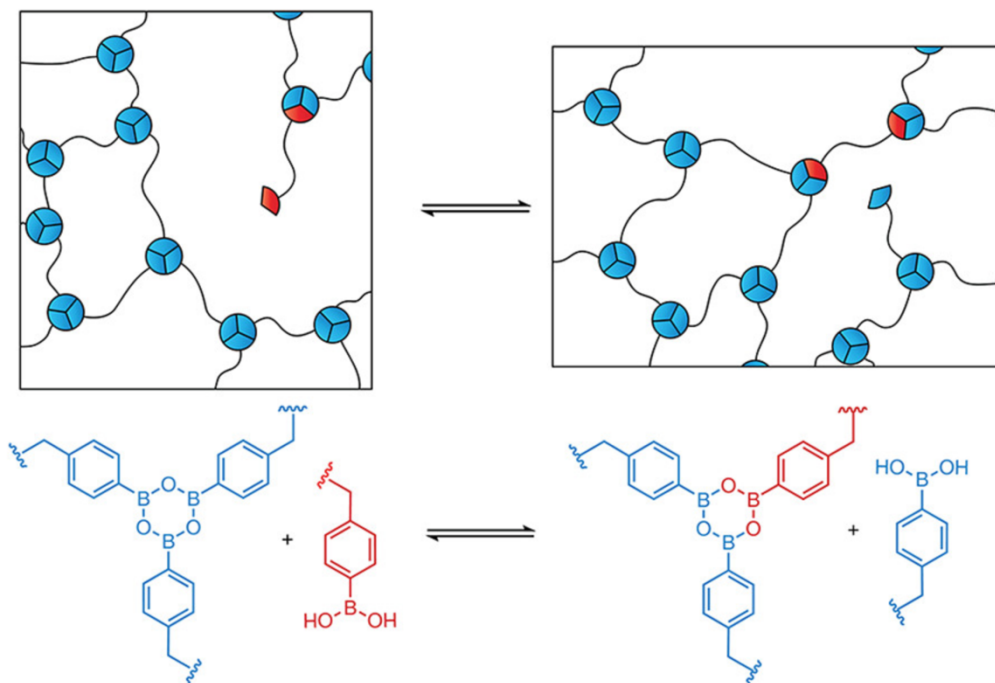


**Figure 1.12.** Boroxine crosslinks generated from the slow dehydration of boronic acid monomers, allowing dynamic exchange in bulk materials without the requirement for hydrolysis, rearrangement, and dehydration. Residual boronic acid undergoes transesterification into the boroxine ring thereby relieving stress in the crosslinked network. Reproduced from Ogden, W., Guan, Z. *J. Am. Chem. Soc.* **2018**.

Along with pushing developments in B-O exchange, our lab has also developed vitrimers that use using Si-O exchange. Siloxane/silyl ether exchange is an interesting motif for vitrimers due to the significant bond strength in Si-O bonds (bond dissociation energy = 535 kJ/mol).<sup>96</sup> Despite its recent use as a dynamic crosslinker, Si-O chemistry has been used for millennia to prepare glass where the exchange temperature occurs at several hundred degrees.<sup>97</sup> Siloxane exchange was one of the earliest discoveries of malleability in crosslinked networks and was initially reported in 1954.<sup>98</sup> They found that crosslinked

polydimethylsiloxane (PDMS) dissipated tensile stress in the presence of acid and base catalyst. They proposed that when potassium hydroxide was dissolved into the elastomer, the siloxane linkages were hydrolyzed to form potassium silanolate, which can exchange with adjacent siloxane linkages. Such chemistry was unearthed in 2012 by McCarthy and coworkers when they applied this concept to self-healing materials.<sup>99</sup> Using a tetramethylammonium counterion to stabilize the exchanging silanolate (Figure 1.13), they could mold the PDMS elastomer at temperature as low as 90 °C. Because the exchange occurs

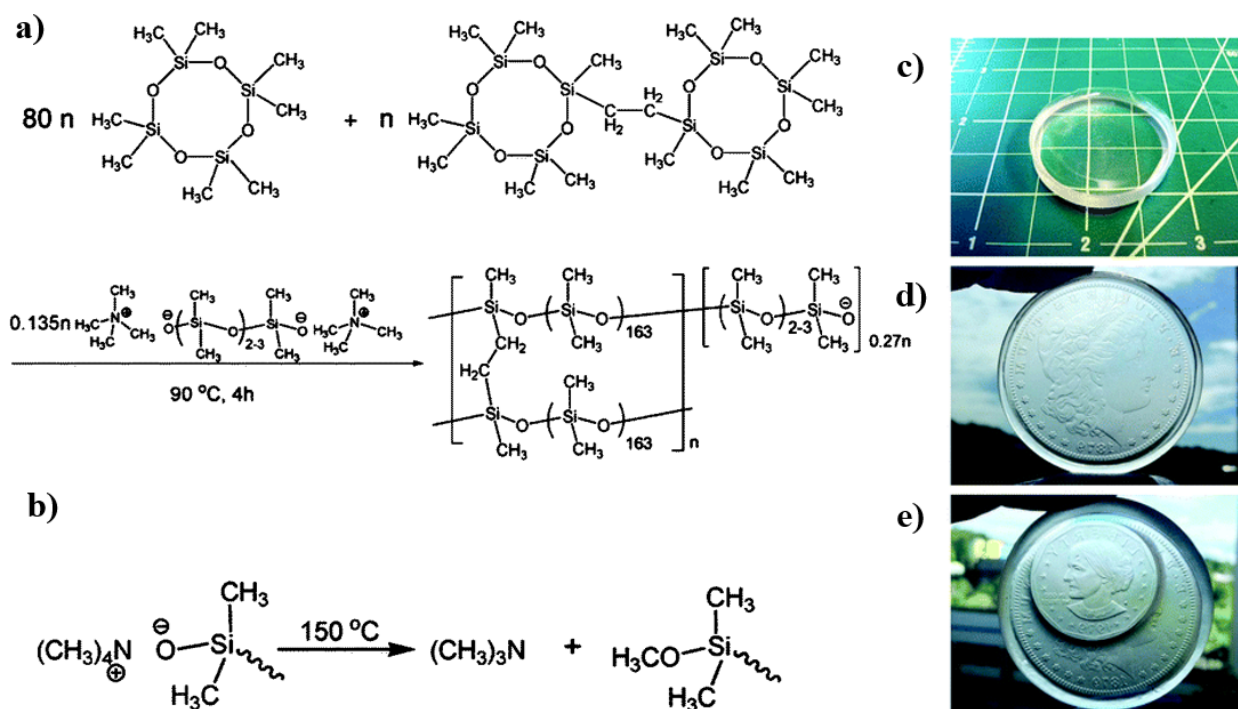


**Figure 1.13.** (a) PDMS elastomers were prepared from the anionic ring opening polymerization of cyclooctamethyltetrasiloxane. The trimethylammonium counterion provided stability in for the living anionic chain end. The living end could substitute onto neighboring siloxane units allowing for network rearrangement. (b) When heated beyond 150 °C, the trimethylammonium counterion decomposed to form trimethylamine and methoxysilane. This allowed the self-healing behavior to be permanently “turned off”. (c) Pristine PDMS elastomer. (d) PDMS elastomer remolded with an American 1879 Silver Dollar. (e) The same PDMS elastomer remolded with an American 1979 dollar. Reproduced from Zheng, P., McCarthy, T. J. *Am. Chem. Soc.* **2012**.

through a 5-membered intermediate, there was no decrease in crosslink density and the material remained relatively robust at elevated temperatures. The tetramethylammonium counterion had the added benefit of dealkylating to triethylamine at temperatures above 150 °C so the catalytic activity could be quenched without explicit removal of the catalyst. Despite the good exchange characteristics, the main challenge of anionic silanolate exchange is the susceptibility to moisture. The silanolate can be quenched to the more stable silanol which will not be able to participate in dynamic exchange under the required conditions, therefore the use of a neutrally charged Si-O exchange route would provide the moisture resistance required for expanded applications.

In an attempt to incorporate neutrally charged silyl ether exchange, our lab worked on using alcohol-silyl ether exchange to provide the dynamic motif.<sup>100</sup> The use of alcohols to displace silyl groups has long been used in traditional organic chemistry as a protection/deprotection step in preserving sensitive functional groups.<sup>101</sup> Using this well-known exchange chemistry, we worked to broaden the scope of Si-O exchange into more traditional commodity polymer backbones such as polystyrene. A bis-trimethoxysilane crosslinker was added to poly(styrene-co-styryl alcohol such that the free -OH on the polymer backbone would displace the methoxy group on the crosslinker (Figure 1.14). Once the crosslinker had been anchored to the polymer backbone, free alcohol groups throughout the polymer backbone facilitate shuffling of the crosslinker between chains. It was found that by incorporating an internal amine catalyst into the crosslinker (Figure 1.14a) the energy of activation of the exchange reaction was cut in half from approximately 174 kJ/mol in the aliphatic crosslinker to 81 kJ/mol in the amine-containing crosslinker. It is hypothesized that



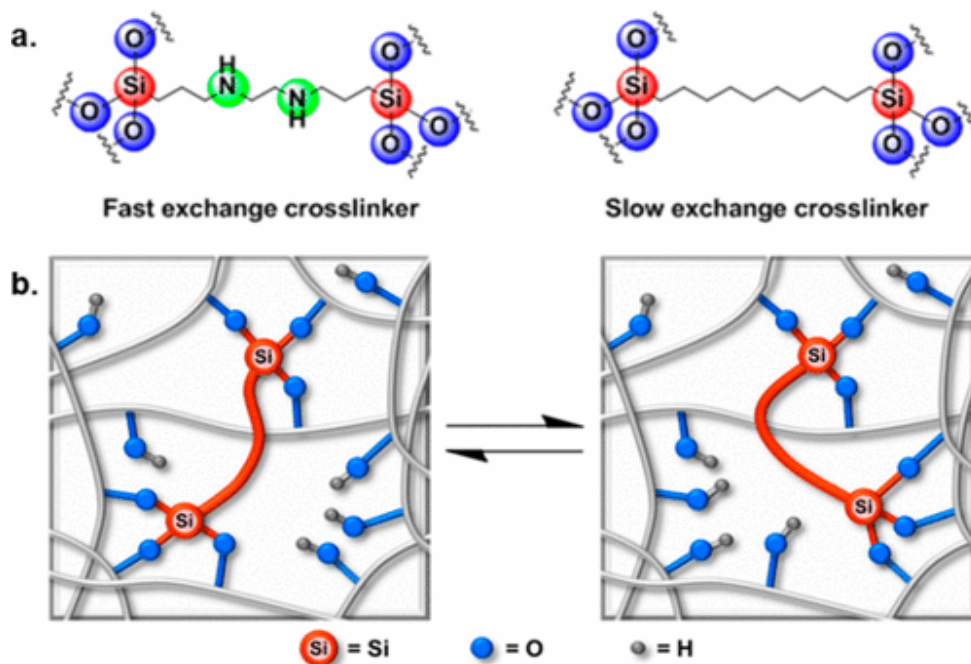


**Figure 1.14.** Linear polystyrene co-polymerized with pendant free alcohols were blended with methoxy silane crosslinkers. The silyl ether crosslinker containing secondary amines catalyzed the exchange rate through neighboring group effects. The amine acted as a proton transfer catalyst during the transesterification reaction. Reproduced from Nishimura, Y., *et al. J. Am. Chem. Soc.* **2017**.

the amine does not directly interact with the silicon, and instead acts as a proton transfer catalyst to increase the rate of the exchange. In chapters 3 and 4 of this thesis, I will describe my efforts towards expanding this chemistry and modifying the exchange dynamics for both silyl ethers and siloxane linkages.

Thus far I have discussed some representative contributions to the field of dynamic polymer networks. The dynamic motifs mentioned in this chapter have played an integral role in the development of the field. Nevertheless, there does not yet exist a ‘silver bullet’ that allows for their broad adoption. This is due to an inherent contrast in the desired properties of DCCs, *i.e.*, we seek a dynamic linkage that has high stability while also retaining rapid exchange rates. Faster exchange in dynamic networks generally requires the linkage

to be more labile, thus lowering the stability. In contrast, a strong dynamic bond generally has lower exchange kinetics. As mentioned in the above discussion, common weaknesses in dynamic materials include sensitivity towards moisture and other nucleophiles, oxygen, high temperatures, and low compatibility with common functional groups. For dynamic polymer networks to reach broad adoption, they need to have low cost, good physical behavior, and resistance towards common atmospheric and processing conditions. Current efforts are underway in our lab as well as many others towards the development of dynamic linkages that meet the above criteria. In chapter 2 of this thesis, I describe my efforts towards developing a self-healing material based on the dissociative exchange of sterically hindered thioureas that have improved hydrolytic stability over their urea-based counterparts. In chapters 3 of this thesis, I report my effort toward expanding the scope of thermally stable silyl ether chemistry into more industrially relevant polymers. In chapter 4, I describe my efforts towards the development of fluoride-catalyzed siloxane exchange as a rapid and selective exchange chemistry for dynamic polymer networks. In the final chapter, I describe my efforts towards the development of a thermally stable dynamic network to facilitate the kinetic trapping of immiscible polymer blends. This thesis represents my efforts to overcome common drawbacks of dynamic networks and to provide viable solutions to the challenges faced in the pursuit of sustainable polymer designs.

## References:

- (1) Staudinger, H. Über Polymerisation. *Berichte Dtsch. Chem. Ges. B Ser.* **1920**, *53* (6), 1073–1085. <https://doi.org/10.1002/cber.19200530627>.
- (2) Staudinger, H.; Fritsch, J. Über Isopren Und Kautschuk. 5. Mitteilung. Über Die Hydrierung Des Kautschuks Und Über Seine Konstitution. *Helv. Chim. Acta* **1922**, *5* (5), 785–806. <https://doi.org/10.1002/hlca.19220050517>.
- (3) Baekeland, L. H. The Synthesis, Constitution, and Uses of Bakelite. *J. Ind. Eng. Chem.* **1909**, *1* (3), 149–161. <https://doi.org/10.1021/ie50003a004>.
- (4) Odian, G. *Principles of Polymerization*; John Wiley & Sons, 2004.
- (5) Rudolph, N. S.; Kiesel, R.; Aumanate, C. *Understanding Plastics Recycling: Economic, Ecological, and Technical Aspects of Plastic Waste Handling*; Hanser Publishers, 2017.
- (6) Sakai, T.; Somiya, S. Analysis of Creep Behavior in Thermoplastics Based on Visco-Elastic Theory. *Mech. Time-Depend. Mater.* **2011**, *15* (3), 293–308. <https://doi.org/10.1007/s11043-011-9136-y>.
- (7) Ferry, J. D. *Viscoelastic Properties of Polymers*; John Wiley & Sons, 1980.
- (8) Pascault, J.-P.; Sautereau, H.; Verdu, J.; Williams, R. J. J. *Thermosetting Polymers*; CRC Press, 2002.
- (9) Winne, J. M.; Leibler, L.; Prez, F. E. D. Dynamic Covalent Chemistry in Polymer Networks: A Mechanistic Perspective. *Polym. Chem.* **2019**, *10* (45), 6091–6108. <https://doi.org/10.1039/C9PY01260E>.
- (10) Rowan, S. J.; Cantrill, S. J.; Cousins, G. R. L.; Sanders, J. K. M.; Stoddart, J. F. Dynamic Covalent Chemistry. *Angew. Chem. Int. Ed.* **2002**, *41* (6), 898–952. [https://doi.org/10.1002/1521-3773\(20020315\)41:6<898::AID-ANIE898>3.0.CO;2-E](https://doi.org/10.1002/1521-3773(20020315)41:6<898::AID-ANIE898>3.0.CO;2-E).
- (11) Maeda, T.; Otsuka, H.; Takahara, A. Dynamic Covalent Polymers: Reorganizable Polymers with Dynamic Covalent Bonds. *Prog. Polym. Sci.* **2009**, *34* (7), 581–604. <https://doi.org/10.1016/j.progpolymsci.2009.03.001>.
- (12) Jin, Y.; Yu, C.; J. Denman, R.; Zhang, W. Recent Advances in Dynamic Covalent Chemistry. *Chem. Soc. Rev.* **2013**, *42* (16), 6634–6654. <https://doi.org/10.1039/C3CS60044K>.
- (13) Diels, O.; Alder, K. Synthesen in Der Hydroaromatischen Reihe. *Justus Liebigs Ann. Chem.* **1928**, *460* (1), 98–122. <https://doi.org/10.1002/jlac.19284600106>.
- (14) Brieger, G.; Bennett, J. N. The Intramolecular Diels-Alder Reaction. *Chem. Rev.* **1980**, *80* (1), 63–97. <https://doi.org/10.1021/cr60323a004>.
- (15) Fuerstner, A. *Alkene Metathesis in Organic Synthesis*; Springer, 2003.
- (16) Calderon, N.; Ofstead, E. A.; Ward, J. P.; Judy, W. A.; Scott, K. W. Olefin Metathesis. I. Acyclic Vinylenic Hydrocarbons. *J. Am. Chem. Soc.* **1968**, *90* (15), 4133–4140. <https://doi.org/10.1021/ja01017a039>.

- (17) Vougioukalakis, G. C.; Grubbs, R. H. Ruthenium-Based Heterocyclic Carbene-Coordinated Olefin Metathesis Catalysts. *Chem. Rev.* **2010**, *110* (3), 1746–1787. <https://doi.org/10.1021/cr9002424>.
- (18) Pennella, F.; Banks, R. L.; Bailey, G. C. Disproportionation of Alkynes. *Chem. Commun. Lond.* **1968**, No. 23, 1548–1549. <https://doi.org/10.1039/C19680001548>.
- (19) Fürstner, A.; W. Davies, P. Alkyne Metathesis. *Chem. Commun.* **2005**, No. 18, 2307–2320. <https://doi.org/10.1039/B419143A>.
- (20) Liu, T.; Zhao, B.; Zhang, J. Recent Development of Repairable, Malleable and Recyclable Thermosetting Polymers through Dynamic Transesterification. *Polymer* **2020**, *194*, 122392. <https://doi.org/10.1016/j.polymer.2020.122392>.
- (21) Rezania, S.; Oryani, B.; Park, J.; Hashemi, B.; Yadav, K. K.; Kwon, E. E.; Hur, J.; Cho, J. Review on Transesterification of Non-Edible Sources for Biodiesel Production with a Focus on Economic Aspects, Fuel Properties and by-Product Applications. *Energy Convers. Manag.* **2019**, *201*, 112155. <https://doi.org/10.1016/j.enconman.2019.112155>.
- (22) Otera, Junzo. Transesterification. *Chem. Rev.* **1993**, *93* (4), 1449–1470. <https://doi.org/10.1021/cr00020a004>.
- (23) Layer, R. W. The Chemistry of Imines. *Chem. Rev.* **1963**, *63* (5), 489–510. <https://doi.org/10.1021/cr60225a003>.
- (24) Levrard, B. B.; Godin, G.; Trachsel, A.; Laumer, J.-Y. de S.; Lehn, J.-M.; Herrmann, A. Reversible Amino Formation: Controlling the Evaporation of Bioactive Volatiles by Dynamic Combinatorial/Covalent Chemistry. *Eur. J. Org. Chem.* **2011**, *2011* (4), 681–695. <https://doi.org/10.1002/ejoc.201001433>.
- (25) You, L.; Berman, J. S.; Anslyn, E. V. Dynamic Multi-Component Covalent Assembly for the Reversible Binding of Secondary Alcohols and Chirality Sensing. *Nat. Chem.* **2011**, *3* (12), 943–948. <https://doi.org/10.1038/nchem.1198>.
- (26) P. Black, S.; M. Sanders, J. K.; R. Stefankiewicz, A. Disulfide Exchange: Exposing Supramolecular Reactivity through Dynamic Covalent Chemistry. *Chem. Soc. Rev.* **2014**, *43* (6), 1861–1872. <https://doi.org/10.1039/C3CS60326A>.
- (27) L. Korich, A.; M. Iovine, P. Boroxine Chemistry and Applications: A Perspective. *Dalton Trans.* **2010**, *39* (6), 1423–1431. <https://doi.org/10.1039/B917043J>.
- (28) Tokunaga, Y.; Ito, T.; Sugawara, H.; Nakata, R. Dynamic Covalent Chemistry of a Boronylammonium Ion and a Crown Ether: Formation of a C<sub>3</sub>-Symmetric [4]Rotaxane. *Tetrahedron Lett.* **2008**, *49* (21), 3449–3452. <https://doi.org/10.1016/j.tetlet.2008.03.106>.
- (29) Tretbar, C. A.; Neal, J. A.; Guan, Z. Direct Silyl Ether Metathesis for Vitrimers with Exceptional Thermal Stability. *J. Am. Chem. Soc.* **2019**, *141* (42), 16595–16599. <https://doi.org/10.1021/jacs.9b08876>.
- (30) Scott, T. F.; Schneider, A. D.; Cook, W. D.; Bowman, C. N. Photoinduced Plasticity in Cross-Linked Polymers. *Science* **2005**, *308* (5728), 1615–1617. <https://doi.org/10.1126/science.1110505>.

- (31) Ciriano, M. V.; Korth, H.-G.; van Scheppingen, W. B.; Mulder, P. Thermal Stability of 2,2,6,6-Tetramethylpiperidine-1-Oxyl (TEMPO) and Related N-Alkoxyamines. *J. Am. Chem. Soc.* **1999**, *121* (27), 6375–6381. <https://doi.org/10.1021/ja9837102>.
- (32) Wang, J.-S.; Matyjaszewski, K. Controlled/"living" Radical Polymerization. Atom Transfer Radical Polymerization in the Presence of Transition-Metal Complexes. *J. Am. Chem. Soc.* **1995**, *117* (20), 5614–5615. <https://doi.org/10.1021/ja00125a035>.
- (33) Chiefari, J.; Chong, Y. K. (Bill); Ercole, F.; Krstina, J.; Jeffery, J.; Le, T. P. T.; Mayadunne, R. T. A.; Meijs, G. F.; Moad, C. L.; Moad, G.; Rizzardo, E.; Thang, S. H. Living Free-Radical Polymerization by Reversible Addition–Fragmentation Chain Transfer: The RAFT Process. *Macromolecules* **1998**, *31* (16), 5559–5562. <https://doi.org/10.1021/ma9804951>.
- (34) Greenlee, A. J.; Wendell, C. I.; Cencer, M. M.; Laffoon, S. D.; Moore, J. S. Kinetic and Thermodynamic Control in Dynamic Covalent Synthesis. *Trends Chem.* **2020**, *2* (12), 1043–1051. <https://doi.org/10.1016/j.trechm.2020.09.005>.
- (35) Smith, J. G. *Organic Chemistry*; McGraw-Hill Education, 2016.
- (36) Wang, S.; Urban, M. W. Self-Healing Polymers. *Nat. Rev. Mater.* **2020**, *5* (8), 562–583. <https://doi.org/10.1038/s41578-020-0202-4>.
- (37) Denissen, W.; Winne, J. M.; Du Prez, F. E. Vitrimers: Permanent Organic Networks with Glass-like Fluidity. *Chem. Sci.* **2016**, *7* (1), 30–38. <https://doi.org/10.1039/c5sc02223a>.
- (38) Zheng, N.; Xu, Y.; Zhao, Q.; Xie, T. Dynamic Covalent Polymer Networks: A Molecular Platform for Designing Functions beyond Chemical Recycling and Self-Healing. *Chem. Rev.* **2021**, *121* (3), 1716–1745. <https://doi.org/10.1021/acs.chemrev.0c00938>.
- (39) Craven, J. M. Cross-Linked Thermally Reversible Polymers Produced from Condensation Polymers with Pendant Furan Groups Cross-Linked with Maleimides. US3435003A, March 25, 1969.
- (40) Kennedy, J. P.; Carlson, G. M. Synthesis, Characterization, and Diels–Alder Extension of Cyclopentadiene Telechelic Polyisobutylene. III. Silylcyclopentadiene-Telechelic Polyisobutylene. *J. Polym. Sci. Polym. Chem. Ed.* **1983**, *21* (10), 2973–2986. <https://doi.org/10.1002/pol.1983.170211013>.
- (41) Chen, X.; Dam, M. A.; Ono, K.; Mal, A.; Shen, H.; Nutt, S. R.; Sheran, K.; Wudl, F. A Thermally Re-Mendable Cross-Linked Polymeric Material. *Science* **2002**, *295* (5560), 1698–1702. <https://doi.org/10.1126/science.1065879>.
- (42) Gandini, A. The Furan/Maleimide Diels–Alder Reaction: A Versatile Click–Unclick Tool in Macromolecular Synthesis. *Prog. Polym. Sci.* **2013**, *38* (1), 1–29. <https://doi.org/10.1016/j.progpolymsci.2012.04.002>.
- (43) Chujo, Y.; Sada, K.; Saegusa, T. Reversible Gelation of Polyoxazoline by Means of Diels–Alder Reaction. *Macromolecules* **1990**, *23* (10), 2636–2641. <https://doi.org/10.1021/ma00212a007>.
- (44) Defize, T.; Riva, R.; Raquez, J.-M.; Dubois, P.; Jérôme, C.; Alexandre, M. Thermoreversibly Crosslinked Poly( $\epsilon$ -Caprolactone) as Recyclable Shape-Memory Polymer Network.

- Macromol. Rapid Commun.* **2011**, *32* (16), 1264–1269.  
<https://doi.org/10.1002/marc.201100250>.
- (45) Yamashiro, M.; Inoue, K.; Iji, M. Recyclable Shape-Memory and Mechanical Strength of Poly(Lactic Acid) Compounds Cross-Linked by Thermo-Reversible Diels-Alder Reaction. *Polym. J.* **2008**, *40* (7), 657–662. <https://doi.org/10.1295/polymj.PJ2008042>.
- (46) Sun, H.; Kabb, C. P.; Dai, Y.; Hill, M. R.; Ghiviriga, I.; Bapat, A. P.; Sumerlin, B. S. Macromolecular Metamorphosis via Stimulus-Induced Transformations of Polymer Architecture. *Nat. Chem.* **2017**, *9* (8), 817–823. <https://doi.org/10.1038/nchem.2730>.
- (47) Christensen, E.; Fioroni, G. M.; Kim, S.; Fouts, L.; Gjersing, E.; Paton, R. S.; McCormick, R. L. Experimental and Theoretical Study of Oxidative Stability of Alkylated Furans Used as Gasoline Blend Components. *Fuel* **2018**, *212*, 576–585.  
<https://doi.org/10.1016/j.fuel.2017.10.066>.
- (48) Chan, J. W.; Hoyle, C. E.; Lowe, A. B.; Bowman, M. Nucleophile-Initiated Thiol-Michael Reactions: Effect of Organocatalyst, Thiol, and Ene. *Macromolecules* **2010**, *43* (15), 6381–6388. <https://doi.org/10.1021/ma101069c>.
- (49) Okumoto, S.; Yamabe, S. A Theoretical Study of Curing Reactions of Maleimide Resins through Michael Additions of Amines. *J. Org. Chem.* **2000**, *65* (5), 1544–1548.  
<https://doi.org/10.1021/jo9905773>.
- (50) Matsumoto, A.; Kubota, T.; Otsu, T. Radical Polymerization of N-(Alkyl-Substituted Phenyl)Maleimides: Synthesis of Thermally Stable Polymers Soluble in Nonpolar Solvents. *Macromolecules* **1990**, *23* (21), 4508–4513. <https://doi.org/10.1021/ma00223a002>.
- (51) Atilla Tasdelen, M. Diels–Alder “Click” Reactions: Recent Applications in Polymer and Material Science. *Polym. Chem.* **2011**, *2* (10), 2133–2145.  
<https://doi.org/10.1039/C1PY00041A>.
- (52) Ling, J.; Rong, M. Z.; Zhang, M. Q. Photo-Stimulated Self-Healing Polyurethane Containing Dihydroxyl Coumarin Derivatives. *Polymer* **2012**, *53* (13), 2691–2698.  
<https://doi.org/10.1016/j.polymer.2012.04.016>.
- (53) López-Vilanova, L.; Martínez, I.; Corrales, T.; Catalina, F. Photochemical Crosslinking of Poly-(Ethylene–Butyl–Acrylate) Copolymers Functionalized with Anthracene Moieties by Reactive Extrusion. *Eur. Polym. J.* **2014**, *56*, 69–76.  
<https://doi.org/10.1016/j.eurpolymj.2014.04.005>.
- (54) Chung, C.-M.; Roh, Y.-S.; Cho, S.-Y.; Kim, J.-G. Crack Healing in Polymeric Materials via Photochemical [2+2] Cycloaddition. *Chem. Mater.* **2004**, *16* (21), 3982–3984.  
<https://doi.org/10.1021/cm049394+>.
- (55) Yang, K.; Zeng, M. Multiresponsive Hydrogel Based on Polyacrylamide Functionalized with Thymine Derivatives. *New J. Chem.* **2013**, *37* (4), 920–926.  
<https://doi.org/10.1039/C3NJ41013G>.
- (56) Marschner, D. E.; Frisch, H.; Offenloch, J. T.; Tuten, B. T.; Becer, C. R.; Walther, A.; Goldmann, A. S.; Tzvetkova, P.; Barner-Kowollik, C. Visible Light [2 + 2] Cycloadditions for Reversible

- Polymer Ligation. *Macromolecules* **2018**, *51* (10), 3802–3807.  
<https://doi.org/10.1021/acs.macromol.8b00613>.
- (57) Ying, H.; Zhang, Y.; Cheng, J. Dynamic Urea Bond for the Design of Reversible and Self-Healing Polymers. *Nat. Commun.* **2014**, *5* (3218), 1–9.  
<https://doi.org/10.1038/ncomms4218>.
- (58) Salvestrini, S.; Di Cerbo, P.; Capasso, S. Kinetics of the Chemical Degradation of Diuron. *Chemosphere* **2002**, *48* (1), 69–73. [https://doi.org/10.1016/S0045-6535\(02\)00043-7](https://doi.org/10.1016/S0045-6535(02)00043-7).
- (59) Otsuka, H.; Aotani, K.; Higaki, Y.; Takahara, A. Polymer Scrambling: Macromolecular Radical Crossover Reaction between the Main Chains of Alkoxyamine-Based Dynamic Covalent Polymers. *J. Am. Chem. Soc.* **2003**, *125* (14), 4064–4065.  
<https://doi.org/10.1021/ja0340477>.
- (60) Yuan, C.; Rong, M. Z.; Zhang, M. Q.; Zhang, Z. P.; Yuan, Y. C. Self-Healing of Polymers via Synchronous Covalent Bond Fission/Radical Recombination. *Chem. Mater.* **2011**, *23* (22), 5076–5081. <https://doi.org/10.1021/cm202635w>.
- (61) Mannan, Md. A.; Ichikawa, A.; Miura, Y. Living Radical Polymerization of Styrene Mediated by a Piperidinyl-N-Oxyl Radical Having Very Bulky Substituents. *Polymer* **2007**, *48* (3), 743–749. <https://doi.org/10.1016/j.polymer.2006.12.002>.
- (62) Imato, K.; Nishihara, M.; Kanehara, T.; Amamoto, Y.; Takahara, A.; Otsuka, H. Self-Healing of Chemical Gels Cross-Linked by Diarylbibenzofuranone-Based Trigger-Free Dynamic Covalent Bonds at Room Temperature. *Angew. Chem.* **2012**, *124* (5), 1164–1168.  
<https://doi.org/10.1002/ange.201104069>.
- (63) Scaiano, J. C.; Martin, A.; Yap, G. P. A.; Ingold, K. U. A Carbon-Centered Radical Unreactive Toward Oxygen: Unusual Radical Stabilization by a Lactone Ring. *Org. Lett.* **2000**, *2* (7), 899–901. <https://doi.org/10.1021/ol9913946>.
- (64) Frenette, M.; MacLean, P. D.; Barclay, L. R. C.; Scaiano, J. C. Radically Different Antioxidants: Thermally Generated Carbon-Centered Radicals as Chain-Breaking Antioxidants. *J. Am. Chem. Soc.* **2006**, *128* (51), 16432–16433. <https://doi.org/10.1021/ja066870j>.
- (65) Korth, H.-G. Gegen Sauerstoff Wenig Reaktive C-Radikale: Radikal Andere Antioxidantien. *Angew. Chem.* **2007**, *119* (28), 5368–5370. <https://doi.org/10.1002/ange.200701569>.
- (66) Marque, S.; Le Mercier, C.; Tordo, P.; Fischer, H. Factors Influencing the C–O–Bond Homolysis of Trialkylhydroxylamines. *Macromolecules* **2000**, *33* (12), 4403–4410.  
<https://doi.org/10.1021/ma9918452>.
- (67) Bejan, E. V.; Font-Sanchis, E.; Scaiano, J. C. Lactone-Derived Carbon-Centered Radicals: Formation and Reactivity with Oxygen. *Org. Lett.* **2001**, *3* (25), 4059–4062.  
<https://doi.org/10.1021/ol0167917>.
- (68) Cunningham, M. F. Recent Progress in Nitroxide-Mediated Polymerizations in Miniemulsion. *Comptes Rendus Chim.* **2003**, *6* (11), 1351–1374.  
<https://doi.org/10.1016/j.crci.2003.07.013>.

- (69) Elling, B. R.; Dichtel, W. R. Reprocessable Cross-Linked Polymer Networks: Are Associative Exchange Mechanisms Desirable? *ACS Cent. Sci.* **2020**, *6* (9), 1488–1496. <https://doi.org/10.1021/acscentsci.0c00567>.
- (70) Montarnal, D.; Capelot, M.; Tournilhac, F.; Leibler, L. Silica-Like Malleable Materials from Permanent Organic Networks. *Science* **2011**, *334* (6058), 965–968. <https://doi.org/10.1126/science.1212648>.
- (71) Lu, Y.-X.; Tournilhac, F.; Leibler, L.; Guan, Z. Making Insoluble Polymer Networks Malleable via Olefin Metathesis. *J. Am. Chem. Soc.* **2012**, *134* (20), 8424–8427. <https://doi.org/10.1021/ja303356z>.
- (72) Scholl, M.; Ding, S.; Lee, C. W.; Grubbs, R. H. Synthesis and Activity of a New Generation of Ruthenium-Based Olefin Metathesis Catalysts Coordinated with 1,3-Dimesityl-4,5-Dihydroimidazol-2-Ylidene Ligands. *Org. Lett.* **1999**, *1* (6), 953–956. <https://doi.org/10.1021/ol990909q>.
- (73) Lu, Y.-X.; Guan, Z. Olefin Metathesis for Effective Polymer Healing via Dynamic Exchange of Strong Carbon–Carbon Double Bonds. *J. Am. Chem. Soc.* **2012**, *134* (34), 14226–14231. <https://doi.org/10.1021/ja306287s>.
- (74) Román-Leshkov, Y.; Davis, M. E. Activation of Carbonyl-Containing Molecules with Solid Lewis Acids in Aqueous Media. *ACS Catal.* **2011**, *1* (11), 1566–1580. <https://doi.org/10.1021/cs200411d>.
- (75) Demongeot, A.; J. Mougner, S.; Okada, S.; Soulié-Ziakovic, C.; Tournilhac, F. Coordination and Catalysis of Zn<sup>2+</sup> in Epoxy-Based Vitrimers. *Polym. Chem.* **2016**, *7* (27), 4486–4493. <https://doi.org/10.1039/C6PY00752J>.
- (76) Capelot, M.; Unterlass, M. M.; Tournilhac, F.; Leibler, L. Catalytic Control of the Vitrimer Glass Transition. *ACS Macro Lett.* **2012**, *1* (7), 789–792. <https://doi.org/10.1021/mz300239f>.
- (77) Self, J. L.; Dolinski, N. D.; Zayas, M. S.; Read de Alaniz, J.; Bates, C. M. Brønsted-Acid-Catalyzed Exchange in Polyester Dynamic Covalent Networks. *ACS Macro Lett.* **2018**, *7* (7), 817–821. <https://doi.org/10.1021/acsmacrolett.8b00370>.
- (78) Brutman, J. P.; Delgado, P. A.; Hillmyer, M. A. Polylactide Vitrimers. *ACS Macro Lett.* **2014**, *3* (7), 607–610. <https://doi.org/10.1021/mz500269w>.
- (79) Eldred, S. E.; Stone, D. A.; Gellman, S. H.; Stahl, S. S. Catalytic Transamidation under Moderate Conditions. *J. Am. Chem. Soc.* **2003**, *125* (12), 3422–3423. <https://doi.org/10.1021/ja028242h>.
- (80) Denissen, W.; Rivero, G.; Nicolaÿ, R.; Leibler, L.; Winne, J. M.; Prez, F. E. D. Vinylogous Urethane Vitrimers. *Adv. Funct. Mater.* **2015**, *25* (16), 2451–2457. <https://doi.org/10.1002/adfm.201404553>.
- (81) Denissen, W.; Droesbeke, M.; Nicolaÿ, R.; Leibler, L.; Winne, J. M.; Du Prez, F. E. Chemical Control of the Viscoelastic Properties of Vinylogous Urethane Vitrimers. *Nat. Commun.* **2017**, *8*, 14857. <https://doi.org/10.1038/ncomms14857>.



- (82) Sprung, M. A. A Summary of the Reactions of Aldehydes with Amines. *Chem. Rev.* **1940**, *26* (3), 297–338. <https://doi.org/10.1021/cr60085a001>.
- (83) Chatterjee, S.; V. Anslyn, E.; Bandyopadhyay, A. Boronic Acid Based Dynamic Click Chemistry: Recent Advances and Emergent Applications. *Chem. Sci.* **2021**, *12* (5), 1585–1599. <https://doi.org/10.1039/D0SC05009A>.
- (84) Qin, Y.; Cui, C.; Jäkle, F. Silylated Initiators for the Efficient Preparation of Borane-End-Functionalized Polymers via ATRP. *Macromolecules* **2007**, *40* (5), 1413–1420. <https://doi.org/10.1021/ma061704h>.
- (85) De, P.; Gondi, S. R.; Roy, D.; Sumerlin, B. S. Boronic Acid-Terminated Polymers: Synthesis by RAFT and Subsequent Supramolecular and Dynamic Covalent Self-Assembly. *Macromolecules* **2009**, *42* (15), 5614–5621. <https://doi.org/10.1021/ma900835y>.
- (86) Niu, W.; O’Sullivan, C.; Rambo, B. M.; Smith, M. D.; Lavigne, J. J. Self-Repairing Polymers: Poly(Dioxaborolane)s Containing Trigonal Planar Boron. *Chem. Commun.* **2005**, No. 34, 4342–4344. <https://doi.org/10.1039/B504634C>.
- (87) Cash, J. J.; Kubo, T.; Bapat, A. P.; Sumerlin, B. S. Room-Temperature Self-Healing Polymers Based on Dynamic-Covalent Boronic Esters. *Macromolecules* **2015**, *48* (7), 2098–2106. <https://doi.org/10.1021/acs.macromol.5b00210>.
- (88) Cromwell, O. R.; Chung, J.; Guan, Z. Malleable and Self-Healing Covalent Polymer Networks through Tunable Dynamic Boronic Ester Bonds. *J. Am. Chem. Soc.* **2015**, *137* (20), 6492–6495. <https://doi.org/10.1021/jacs.5b03551>.
- (89) Delahaye, M.; Winne, J. M.; Du Prez, F. E. Internal Catalysis in Covalent Adaptable Networks: Phthalate Monoester Transesterification As a Versatile Dynamic Cross-Linking Chemistry. *J. Am. Chem. Soc.* **2019**, *141* (38), 15277–15287. <https://doi.org/10.1021/jacs.9b07269>.
- (90) Zhang, X.; Wang, S.; Jiang, Z.; Li, Y.; Jing, X. Boronic Ester Based Vitrimers with Enhanced Stability via Internal Boron–Nitrogen Coordination. *J. Am. Chem. Soc.* **2020**, *142* (52), 21852–21860. <https://doi.org/10.1021/jacs.0c10244>.
- (91) Zhang, H.; Majumdar, S.; van Benthem, R. A. T. M.; Sijbesma, R. P.; Heuts, J. P. A. Intramolecularly Catalyzed Dynamic Polyester Networks Using Neighboring Carboxylic and Sulfonic Acid Groups. *ACS Macro Lett.* **2020**, *9* (2), 272–277. <https://doi.org/10.1021/acsmacrolett.9b01023>.
- (92) Altuna, F. I.; Hoppe, C. E.; Williams, R. J. J. Epoxy Vitrimers with a Covalently Bonded Tertiary Amine as Catalyst of the Transesterification Reaction. *Eur. Polym. J.* **2019**, *113*, 297–304. <https://doi.org/10.1016/j.eurpolymj.2019.01.045>.
- (93) Ogden, W. A.; Guan, Z. Recyclable, Strong, and Highly Malleable Thermosets Based on Boroxine Networks. *J. Am. Chem. Soc.* **2018**, *140* (20), 6217–6220. <https://doi.org/10.1021/jacs.8b03257>.
- (94) Delpierre, S.; Willocq, B.; Manini, G.; Lemaire, V.; Goole, J.; Gerbaux, P.; Cornil, J.; Dubois, P.; Raquez, J.-M. Simple Approach for a Self-Healable and Stiff Polymer Network from Iminoboronate-Based Boroxine Chemistry. *Chem. Mater.* **2019**, *31* (10), 3736–3744. <https://doi.org/10.1021/acs.chemmater.9b00750>.

- (95) Delpierre, S.; Willocq, B.; De Winter, J.; Dubois, P.; Gerbaux, P.; Raquez, J.-M. Dynamic Iminoboronate-Based Boroxine Chemistry for the Design of Ambient Humidity-Sensitive Self-Healing Polymers. *Chem. – Eur. J.* **2017**, *23* (28), 6730–6735. <https://doi.org/10.1002/chem.201700333>.
- (96) Walsh, R. Bond Dissociation Energy Values in Silicon-Containing Compounds and Some of Their Implications. *Acc. Chem. Res.* **1981**, *14* (8), 246–252. <https://doi.org/10.1021/ar00068a004>.
- (97) Napolitano, A.; Hawkins, E. G. Viscosity of a Standard Soda-Lime-Silica Glass. *J. Res. Natl. Bur. Stand. Sect. Phys. Chem.* **1964**, *68A* (5), 439–448. <https://doi.org/10.6028/jres.068A.042>.
- (98) Osthoff, R. C.; Bueche, A. M.; Grubb, W. T. Chemical Stress-Relaxation of Polydimethylsiloxane Elastomers<sup>1</sup>. *J. Am. Chem. Soc.* **1954**, *76* (18), 4659–4663. <https://doi.org/10.1021/ja01647a052>.
- (99) Zheng, P.; McCarthy, T. J. A Surprise from 1954: Siloxane Equilibration Is a Simple, Robust, and Obvious Polymer Self-Healing Mechanism. *J. Am. Chem. Soc.* **2012**, *134* (4), 2024–2027. <https://doi.org/10.1021/ja2113257>.
- (100) Nishimura, Y.; Chung, J.; Muradyan, H.; Guan, Z. Silyl Ether as a Robust and Thermally Stable Dynamic Covalent Motif for Malleable Polymer Design. *J. Am. Chem. Soc.* **2017**, *139* (42), 14881–14884. <https://doi.org/10.1021/jacs.7b08826>.
- (101) Crouch, R. D. Recent Advances in Silyl Protection of Alcohols. *Synth. Commun.* **2013**, *43* (17), 2265–2279. <https://doi.org/10.1080/00397911.2012.717241>.

## **Chapter 2: Combining Supramolecular & Dynamic Covalent Interactions for Advanced Self-Healing Polymers**

### **2.1 Introduction**

#### **2.1.1 Designs for extrinsic and intrinsic self-healing materials**

Healing behaviors in complex biological organisms require an extensive network of cells, proteins, and fuel to close fractures and regenerate lost performance. Mimicking biology's ability to heal fractures in materials is desirable for applications with poor accessibility or for long term reliability.<sup>1</sup> In lieu of being able to chemically engineer such a complex network, chemists have turned towards self-healing polymers to mimic this behavior.

Within the field of self-healing materials, two main types of healing mechanisms are used: extrinsically healing and intrinsically healing.<sup>2</sup> Extrinsic healing relies on the triggering of a latent healing component that can be activated in the event of damage. Examples of such are monomer-filled microcapsules<sup>3,4</sup> or an external stimulus such as heat<sup>5,6</sup> or light.<sup>7</sup> The main challenge with extrinsic healing is that it can generally be used only once before the latent healing components are depleted after use. Another drawback is that human intervention is needed, as well as knowledge of when and where to apply the stimulus. Alternatively, intrinsic healing has the healing functionality integrated into the polymer itself allowing for a material to automatically self-repair without the need of an external reagent or intervention. Intrinsically self-healing materials offer the ability to heal without the requirement of an external stimuli, reproducible healing with little to no decrease in efficacy,

and healing near ambient temperatures.<sup>8</sup> While intrinsically self-healing polymers offer many benefits over other approaches, noted drawbacks include a reliance on catalysts,<sup>9,10</sup> low mechanical strength,<sup>11,12</sup> and water sensitivity.<sup>13,14,15,16</sup> Here we propose a tough, intrinsically self-healing polymer network that is catalyst-free, mechanically robust, and water-stable. We achieve this by using thiourea groups to promote dynamic covalent exchange as well as supramolecular interactions.

### 2.1.2 Our design for hydrolytically stable intrinsically self-healing polymers

Urea linkages are traditionally strong connections and are known to be stable under a variety of conditions.<sup>17</sup> However, when a bulky substituent is added to a nitrogen in the urea, it can perturb the equilibrium and cause reversibility back to the isocyanate and primary amine starting material (Figure 2.1A).<sup>18</sup> By leveraging this functionality, dynamic polymer gels have been prepared from isocyanate and secondary amine monomers that constantly dissociate and re-associate at substituted urea linkages.<sup>13</sup> It was found that when the reaction was driven back to the starting materials, the isocyanate and amine would find new motifs to recombine with leading to connection changes in the gel. The size of the

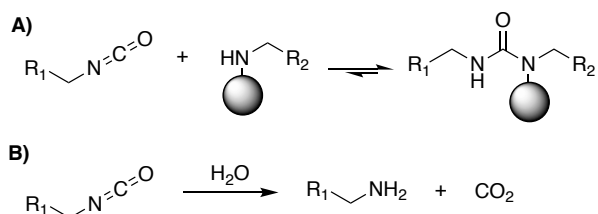


**Figure 2.1.** (A) Isocyanate reacting with a bulky amine to form a bulky urea. (B) Hydrolysis of isocyanate to amine.

sterically hindered amine was found to have a direct effect on the disruption of the urea. While conceptually interesting, a drawback of this functionality is that isocyanates react quickly with ambient moisture, causing irreversible decomposition of the structural framework (Figure 2.1B). We propose that by using the more hydrolytically stable isothiocyanate instead of isocyanate, crosslinked network will have reduced susceptibility to hydrolysis.

Complementing the benefit of hydrolytic stability, a secondary benefit of thiourea linkages is that they do not aggregate to form crystalline domains as seen in polyureas and polyurethanes.<sup>19,20</sup> Polyureas are semi-crystalline due to their bifurcated hydrogen bonding nature as shown in Figure 2.2A.<sup>21</sup> While crystalline domains are desirable for impact resistance, their stiffness limits their mobility and therefore their ability to self-heal.<sup>22</sup> Bifurcated hydrogen bonding is partly caused by the *trans-trans* planarity of the urea group, as well as it being both a strong hydrogen bond donor and acceptor. In contrast to urea linkages, it has been shown that *N,N'*-disubstituted thioureas are able to adopt both *trans-trans* and *cis-trans* conformations (Figure 2.2B).<sup>23,24</sup> The free energy of rotation around the

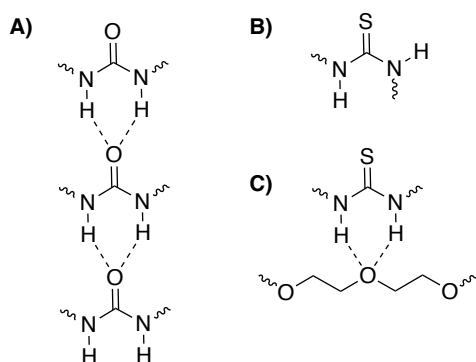


**Figure 2.2.** (A) Urea hydrogen bonding leading to crystallinity. (B) *Trans-cis* conformation of thiourea. (C) *Trans-trans* conformation of thiourea H-bonding to PEG.

N(H)-C(S) sigma bond in 1,1-dimethyl-3-phenylthiourea was found to be 10.7–11.5 kcal/mol at -40 °C, which is significantly lower than that of an oxygen analogue, 14.3-15.8 kcal/mol.<sup>25</sup> This can be attributed to reduced  $Sp_{\pi}-Cp_{\pi}$  orbital overlap in relation to  $Op_{\pi}-Cp_{\pi}$ , thereby reducing bond order of the C–N bond. Decreasing C–N bond order leads to an easier rotation of substituents, and therefore a decrease in self-specific hydrogen bonding.

Previous work has investigated the supramolecular effects of combining thiourea and ether linkages as H-bond donors/acceptors in polymers (Figure 2.2C).<sup>26</sup> They observed robust supramolecular self-healing behavior, as the *cis-trans* conformation allowed the thiourea to ‘walk’ down the polymer chain to dissipate energy and increase toughness. For self-healing, they relied on diffusion of short polymers chains across the interface of the cut. The main drawback of this system was extensive creep caused by low  $M_w$  polymers, which was corroborated by a decrease in self-healing behavior at higher molecular weights.

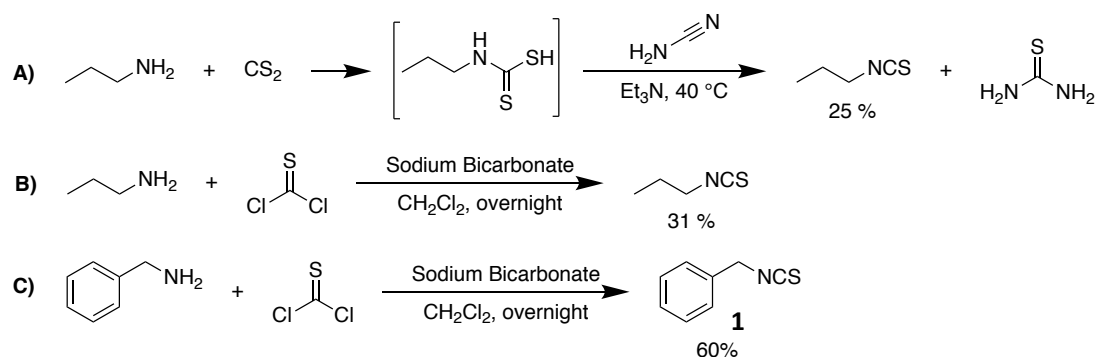
We envision that by combining supramolecular interactions with dynamic covalent linkages, we can increase molecular weight to target robust self-healing polymers. The goal of this work is to use bulky thioureas to: *i*) impart hydrolytically stable dynamic covalent linkages, *ii*) reduce crystallinity to limit stiffness, *iii*) act as hydrogen bond donors to the ether backbone to facilitate supramolecular self-healing. These goals will be achieved by studying the effects of sterics on bulky thiourea formation, studying the extent of polymerization, and finally by optimizing bulk polymer samples for self-healing.

## 2.2 Results and Discussion

### 2.2.1 Small molecule synthesis

Optimization of isothiocyanate-amine association and dissociation kinetic rates is paramount to the formation of tough, intrinsically self-healing polymers. First, the kinetic rate constants,  $k_1$  and  $k_{-1}$ , must be fast to afford quick interplay between reactive species. Secondly, to form high molecular weight polymers the equilibrium constant ( $K_{eq} = k_1/k_{-1}$ ) must be large. Model studies were used to analyze the effect of bulky substituents on the  $K_{eq}$  of thiourea formation. Model reactions between a monofunctional isothiocyanate and a monofunctional secondary amine were carried out to mimic the behavior of the difunctional monomers to be used in bulk polymerization.

**Scheme 2.1.** Small molecule synthesis for model bulky thiourea study.



Synthesis of the model isothiocyanate (Scheme 2.1A) was adopted from the procedure by Yamamoto et. al.<sup>27</sup> As seen in Scheme 2.1A, *n*-propylamine was converted to the corresponding *n*-propyl isothiocyanate via addition of CS<sub>2</sub> and cyanamide. Initial yields were very low, as the low pressure required for drying also caused the *n*-propyl isothiocyanate to evaporate. In Scheme 2.1B, a secondary method of *n*-propyl isothiocyanate

preparation was used, which resulted in a slightly higher yield.<sup>28</sup> To combat product volatility, benzyl amine was substituted in place of propylamine (Scheme 2.1C). Benzyl isothiocyanate (**1**) was generated at 60% yield at >10-gram scale, which is in good agreement with literature values.<sup>27</sup>

Three representative bulky amines were chosen for the model reaction due to their small size, easily identifiable peaks in <sup>1</sup>H and <sup>13</sup>C NMR, and commercial availability of their monomer analogues. The amines used were: *tert*-butylethylamine (**2**), diisopropylamine (**3**), and diethylamine (**4**). A fourth amine (2,2,6,6-tetramethylpiperidine) was used, but it was found that no observable reaction occurred when added to **1**. This is attributed to its high steric hindrance.

#### Model thiourea $K_{eq}$ results

To form high molecular weight polymers, high degrees of monomer conversion are necessary. As a result, the equilibrium constant was studied via <sup>1</sup>H-NMR for three different sterically hindered amines in a model reaction, as shown in Figure 2.3. The addition of **1** and **2** (Scheme 2.2A) yielded  $K_{eq,2} = 4.81 \text{ M}^{-1}$ , however the reactions between **1** and **3** ( $K_{eq,3}$ ), and **1** and **4** ( $K_{eq,4}$ ) proceeded too far to accurately measure via <sup>1</sup>H-NMR. An indirect method of

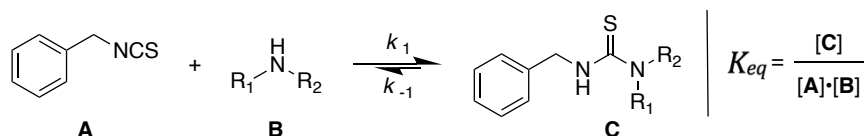


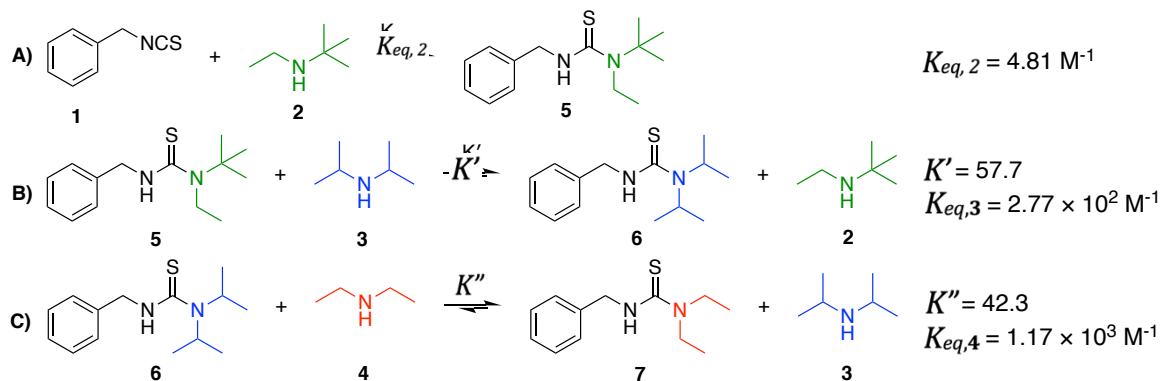
**Figure 2.3.** General reaction for the addition reaction between benzyl isothiocyanate, **A**, and a 2° amine, **B**, to form a bulky thiourea. The equilibrium constant,  $K_{eq} = [C]/[A] \cdot [B]$ .



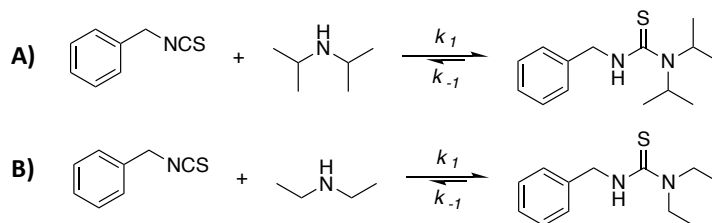
determining  $K_{eq,3}$  and  $K_{eq,4}$  was used through use of an intermediate exchange reaction (Scheme 2.2B,C). Since the addition of **1** and **2** is accurately measurable via  $^1\text{H-NMR}$ ,  $K_{eq,2}$  was used to determine  $K_{eq,3}$  using the equation  $K_{eq,3} = K' \cdot K_{eq,2}$ , where  $K'$  is the equilibrium constant for the reaction in Scheme 2.2B. Once  $K_{eq,3}$  was determined, the same indirect procedure was used to determine the equilibrium constant  $K_{eq,4}$ . Model reaction results show that the  $K_{eq}$  of isopropyl and ethyl substituents ( $K_{eq,3} = 2.77 \times 10^2 \text{ M}^{-1}$  and  $K_{eq,4} = 1.17 \times 10^3 \text{ M}^{-1}$ , respectively) on the thiourea will allow for polymer formation, while *tert*-butyl ( $K_{eq,2} = 4.81 \text{ M}^{-1}$ ) will only form oligomers.

After equilibrium constants had been determined, the reverse rate constant,  $k_{-1}$ , was found. Larger  $k_{-1}$  values afford quick interplay between the thiourea and its reactive precursors, which should be favorable for dynamic exchange. To elucidate  $k_{-1}$  for the decomposition of the bulky thiourea, the reverse reaction was studied (Figure S22, S23). Using the reactivity information gathered from isothiocyanate-isocyanate competitive studies (Table S2), benzyl isocyanate (5x mol. excess) was used as a kinetic trapping agent

**Scheme 2.2.** The indirect method for determining  $K_{eq}$  values for the addition of **1** and **2** ( $K_{eq,2}$ ), **1** and **3** ( $K_{eq,3}$ ), and **1** and **4** ( $K_{eq,4}$ ).



**Scheme 2.3.** Determination of rate constants for the synthesis of sterically hindered model compounds.



to capture free amine upon dissociation of the bulky thiourea bond. The rate constant,  $k_{-1}$  for the reaction in Scheme 2.3A was determined to be  $7.0 \times 10^{-6} \text{ h}^{-1}$ , while reaction in Scheme 2.3B was determined to be  $6.0 \times 10^{-6} \text{ h}^{-1}$ .

After measuring the kinetics for bulky thiourea formation and dissociation, we then turned to analyzing the effect of temperature on dynamic exchange. Conversion dependence on temperature was measured by purifying **6** and varying its temperature in DMSO- $d_6$  at 22 °C, 30 °C, 40 °C, and 50 °C until equilibrium was reached. At elevated temperatures, the

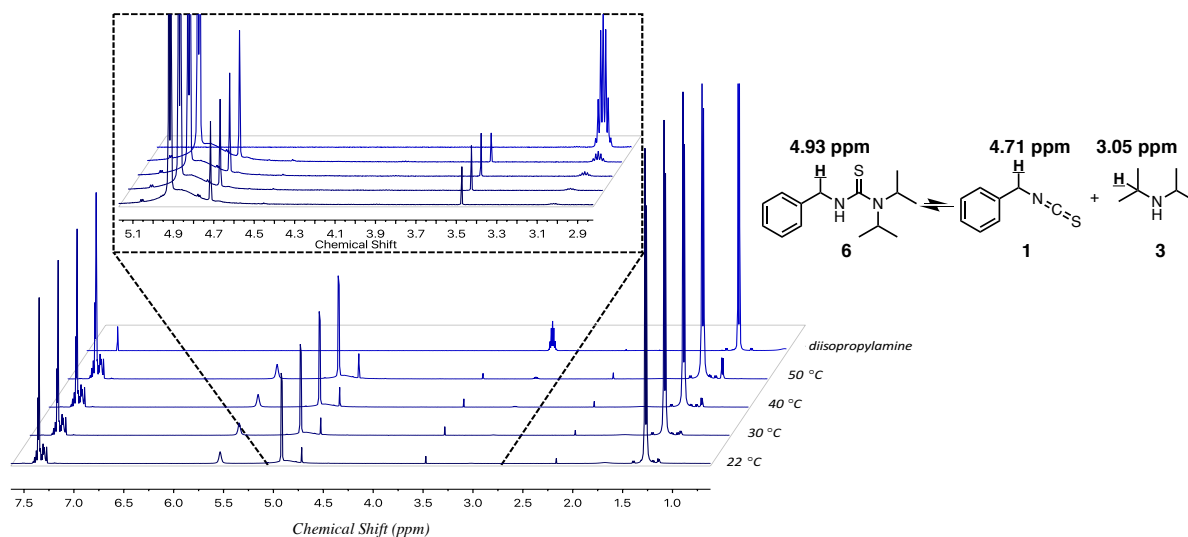


**Figure 2.4.**  $^1\text{H}$  NMR spectra of **6** upon heating. From bottom to top: 22 °C, 30 °C, 40 °C, 50 °C, and neat diisopropylamine. Note the **3** methine peak at 3.05 ppm growing at elevated temperatures.

diisopropylamine methine peak (3.05 ppm) in Figure 2.4 can be observed gaining intensity as the equilibrium begins to favor the reactants. This is consistent with our hypothesis that elevated temperatures may be beneficial in reprocessing the samples due to dynamic shortening of the polymer chain length.

## 2.2.2 Synthesis and characterization of polymers

### *Polymerizations and supramolecular H-bonding incorporation*

After concluding small molecule studies, effort was put forth to incorporate bulky thiourea groups into polymers. To examine the extent of polymerization and the effect of temperature on the dynamic networks, *m*-xylylenediisothiocyanate (**8**) was synthesized and used for AA-BB step-growth polymerizations with three separate bulky di-amines: diethylethylenediamine (**9**), diisopropylethylenediamine (**10**), and di-*tert*-butylethylenediamine (**11**) (Figure 2.5). After allowing the reaction to proceed for 24 hours at room temperature, the samples were then heated at 50 °C for 8 hours to observe if changes in molecular weight would occur. Polymerization 6C did not proceed past oligomers, which

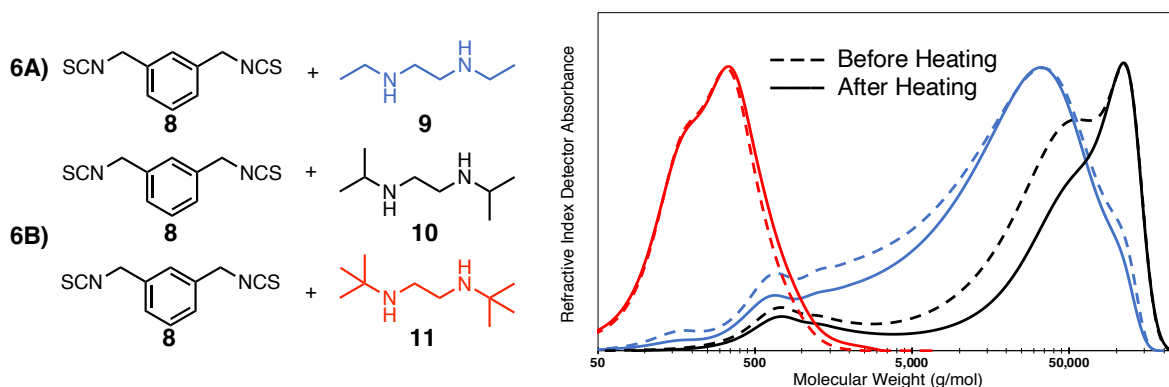
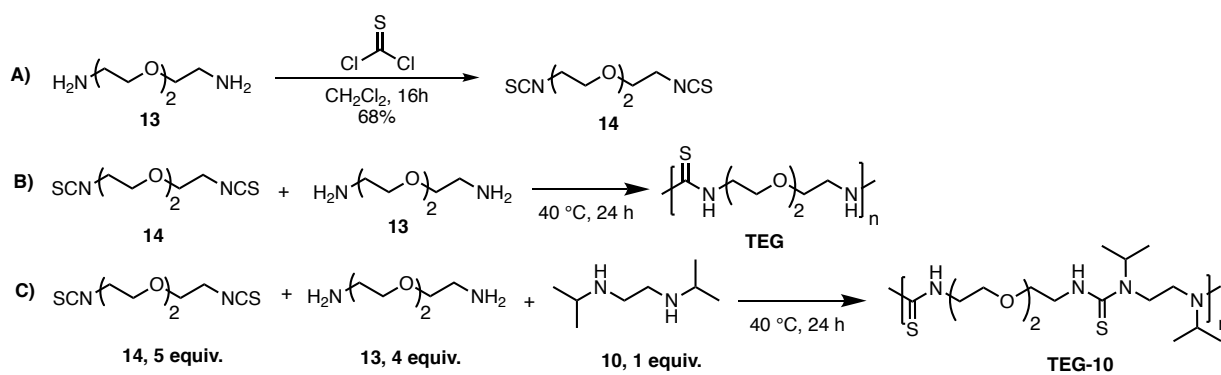


**Figure 2.5.** GPC chromatogram for polymerization 6A, 6B, and 6C. Polymerizations proceeded at room temperature for 24 hours, followed by heating at 50 °C for 8 hours.

is in line with the results of our small molecule studies. Both polymerizations 6A and 6B afforded high molecular weight polymers ( $M_n = 1.53 \times 10^4$  g/mol (PDI = 2.55) and  $M_n = 4.06 \times 10^4$  g/mol (PDI = 1.73), respectively) and showed changes in polydispersity after heating with an observed trend toward a Gaussian distribution ( $M_n = 1.63 \times 10^4$  g/mol (PDI = 2.35) and  $M_n = 5.21 \times 10^4$  g/mol (PDI = 1.53), respectively). This evidence corroborates our hypothesis of polymer reorganization at elevated temperatures due to the dynamic bulky thioureas.

With evidence that bulky thiourea polymers exhibit dynamic characteristics in bulk, attention was turned to constructing supramolecular interactions between polymers. A preliminary test using a three-component system with varying ratios of **8**, **10**, and 4,7,10-trioxa-1,13-tridecanediamine was used to examine the effect hydrogen-bond acceptors in supramolecular interactions between thiourea and ether groups (Figure S28). When comparing the tensile properties of the three formulations, an optimal ratio of 10 mol% bulky amine was found. As the amount of bulky amine increased, mechanical properties diminished. We propose that as more dynamic backbones are added, the mechanical

**Scheme 2.4.** Synthesis of monomer **14** and the synthesis of polymers **TEG** and **TEG-10**.



properties suffer due to shorter effective polymer lengths as well as a decrease in the fraction of available hydrogen bond acceptors.

To simplify the system, two new monomers (**13** and **14**, Scheme 2.4) were used to replace **10** and **12** to make the well-defined repeating polymers: thiourea ethylene glycol (TEG) and thiourea ethylene glycol with 10% bulky amine (TEG-10). For the polymerization of B and C in Scheme 2.4, the monomers were mixed in a PTFE mold and heated at 40 °C for 24 hours. Samples were then purified through precipitation and dried at 120 °C for three hours.

#### *Self-healing experiments*

TEG and TEG-10 were investigated for their self-healing abilities. Many processing parameters (drying time, maximum heat, cooling rate, molding pressure, dwell time, and annealing time) for the processing of samples were studied. Optimized pristine TEG and TEG-10 samples were melt pressed at 80 °C through manual compression in a vice-clamp and allowed to cool naturally in the compressed mold for 8 hours. Following reported protocols,<sup>29</sup> samples were cut 90% of the way through and pressed back together to facilitate self-healing. Optimal self-healing conditions were found when the samples were gently pressed together for 1 minute followed by heating at 50 °C for 20 minutes. The samples were then gently compressed for 14 hours at room temperature in an air-free environment. Figure 2.6 shows the comparison between pristine and healed TEG and TEG-10 samples. Both TEG and TEG-10 showed very good self-healing with approximately 70% strain recovery. It is also of note that similar ultimate strengths were achieved before and after healing between

TEG and TEG-10, indicating that sufficient healing occurred to allow large amounts of stress to be exerted without material failure.

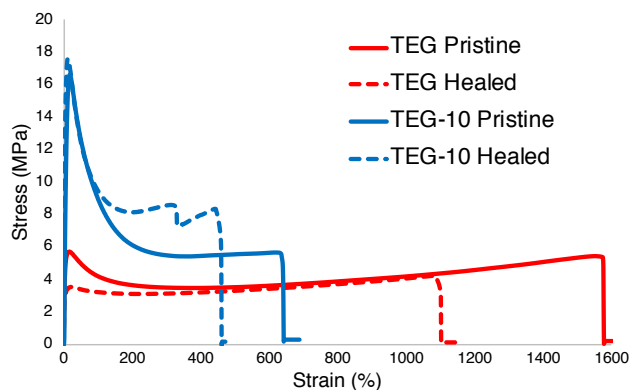


**Figure 2.6.** Comparison between pristine and healed samples. Samples were tested at room temperature under a strain rate of 100 mm/min.

### 2.3 Conclusion and Future Work

In summary, we have demonstrated that using dynamic covalent motifs and supramolecular interactions in the formation of self-healing polymers allows for a robust, catalyst-free, and hydrolysis-resistant network. By examining the equilibrium constant of the reaction between isothiocyanate and secondary amines, isopropyl and ethyl motifs were found to be optimal for generating sufficiently long polymers while retaining dynamic behavior. Thiourea formation was found to be reversible at elevated temperatures, which was required to facilitate self-healing. Polymerizations between diisothiocyanates and bulky diamines showed dynamic exchange properties when heated, and self-healing profiles were evaluated under different healing conditions. It was found that gentle pressure and short-term elevated temperatures yielded polymer networks with 70% strain recovery. We anticipate that the bulky thiourea functionality will be employed in future self-healing systems due to its catalyst free and hydrolysis-resistant nature.

Future directions for this work should focus on polymers generated from monomers containing ether linkages in the backbone, such as TEG and TEG-10. Those polymers exhibited higher degrees of toughness and elongation than similarly prepared aliphatic polymers, indicating that good H-bonding acceptor sites in the backbone are critical to the mechanical behavior of the material. Furthermore, additional polymer processing would be beneficial for the preparation of more uniform high-molecular weight polymers. It was observed that the addition of amine to isothiocyanate was a rapid reaction, and it is likely that cyclic oligomers are generated which do not contribute to improved mechanical behavior. By annealing at sufficiently high temperatures, I predict that the molecular weight distribution will shift from multimodal to monomodal due to the dissociation/association of the thiourea groups along the backbone. Both the self-healing behavior and mechanical properties would greatly benefit from a monomodal molecular weight distribution. Along with a new annealing process, varying the ether linkages along the backbone would help to optimize the physical properties of the self-healing networks. Screening monomers containing two, three, and four ether linkages per monomer would affect the self-healing behavior due to changes in supramolecular interactions. Also, modifying the ether linkage content has the effect of modifying the glass transition which greatly influences the physical behavior. Finally, testing the hydrolytic stability of these polymers is critical to demonstrate the overall premise of this project.

## 2.4 References

- (1) Hager, M. D.; Greil, P.; Leyens, C.; van der Zwaag, S.; Schubert, U. S. Self-Healing Materials. *Adv. Mater.* **2010**, *22* (47), 5424–5430. <https://doi.org/10.1002/adma.201003036>.
- (2) Wu, D. Y.; Meure, S.; Solomon, D. Self-Healing Polymeric Materials: A Review of Recent Developments. *Progress in Polymer Science* **2008**, *33* (5), 479–522. <https://doi.org/10.1016/j.progpolymsci.2008.02.001>.
- (3) White, S. R.; Sottos, N. R.; Geubelle, P. H.; Moore, J. S.; Kessler, M. R.; Srilram, S. R.; Brown, E. N.; Viswanathan, S. Autonomic Healing of Polymer Composites. *Nature* **2001**, *409* (6822), 794–797. <https://doi.org/10.1038/35057232>.
- (4) Pang, J. W. C.; Bond, I. P. A Hollow Fibre Reinforced Polymer Composite Encompassing Self-Healing and Enhanced Damage Visibility. *Composites Science and Technology* **2005**, *65* (11), 1791–1799. <https://doi.org/10.1016/j.compscitech.2005.03.008>.
- (5) Ghosh, B.; Urban, M. W. Self-Repairing Oxetane-Substituted Chitosan Polyurethane Networks. *Science* **2009**, *323* (5920), 1458–1460. <https://doi.org/10.1126/science.1167391>.
- (6) Zhang, P.; Li, G. Healing-on-Demand Composites Based on Polymer Artificial Muscle. *Polymer* **2015**, *64*, 29–38. <https://doi.org/10.1016/j.polymer.2015.03.022>.
- (7) Ji, S.; Cao, W.; Yu, Y.; Xu, H. Visible-Light-Induced Self-Healing Diselenide-Containing Polyurethane Elastomer. *Adv. Mater.* **2015**, *27* (47), 7740–7745. <https://doi.org/10.1002/adma.201503661>.
- (8) Cordier, P.; Tournilhac, F.; Soulié-Ziakovic, C.; Leibler, L. Self-Healing and Thermoreversible Rubber from Supramolecular Assembly. *Nature* **2008**, *451* (7181), 977–980. <https://doi.org/10.1038/nature06669>.
- (9) Cho, S. H.; Andersson, H. M.; White, S. R.; Sottos, N. R.; Braun, P. V. Polydimethylsiloxane-Based Self-Healing Materials. *Adv. Mater.* **2006**, *18* (8), 997–1000. <https://doi.org/10.1002/adma.200501814>.
- (10) Yoon, J. A.; Kamada, J.; Koynov, K.; Mohin, J.; Nicolaÿ, R.; Zhang, Y.; Balazs, A. C.; Kowalewski, T.; Matyjaszewski, K. Self-Healing Polymer Films Based on Thiol–Disulfide Exchange Reactions and Self-Healing Kinetics Measured Using Atomic Force Microscopy. *Macromolecules* **2012**, *45* (1), 142–149. <https://doi.org/10.1021/ma2015134>.
- (11) Zheng, P.; McCarthy, T. J. A Surprise from 1954: Siloxane Equilibration Is a Simple, Robust, and Obvious Polymer Self-Healing Mechanism. *J. Am. Chem. Soc.* **2012**, *134* (4), 2024–2027. <https://doi.org/10.1021/ja2113257>.
- (12) Chung, C.-M.; Roh, Y.-S.; Cho, S.-Y.; Kim, J.-G. Crack Healing in Polymeric Materials via Photochemical [2+2] Cycloaddition. *Chem. Mater.* **2004**, *16* (21), 3982–3984. <https://doi.org/10.1021/cm049394+>.



- (13) Ying, H.; Zhang, Y.; Cheng, J. Dynamic Urea Bond for the Design of Reversible and Self-Healing Polymers. *Nature Communications* **2014**, *5* (3218), 1–9. <https://doi.org/10.1038/ncomms4218>.
- (14) Ying, H.; Cheng, J. Hydrolyzable Polyureas Bearing Hindered Urea Bonds. *J. Am. Chem. Soc.* **2014**, *136* (49), 16974–16977. <https://doi.org/10.1021/ja5093437>.
- (15) Zhang, Y.; Ying, H.; Hart, K. R.; Wu, Y.; Hsu, A. J.; Coppola, A. M.; Kim, T. A.; Yang, K.; Sottos, N. R.; White, S. R.; Cheng, J. Malleable and Recyclable Poly(Urea-Urethane) Thermosets Bearing Hindered Urea Bonds. *Adv. Mater.* **2016**, *28* (35), 7646–7651. <https://doi.org/10.1002/adma.201601242>.
- (16) Zechel, S.; Geitner, R.; Abend, M.; Siegmann, M.; Enke, M.; Kuhl, N.; Klein, M.; Vitz, J.; Gräfe, S.; Dietzek, B.; Schmitt, M.; Popp, J.; Schubert, U. S.; Hager, M. D. Intrinsic Self-Healing Polymers with a High *E*-Modulus Based on Dynamic Reversible Urea Bonds. *NPG Asia Materials* **2017**, *9* (420), 1–8. <https://doi.org/10.1038/am.2017.125>.
- (17) Delebecq, E.; Pascault, J.-P.; Boutevin, B.; Ganachaud, F. On the Versatility of Urethane/Urea Bonds: Reversibility, Blocked Isocyanate, and Non-Isocyanate Polyurethane. *Chem. Rev.* **2013**, *113* (1), 80–118. <https://doi.org/10.1021/cr300195n>.
- (18) Hutchby, M.; Houlden, C. E.; Haddow, M. F.; Tyler, S. N. G.; Lloyd-Jones, G. C.; Booker-Milburn, K. I. Switching Pathways: Room-Temperature Neutral Solvolysis and Substitution of Amides. *Angewandte Chemie International Edition* **2012**, *51* (2), 548–551. <https://doi.org/10.1002/anie.201107117>.
- (19) Coleman, M. M.; Sobkowiak, M.; Pehlert, G. J.; Painter, P. C.; Iqbal, T. Infrared Temperature Studies of a Simple Polyurea. *Macromol. Chem. Phys.* **1997**, *198* (1), 117–136. <https://doi.org/10.1002/macp.1997.021980110>.
- (20) Yi, J.; Boyce, M. C.; Lee, G. F.; Balizer, E. Large Deformation Rate-Dependent Stress–Strain Behavior of Polyurea and Polyurethanes. *Polymer* **2006**, *47* (1), 319–329. <https://doi.org/10.1016/j.polymer.2005.10.107>.
- (21) Jiang, S.; Shi, R.; Cheng, H.; Zhang, C.; Zhao, F. Synthesis of Polyurea from 1,6-Hexanediamine with CO<sub>2</sub> through a Two-Step Polymerization. *Green Energy & Environment* **2017**, *2* (4), 370–376. <https://doi.org/10.1016/j.gee.2017.05.001>.
- (22) Qian, B.; Todd, D. B.; Gogos, C. G. Plastic Energy Dissipation and Its Role on Heating/Melting of Single-Component Polymers and Multi-Component Polymer Blends. *Advances in Polymer Technology* **2003**, *22* (2), 85–95. <https://doi.org/10.1002/adv.10039>.
- (23) Qian, X.; Liu, F. Promoting Effects of the Hydroxymethyl Group on the Fluorescent Signaling Recognition of Anions by Thioureas. *Tetrahedron Letters* **2003**, *44* (4), 795–799. [https://doi.org/10.1016/S0040-4039\(02\)02671-0](https://doi.org/10.1016/S0040-4039(02)02671-0).
- (24) Liu, W.-X.; Jiang, Y.-B. Intramolecular Hydrogen Bonding and Anion Binding of *N*-Benzamido-*N'*-Benzoylthioureas. *J. Org. Chem.* **2008**, *73* (3), 1124–1127. <https://doi.org/10.1021/jo702159r>.

- (25) Stewart, W. Esley.; Siddall, T. H. Nuclear Magnetic Resonance Studies of Amides. *Chem. Rev.* **1970**, *70* (5), 517–551. <https://doi.org/10.1021/cr60267a001>.
- (26) Yanagisawa, Y.; Nan, Y.; Okuro, K.; Aida, T. Mechanically Robust, Readily Repairable Polymers via Tailored Noncovalent Cross-Linking. *Science* **2018**, *359* (6371), 72–76. <https://doi.org/10.1126/science.aam7588>.
- (27) Yamamoto, T.; Sugiyama, S.; Akimoto, K.; Hayashi, K. One-Pot Synthesis of Isothiocyanates from Primary Amines Synthesis Using Cyanamide? *Organic Preparations and Procedures International* **1992**, *24* (3), 346–349. <https://doi.org/10.1080/00304949209355899>.
- (28) Sureshbabu, V. V.; Naik, S. A.; Hemantha, H. P.; Narendra, N.; Das, U.; Guru Row, T. N. N-Urethane-Protected Amino Alkyl Isothiocyanates: Synthesis, Isolation, Characterization, and Application to the Synthesis of Thioureidopeptides. *J. Org. Chem.* **2009**, *74* (15), 5260–5266. <https://doi.org/10.1021/jo900675s>.
- (29) Mozhdehi, D.; Ayala, S.; Cromwell, O. R.; Guan, Z. Self-Healing Multiphase Polymers via Dynamic Metal–Ligand Interactions. *J. Am. Chem. Soc.* **2014**, *136* (46), 16128–16131. <https://doi.org/10.1021/ja5097094>.

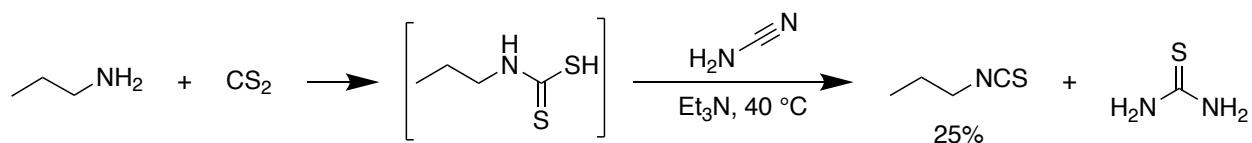
## 2.5 Supporting Information

### General Experimental information

Unless otherwise noted, reactions were carried out with a magnetic stir bar under a nitrogen atmosphere. Commercial reagents were used as received with no further purification, unless otherwise noted. *N,N'*-Di-*tert*-butylethylenediamine (DtBuEDA), *N,N'*-Dimethylethylene-diamine (DMEDA), and *N,N'*-Diethylethylenediamine (DEEDA) were purified via vacuum distillation and stored under activated 3Å molecular sieves. Flash column chromatography was performed by forced flow of indicated solvent using automated silica columns (CombiFlash, Teledyne Isco). <sup>1</sup>H NMR spectra were recorded at 500 MHz on a Bruker DRX500 spectrometer using a TCI three channel inverse cryoprobe. <sup>13</sup>C NMR spectra were recorded at 125.2 MHz on a Bruker AVANCE600 spectrometer using a BBFO cryoprobe. NMR spectra peaks are reported as δ values in ppm relative to TMS or residual solvent: CDCl<sub>3</sub>-t (7.26 ppm; 77.0 ppm), d<sub>6</sub>-DMSO-t (2.50 ppm, 39.5 ppm). <sup>1</sup>H NMR data are reported as follows: chemical shift in ppm, multiplicity (s = singlet, d = doublet, t = triplet), coupling constants in Hz, and relative integration of the number of protons. Multiplets (m) are reported over the range of chemical shift at which they appear. For <sup>13</sup>C NMR, only chemical shift values are reported. Tensile tests were performed on an Instron 3365 tensometer. Stress/strain experiments were performed at room temperature with a strain rate of 100 mm/min unless otherwise noted. The average samples size was 25 mm x 20 mm x 1 mm. DSC thermograms were evaluated using a TA Instruments Q700, while TGA thermograms were evaluated using a TA Instruments Q500. Gel Permeation Chromatography (GPC) measurements were taken with an Agilent 1100 series GPC with an Agilent PLgel Mixed-C

column. The solvent was 0.2  $\mu\text{m}$  filtered dimethylformamide (DMF) containing 0.1% LiBr that had been warmed to 40  $^{\circ}\text{C}$ . All molecular weights were referenced to polymethyl methacrylate standards and detected with a refractive index detector.

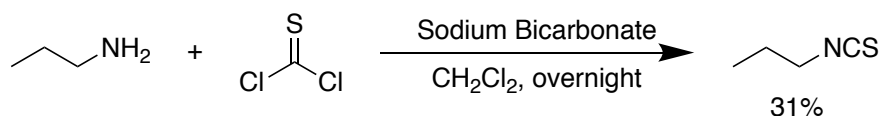
### Supplementary Scheme S1



#### *Synthesis of propylisothiocyanate.*

A stir bar and 20 mL of anhydrous THF were added to a capped round bottom flask and capped with a rubber septum. Propylamine (1.00 equiv., 6.00 mmol, 354 mg) was added, and the temperature was reduced to 0  $^{\circ}\text{C}$ . Carbon disulfide (1.30 equiv., 7.80 mmol, 735  $\mu\text{L}$ ) was added dropwise via syringe. The reaction was allowed to stir for 3 hours at 0  $^{\circ}\text{C}$ . Cyanamide (1.30 equiv., 7.80 mmol, 328 mg) was dissolved in 10 mL of THF and then added to the round bottom flask, followed by two drops of triethylamine. The temperature was raised to 40  $^{\circ}\text{C}$  and was stirred for 3 hours. Upon workup, the reaction was extracted with ether (5 x 15 mL) and the solvent was removed. The remaining oil was passed through a silica column (70% hexane : 30%  $\text{CH}_2\text{Cl}_2$ ), followed by solvent removal. The product was isolated in 25% yield (152 mg). Propylisothiocyanate was characterized via  $^1\text{H}$  NMR spectroscopy and was found to contain 8 mol% ethyl acetate.  $^1\text{H}$  NMR (499 MHz, Chloroform- $d$ )  $\delta$  4.11 3.48 (t,  $J$  = 6.6 Hz, 2H), 1.73 (dtd,  $J$  = 13.8, 7.4, 6.6 Hz, 2H), 1.02 (t,  $J$  = 7.4 Hz, 3H).

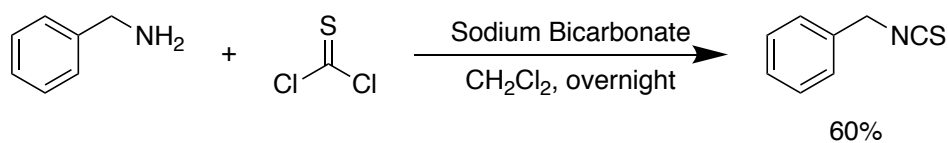
## Supplementary Scheme S2



### *Modified synthesis of propylisothiocyanate*

Into a round bottom flask 30 mL CHCl<sub>3</sub>, a stir bar, and sodium bicarbonate (4.32 equiv., 100 mmol, 8.40 g) were added and capped. Temperature was reduced to 0 °C. Propylamine (1.00 equiv., 23.0 mmol, 1.36 g) was added via syringe, followed by thiophosgene (1.08 equiv., 25.0 mmol, 1.93 mL) dropwise. After 20 minutes, the temperature was brought up to room temperature. The mixture was allowed to stir overnight. Solvent was removed to a slurry and then filtered through a zeolite plug. The filtered solution was passed through a silica column (70% hexane : 30% CH<sub>2</sub>Cl<sub>2</sub>) and had solvent removed. The resulting product was isolated in 31% yield (721 mg). <sup>1</sup>H NMR (499 MHz, Chloroform-d) δ 3.48 (t, J = 6.6 Hz, 2H), 1.73 (dtd, J = 13.8, 7.4, 6.6 Hz, 2H), 1.02 (t, J = 7.4 Hz, 3H).

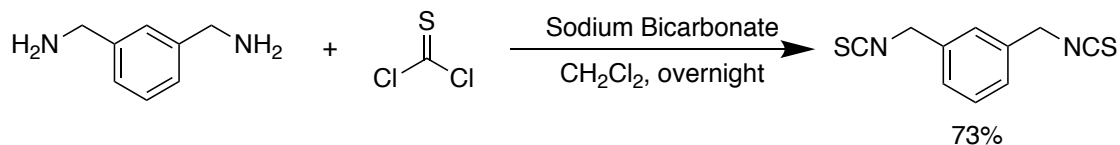
### Supplementary Scheme S3



#### *Synthesis of benzyl isothiocyanate*

Into a round bottom flask 200 mL CHCl<sub>3</sub>, benzylamine (1.00 equiv., 120 mmol, 12.9 g), and sodium bicarbonate (5.00 equiv., 600 mmol, 50.4 g) were added and capped. The temperature of the reaction was lowered to 0 °C. Thiophosgene (2.20 equiv., 264 mmol, 20.4 mL) was added dropwise. The temperature was held at 0 °C for 1 hour, and then brought up to room temperature. The reaction was allowed to stir overnight. The CHCl<sub>3</sub> was removed until a slurry and filtered through a zeolite plug. The filtered solution was passed through a silica column (70% hexane : 30% CH<sub>2</sub>Cl<sub>2</sub>) and had solvent removed. The resulting product was found in 60% yield (10.7 g). <sup>1</sup>H NMR (600 MHz, Chloroform-d) δ 7.53 – 7.35 (m, 5H), 4.79 (d, 2H). <sup>13</sup>C NMR (151 MHz, Chloroform-d) δ 134.21, 132.04, 129.05, 128.48, 126.91, 77.35 – 76.92 (t, CHCl<sub>3</sub>), 48.71.

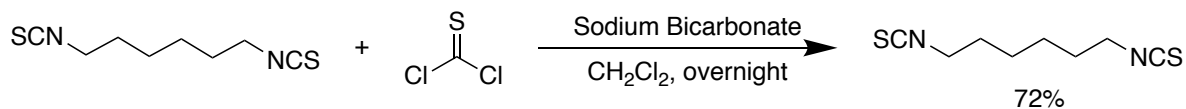
### Supplementary Scheme S4



#### *Synthesis of xylylenediisothiocyanate (XDI)*

Into a capped round bottom flask 200 mL  $\text{CHCl}_3$ , xylylenediamine (1.00 equiv., 80.0 mmol, 10.9 g), and sodium bicarbonate (5.00 equiv, 400 mmol, 33.6 g) were added. The temperature of the reaction was lowered to 0 °C. Thiophosgene (2.40 eq., 192 mmol, 22.1 g) was added dropwise. The temperature was held at 0 °C for 1 hour, and then brought up to room temperature. The reaction was allowed to stir overnight. Solvent was removed until a slurry, and then filtered through a zeolite plug. The filtered solution was passed through a silica column (95% hexane : 5%  $\text{CH}_2\text{Cl}_2$ ) and had solvent removed. XDI was found in 73% yield (12.9 g).  $^1\text{H}$  NMR (499 MHz, Chloroform-*d*)  $\delta$  7.49 (t,  $J = 7.7$  Hz, 1H), 7.37 (dd,  $J = 7.6, 1.8$  Hz, 2H), 7.32 (d,  $J = 1.6$  Hz, 1H), 4.81 (s, 4H).  $^{13}\text{C}$  NMR (151 MHz, Chloroform-*d*)  $\delta$  135.27, 133.10, 129.76, 126.88, 125.30, 78.68 – 74.87 (t), 48.50.  $m/z$  calculated for  $\text{C}_{10}\text{H}_8\text{N}_2\text{S}_2\text{Na}^+$  (M+Na) $^+$  243.0, found 243.0.  $m/z$  calculated for  $\text{C}_{10}\text{H}_8\text{N}_2\text{S}_2\text{K}^+$  (M+K) $^+$  259.0, found 259.0.

### Supplementary Scheme S5

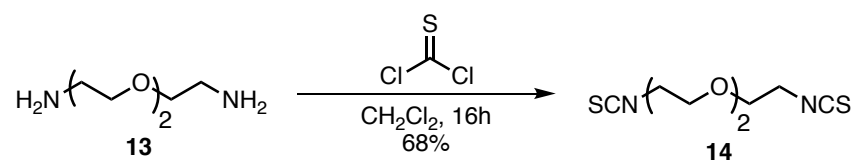


#### *Synthesis of hexamethylenediisothiocyanate (HMDI)*

Into a round bottom flask 200 mL CHCl<sub>3</sub>, 1,6-hexanediamine (1.00 equiv., 80.0 mmol, 9.30 g), and sodium bicarbonate (4.00 equiv., 360 mmol, 30.2 g) were added and capped. The temperature of the reaction was lowered to 0 °C. Thiophosgene (2.40 equiv., 192 mmol, 22.1 g) was added dropwise. The temperature was held at 0 °C for 1 hour, and then brought up to room temperature. The reaction was allowed to stir overnight. Solvent was removed and filtered through a zeolite plug. The filtered solution was passed through a silica column (95% hexane: 5% CH<sub>2</sub>Cl<sub>2</sub>) and had solvent removed. HMDI was found in 72% yield (11.5 g). <sup>1</sup>H NMR (500 MHz, Chloroform-*d*) δ 7.32 (s), 3.60 (t, *J* = 6.5 Hz, 4H), 1.79 (ddt, *J* = 10.5, 7.0, 3.4 Hz, 4H), 1.58 – 1.50 (m, 4H). <sup>13</sup>C NMR (151 MHz, Chloroform-*d*) δ 130.22, 79.81 – 74.87 (m), 44.95, 29.80, 25.94. *m/z* calculated for C<sub>8</sub>H<sub>12</sub>N<sub>2</sub>NaS<sub>2</sub><sup>+</sup> (M+Na)<sup>+</sup> 223.0, found 223.0. *m/z* calculated for C<sub>8</sub>H<sub>12</sub>N<sub>2</sub>KS<sub>2</sub><sup>+</sup> (M+K)<sup>+</sup> 239.0, found 239.0.



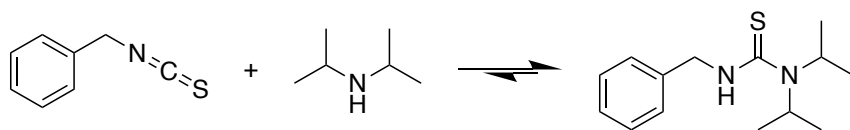
## Supplementary Scheme S6



### *Synthesis of 1,2-bis(2-isothiocyanatoethoxy)ethane*

Into a round bottom flask 200 mL  $\text{CHCl}_3$ , **12** (1.00 equiv., 50.0 mmol, 7.40 g), and sodium bicarbonate (4.50 equiv., 225 mmol, 18.9 g) were added and capped. The temperature of the reaction was lowered to 0 °C. Thiophosgene (2.20 equiv., 111 mmol, 9.91 mL) was added dropwise. The temperature was held at 0 °C for 1 hour, and then brought up to room temperature. The reaction was allowed to stir overnight. Solvent was removed, and the slurry filtered through a celite plug. The filtered solution was passed through a silica column (50% hexane : 50%  $\text{CH}_2\text{Cl}_2$ ) and had solvent removed. **14** was found in 68% yield (7.89 g).  $^1\text{H}$  NMR (500 MHz, Chloroform-d)  $\delta$  7.32 (s), 3.75 – 3.66 (m, 12H).  $m/z$  calculated for  $\text{C}_8\text{H}_{12}\text{N}_2\text{O}_2\text{NaS}_2^+$  ( $\text{M}+\text{Na}$ ) $^+$  255.0, found 255.1.

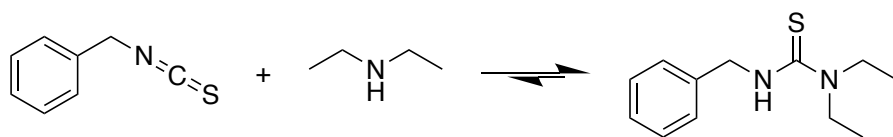
## Supplementary Scheme S7



### *Synthesis and isolation of 3-benzyl-1,1-diisopropylthiourea*

Benzyl isothiocyanate (1.00 equiv., 5.00 mmol, 746 mg) was weighed into a test tube and dissolved with 10 mL of hexanes. Diisopropylamine (2.00 equiv., 10.0 mmol, 1.01 g) was added to the test tube and mixed thoroughly. The resulting white precipitant was concentrated via centrifugation, and washed with hexanes (7 x 10 mL), centrifuging each wash. The precipitant was filtered and dried. It should be noted that due to the molecule's reversibility, low pressures for extended time periods causes volatilization of diisopropylamine and an increase in impurities.  $^1\text{H}$  NMR (500 MHz, Chloroform- $d$ )  $\delta$  7.46 – 7.33 (m, 5H), 5.58 (s, 2H), 4.98 (dd,  $J$  = 4.7, 0.9 Hz, 2H), 1.33 (dd,  $J$  = 7.0, 0.9 Hz, 12H).  $^{13}\text{C}$  NMR (151 MHz, DMSO- $d_6$ )  $\delta$  180.98, 140.73, 128.45, 127.54, 126.73, 49.08, 48.74, 40.02 (dp,  $J$  = 42.0, 21.0 Hz), 20.54.  $m/z$  calculated for  $\text{C}_{14}\text{H}_{22}\text{N}_2\text{HS}^+$  ( $\text{M}+\text{H}$ ) $^+$  251.2, found 251.1.  $m/z$  calculated for  $\text{C}_{14}\text{H}_{22}\text{N}_2\text{NaS}^+$  ( $\text{M}+\text{Na}$ ) $^+$  273.1, found 273.0.

### Supplementary Scheme S8



#### *Synthesis and isolation of 3-benzyl-1,1-diethylthiourea.*

Benzyl isothiocyanate (1.00 equiv., 5.00 mmol, 746 mg) was weighed into a test tube and dissolved with 10 mL of hexanes. Diethylamine (2.00 equiv., 10.0 mmol, 731 mg) was added to the test tube and mixed thoroughly. The resulting yellow oily precipitant was concentrated via centrifugation, and washed with hexanes (7 x 10 mL), mixing and centrifuging each wash. The precipitant was filtered and dried. It should be noted that due to the molecule's reversibility, low pressures for extended time periods causes volatilization of diethylamine and an increase in impurities. <sup>1</sup>H NMR (500 MHz, Chloroform-d) δ 7.44 – 7.37 (m, 5H), 5.53 (s, 0.75H), 4.95 (d, 2H), 3.76 – 3.72 (m, 4H), 1.36 – 1.28 (t, 6H). <sup>13</sup>C NMR (151 MHz, DMSO-*d*<sub>6</sub>) δ 180.41, 140.73, 128.48, 127.47, 126.84, 48.66, 44.84, 13.28. *m/z* calculated for C<sub>12</sub>H<sub>18</sub>N<sub>2</sub>SH<sup>+</sup> (M+H)<sup>+</sup> 223.1, found 223.1. *m/z* calculated for C<sub>12</sub>H<sub>18</sub>N<sub>2</sub>SNa<sup>+</sup> (M+Na)<sup>+</sup> 245.1, found 245.0.

### Conversion vs. temperature $^1\text{H}$ NMR study

For the extent of reaction vs. temperature  $^1\text{H}$  NMR study, benzyl isothiocyanate (1 equiv., 50.4 mg) was weighed into a vial. Diisopropylamine (1 equiv., 47.0  $\mu\text{L}$ ) was dissolved in 2 mL  $\text{CDCl}_3$  to yield a 0.168 M solution. The solution containing diisopropylamine was then transferred to the vial containing benzyl isothiocyanate. After mixing for 40 hours at 22  $^\circ\text{C}$ , 0.7 mL of the mixture was transferred to an NMR tube and characterized via  $^1\text{H}$  NMR. After characterization, the NMR tube was placed into an oil bath at 30  $^\circ\text{C}$  for 24 hours and subsequently characterized via  $^1\text{H}$  NMR. Establishing equilibrium and  $^1\text{H}$  NMR characterization was repeated at 40  $^\circ\text{C}$  and 50  $^\circ\text{C}$ . Results were plotted in Figure S9.

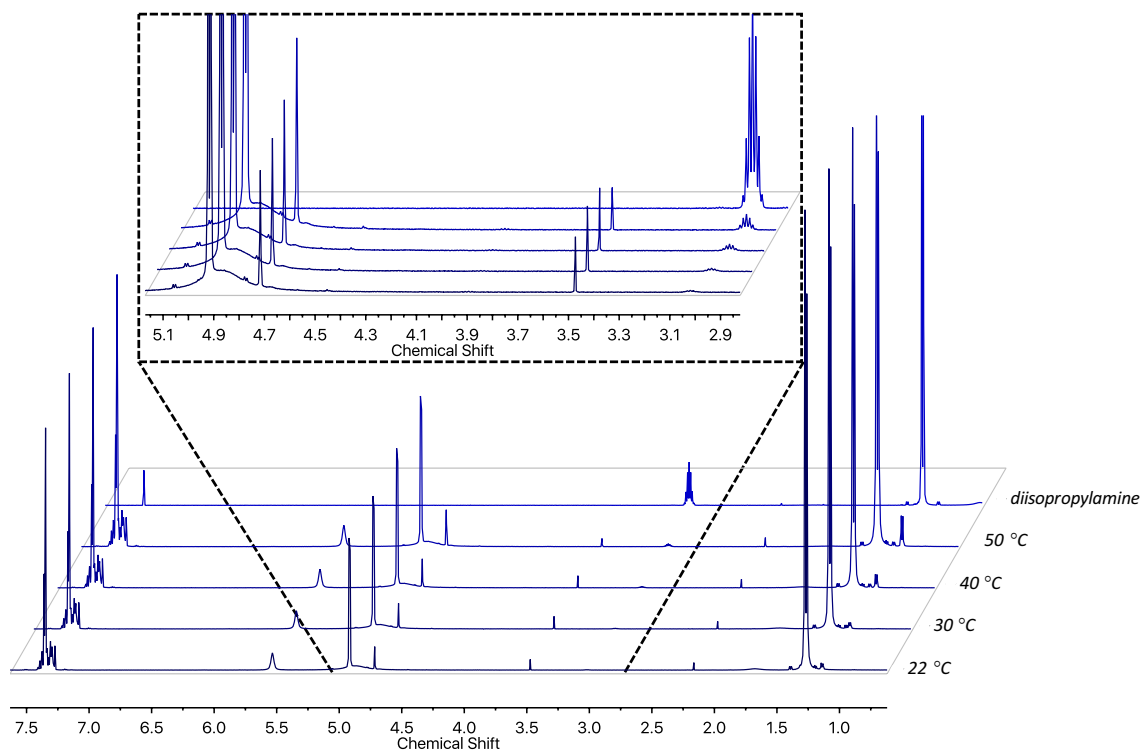


**Figure S9**  $^1\text{H}$  NMR plot showing the conversion of 1 and 2c in equilibrium with 3c. Equilibrated reaction between 1 and 2c to form a bulkythiourea conversion vs temperature

$^1\text{H}$  NMR spectra The methine peak of diisopropylamine (3.06 ppm) increases with increasing temperature.

Conversion vs. time  $^1\text{H}$  NMR study

Benzyl isothiocyanate (50.4 mg, 0.168 M) and diisopropylamine (47  $\mu\text{L}$ , 0.168 M) were dissolved into 2 mL  $\text{CDCl}_3$ . The mixture was then mixed and transferred to an NMR tube.  $^1\text{H}$  NMR spectra were taken at 45 min, 75 min, 22 hours, and 40 hours. Using the integration of **a** (Figure S10) to determine the depletion of diisopropylamine, it was found that at 45 min, 70.4% of **a** had been depleted. At 75 minutes, it was found that 74.3% of **a** had been depleted. At 22 hours, 98.1% had been depleted, and at 40 hours the peak was too small to accurately integrate.

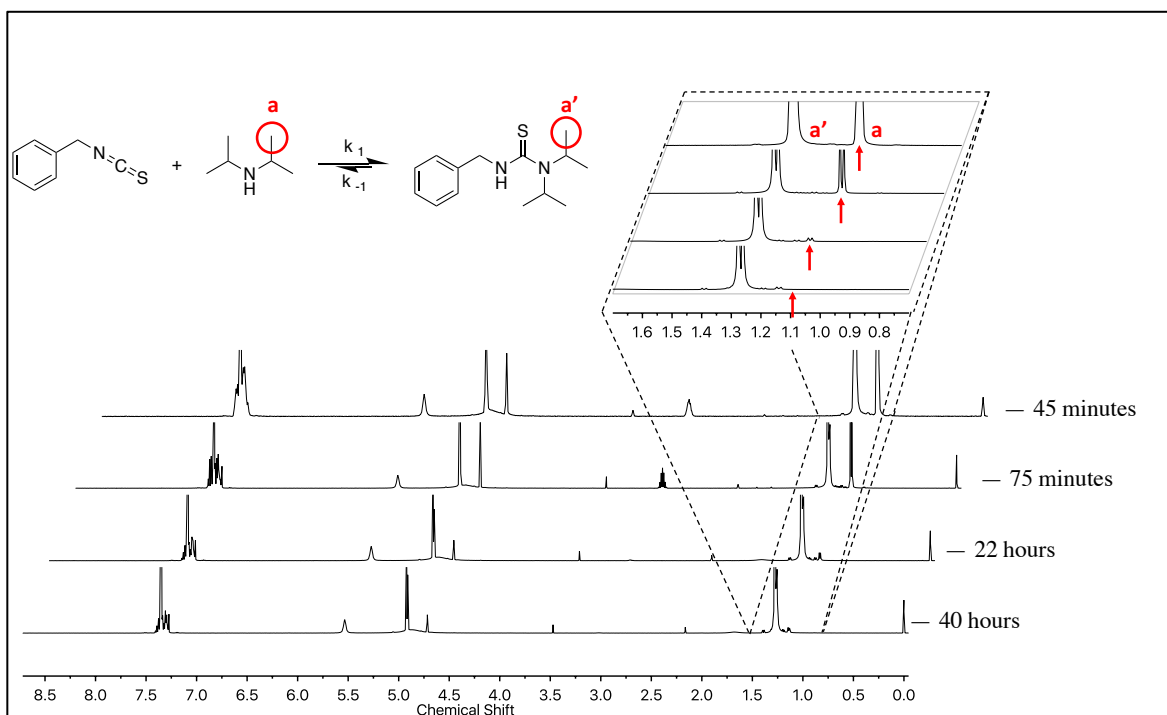
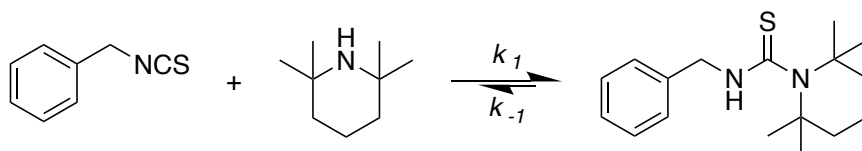


**Figure S10** Conversion vs. time  $^1\text{H}$  NMR study of benzyl isothiocyanate and diisopropylamine

### *K<sub>eq</sub>* determination

Since a large equilibrium constant is critical to forming high molecular weight polymers,  $K_{eq}$  was for each of the four hindered amines (1,1,5,5-tetramethylpiperidine, *tert*-butylethylamine, diisopropylamine, and diethylamine). To establish the accuracy of  $K_{eq}$ , three concentrations of benzyl isothiocyanate were used for each of the amines. Since equilibrium constants are independent of starting material concentration, there should be good agreement between the three measure  $K_{eq}$  values for each experiment.

### Supplementary Scheme S11



*K<sub>eq</sub>* model reaction between benzyl isothiocyanate and 1,1,5,5-tetramethylpiperidine.

Three vials containing different amounts of benzyl isothiocyanate were prepared:

Vial 1 = 0.75 equiv., 0.300 mmol, 45.1 mg.

Vial 2 = 1.00 equiv., 0.400 mmol, 59.4 mg.

Vial 3 = 1.25 equiv., 0.500 mmol, 74.8 mg.

A 2 M stock solution (25 mL) of 1,1,5,5-tetramethylpiperidine was prepared by dissolving 1,1,5,5-tetramethylpiperidine (1.00 equiv., 0.005 mol, 0.706 g) in CDCl<sub>3</sub>. Into each of the three vials, 2 mL portions of the prepared stock solution were added and mixed. The reaction was allowed to stir for three days before being characterized. After <sup>1</sup>H NMR spectra

was acquired, it was observed that no product had been formed. This is due to the large steric bulk of the amine. The three NMR spectra can be found in Figure S12.

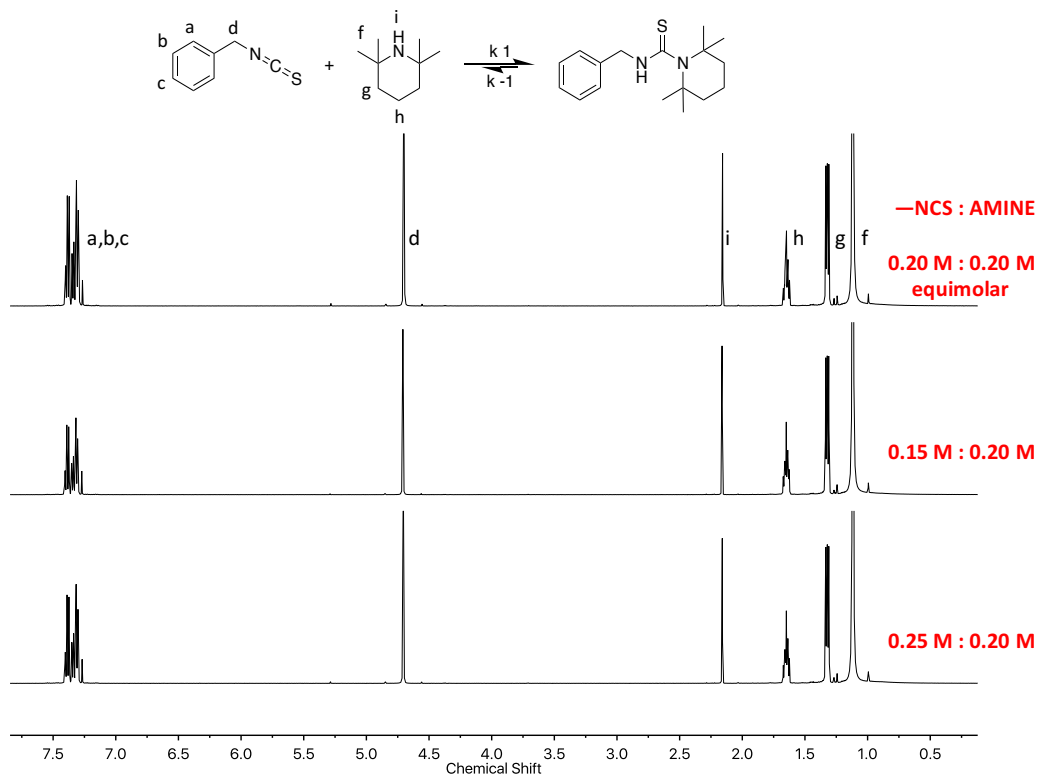
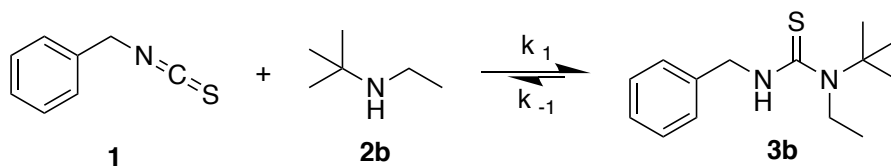


**Figure S12** Model reaction between benzyl isothiocyanate and 1,1,5,5-tetramethylpiperidine. No reaction as observed.

### Supplementary Scheme S13



$K_{eq}$  model reaction between benzyl isothiocyanate and tert-butylethylamine.

Three vials containing different amounts of benzyl isothiocyanate were prepared:

Vial 1 = 0.75 equiv., 0.300 mmol, 45.1 mg.

Vial 2 = 1.00 equiv., 0.400 mmol, 59.4 mg.

Vial 3 = 1.25 equiv., 0.500 mmol, 74.8 mg.

A 2 M stock solution (25 mL) of *tert*-butylethylamine was prepared by dissolving *tert*-butylethylamine (1.00 equiv., 0.005 mol, 0.506 g). Into each of the three vials, 2 mL portions of the prepared stock solution were added and mixed. The reaction was allowed to stir for three days before being characterized via  $^1\text{H}$  NMR. Calculated initial concentration values and  $K_{\text{eq}}$  values can be found in Table S1. Stacked NMR spectra of all three ratios can be found in Figure S14.

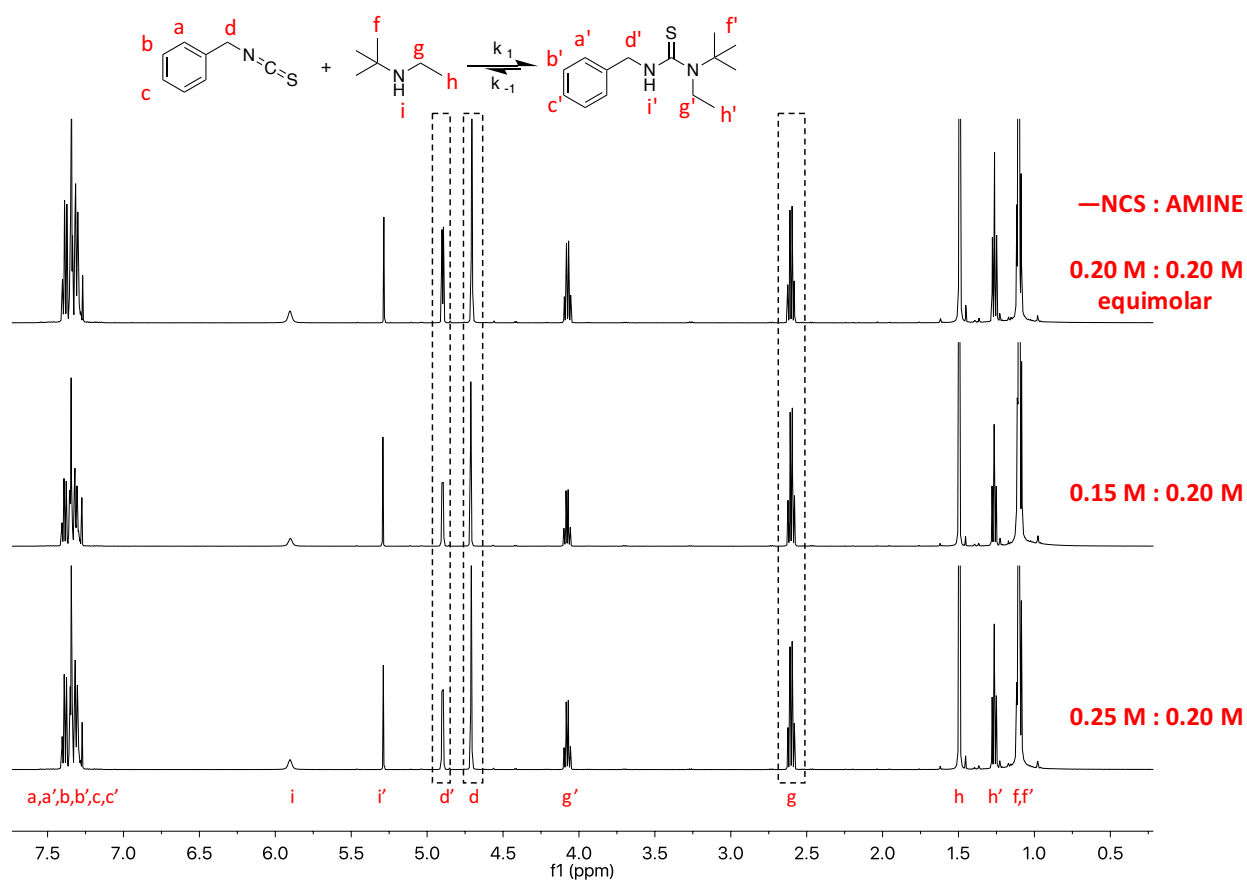
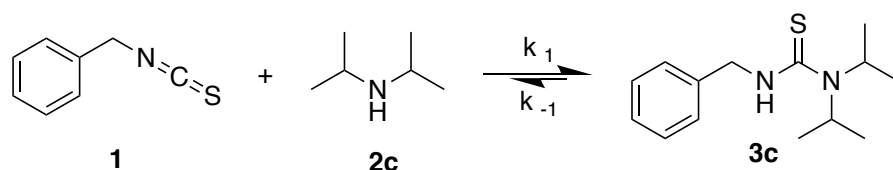


**Figure S14.** Stacked NMR spectra for the addition of benzyl isothiocyanate and *tert*-butylethylamine at equilibrium. Peaks  $d'$ ,  $d$  and  $g$  were used to determine  $K_{\text{eq}}$  for the reaction.



### Supplementary Scheme S15



$K_{eq}$  model reaction between benzyl isothiocyanate and diisopropylamine.

Three vials containing different amounts of benzyl isothiocyanate were prepared:

Vial 1 = 0.75 equiv., 0.300 mmol, 45.1 mg.

Vial 2 = 1.00 equiv., 0.400 mmol, 59.4 mg.

Vial 3 = 1.25 equiv., 0.500 mmol, 74.8 mg.

A 2 M stock solution (25 mL) of *tert*-butylethylamine was prepared by dissolving *tert*-butylethylamine (1.00 equiv., 0.005 mol, 0.506 g). Into each of the three vials, 2 mL portions of the prepared stock solution were added and mixed. The reaction was allowed to stir for three days before being characterized via  $^1\text{H}$  NMR. Calculated initial concentration values and  $K_{eq}$  values can be found in Table S1. Stacked NMR spectra of all three ratios can be found in Figure S16.

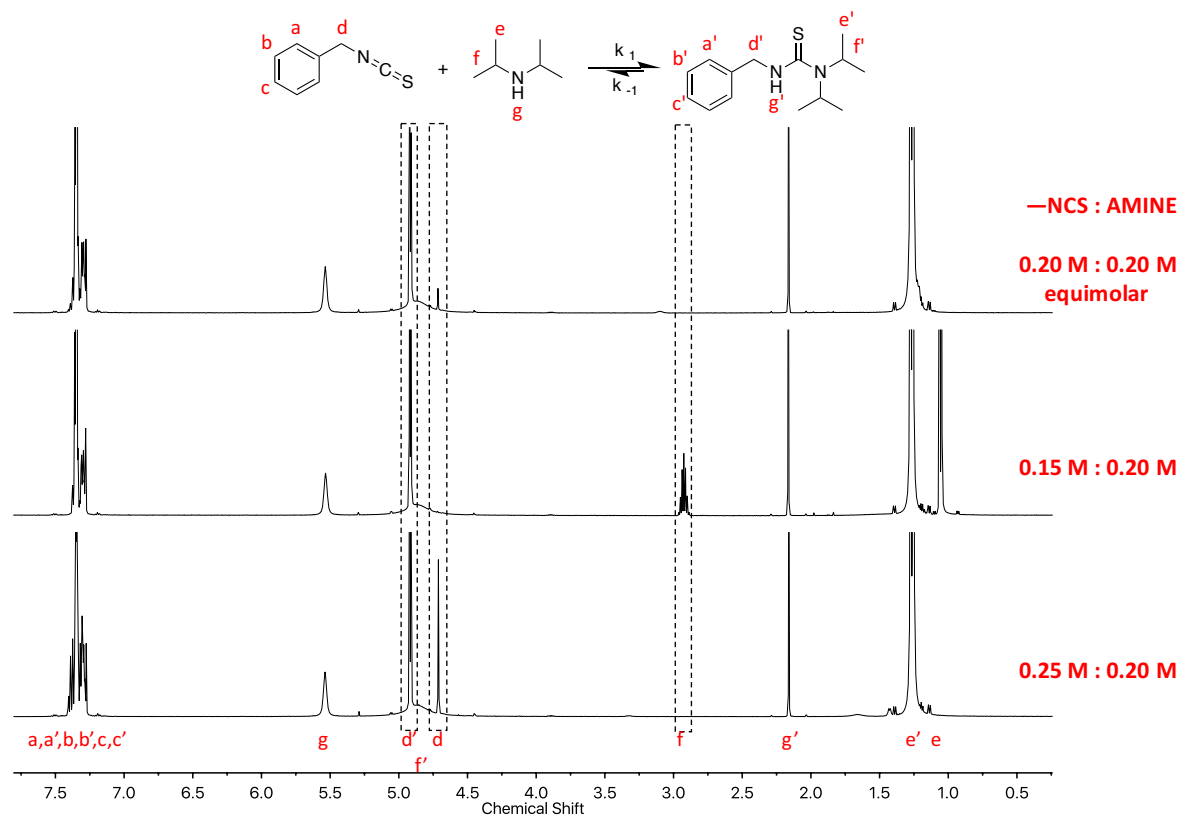
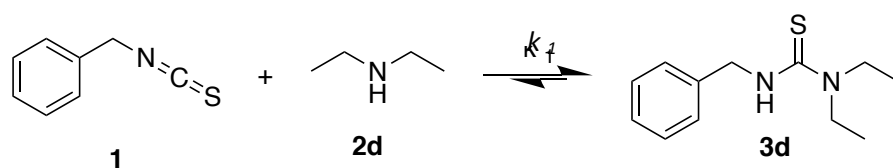


**Figure S16.** Stacked NMR spectra for the addition of benzyl isothiocyanate and diisopropylamine. Peaks d', d, and f were used to determine  $K_{eq}$  for the reaction.

### Supplementary Scheme S17



$K_{eq}$  model reaction between benzyl isothiocyanate and diethylamine.

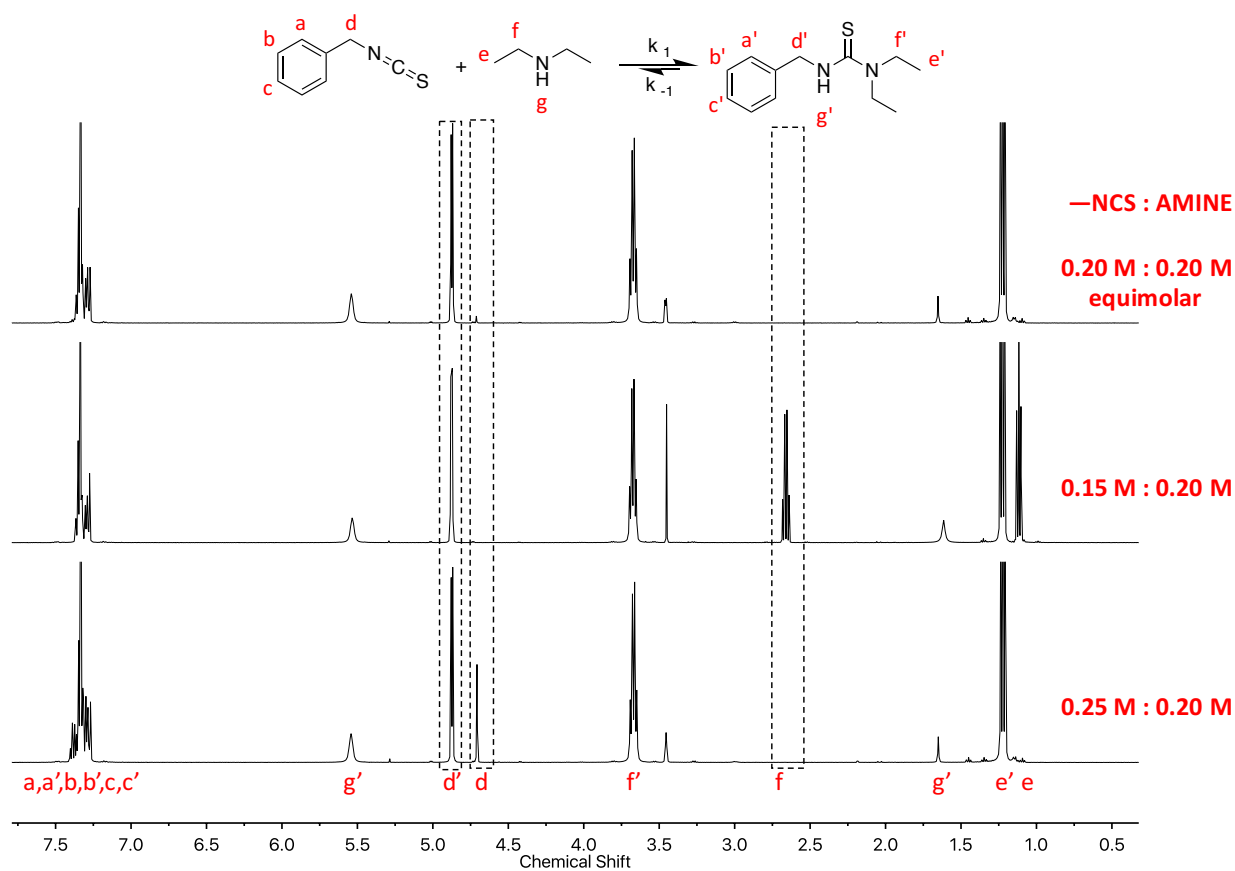
Three vials containing different amounts of benzyl isothiocyanate were prepared:

Vial 1 = 0.75 equiv., 0.300 mmol, 45.1 mg.

Vial 2 = 1.00 equiv., 0.400 mmol, 59.4 mg.

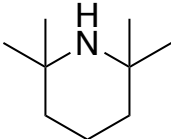
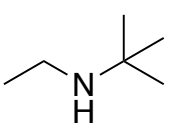
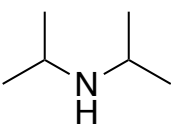
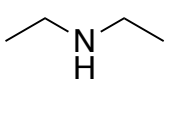
Vial 3 = 1.25 equiv., 0.500 mmol, 74.8 mg.

A 2 M stock solution (25 mL) of *tert*-butylethylamine was prepared by dissolving *tert*-butylethylamine (1.00 equiv., 0.005 mol, 0.366 g). Into each of the three vials, 2 mL portions of the prepared stock solution were added and mixed. The reaction was allowed to stir for three days before being characterized via  $^1\text{H}$  NMR. Calculated initial concentration values and  $K_{eq}$  values can be found in Table S1. Stacked NMR spectra of all three ratios can be found in Figure S18.



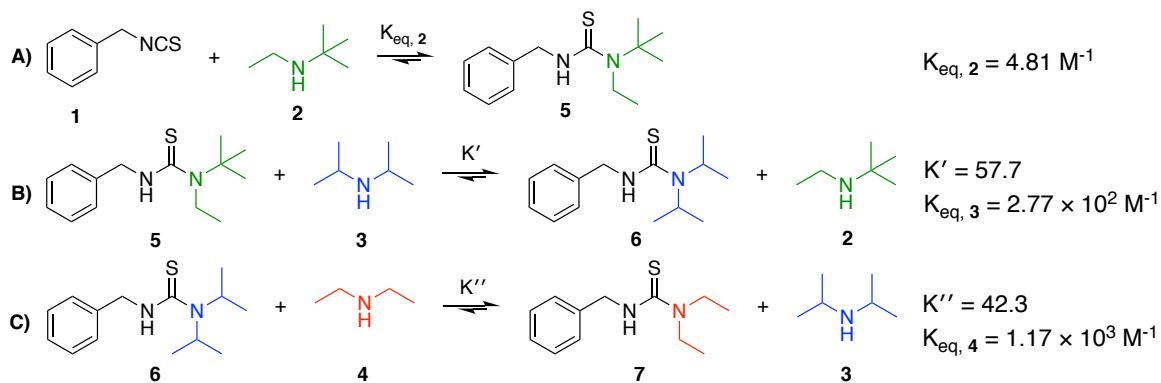
**Figure S18** Stacked NMR spectra for the addition reaction between benzyl isothiocyanate and diethylamine. Peaks d', d, and f were used to determine the  $K_{eq}$  of the reaction.

**Table S1** Initial concentrations and  $K_{eq}$  values for each of  $K_{eq}$  experiment.

	-NCS : amine 0.75 : 1.00	-NCS : amine 1.00 : 1.00 <i>equimolar</i>	-NCS : amine 1.25 : 1.00
	No observable rxn.	No observable rxn.	No observable rxn.
	$[-NCS]_i = 0.150 \text{ M}$ $[NR_2]_i = 0.195 \text{ M}$ $K_{eq} = 4.57 \text{ L/mol}$	$[-NCS]_i = 0.200 \text{ M}$ $[NR_2]_i = 0.193 \text{ M}$ $K_{eq} = 4.42 \text{ L/mol}$	$[-NCS]_i = 0.251 \text{ M}$ $[NR_2]_i = 0.193 \text{ M}$ $K_{eq} = 4.45 \text{ L/mol}$
	$[-NCS]_i = 0.149 \text{ M}$ $[NR_2]_i = 0.196 \text{ M}$ $K_{eq} = \text{unmeasurable}$	$[-NCS]_i = 0.200 \text{ M}$ $[NR_2]_i = 0.198 \text{ M}$ $K_{eq} = \text{unmeasurable}$	$[-NCS]_i = 0.249 \text{ M}$ $[NR_2]_i = 0.197 \text{ M}$ $K_{eq} = \text{unmeasurable}$
	$[-NCS]_i = 0.149 \text{ M}$ $[NR_2]_i = 0.197 \text{ M}$ $K_{eq} = \text{unmeasurable}$	$[-NCS]_i = 0.202 \text{ M}$ $[NR_2]_i = 0.199 \text{ M}$ $K_{eq} = \text{unmeasurable}$	$[-NCS]_i = 0.250 \text{ M}$ $[NR_2]_i = 0.199 \text{ M}$ $K_{eq} = \text{unmeasurable}$

Indirect method to determine  $K_{eq}$

**Scheme S19.**



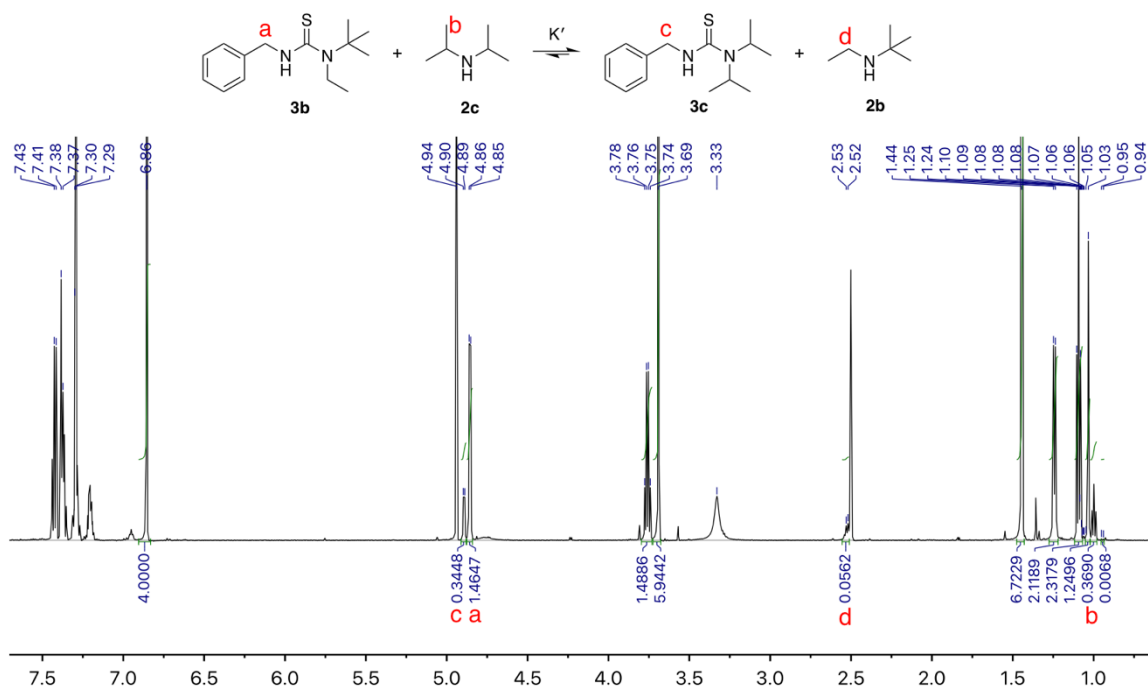
The indirect method for determining  $K_{eq}$  values for the addition of **1** and **2** ( $K_{eq,2}$ ), **1** and **3** ( $K_{eq,3}$ ), and **1** and **4** ( $K_{eq,4}$ ).  $K'$  is the equilibrium constant for reaction B.  $K''$  is the equilibrium constant for reaction C.

As the equilibrium constants for diisopropylamine and diethylamine were difficult to determine through  $^1\text{H-NMR}$ , an indirect method of measuring  $K_{eq}$  was used. A stock solution of **1** (0.2 M, 119.7 mg in 4 mL DMSO- $d_6$ ) was prepared with an internal standard of dimethoxybenzene (0.1 M, 55.7 mg in 4 mL). Stock solutions of **2b** (0.2 M, 40.7 mg in 4 mL DMSO- $d_6$ ), **2c** (0.2 M, 40.7 mg in 4 mL DMSO- $d_6$ ), and **2d** (0.2 M, 58.5 mg in 4 mL DMSO- $d_6$ ) were prepared.

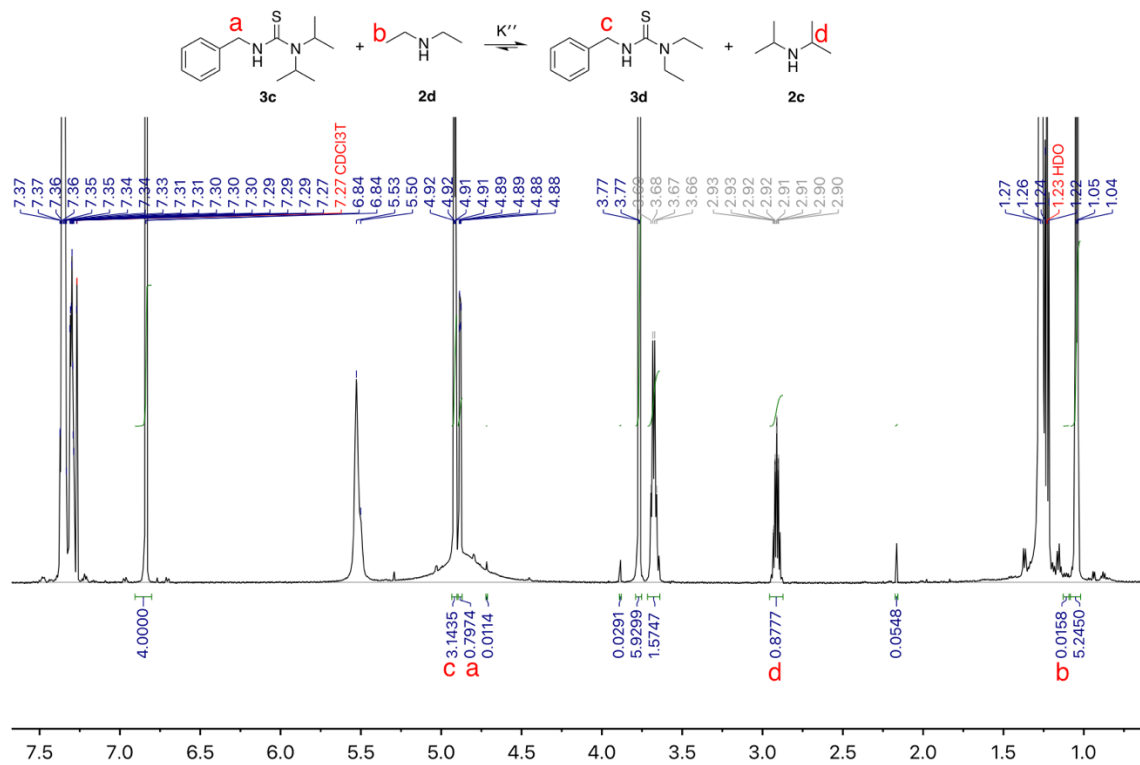
For reaction (B) in Scheme S19, 1 mL portions of the stock solution of **1**, **2b**, and **2c** were added to a capped vial. The reaction was allowed to stir for 72 hours to reach equilibrium. The resulting NMR spectra is shown in Figure S20. For reaction (C) in Scheme S19, 1 mL portions of the stock solution of **1**, **2c**, and **2d** were added to a capped vial. The reaction was allowed to stir for 72 hours to reach equilibrium. The resulting NMR spectra is shown in Figure S21.

The equilibrium constant,  $K'$  (Scheme S19), was found through the equilibrium reaction (B). The equilibrium constant,  $K_{eq,3}$  was determined through the equation  $K_{eq,3} = K' \cdot K_{eq,2}$ . The equilibrium constant,  $K''$ , was found through the equilibrium reaction (C), and the resulting  $K_{eq,4}$  was determined through the equation  $K_{eq,4} = K'' \cdot K_{eq,3}$ . Model reaction results show that the  $K_{eq}$  of isopropyl and ethyl substituents ( $K_{eq,3} = 2.77 \times 10^2 \text{ M}^{-1}$  and  $K_{eq,4} = 1.17 \times 10^3 \text{ M}^{-1}$ , respectively) on the thiourea will allow for polymer formation, while *tert*-butyl ( $K_{eq,2} = 4.81 \text{ M}^{-1}$ ) will only afford oligomers.

**Scheme S20. Reaction (B) from Scheme S19.**



**Scheme S21. Reaction (C) from Scheme S19.**

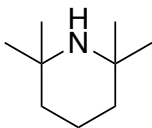
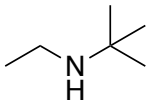
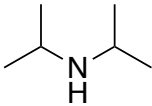
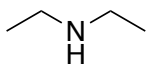


### Isocyanate vs isothiocyanate competitive study

To determine the reactivity difference between isocyanates (-NCO) and isothiocyanates (-NCS), a competitive study was designed. Four stock solutions of bulky amines were prepared in CDCl<sub>3</sub>-t: 1,1,5,5-tetramethylpiperidine (0.200 M, 0.005 mol, 0.706 g, dissolved in 25.0 mL), *tert*-butylethylamine (0.200 M, 0.005 mol, 0.506 g, dissolved in 25 mL), diisopropylamine (0.200 M, 0.005 mol, 0.506 g, dissolved in 25 mL), and diethylamine (0.200 M, 0.005 mol, 0.366 g, dissolved in 25.0 mL). Benzyl isocyanate (0.400 mmol, 53.3 mg) was weighed into four vials. Benzyl isothiocyanate (0.400 mmol, 59.7 mg) was weighed into the same four vials, but not mixed with the isocyanate. Into four vials containing the -NCO and -NCS mixture, 2 mL portions of stock solutions were added separately so that each vial only had one type of amine. The mixtures were allowed to mix for 40 minutes before being characterized via <sup>1</sup>H NMR spectroscopy. It was found that 1,1,5,5-tetramethylpiperidine did not react at all with the -NCS, while it reacted with 73.4% of the -NCO. The solution with *tert*-butylethylamine had low reactivity with -NCO to -NCS being 555.1 to 1.0 with 99.2% of the -NCO being consumed. The solution with diisopropylamine was found to react with -NCO 38 times faster, leading to a 38.0 to 1.0 ratio with >99% of the -NCO being consumed. Finally, the solution with diethylamine was found to react with -NCO 11.2 times faster than -NCS, with >99% of the -NCO being consumed. This study tells us that with an amine with enough nucleophilicity can bring the reactivity of an isothiocyanate to within an order of magnitude of the reactivity of an isocyanate. Table S2 shows the reactivity ratio and the corresponding amines.



**Table S2** Reactivity ratios of –NCO to –NCS at 40 minutes.

	<b>–NCO to –NCS reactivity @ 40 min. (based on product integral)</b>
	>1,000.0 to 1.0 (undetectable for –NCS)
	555.1 to 1.0
	38.0 to 1.0
	11.2 to 1.0

Rate constant,  $k_1$ , determination

A stock solution containing benzyl isocyanate (1.000 M, 0.010 mol, 1.332 g) and a NMR standard, dimethoxybenzene (0.116 M, 1.16 mmol), were prepared in 10 mL of  $\text{CDCl}_3$ . 3-benzyl-1,1-diethylthiourea (0.200 M, 0.400 mmol, 88.6 mg) was weighed into a vial, and then dissolved with 2 mL of the prepared stock solution.  $^1\text{H}$  NMR spectra were acquired at several time intervals and plotted in Figure S22. Into a separate vial, benzyl-1,1-diisopropylthiourea (0.200 M, 0.400 mmol, 100 mg) was weighed, and dissolved with 2 mL with the prepared isocyanate stock solution.  $^1\text{H}$  NMR spectra were acquired at several time intervals and plotted in Figure S23.

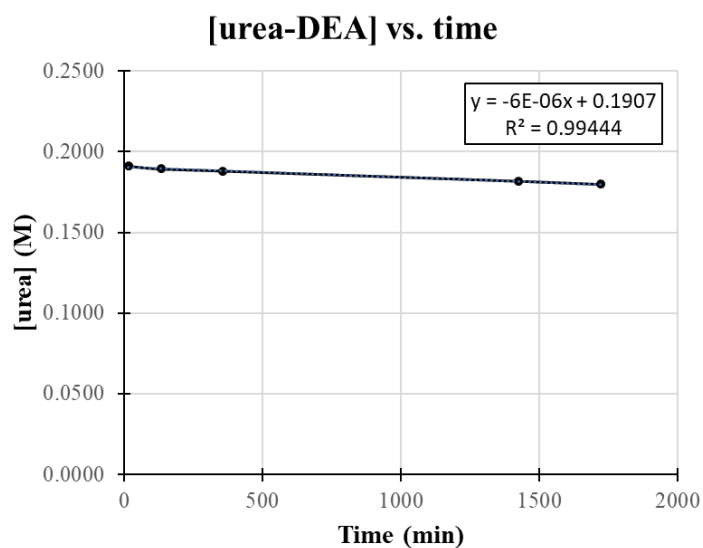


**Figure S22.** Concentration of benzyl-1,1-diethylthiourea decreasing with respect to time.

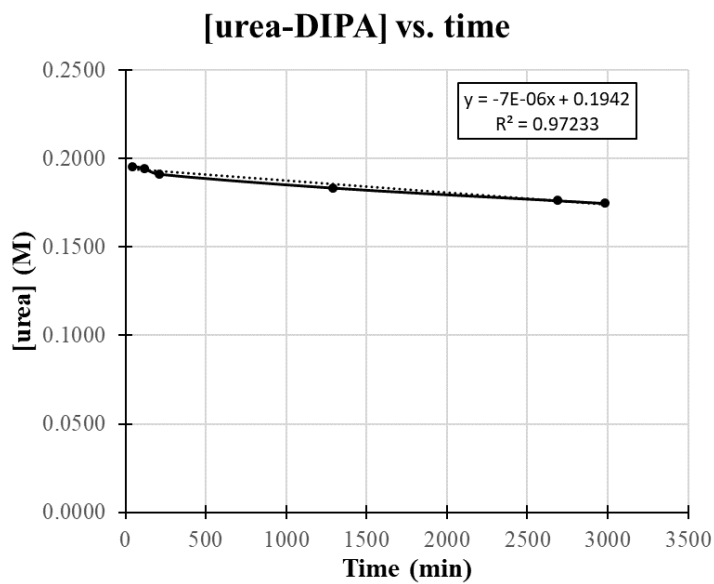


**Figure S23.** Concentration of benzyl-1,1-diisopropylthiourea decreasing with respect to time.

### *Polymerization with and without catalyst*

Commercial production of polyureas and polyurethanes often involve the use of a catalyst to promote polymerization. We investigated the use of dibutyltin diacetate (DBTDA) as a catalyst, as it has been proven to accelerate polymerization.<sup>1</sup> XDI (87.2 mg) was mixed with 2 mL of a stock solution of dimethylethylenediamine (DMEDA) (0.198 M, 175.6 mg in 10.0 mL DMF) and immediately filtered through a 0.2  $\mu\text{m}$  PTFE filter and into a GPC vial. A GPC chromatogram was taken every hour for four hours, and a final time point was taken at 22 hours 15 min. The GPC trace of all time points is plotted in Figure S24. The polymerization occurred very fast, with it nearing completion within 65 minutes of initiation. Number average molecular weight ( $M_n$ ) was found to be  $2.69 \times 10^4$  g/mol.

Likewise, XDI (87.2 mg) was mixed with 2 mL of a stock solution of DMEDA (0.198 M, 175.6 mg in 10 mL DMF). After mixing, DBTDA (0.05 equiv., 0.001 M, 0.500  $\mu\text{L}$ ) was added to the solution, mixed, and immediately filtered through a 0.2  $\mu\text{m}$  PTFE filter and into a GPC vial. A GPC chromatogram was taken every hour for four hours, and a 6<sup>th</sup> time point was taken at 22 hours 10 min. The GPC trace of all time points is plotted in Figure S25. The number average molecular weight ( $M_n$ ) was found to  $4.56 \times 10^3$  g/mol. Interestingly, the polymerization was significantly less than the polymerization without catalyst. We hope to perform this polymerization again in an attempt to eliminate errors.

---

<sup>1</sup> Goredema, A.; Carlini, R.; Bedford, C.; Breton, M.; Toma, E. Bis[urea-urethane] compounds. US20060122427 A1, June 8, 2006.

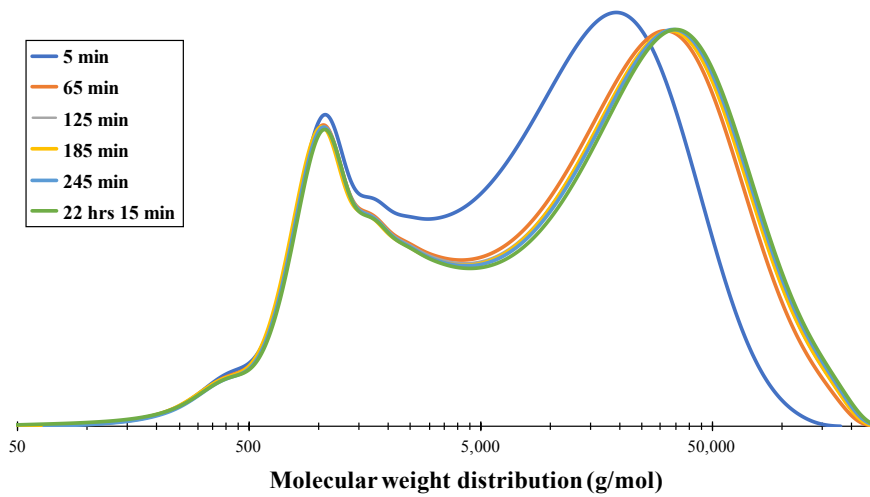


**Figure S24.** Polymerization of XDI and DMEDA in a 1:1 stoichiometric ration without the addition of catalyst.

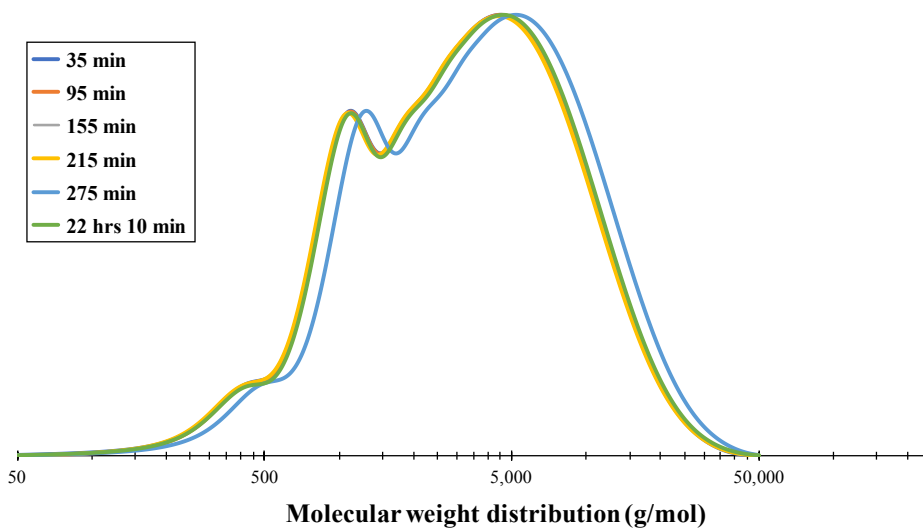


**Figure 25.** Polymerization of XDI and DMEDA in the presence of dibutyltin diacetate catalyst in a 1:1:0.05 stoichiometric ratio.

Polymerizations diiothiocyanate monomer (XDI) and bulky amines.

Stock solutions were prepared at a concentration of 3M in DMF with 0.1 % LiBr. The following table shows the concentration and masses:

**Table S3.** Preparation of stock solutions in DMF.

	<b>XDI</b>	<b>DtBuEDA</b>	<b>DiPrEDA</b>	<b>DEEDA</b>
<b>M<sub>w</sub></b>	220.31	172.32	144.26	116.21
	g/mol	g/mol	g/mol	g/mol
<b>Concentration</b>	3 M	3 M	3 M	3 M
<b>Volume</b>	5 mL	4 mL	4 mL	4 mL
<b>Mol.</b>	15 mmol	12 mmol	12 mmol	12 mmol
<b>Mass</b>	3.3047 g	2.0678 g	1.7311 g	1.3945 g

Polymerization of XDI and DtBuEDA (poly-6A)

Into a GPC vial, 0.5 mL XDI stock solution and 0.5 mL DtBuEDA stock solution were added. The polymerization was allowed to proceed for 24 hours at room temperature before characterization via GPC. After molecular weight analysis, the sample was placed into an oil bath and held at 50 °C for 8 hours before being characterized via GPC again. A plot of the GPC traces can be found in Figure 26. Results can be found in Table S4.

Polymerization of XDI and DiPrEDA (poly-6B)

Into a GPC vial, 0.5 mL XDI stock solution and 0.5 mL DiPrEDA stock solution were added. The polymerization was allowed to proceed for 24 hours at room temperature before

characterization via GPC. After molecular weight analysis, the sample was placed into an oil bath and held at 50 °C for 8 hours before being characterized via GPC again. A plot of the GPC traces can be found in Figure 26. Results can be found in Table S4.

### Polymerization of XDI and DEEDA (poly-6C)

Into a GPC vial, 0.5 mL XDI stock solution and 0.5 mL DEEDA stock solution were added. The polymerization was allowed to proceed for 24 hours at room temperature before characterization via GPC. After molecular weight analysis, the sample was placed into an oil bath and held at 50 °C for 8 hours before being characterized via GPC again. A plot of the GPC traces can be found in Figure 26. Results can be found in Table S4.

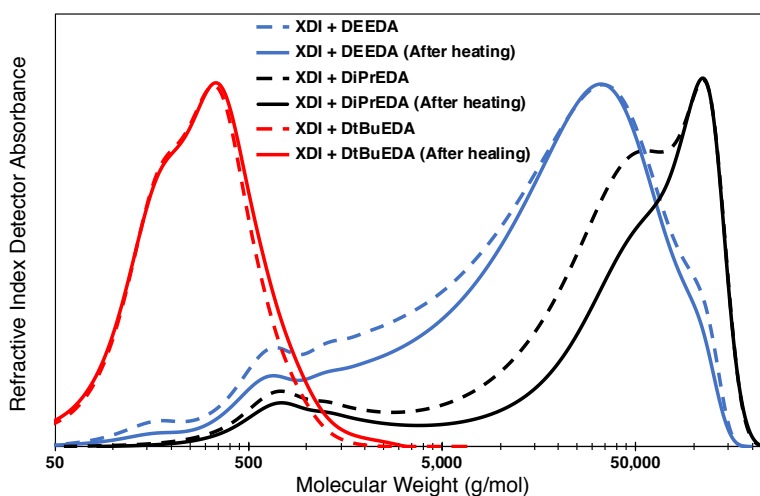


**Figure 26.** Overlaid GPC chromatograms of poly-6A, poly-6B, and poly-6C before and after heating.

**Table S4.** Number average molecular weight ( $M_n$ ), weight average molecular weight ( $M_w$ ) and polydispersity index of poly-6A, poly-6B, and poly-6C.

Sample	$M_n$	$M_w$	PDI
Poly-6A	$2.18 \times 10^2$ g/mol	$3.27 \times 10^2$ g/mol	1.49
Poly-6A after heating	$1.68 \times 10^2$ g/mol	$3.50 \times 10^2$ g/mol	2.08
Poly-6B	$4.06 \times 10^4$ g/mol	$7.02 \times 10^4$ g/mol	1.73
Poly-6B after heating	$5.21 \times 10^4$ g/mol	$7.97 \times 10^4$ g/mol	1.53
Poly-6C	$1.53 \times 10^4$ g/mol	$3.90 \times 10^4$ g/mol	2.55
Poly-6C after heating	$1.63 \times 10^4$ g/mol	$3.84 \times 10^4$ g/mol	2.35

Initial incorporation of ether linkages into polymer backbone

**Scheme S27.** Polymerization of **10**, **8**, and **12** in varying ratios.

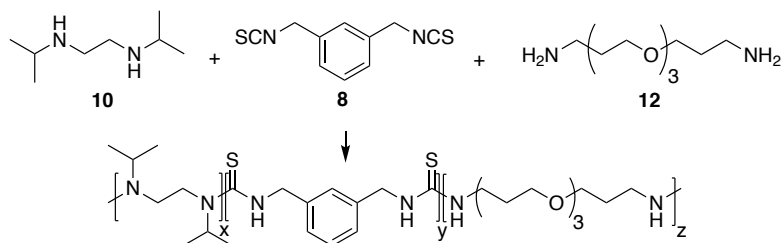


**Table S5.** Varying ratios of bulky amine added to poly-6B.

<b>Sample</b>	<b>Equiv. (mL) of 10</b>	<b>Equiv. (mL) of 8</b>	<b>Equiv. (mL) of 12</b>	<b>Result</b>
5% bulky amine	1 (0.150 mL)	10 (1.501 mL)	9 (1.351 mL)	N/A
10% bulky amine	2 (0.303 mL)	10 (1.513 mL)	8 (1.210 mL)	Robust
15% bulky amine	3 (0.451 mL)	10 (1.499 mL)	7 (1.051 mL)	Weak

The same stock solutions prepared in Table S3 were prepared again for the polymerizations in Table S5. The general procedure for all polymerizations in Scheme S27 were to first mix **10** and **12** in a PTFE mold. In a dropwise manner, **10** was added, followed by rapid manual mixing. The sample was then placed in an oven at 40 °C for 24 hours, followed by dissolving in 40 mL DMF. The solution was then mixed and precipitated into 800 mL of vigorously stirred Et<sub>2</sub>O. The resulting precipitate was centrifuged, decanted, and solvent was removed *in vacuo* at 110 °C for 16 hours.

When 5% bulky amine was added to poly-6B, the sample was too brittle to be removed from the mold. The samples containing 10% and 15% bulky amine were tough enough to remove from the mold, where they then underwent stress vs. strain testing on an Instron tensile testing machine. The plot of their stress vs. strain curve can be found in Figure S28.



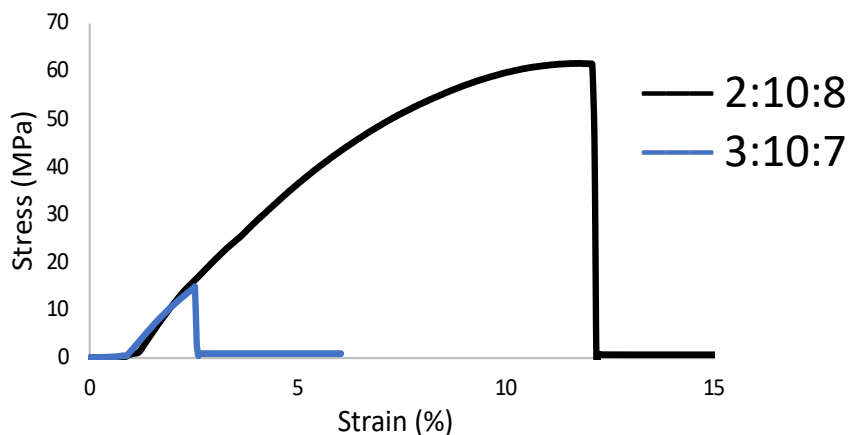
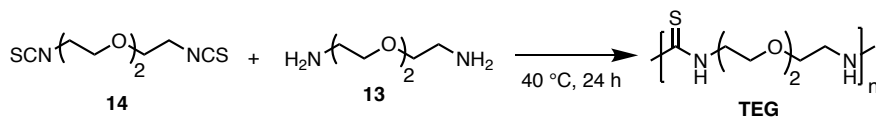


**Figure S28.** Stress vs strain of amine ratios from Table S5.

*Polymerization of TEG and TEG-10*

**Scheme S29.** Polymerization of thiourea ethylene glycol (TEG).



Into a PTFE mold, **13** (7.00 mmol, 1.037 g) was weighed, followed by the addition of 3 mL DMSO. After mixing, **14** (6.74 mmol, 1.566 g) was added in a dropwise manner. The mixture was then manually stirred and placed into an oven at 40 °C for 24 hours. It was then dissolved in 40 mL CHCl<sub>3</sub>, followed by precipitation into 800 mL of vigorously stirred Et<sub>2</sub>O. The resulting precipitate was centrifuged, decanted, and solvent was removed *in vacuo* at 110 °C for 16 hours followed by storage in a desiccator. A small piece (~3 mg) was removed and subjected to GPC measurements to determine molecular weight and dispersity. Molecular weight was referenced to PMMA standards: M<sub>n</sub> = 2.31 × 10<sup>4</sup> g/mol, PDI = 1.80.

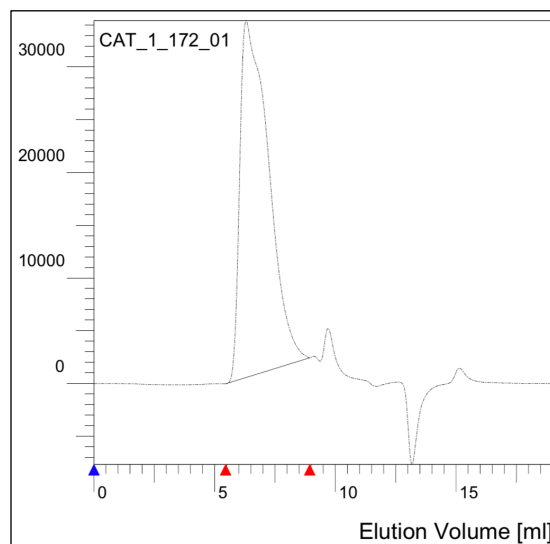
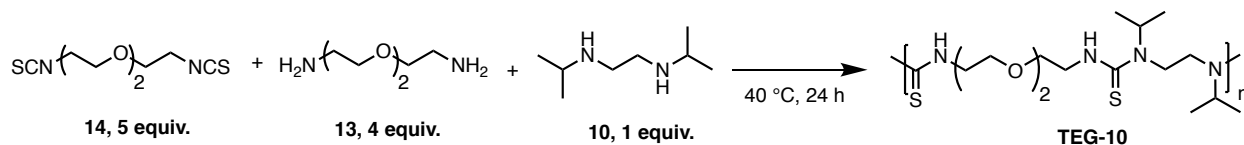


**Figure S29.** GPC chromatogram of TEG.

**Scheme S30.** Polymerization of thiourea ethylene glycol with 10% bulky amine (TEG-10).



Into a PTFE mold, **10** (2.00 mmol, 0.288 g) and **13** (8.00 mmol, 1.186 g) were added, followed by the addition of 1.5 mL DMSO. After mixing, **14** (10 mmol, 2.323 g) was added in a dropwise manner. The mixture was then manually stirred and placed into an oven at 40 °C for 24 hours. It was then dissolved in 40 mL CHCl<sub>3</sub>, followed by precipitation into 800 mL of vigorously stirred Et<sub>2</sub>O. The resulting precipitate was centrifuged, decanted, and solvent was removed *in vacuo* at 110 °C for 16 hours, followed by storage in a desiccator. A small piece (~3 mg) was removed and subjected to GPC measurements to determine molecular weight and dispersity. Molecular weight was referenced to PMMA standards:  $M_n = 3.14 \times 10^4$  g/mol, PDI = 1.86.

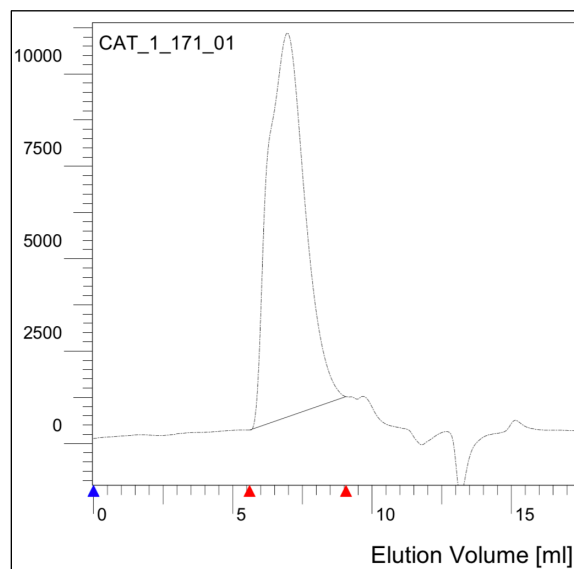


**Figure S30.** GPC chromatogram of TEG-10.

#### *Self-Healing Tests of TEG and TEG-10*

Both TEG and TEG-10 were heated to 80 °C for 15 minutes, placed in a rectangular PTFE mold, and compressed using a benchtop vice. The samples were allowed to cool naturally in the mold to room temperature, where they remained compressed for 8 hours. The bulk samples were then separated into two groups. The first group immediately underwent tensile testing on an Instron tensile testing machine, while the second group was cut 90% through using a razor blade. The cut samples were gently pressed together for 1 minute, followed by heating at 50 °C for 20 minutes. Samples were immediately placed in a room temperature desiccator for 14 hours. Strain rates of 100 mm/min were used for stress vs. strain plots (Figure S31).

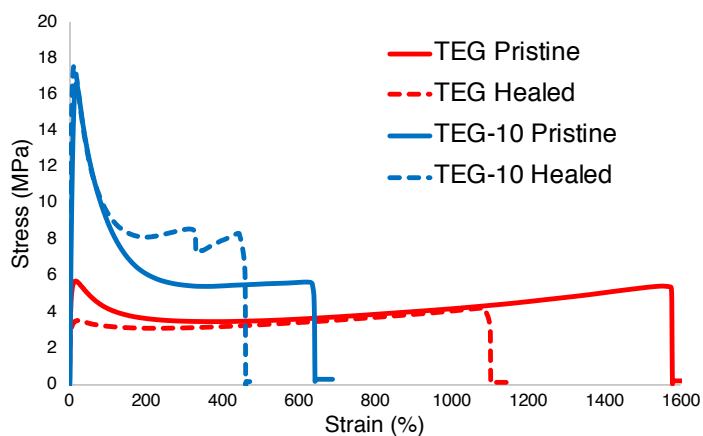


**Figure S31.** Comparison between pristine and healed samples. Samples were tested at room temperature under a strain rate of 100 mm/min.

*Thermal analysis of TEG and TEG-10*

The glass transition temperature ( $T_g$ ) for both TEG and TEG-10 were evaluated using differential scanning calorimetry (DSC, TA Q800). After molding the sample, pieces of flashing (5-10 mg) were trimmed and placed in a non-hermetic aluminum pan and scanned against an empty reference. The temperature was ramped from room temperature to 180 °C at a rate of 10 °C/min to wipe the thermal history. The samples were then cooled to -80 °C at a rate of -5 °C/min. After an isotherm at -80 °C for 10 minutes, the samples' temperature was raised to 180 °C at a ramp rate of 5 °C/min. A thermogram of the heat-cool-heat cycle can be found in Figure S32.

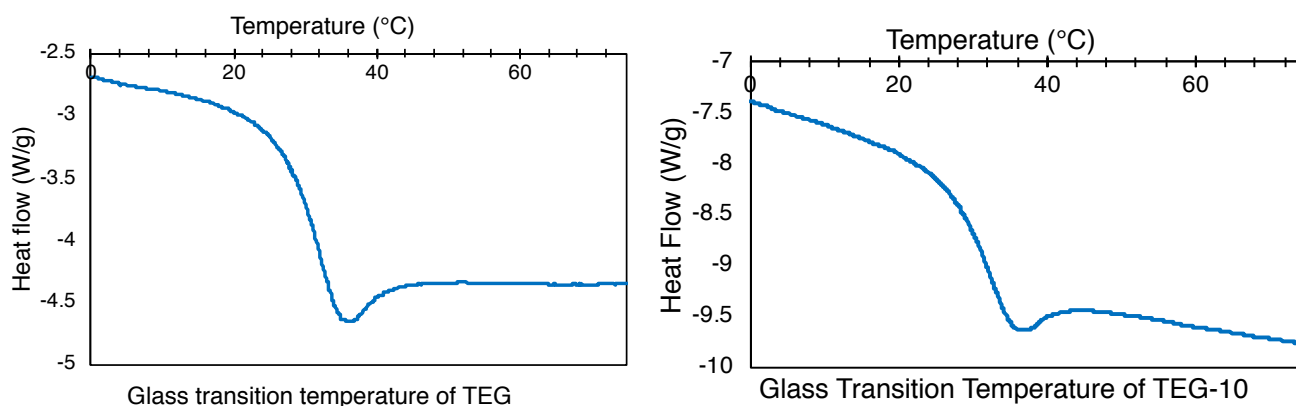


**Figure S32.** The  $T_g$  for both TEG and TEG-10 are very similar at 29–33 °C.

### *Thermogravimetric Analysis*

Thermogravimetric Analysis (TGA) of TEG was performed using a TA Q500 (Figure 33). A small piece of TEG (20–25 mg) was removed from the desiccator and allowed to set on the benchtop for 48 hours. The sample was then placed onto a platinum TGA pan and positioned in the furnace. The sample was flushed with argon at a flow rate of 40 mL/min, where it was heated at 20 °C/min to 130 °C. It was held isothermally at 130 °C for 30 minutes to measure water loss, and was then raised to 800 °C at a ramp rate of 20 °C/min. During the isothermal phase, the sample lost 1.178% mass, meaning that TEG absorbed 1.178% water by mass after sitting in air for 48 hours.

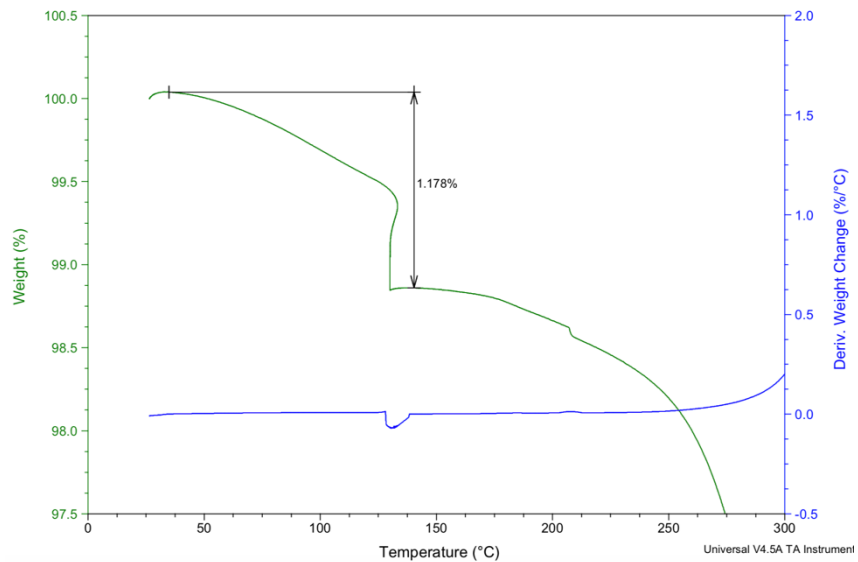
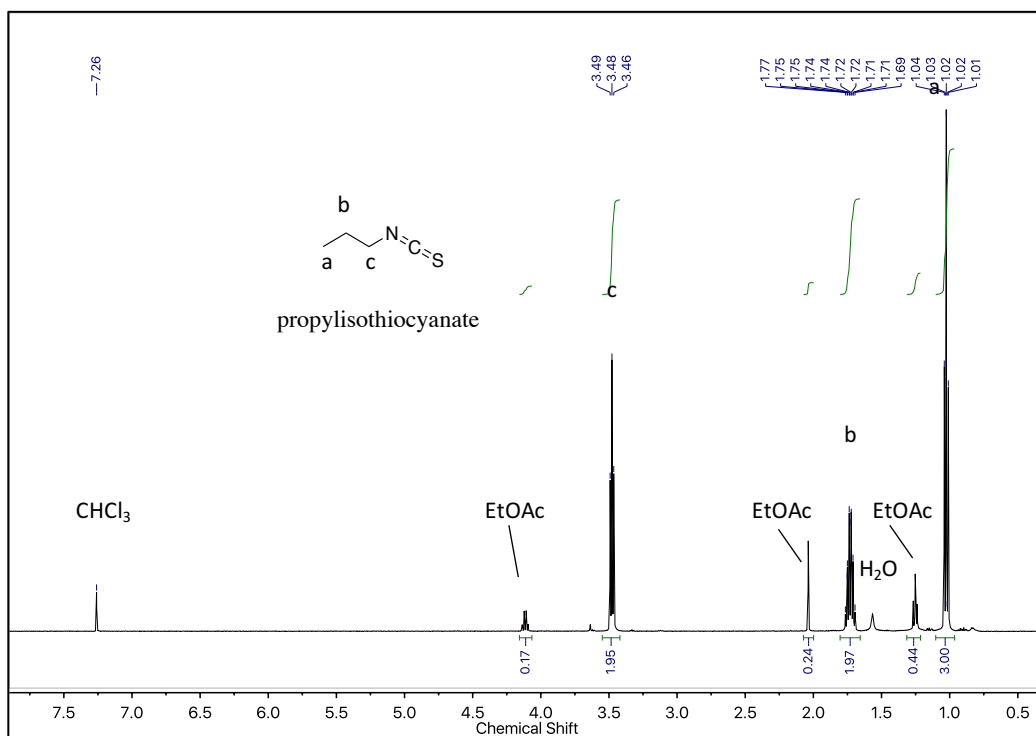
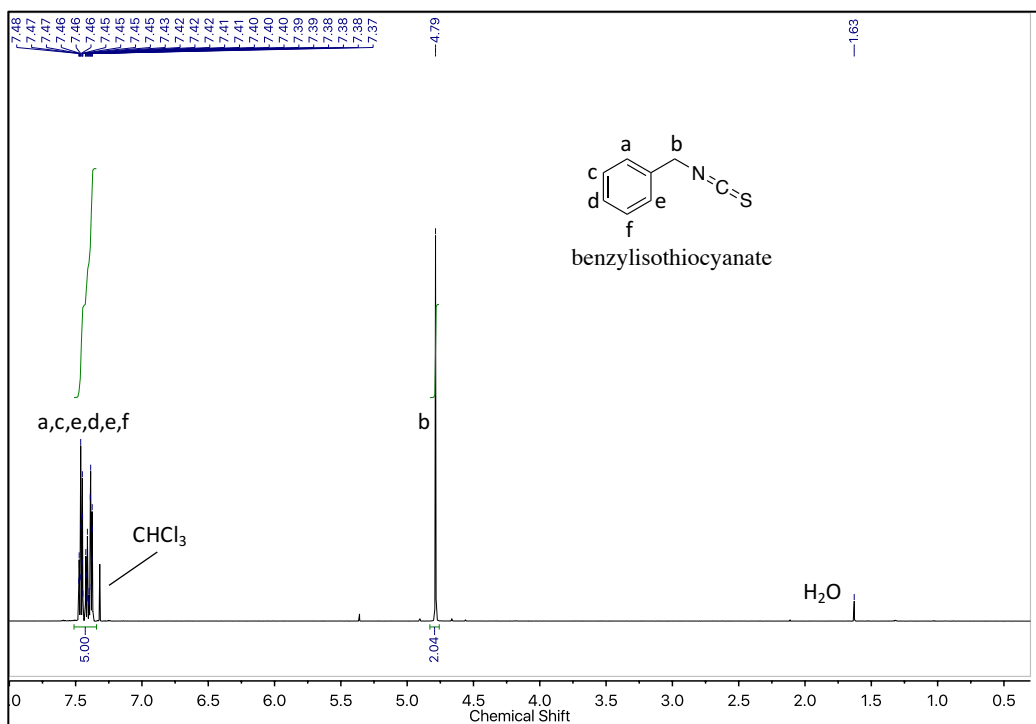


**Figure S33.** TGA of TEG after sitting in air for 48 hours. Figure is inset to better show water loss.

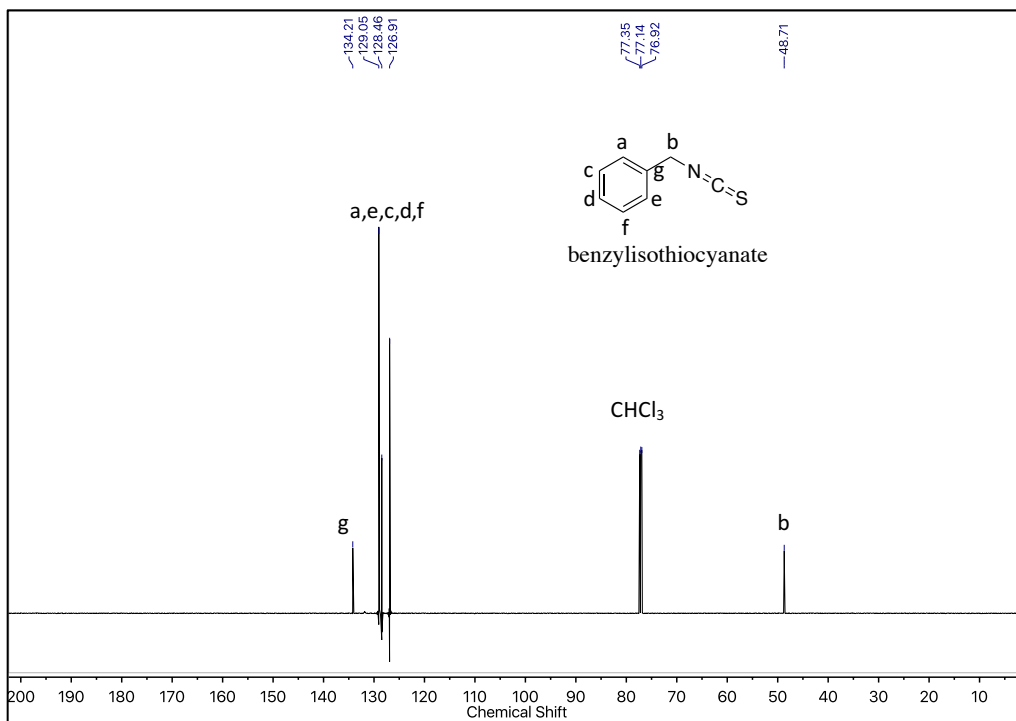
NMR Spectra for synthesized compounds



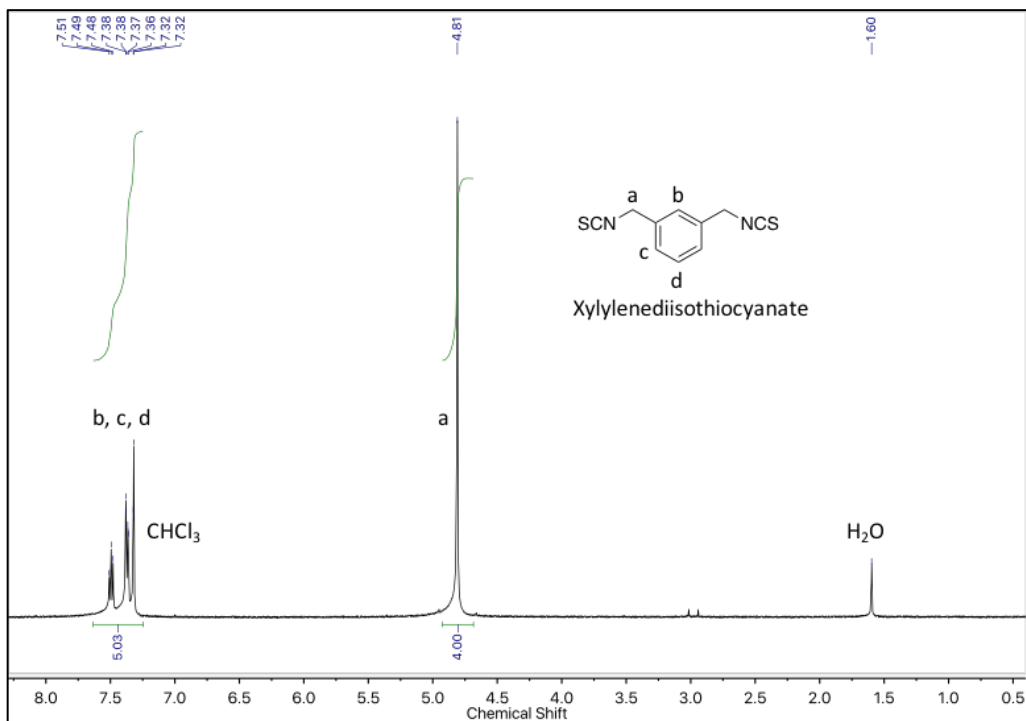
Propylisothiocyanate. <sup>1</sup>H-NMR (500 MHz, CDCl<sub>3</sub>, 298 K)



Benzylisothiocyanate. <sup>1</sup>H-NMR (500 MHz, CDCl<sub>3</sub>, 298 K)

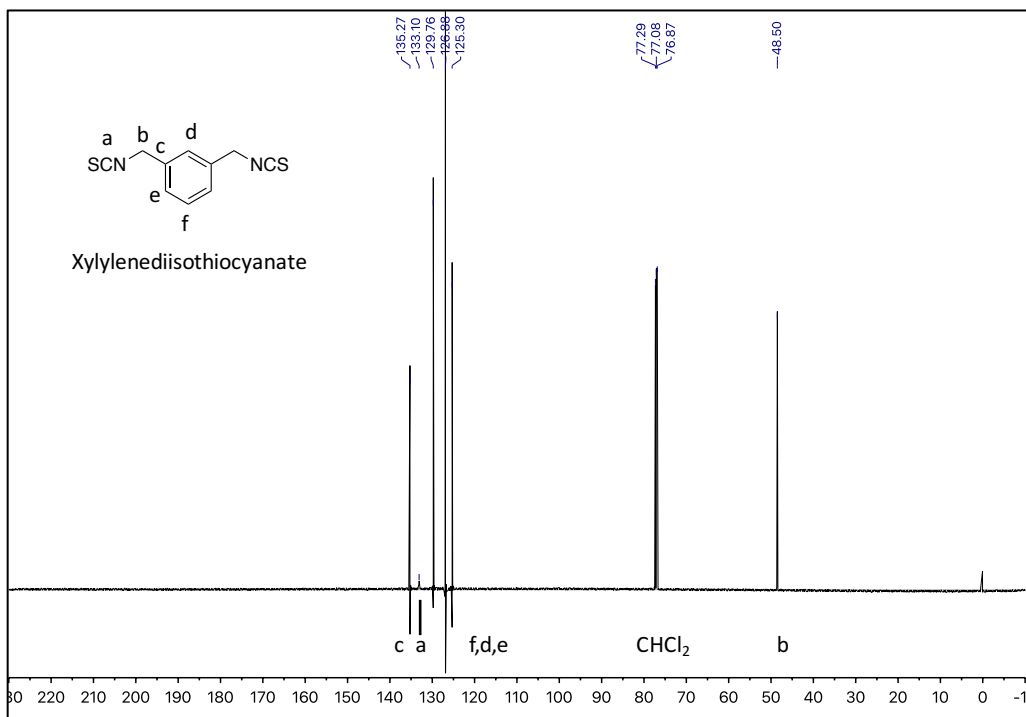


**Benzylisothiocyanate.**  $^{13}\text{C-NMR}$  (125 MHz,  $\text{CDCl}_3$ , 298 K)

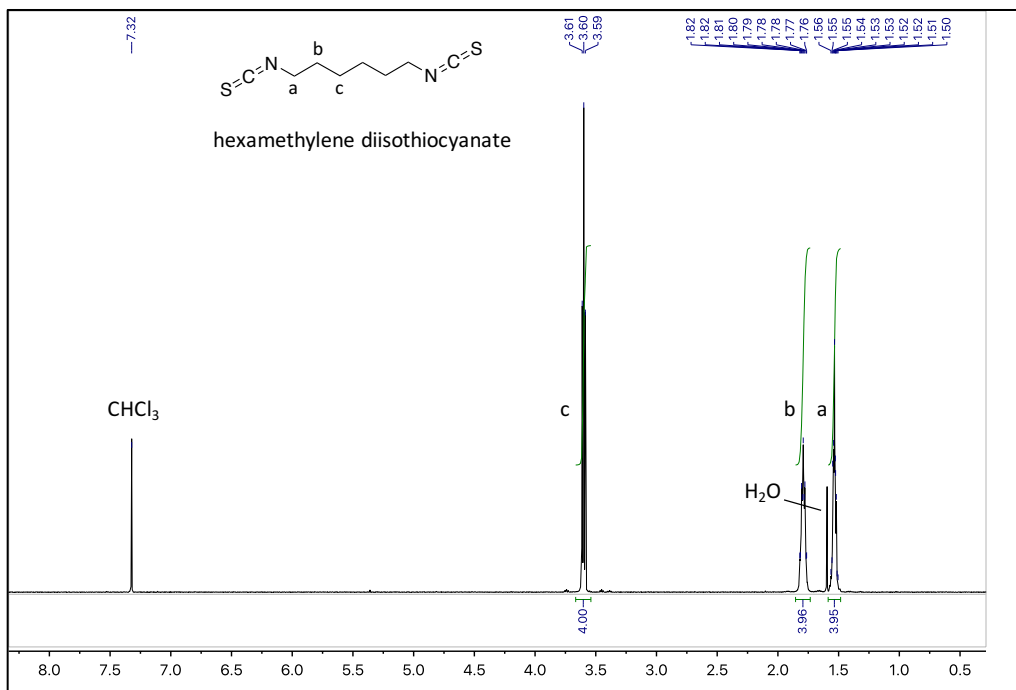


**Xylylenediisothiocyanate.**  $^1\text{H-NMR}$  (500 MHz,  $\text{CDCl}_3$ , 298 K)

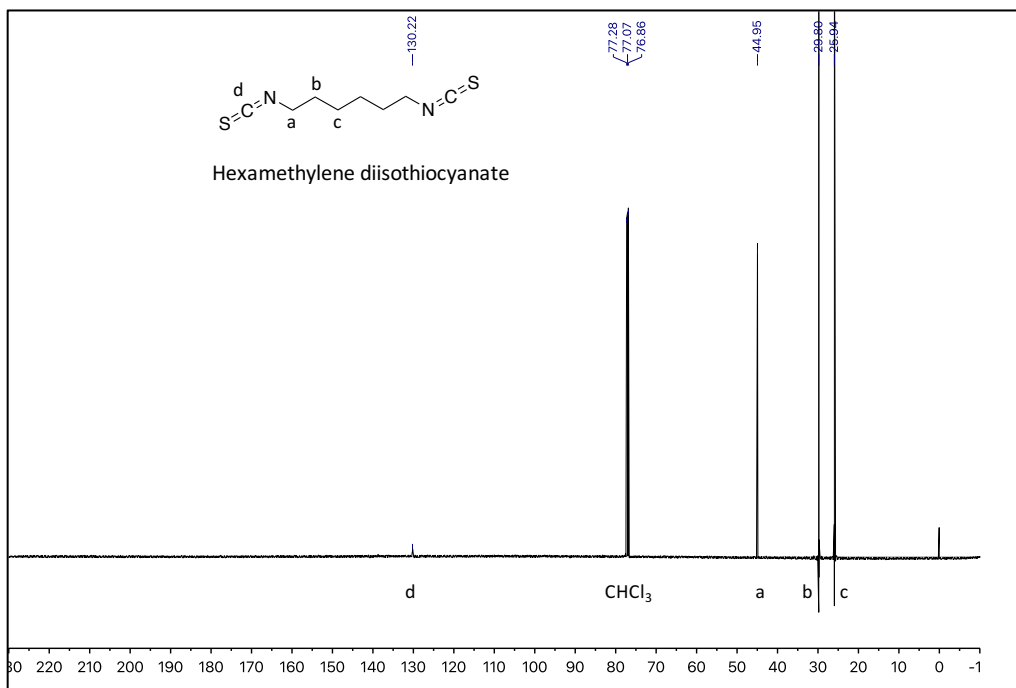




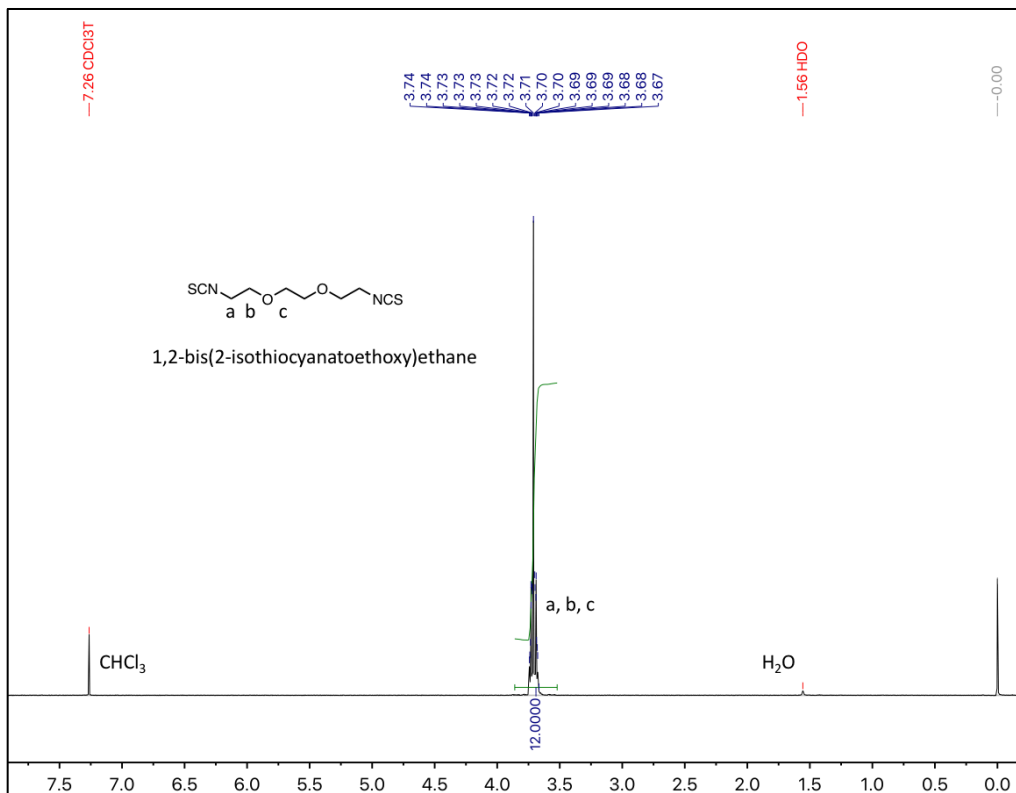
**Xylylenediisothiocyanate.** <sup>13</sup>C-NMR (125 MHz, CDCl<sub>3</sub>, 298 K)



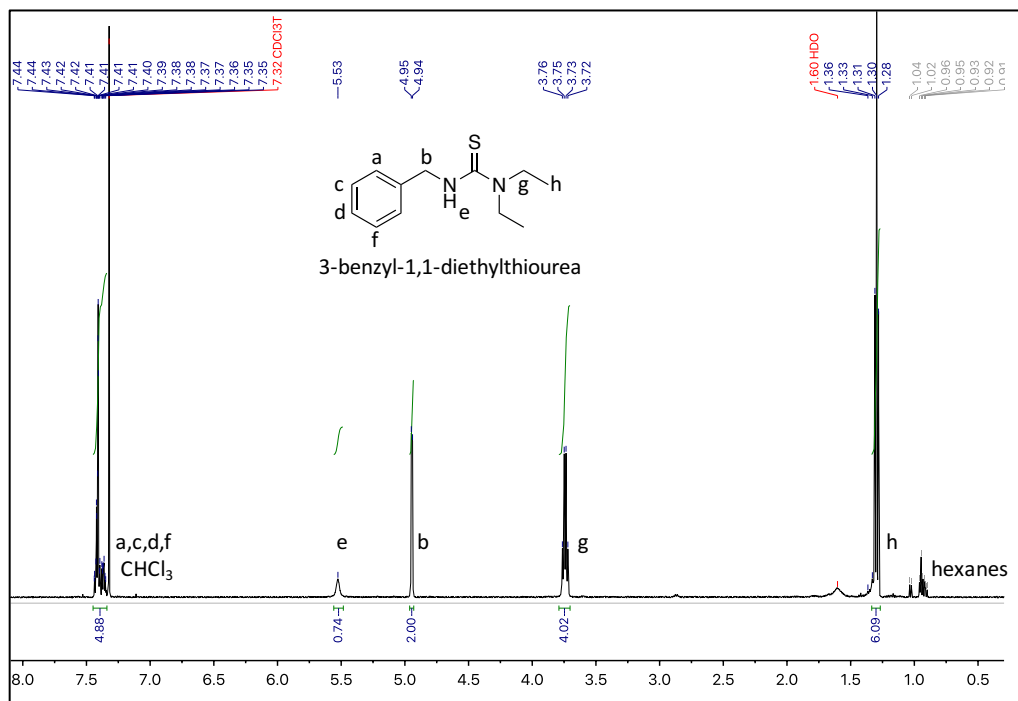
**Hexamethylene diisothiocyanate.** <sup>1</sup>H-NMR (500 MHz, CDCl<sub>3</sub>, 298 K)



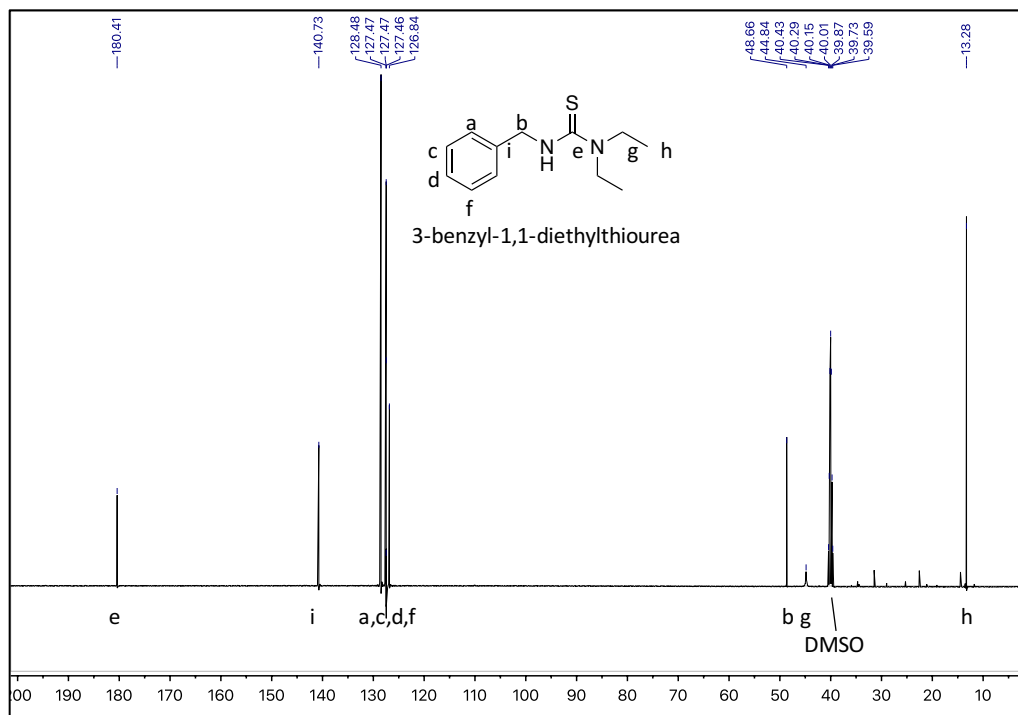
Hexamethylene diisothiocyanate. <sup>13</sup>C-NMR (125 MHz, CDCl<sub>3</sub>, 298 K)



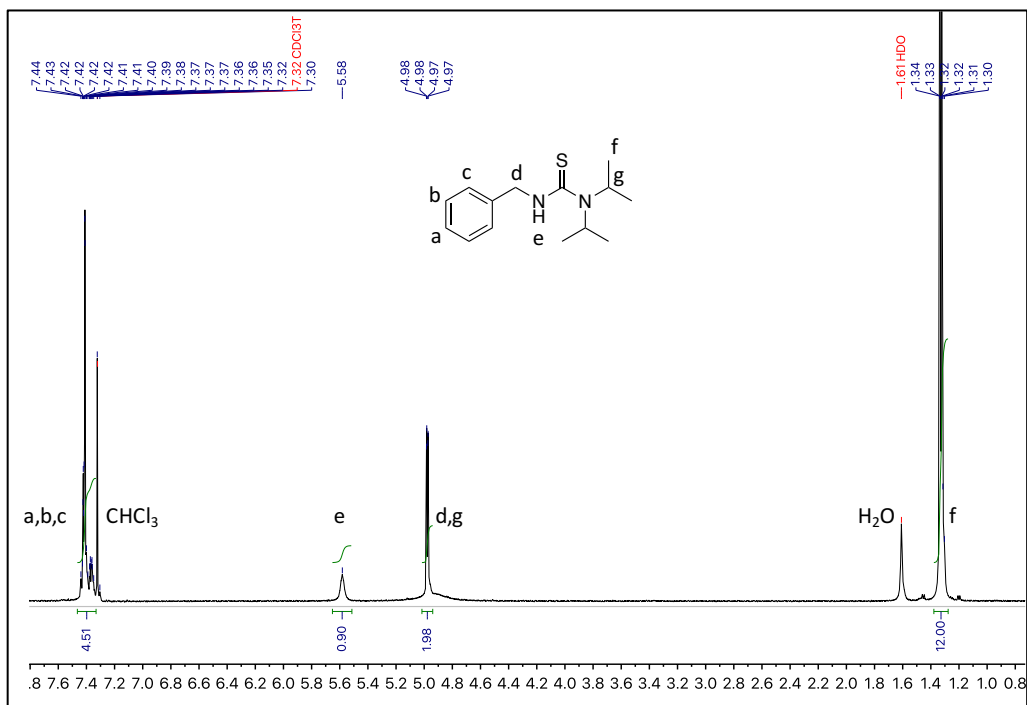
1,2-bis(2-isothiocyanatoethoxy)ethane. <sup>1</sup>H-NMR (500 MHz, CDCl<sub>3</sub>, 298 K)



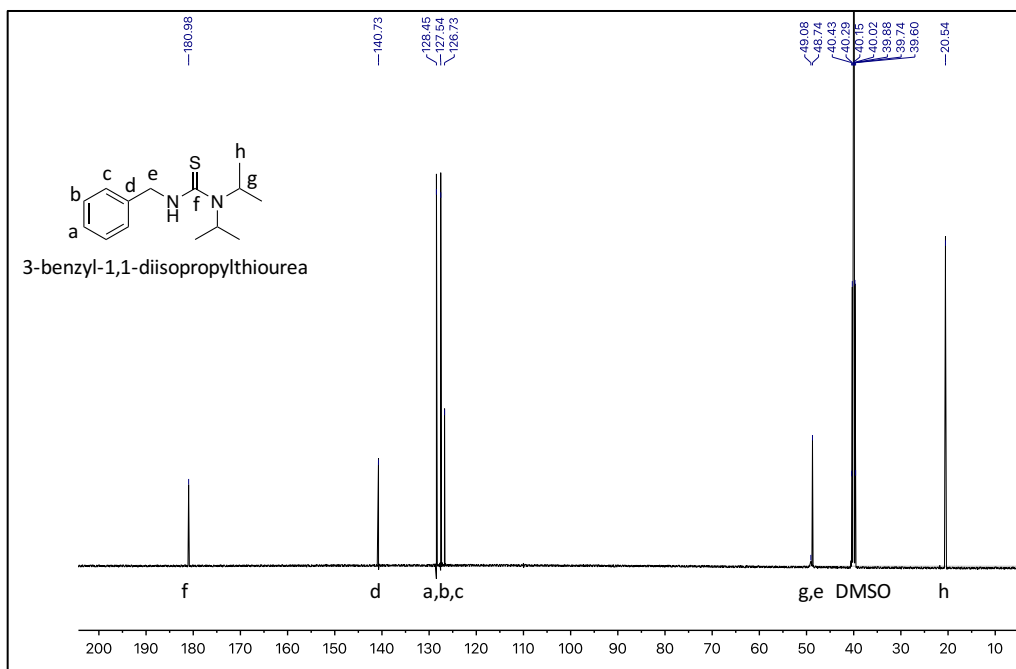
**3-benzyl-1,1-diethylthiourea.** <sup>1</sup>H-NMR (500 MHz, CDCl<sub>3</sub>, 298 K)



**3-benzyl-1,1-diethylthiourea.** <sup>13</sup>C-NMR (125 MHz, CDCl<sub>3</sub>, 298 K)



**3-benzyl-1,1-diisopropylthiourea.**  $^1\text{H-NMR}$  (500 MHz,  $\text{CDCl}_3$ , 298 K)



**3-benzyl-1,1-diisopropylthiourea.**  $^{13}\text{C-NMR}$  (125 MHz,  $\text{CDCl}_3$ , 298 K)

## Chapter 3: Direct Silyl Ether Metathesis for Vitrimers with Exceptional Thermal Stability

### 3.1 Introduction

Permanently cross-linked polymers (i.e., thermosets) have excellent mechanical properties, creep resistance, and chemical/solvent stability. However, a critical limitation of thermoset polymers is that they cannot be reshaped, reprocessed, or recycled by heat or with solvent. In contrast, thermoplastic polymers are reprocessable, but normally have poorer chemical/solvent resistances and both lower mechanical strength and lower dimensional stability at elevated temperatures. With the aim to combine the desirable attributes of both thermoplastics and thermosets, dynamic covalent chemistries have been incorporated into covalent adaptable networks (CANs) to introduce plasticity and make them malleable under external stimuli.<sup>1,2</sup> The plasticity/malleability is imparted by dynamic covalent cross-links that can undergo associative or dissociative exchange mechanisms.<sup>2</sup> Of the associative exchange-based CANs, vitrimers have generated considerable interest as they offer increased mechanical properties and solvent resistance while maintaining malleability/reprocessability.<sup>3</sup>

Several dynamic covalent motifs have been employed in vitrimer designs, such as trans-amination of vinylogous urethanes,<sup>4,5</sup> transesterification,<sup>3,6-8</sup> olefin cross metathesis,<sup>9,10</sup> trans-carbamoylation,<sup>11</sup> triazolium trans-alkylation,<sup>12</sup> poly(alkylurea-urethane),<sup>13</sup> boronic ester or boroxine exchange,<sup>14-16</sup> imine exchange,<sup>17</sup> and acetal exchange.<sup>18</sup> Despite the rapid progress in this field, the dynamic covalent chemistries involved in the reported systems have major limitations as some motifs are thermally and/or

oxidatively unstable, while others only suitable for a relatively narrow range of polymers. For further development, a critical need is to develop robust dynamic covalent chemistries for making mechanically strong and thermally stable vitrimers.

Toward this goal, our lab has recently demonstrated silyl ether as an advantageous dynamic covalent motif for vitrimer design<sup>19</sup> due to its high chemical and thermal stability, facile accessibility, and general applicability. As one of the most ubiquitous chemical bonds in natural and synthetic materials, the Si–O bond is thermodynamically strong (BDE ~ 535 kJ/mol).<sup>20</sup> Accordingly, silyl ethers show excellent stability toward heat and oxidation in contrast to many other dynamic covalent motifs including the promising boronic esters,<sup>14,16</sup> which are susceptible to deboronation and oxidation at elevated temperatures.<sup>21,22</sup> However, one of the major limitations of our initial silyl ether exchange vitrimer<sup>19</sup> as well as several other vitrimer systems<sup>3,11,18</sup> is the requirement of free hydroxyls on the polymers. The presence of many free hydroxyls is undesirable because they can introduce side reactions such as dehydration and oxidation at elevated temperatures, as well as possible reactions with polymers (e.g., transesterification with polyacrylates).<sup>23</sup> This would be undesirable for general vitrimer applications that involve multiple cycles of reprocessing/recycling at elevated temperatures.

To address this key limitation, we have been searching for new strategies for silyl ether exchange without the need of free hydroxyl groups. During our study, we discovered that silyl ether groups can directly exchange (i.e., silyl ether metathesis), which would eliminate the need for free hydroxyls (Figure 3.1). *To the best of our knowledge, this is the first report of direct silyl ether metathesis.* In addition to a new type of dynamic covalent

chemistry, the thermal and oxidative stability of silyl ether functionality lends itself towards general design of thermally robust vitrimers. Different from anionic siloxane exchange, which is limited to polysiloxanes,<sup>24,25</sup> silyl ether groups can be easily introduced post-polymerization by silylation of free hydroxyl,<sup>26</sup> methoxy,<sup>27</sup> and acetate<sup>28</sup> groups or by simple polymerization/co-polymerization with a silyl ether functionalized monomer.

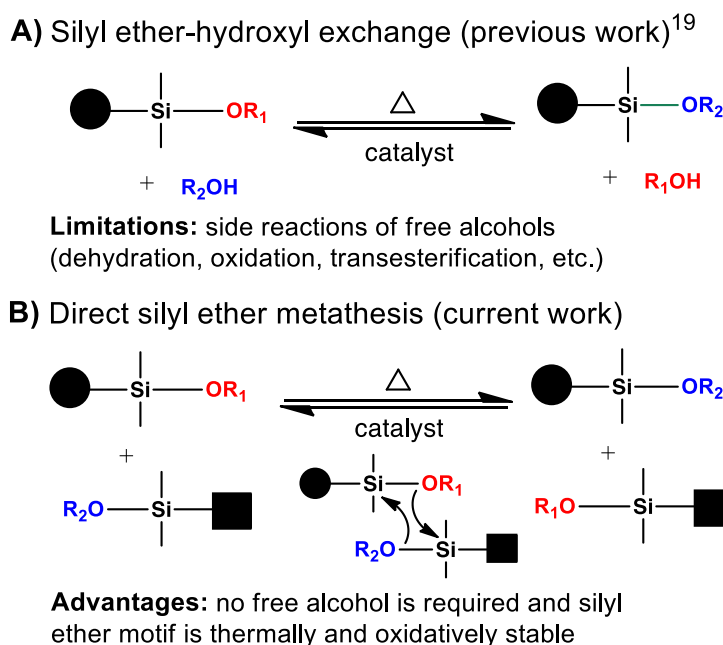


**Figure 3.1** Differences between silyl ether hydroxyl exchange and silyl ether metathesis for vitrimer design.

## 3.2 Results and Discussion

### 3.2.1 Small molecule synthesis and kinetic studies

First, the direct silyl ether metathesis reaction was discovered in our small molecule model studies. As shown in Figure 3.2A, an equimolar amount of ethyltributoxysilane (**B**<sub>3</sub>) and ethyltripentoxysilane (**P**<sub>3</sub>) were mixed in an anhydrous solvent with or without a

catalyst. The mixtures were heated at different temperatures and the exchange between butoxy and pentoxy groups was monitored by GC-MS (see detailed in Supporting Information). At time zero GC-MS showed two peaks with equal intensity for the two starting materials. As exchange proceeded, two additional peaks appeared with the masses matching the exchange products  $B_2P_1$  and  $B_1P_2$ , respectively. The intensity of the new peaks grew with time until reaching the expected 1:3:3:1 statistical distribution for  $B_3:B_2P_1:B_1P_2:P_3$  at equilibrium. Without the addition of any catalyst, the exchange proceeded slowly, reaching full exchange after 16.5 hours at 190 °C.

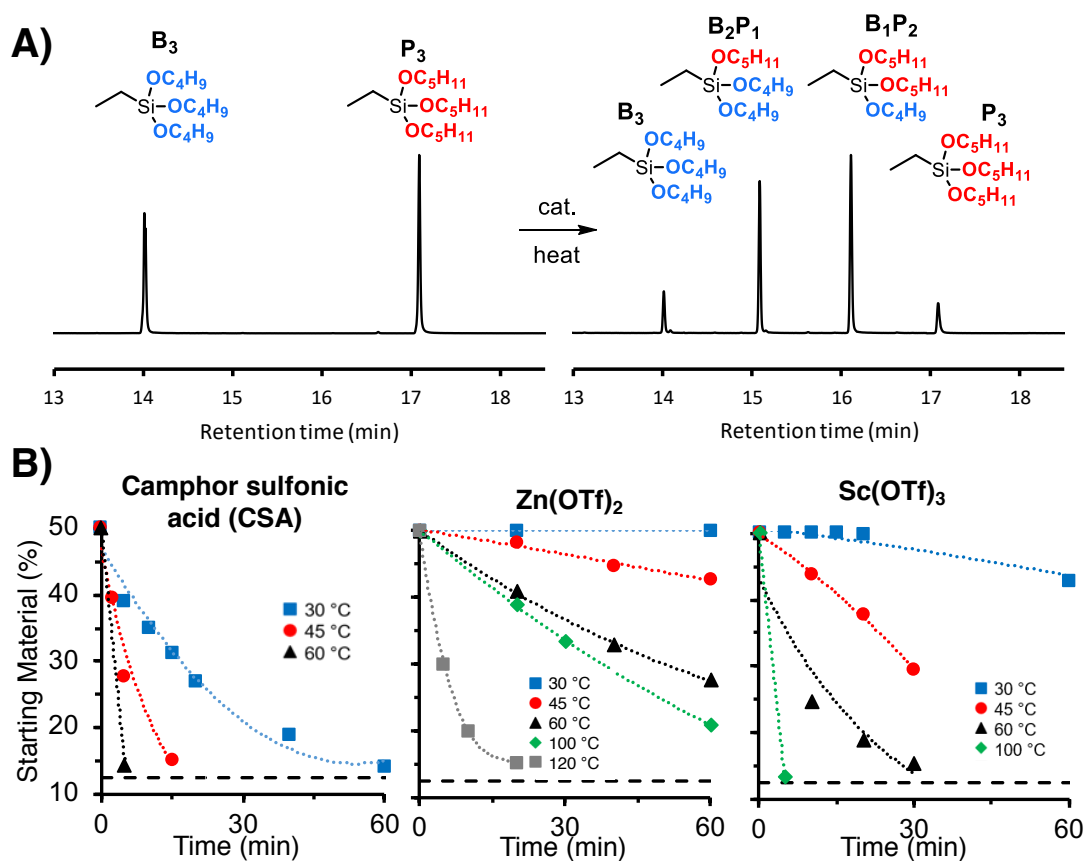


**Figure 3.2** Silyl ether metathesis. (a) Representative GC chromatograms of the equilibration of  $B_3$  and  $P_3$  to  $B_3$ ,  $B_2P_1$ ,  $B_1P_2$  and  $P_3$  with catalyst. (b) Kinetics of silyl ether exchange using different catalysts and temperatures.

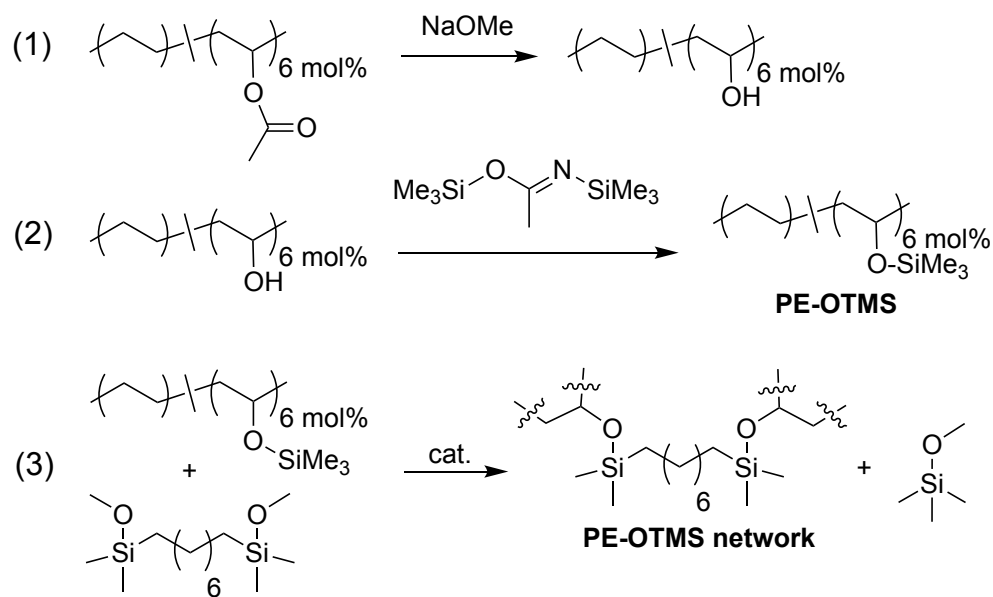


To accelerate the reaction, we added 5 mol% of a Brønsted acid (camphor sulfonic acid, CSA) or a Lewis acid ( $\text{Zn}(\text{OTf})_2$  and  $\text{Sc}(\text{OTf})_3$ ) catalyst (Figure 3.2B). Among the catalysts tested, CSA was found to be the most active catalyst and chosen for subsequent vitrimer studies. The exact mechanism for the direct silyl ether exchange is not clear at the moment. A simple proposal is direct exchange between silyl ethers, i.e., silyl ether metathesis (Figure 1B). Alternatively, the exchange can be facilitated by some transient reactive intermediates formed in the process. Notably, the GC-MS traces showed clean product distributions with no detectable byproducts (Figure 3.2A and S5–7), indicating clean exchange between the silyl ether compounds.

### 3.2.2 Synthesis of PE-OTMS and vitrimer preparation

Encouraged by the direct silyl ether metathesis reaction observed in our small molecule model studies, next we applied this new dynamic covalent chemistry to vitrimer designs. For initial demonstration, a low molecular weight poly(ethylene-co-vinyl acetate) (EVA, 6 mol% vinyl acetate, MFI = 150 g/10 min) was chosen for its inexpensive commercial availability and ease of processing. EVA was hydrolyzed quantitatively with sodium methoxide to yield poly(ethylene-co-vinyl alcohol) with 6 mol% alcohol. The free hydroxyls in the resulting polymer were fully silylated with N,O-bis(trimethylsilyl)acetamide to yield a trimethylsilyl (TMS) ether functional polymer (PE-OTMS) (Scheme 3.1). A divalent cross-linker, bis(methoxydimethyl)silyl octane, was synthesized from bis(chlorodimethyl)silyl octane via one step reaction with methanol. All the details for compound syntheses and characterizations can be found in the Supporting Information.

**Scheme 3.1.** Synthesis of PE-OTMS polymer and its vitrimer.



The vitrimer was prepared by dissolving PE-OTMS, the bis(methoxydimethyl)silyl octane cross-linker, and CSA in toluene at 80 °C. The cross-linker concentration was 3 mol% of the total -OTMS motifs and CSA concentration was held at 2 mol% of total -OTMS motifs. The excess of free -OTMS motifs on PE-OTMS backbone facilitate silyl ether metathesis with the silyl ether cross-links. After mixing, silyl ether metathesis between the cross-linker and PE-OTMS resulted in gelation. The gelled polymer was slowly dried and compression molded at 150 °C for 20 minutes at 400 psi for mechanical testing (see Supporting Information). The insoluble gel fraction of the samples was measured to be ~62% after incubating the processed polymer in hot anhydrous toluene for 16 hours, indicating a relatively high degree of cross-linking within the samples.

### 3.2.3 Mechanical and thermal testing

The thermal and mechanical properties of the vitrimer were carefully investigated. The Differential Scanning Calorimetry (DSC) trace for PE-OTMS showed a broad melting transition with the peak at 93 °C (Figure S12), consistent with the semi-crystalline structure of the PE backbone. Thermogravimetric Analysis (TGA) demonstrated the vitrimer having

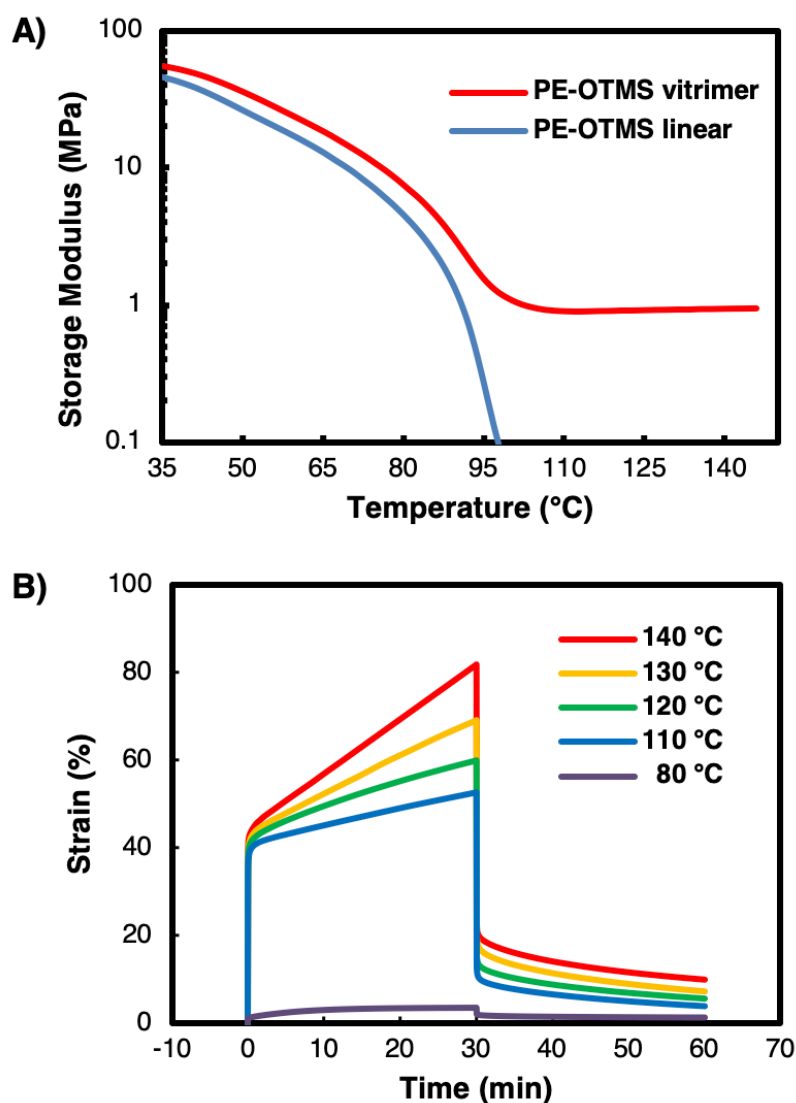


**Figure 3.3** Mechanical analysis of the linear control polymer and PE-OTMS vitrimer. (a) DMTA analysis of both the linear and crosslinked PE-OTMS. (b) Creep tests of the PE-OTMS vitrimer at different temperatures under 0.1 MPa stress.

exceptional thermal stability, with minimal loss below 400 °C and 5% loss of its original mass at 427 °C (Figure S14). To the best of our knowledge, this is the most thermally stable vitrimer reported so far. Because of no free hydroxyl groups, the current vitrimer has substantially higher thermal stability than our previous system using silyl ether-hydroxyl exchange.<sup>19</sup> The robustness of silyl ether moieties and lack of free hydroxyls should contribute to the high thermal stability.

Dynamic Mechanical Thermal Analysis (DMTA) clearly showed a rubber plateau after the melting transition at ~93 °C for the vitrimer in contrast to the linear polymer PE-OTMS which completely flowed after melting (Figure 3.3A). The vitrimer network retains mechanical strength after melting due to covalent cross-links. The molecular weight between cross-links ( $M_c$ ) was calculated to be 9.61 kD (see details in the Supporting Information). Furthermore, introducing silyl ether cross-links significantly improved the vitrimer creep resistance as compared to the PE-OTMS linear polymer. The linear polymer crept rapidly at 80 °C under 0.1 MPa stress (Figure S17). On the contrary, the vitrimer showed negligible creep under the same condition (80 °C, 0.1 MPa) (Figure 3.3B). At temperatures above the  $T_m$ , the vitrimers exhibit an initial elastic response followed by a transition into a linear creep region whereby dynamic silyl ether exchange occurs. As expected, the vitrimers display faster creep at increasing temperatures as the silyl metathesis reaction accelerates at higher temperatures.

To further quantify the silyl ether exchange dynamics in bulk, the silyl ether vitrimers were subjected to stress relaxation testing at elevated temperatures (130 – 170 °C) by applying a constant strain to the sample while monitoring the decrease of stress over time (Figure 3.4A). Consistent with the creep data, we observed faster stress relaxation at higher temperatures. The characteristic relaxation time,  $\tau^*$ , is defined as the time required for the modulus to decrease to  $e^{-1}$  (~37%) from the initial value. The relaxation time decreased from

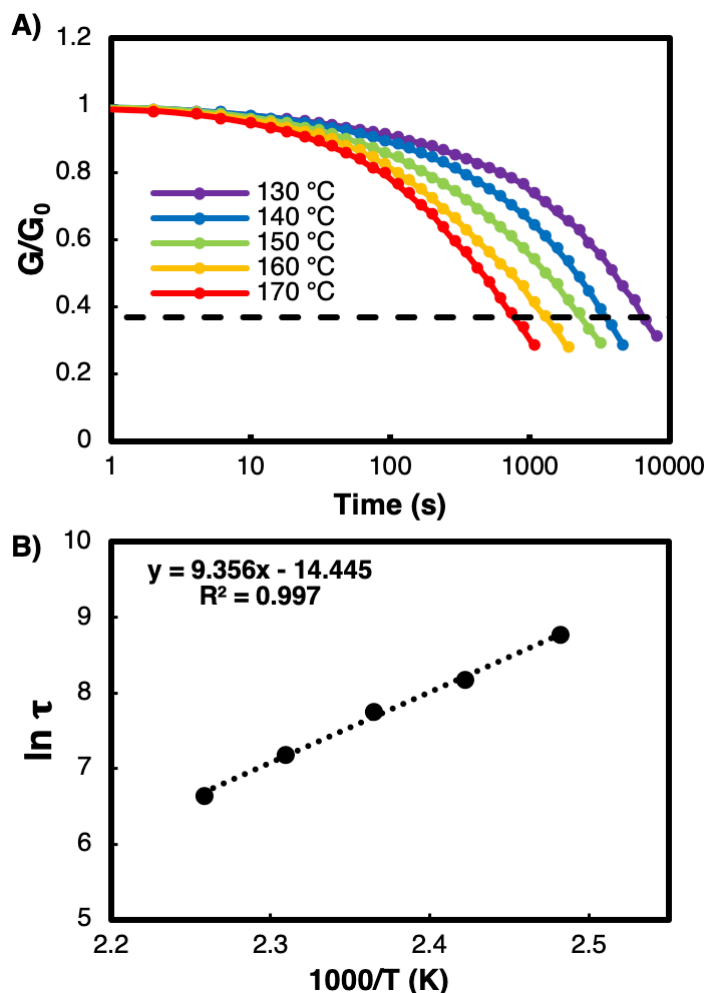


**Figure 3.4** Stress relaxation studies of PE-OTMS vitrimer. (a) Stress relaxations experiments were performed on using 5% strain in tensile mode. (b) An Arrhenius treatment was performed to the stress relaxation data to yield an energy of activation of 77.8 kJ/mol.

6,456 s to 770 s as the temperature increased from 130 °C to 170 °C. As silyl ethers appear to undergo direct exchange with temperature dependency, they should follow the characteristic vitrimer Arrhenius behavior as defined by equation 1:<sup>4,8,29</sup>

$$\tau^* = \tau_o \exp\left(\frac{E_A}{RT}\right) \quad (1)$$

By performing Arrhenius treatment to the stress relaxation data (Figure 3.4B), we can calculate the energy of activation for the silyl ether exchange. Plotting  $\ln(\tau)$  vs  $1000/T$  yields a straight line with the slope correlating to an energy of activation of 77.8 kJ/mol. The activation energy for our CSA-catalyzed silyl ether exchange is comparable to the 81 kJ/mol value previously reported for amine-catalyzed silyl ether-hydroxyl exchange by our lab.<sup>19</sup>

Another important parameter of vitrimers is the topology-freezing transition temperature ( $T_v$ ), the temperature at which the network topology is frozen through kinetic trapping of its internal dynamic chemistry. Following the reported protocols,<sup>3</sup> the  $T_v$  of the silyl ether vitrimer is calculated to be 45 °C. This transition temperature sits between the glass transition temperature ( $T_g \sim -125$  °C)<sup>30</sup> and melting temperature ( $T_m \sim 93$  °C) for the PE backbone.

The chemical cross-linking also significantly enhanced the mechanical properties of the polymer. Tensile stress-strain tests showed a five-fold increase in Young's Modulus from  $19.2 \pm 1$  to  $101 \pm 19$  for the PE-OTMS polymer and vitrimer, respectively (Figures 3.5C, S15, S16). The ultimate tensile strength also increased from  $5.5 \pm 0.6$  to  $8.3 \pm 0.2$  for the PE-OTMS polymer and vitrimer, respectively. Finally, we tested the reprocessability of the silyl ether vitrimers. To demonstrate reprocessability, a vitrimer sample was repetitively diced into

small pieces, melt pressed at 150 °C (Figure 3.5B), and subjected to mechanical and gel fraction tests. The tensile testing results show that the mechanical properties – including the Young’s modulus, tensile strength, elongation at break, and toughness – remain almost

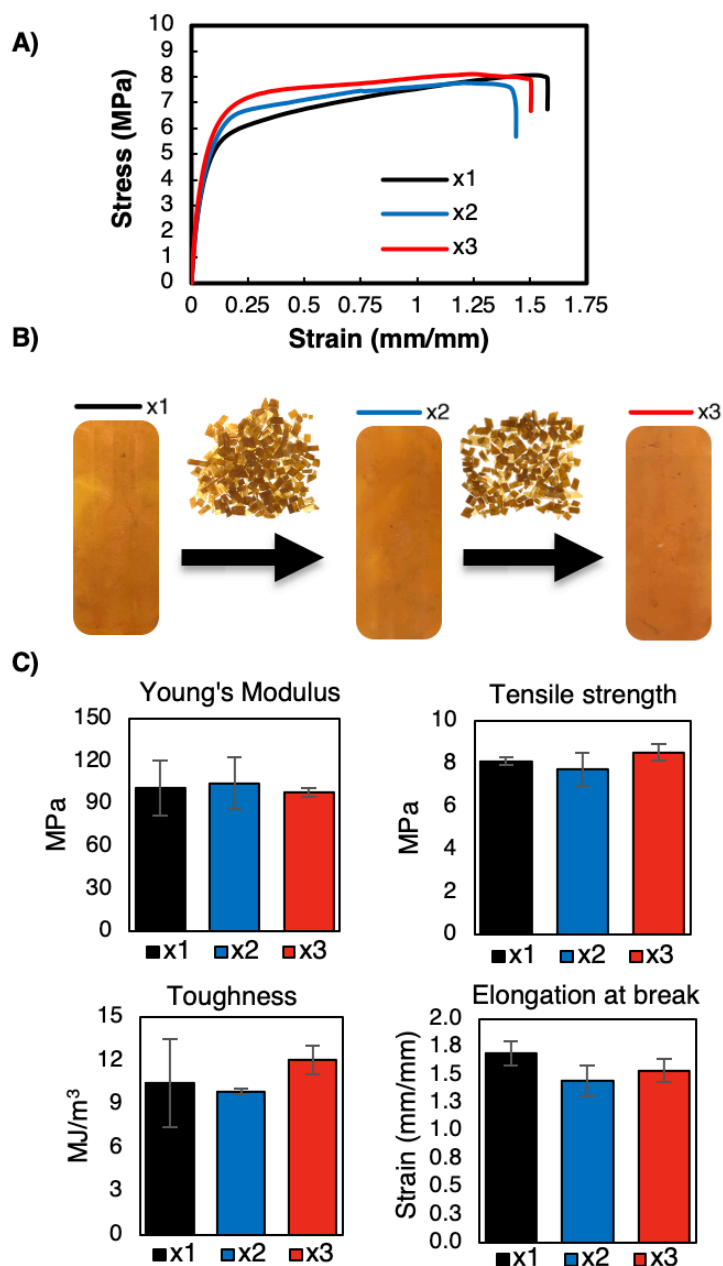


**Figure 3.5** Reprocessability testing for the PE-OTMS vitrimers. (a) Tensile test for the samples that were reprocessed x1, x2, and x3 times. (b) PE-OTMS samples were diced into small pieces, compression molded and reprocessed three times. (b) Mechanical properties of the recycled vitrimer (in triplicates).

constant for the repetitively reprocessed samples (Figure 3.5A). The gel fractions for the reprocessed samples also remain nearly constant (Table S1).

### 3.3 Conclusion

In summary, we report our discovery of a new silyl ether metathesis reaction and its application for vitrimer design. Owing to the thermal and oxidative stability of silyl ether motifs, this new dynamic covalent chemistry was demonstrably suitable for making mechanically robust and thermally stable vitrimers. Compared to previously reported transesterification<sup>3</sup> and silyl ether-hydroxyl exchange<sup>19</sup> for vitrimer designs, the current silyl ether metathesis avoids free hydroxyls which are susceptible to side reactions such as dehydration and oxidation at elevated temperatures. Indeed, the PE-OTMS vitrimers show exceptional thermal stability. To the best of our knowledge, this represents the most thermally stable vitrimers reported to date. The introduction of silyl ether cross-links to PE-OTMS significantly enhances its mechanical properties and creep resistance. The silyl ether vitrimer shows good creep resistance at temperatures below its  $T_m$  while maintaining malleability at temperatures above the  $T_m$ . Facilitated by silyl ether metathesis, the silyl ether vitrimers are fully reprocessable at elevated temperatures. Silyl ethers can be easily prepared by silylation of polymers bearing hydroxyl or its derivatives, copolymerization of monomers having silyl ether groups, or radical grafting with a silyl ether-containing a silyl ether motif. With the excellent attributes and synthetic feasibility of silyl ethers, we envision this new dynamic covalent chemistry can be generalized for various vitrimer synthesis and studies are currently underway toward this direction.



### 3.4 References

- (1) Kloxin, C. J.; Scott, T. F.; Adzima, B. J.; Bowman, C. N. Covalent Adaptable Networks (CANs): A Unique Paradigm in Cross-Linked Polymers. *Macromolecules* **2010**, *43* (6), 2643–2653.
- (2) Denissen, W.; Winne, J. M.; Du Prez, F. E. Vitrimers: Permanent Organic Networks with Glass-like Fluidity. *Chem Sci* **2016**, *7* (1), 30–38.
- (3) Montarnal, D.; Capelot, M.; Tournilhac, F.; Leibler, L. Silica-Like Malleable Materials from Permanent Organic Networks. *Science* **2011**, *334* (6058), 965–968.
- (4) Denissen, W.; Rivero, G.; Nicolaÿ, R.; Leibler, L.; Winne, J. M.; Prez, F. E. D. Vinylogous Urethane Vitrimers. *Advanced Functional Materials* **2015**, *25* (16), 2451–2457.
- (5) Denissen, W.; Droesbeke, M.; Nicolaÿ, R.; Leibler, L.; Winne, J. M.; Du Prez, F. E. Chemical Control of the Viscoelastic Properties of Vinylogous Urethane Vitrimers. *Nature Communications* **2017**, *8*, 14857.
- (6) Capelot, M.; Montarnal, D.; Tournilhac, F.; Leibler, L. Metal-Catalyzed Transesterification for Healing and Assembling of Thermosets. *J. Am. Chem. Soc.* **2012**, *134* (18), 7664–7667.
- (7) Pei, Z.; Yang, Y.; Chen, Q.; Terentjev, E. M.; Wei, Y.; Ji, Y. Mouldable Liquid-Crystalline Elastomer Actuators with Exchangeable Covalent Bonds. *Nature Materials* **2014**, *13* (1), 36–41. <https://doi.org/10.1038/nmat3812>.
- (8) Brutman, J. P.; Delgado, P. A.; Hillmyer, M. A. Polylactide Vitrimers. *ACS Macro Lett.* **2014**, *3* (7), 607–610. <https://doi.org/10.1021/mz500269w>.
- (9) Lu, Y.-X.; Guan, Z. Olefin Metathesis for Effective Polymer Healing via Dynamic Exchange of Strong Carbon–Carbon Double Bonds. *J. Am. Chem. Soc.* **2012**, *134* (34), 14226–14231.
- (10) Lu, Y.-X.; Tournilhac, F.; Leibler, L.; Guan, Z. Making Insoluble Polymer Networks Malleable via Olefin Metathesis. *J. Am. Chem. Soc.* **2012**, *134* (20), 8424–8427.
- (11) Fortman, D. J.; Brutman, J. P.; Cramer, C. J.; Hillmyer, M. A.; Dichtel, W. R. Mechanically Activated, Catalyst-Free Polyhydroxyurethane Vitrimers. *J. Am. Chem. Soc.* **2015**, *137* (44), 14019–14022.
- (12) Obadia, M. M.; Mudraboyina, B. P.; Serghei, A.; Montarnal, D.; Drockenmuller, E. Reprocessing and Recycling of Highly Cross-Linked Ion-Conducting Networks through Transalkylation Exchanges of C–N Bonds. *J. Am. Chem. Soc.* **2015**, *137* (18), 6078–6083.
- (13) Zhang, L.; Rowan, S. J. Effect of Sterics and Degree of Cross-Linking on the Mechanical Properties of Dynamic Poly(Alkylurea–Urethane) Networks. *Macromolecules* **2017**, *50* (13), 5051–5060.

- (14) Cromwell, O. R.; Chung, J.; Guan, Z. Malleable and Self-Healing Covalent Polymer Networks through Tunable Dynamic Boronic Ester Bonds. *J. Am. Chem. Soc.* **2015**, *137* (20), 6492–6495.
- (15) Ogden, W. A.; Guan, Z. Recyclable, Strong, and Highly Malleable Thermosets Based on Boroxine Networks. *J. Am. Chem. Soc.* **2018**, *140* (20), 6217–6220.
- (16) Röttger, M.; Domenech, T.; Weegen, R. van der; Breuillac, A.; Nicolaÿ, R.; Leibler, L. High-Performance Vitrimers from Commodity Thermoplastics through Dioxaborolane Metathesis. *Science* **2017**, *356* (6333), 62–65.
- (17) Taynton, P.; Yu, K.; Shoemaker, R. K.; Jin, Y.; Qi, H. J.; Zhang, W. Heat- or Water-Driven Malleability in a Highly Recyclable Covalent Network Polymer. *Advanced Materials* **2014**, *26* (23), 3938–3942.
- (18) Li, Q.; Ma, S.; Wang, S.; Yuan, W.; Xu, X.; Wang, B.; Huang, K.; Zhu, J. Facile Catalyst-Free Synthesis, Exchanging, and Hydrolysis of an Acetal Motif for Dynamic Covalent Networks. *Journal of Materials Chemistry A* **2019**, *7*, 18039–18049.
- (19) Nishimura, Y.; Chung, J.; Muradyan, H.; Guan, Z. Silyl Ether as a Robust and Thermally Stable Dynamic Covalent Motif for Malleable Polymer Design. *J. Am. Chem. Soc.* **2017**, *139* (42), 14881–14884.
- (20) Walsh, R. Bond Dissociation Energy Values in Silicon-Containing Compounds and Some of Their Implications. *Acc. Chem. Res.* **1981**, *14* (8), 246–252.
- (21) Lappert, M. F. Organic Compounds of Boron. *Chem. Rev.* **1956**, *56* (5), 959–1064.
- (22) Hall, D. G. *Structure, Properties, and Preparation of Boronic Acid Derivatives. Overview of Their Reactions and Applications*; Wiley: New York, NY, 2005.
- (23) Smith, M.; March, J. *March's Advanced Organic Chemistry*, 6th ed.; John Wiley & Sons, Ltd: Hoboken, NJ, 2006.
- (24) Zheng, P.; McCarthy, T. J. A Surprise from 1954: Siloxane Equilibration Is a Simple, Robust, and Obvious Polymer Self-Healing Mechanism. *J. Am. Chem. Soc.* **2012**, *134* (4), 2024–2027.
- (25) Schmolke, W.; Perner, N.; Seiffert, S. Dynamically Cross-Linked Polydimethylsiloxane Networks with Ambient-Temperature Self-Healing. *Macromolecules* **2015**, *48* (24), 8781–8788.
- (26) Mormann, W.; Wagner, T. Silylation of Poly(Vinyl Alcohol) with Hexamethyldisilazane in Liquid Ammonia. *Journal of Polymer Science Part A: Polymer Chemistry* **1995**, *33* (7), 1119–1124.
- (27) Yang, J.; White, P. S.; Brookhart, M. Scope and Mechanism of the Iridium-Catalyzed Cleavage of Alkyl Ethers with Triethylsilane. *J. Am. Chem. Soc.* **2008**, *130* (51), 17509–17518.
- (28) Adachi, K.; Toyomura, S.; Miyakuni, Y.; Yamazaki, S.; Honda, K.; Hirano, T. Dioxomolybdenum(VI) and Dioxotungsten(VI) Complexes: Efficient Catalytic Activity

for Crosslinking Reaction in Ethylene-Vinyl Acetate Copolymer/Alkoxysilane Composites. *Polymers for Advanced Technologies* **2015**, 26 (6), 597–605.

- (29) Self, J. L.; Dolinski, N. D.; Zayas, M. S.; Read de Alaniz, J.; Bates, C. M. Brønsted-Acid-Catalyzed Exchange in Polyester Dynamic Covalent Networks. *ACS Macro Lett.* **2018**, 7 (7), 817–821.
- (30) Brandrup, J.; Immergut, E. H. *Polymer Handbook*, 3rd ed.; John Wiley & Sons, 1989.

## 3.5 Experimental

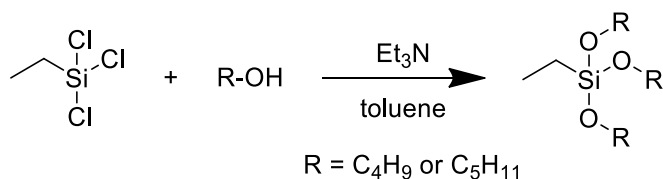
### General Experimental information

Unless otherwise noted, reactions were carried out with dry solvents using a magnetic stir bar. Commercial reagents were used as received with no further purification, unless otherwise noted.  $^1\text{H}$  NMR spectra were recorded at either 500 MHz on a Bruker DRX500 spectrometer or at 600 MHz on a Bruker AVANCE600 spectrometer.  $^{13}\text{C}$  NMR spectra were recorded at 125.2 MHz using a Bruker AVANCE600 with a BBFO cryoprobe. NMR spectra peaks are reported as  $\delta$  values in ppm relative to TMS or residual solvent:  $\text{CDCl}_3$  ( $^1\text{H} = 7.26$  ppm;  $^{13}\text{C} = 77.0$  ppm),  $\text{C}_6\text{D}_6$  ( $^1\text{H} = 7.16$  ppm,  $^{13}\text{C} = 128.06$  ppm).  $^1\text{H}$  NMR data are reported as follows: chemical shift in ppm, multiplicity (s = singlet, d = doublet, t = triplet), coupling constants in Hz, and relative integration of the number of protons. Multiplets (m) are reported over the range of chemical shift at which they appear. For  $^{13}\text{C}$  NMR, only chemical shift values are reported. Tensile tests were performed on an Instron 3365 mechanical tester. Differential Scanning Calorimetry (DSC) thermograms were evaluated using a TA Instruments Q2500. Thermogravimetric Analysis (TGA) thermograms were evaluated using a TA Instruments Q500. Dynamic Mechanical Thermal Analysis (DMTA) analysis was evaluated using a TA Instruments Q800. Gas chromatography-mass spectrometry experiments (GC-MS) were taken using a Thermo Scientific ISQ GC Ultra.

## Small molecule model studies for silyl ether metathesis

### *Synthesis of model compounds*

**Scheme S1.** Synthesis of ethyltributoxysilane and ethyltripentoxysilane.



Representative synthesis of alkoxy silanes: To a flame-dried N<sub>2</sub>-purged round bottom flask equipped with an air condenser, toluene (30 mL), triethylamine (5 equiv., 8.82 g, 13.77 mL), and alcohol (5 equiv.) were added. The flask was cooled to 0 °C followed by the dropwise addition of trichloroethylsilane (1 equiv., 2.64 mL). The vessel was brought to reflux at 115 °C for 5 hours. After cooling to room temperature, the reaction mixture was filtered to remove TEA-HCl salts followed by the removal of excess alcohol by rotary evaporation. The crude mixture was purified by vacuum distillation to yield a clear liquid. The identity and purity of the product was confirmed by <sup>1</sup>H NMR and <sup>13</sup>C NMR.

R = C<sub>4</sub>H<sub>9</sub>: 3.53 g, 64% yield

R = C<sub>5</sub>H<sub>9</sub>: 3.26 g, 51% yield

**EtSi(OBu)<sub>3</sub>** <sup>1</sup>H NMR (500 MHz, CDCl<sub>3</sub>, 298 K) δ 3.74 (t, J=6.7, 6H), 1.56 (m, 6H), 1.38 (sxt, J=7.6, 6H), 0.99 (t, J=8.0, 3H), 0.92 (t, J=7.4, 9H), 0.62 (q, J=8.0, 2H). <sup>13</sup>C NMR (125 MHz, CDCl<sub>3</sub>, 298 K) δ 62.60, 34.83, 19.07, 14.00, 6.69, 2.32.

**EtSi(OPn)<sub>3</sub>** <sup>1</sup>H NMR (500 MHz, CDCl<sub>3</sub>, 298 K) δ 3.73 (t, J=6.8, 6H), 1.57 (m, 6H), 1.33 (m, 12H), 0.99 (t, J=8.0, 3H), 0.90 (m, 9H), 0.62 (q, J=8.0, 2H). <sup>13</sup>C NMR (125 MHz, CDCl<sub>3</sub>, 298 K) δ 62.92, 32.42, 28.10, 22.62, 14.21, 6.70, 2.33.

***NMR Spectra of small molecule model compounds***

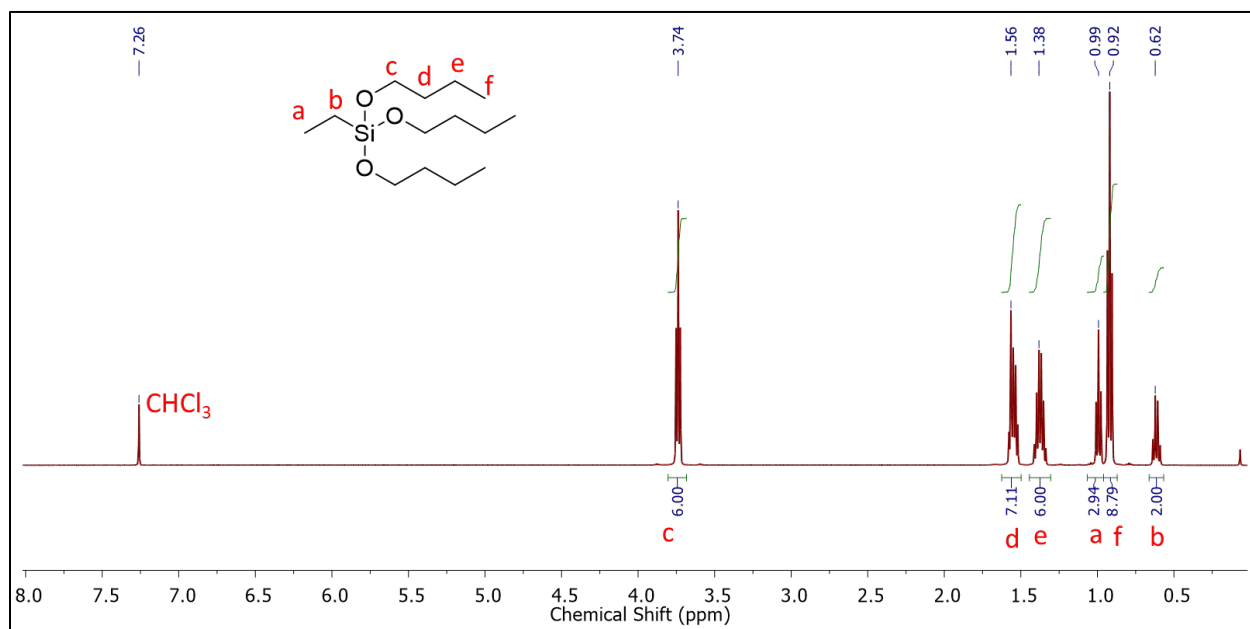


**Figure S1.** <sup>1</sup>H NMR (500 MHz, CDCl<sub>3</sub>, 298 K) spectrum for **EtSi(OBu)<sub>3</sub>**

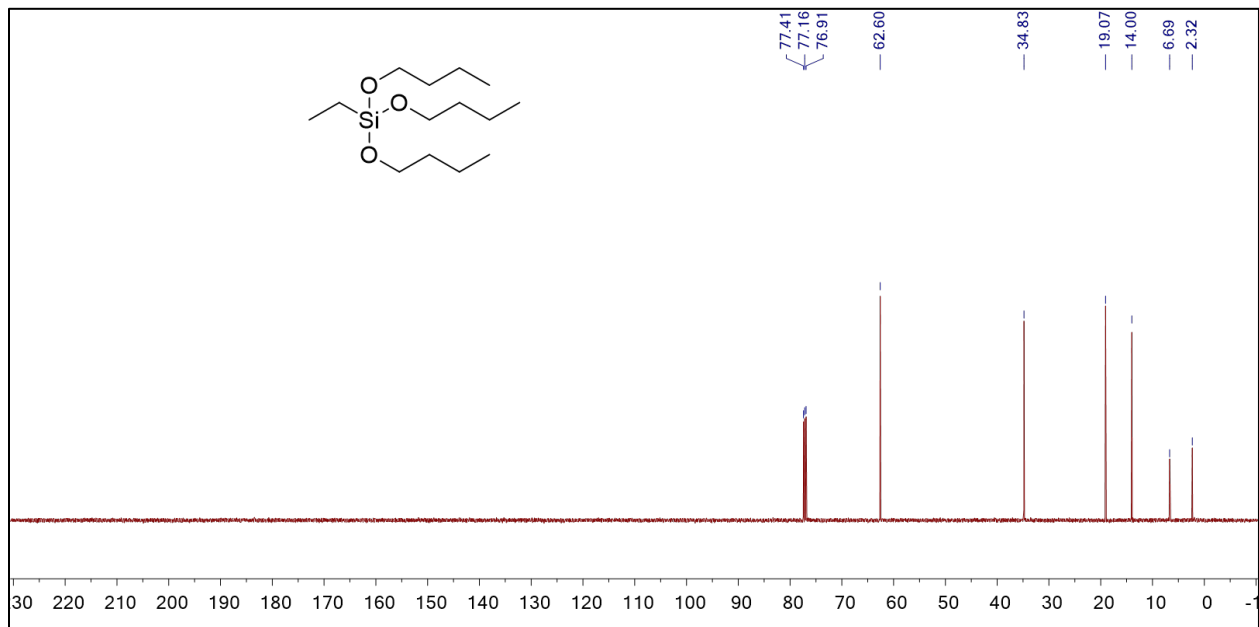


**Figure S2.**  $^{13}\text{C}$  NMR (125 MHz,  $\text{CDCl}_3$ , 298 K) spectrum for **EtSi(OBu) $_3$**

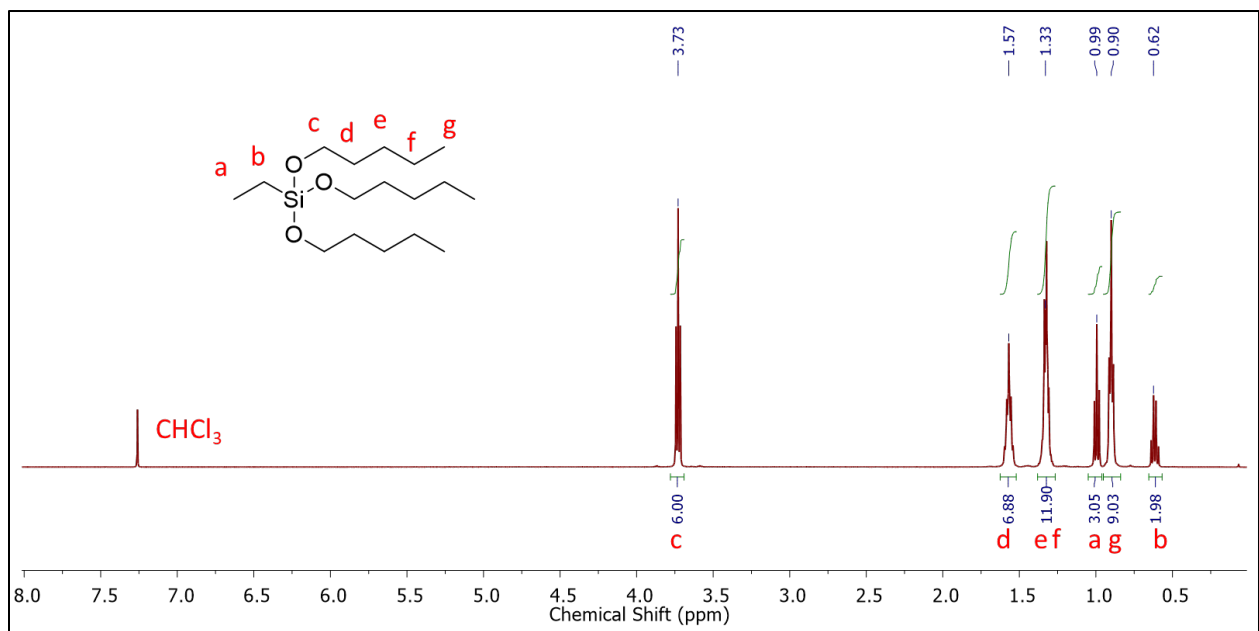


**Figure S3.**  $^1\text{H}$  NMR (500 MHz,  $\text{CDCl}_3$ , 298 K) spectrum for **EtSi(OPn) $_3$**

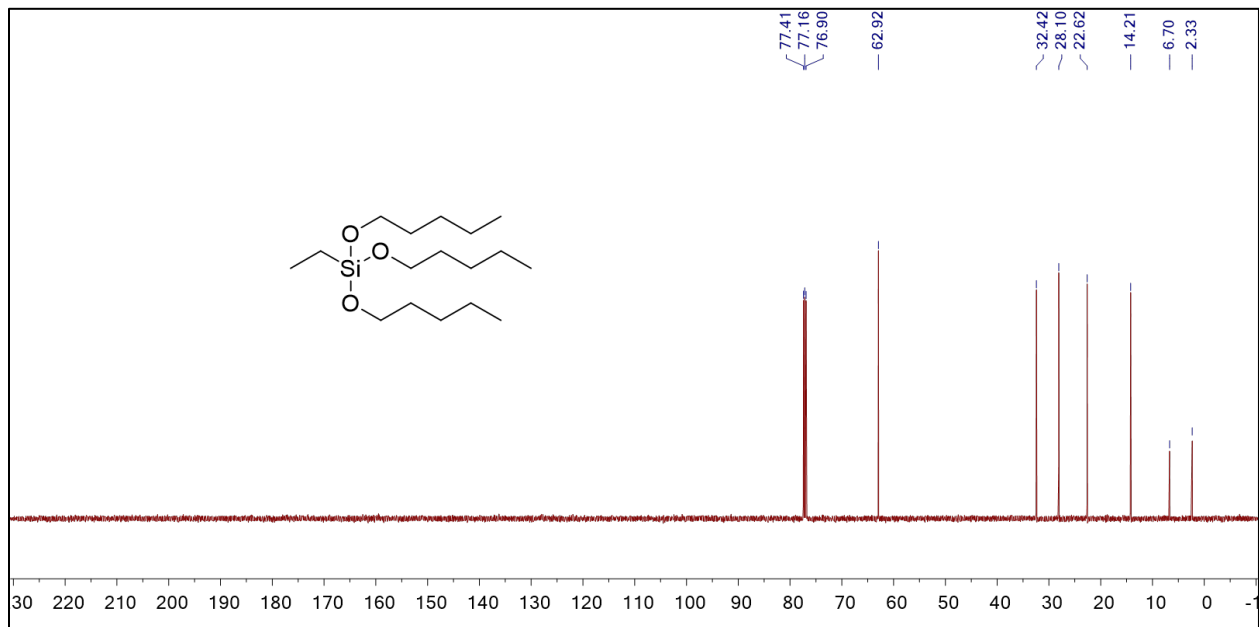


**Figure S4.**  $^{13}\text{C}$  NMR (125 MHz,  $\text{CDCl}_3$ , 298 K) spectrum for  $\text{EtSi}(\text{OPn})_3$



### ***Small molecule silyl ether exchange studies***

Silyl ether metathesis model reactions were investigated under different temperatures with different acid catalysts. After a brief screen of multiple Lewis acid and Brønsted acid catalysts, the three most promising were found to be camphor sulfonic acid (CSA),  $\text{Zn}(\text{OTf})_2$ , and  $\text{Sc}(\text{OTf})_3$ . The model exchange reaction was performed as following: Dimethylacetamide (0.33 mL) and catalyst (0.1 equiv., 0.033 mmol) were added to a flame dried and  $\text{N}_2$ -purged flask, followed by  $\text{EtSi}(\text{OBu})_3$  (1 equiv., 0.33 mmol, 0.092 g) and  $\text{EtSi}(\text{OPn})_3$  (1 equiv., 0.33 mmol, 0.106 g) via tared syringe. For the small molecule model exchange without catalyst, anhydrous trichlorobenzene was used instead of dimethylacetamide due to its higher boiling point. The flask was heated to the indicated reaction temperature. Aliquots were taken at different points and analyzed via gas chromatography mass spectrometry (GC-MS).

**Representative GC-MS chromatograms for model reaction studies**

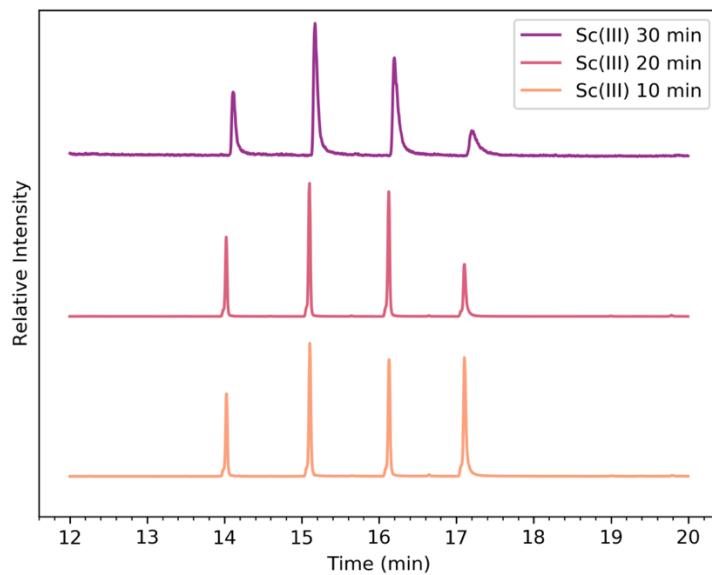


**Figure S5.** GC-MS chromatogram for Sc(OTf)<sub>3</sub> catalyzed silyl ether exchange at 60 °C.

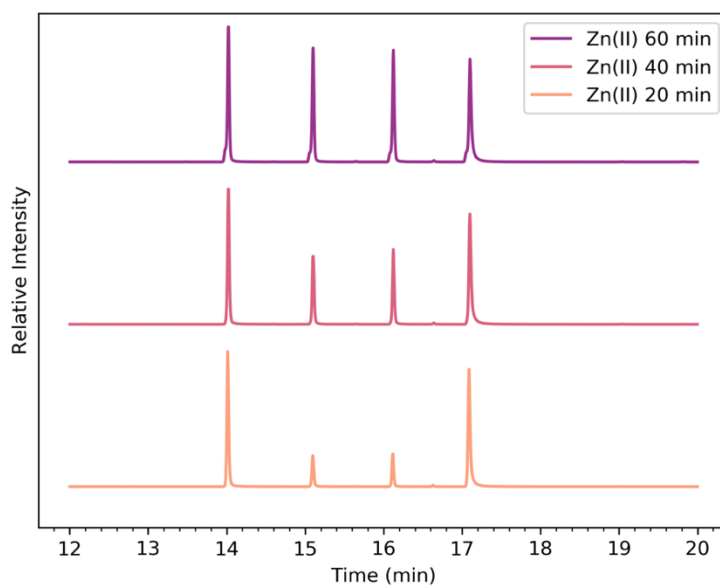


**Figure S6.** GC-MS chromatogram for Zn(OTf)<sub>2</sub> catalyzed silyl ether exchange at 60 °C.

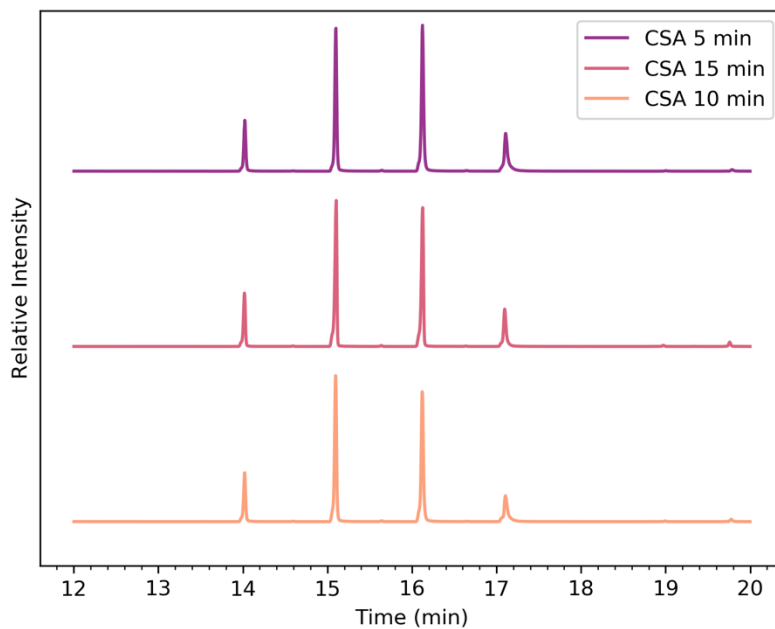
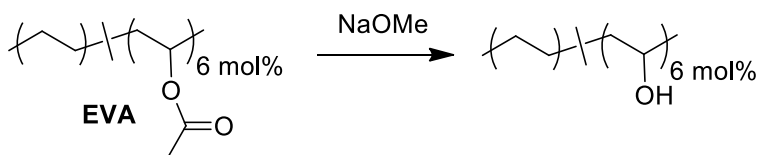


**Figure S7.** GC-MS chromatogram for CSA catalyzed silyl ether exchange at 60 °C.

## Synthesis of silyl ether functionalized polymer and cross-linker

### *Modification of polymer backbone*

#### **Scheme S2.** Hydrolysis of EVA.



Poly(ethylene-co-vinyl acetate) (**EVA**) (50 g, Celanese 1850A, 18.2 wt% VA, MFI = 150 g/10 min) was dissolved in 1 L toluene and heated to 75 °C. To the stirred solution, 25 wt.%

sodium methoxide in methanol (1.5 equiv., 34.3 g) was added and the solution was stirred overnight. Finally, to the gently stirring solution HCl (1 equiv., 3 M, 52.3 mL) was added followed by stirring for 20 minutes. The aqueous layer was removed via cannulation and the organic phase was washed twice with hot brine to reduce the emulsion. The resulting organic phase was washed twice with hot brine to reduce the emulsion. The resulting organic phase was precipitated into vigorously stirred MeOH, filtered and dried under vacuum overnight at 85 °C to yield poly(ethylene-co-vinyl alcohol) which was characterized by  $^1\text{H}$  NMR spectroscopy.

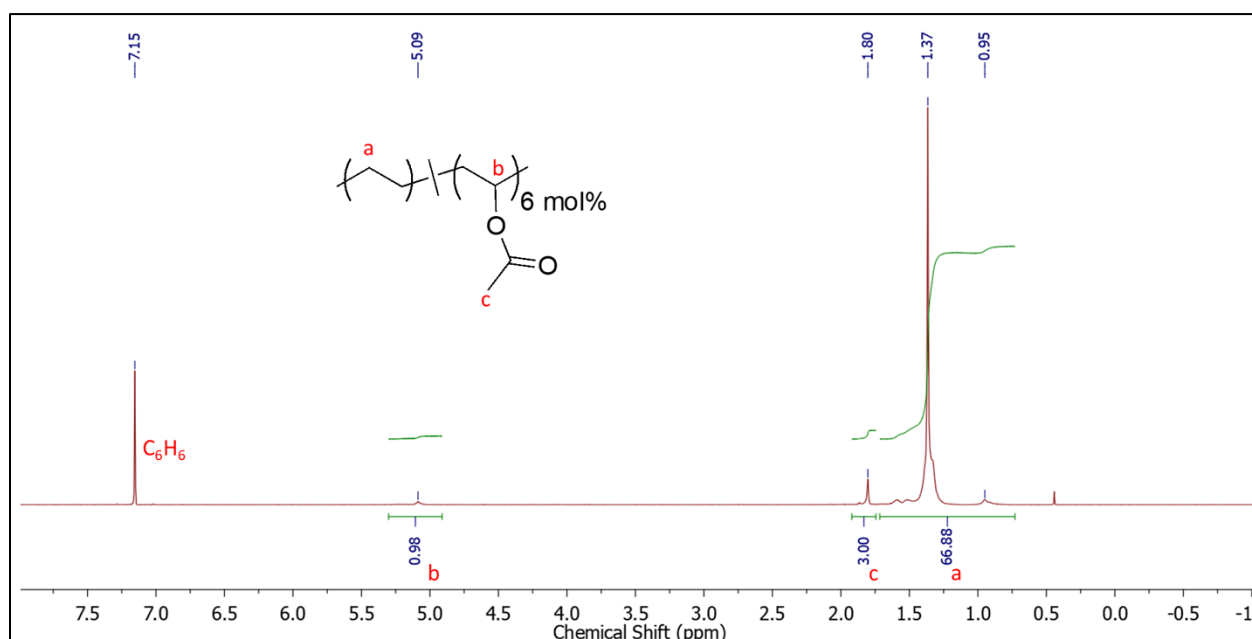


**Figure S8.**  $^1\text{H}$  NMR (600 MHz,  $\text{C}_6\text{D}_6$ , 333 K) spectrum of EVA

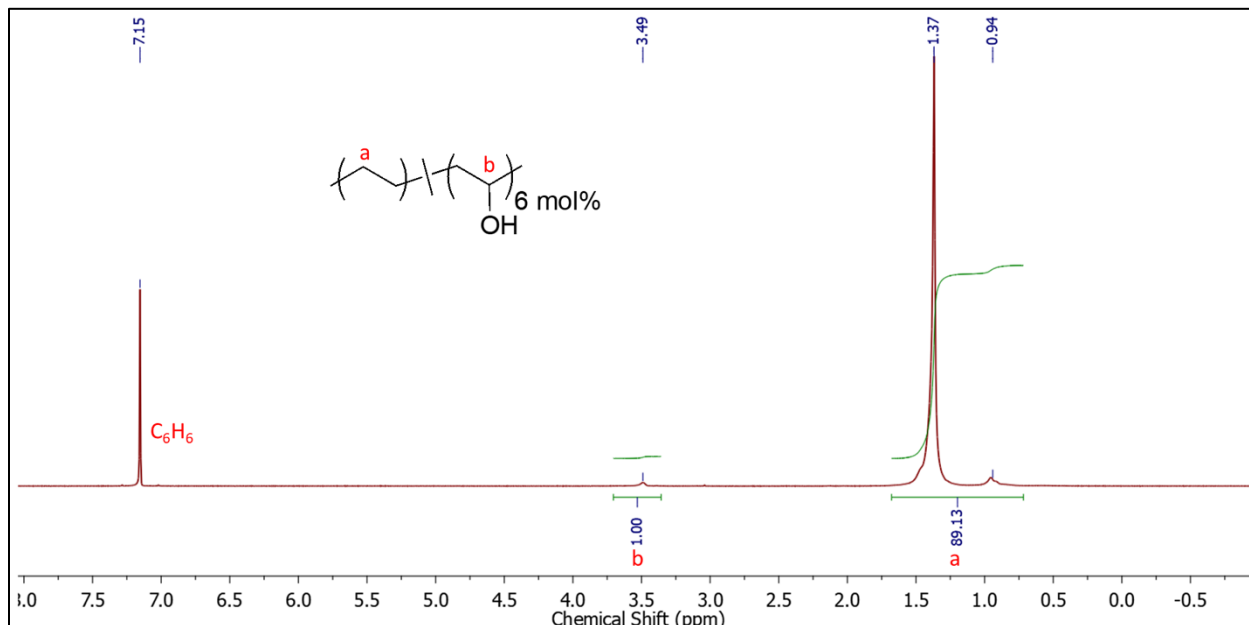
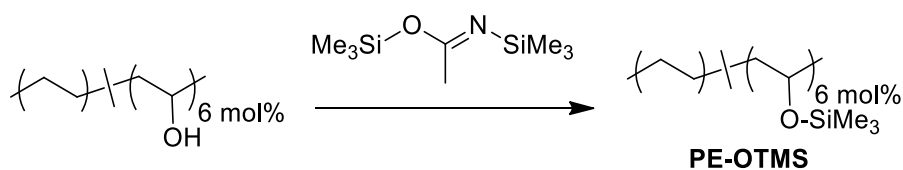


**Figure S9.**  $^1\text{H}$  NMR (600 MHz,  $\text{C}_6\text{D}_6$ , 333 K) spectrum of **Poly(ethylene-co-vinyl alcohol)**

**Scheme S3.** Silylation of poly(ethylene-co-vinyl alcohol)



Poly(ethylene-co-vinyl alcohol) (10.1 g) was dissolved in 200 mL toluene and heated to 75 °C. To the stirred solution, N,O-bis(trimethylsilyl) acetamide (BSA, 3 equiv., 14.28 g, 17.16 mL) was added dropwise via syringe. The reaction mixture stirred overnight, followed by rotary evaporation to remove excess solvent. The light orange polymer was then further dried under high vacuum to remove residual BSA and N-trimethylsilyl acetamide by-product, yielding **PE-OTMS** as the final product.

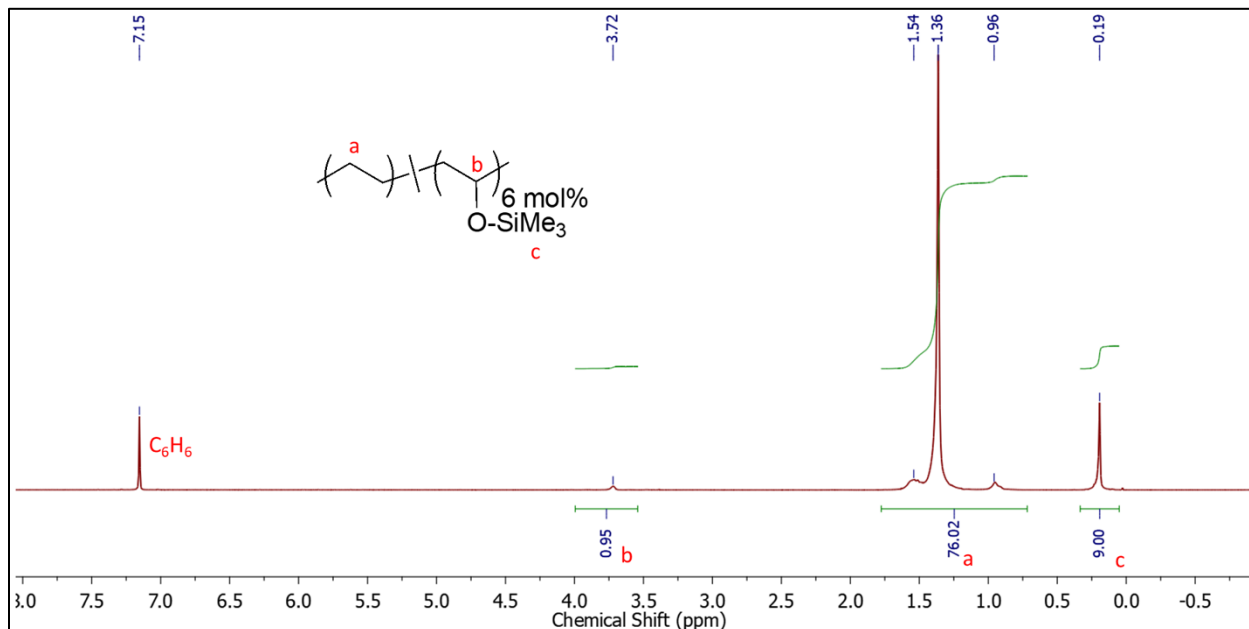
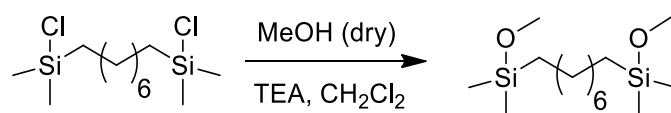


**Figure S10.**  $^1\text{H}$  NMR (600 MHz,  $\text{C}_6\text{D}_6$ , 333 K) spectrum of **PE-OTMS**.

### *Synthesis of cross-linker*

#### **Scheme S4.** Synthesis of cross-linker.



To a flame-dried round bottom flask, anhydrous dichloromethane (20 mL) and 1,8-bis(chlorodimethylsilyl)octane (1 equiv., 15 mmol, 4.61 mL) were added. The flask was sealed with a septum and anhydrous methanol (2.2 equiv., 33 mmol, 1.33 mL) was added, followed by the dropwise addition of TEA (2.2 equiv., 33 mmol, 4.60 mL). The mixture stirred for 1 hour followed by rotary evaporation. The resulting crude product was washed with diethyl ether (50 mL x 2) and filtered through a pad of celite to remove ammonium salts. The

diethyl ether was removed via rotary evaporation to yield a clear, slightly yellow liquid (95% yield). The identity of the product was determined via  $^1\text{H}$  NMR.

**1,8-bis(methoxydimethylsilyl)octane**  $^1\text{H}$  NMR (500 MHz,  $\text{CDCl}_3$ , 298K)  $\delta$  3.42 (s, 6H), 1.31 (m, 6H), 1.27 (m, 6H), 0.59 (t,  $J = 7$  Hz, 3H), 0.09 (s, 12 H).

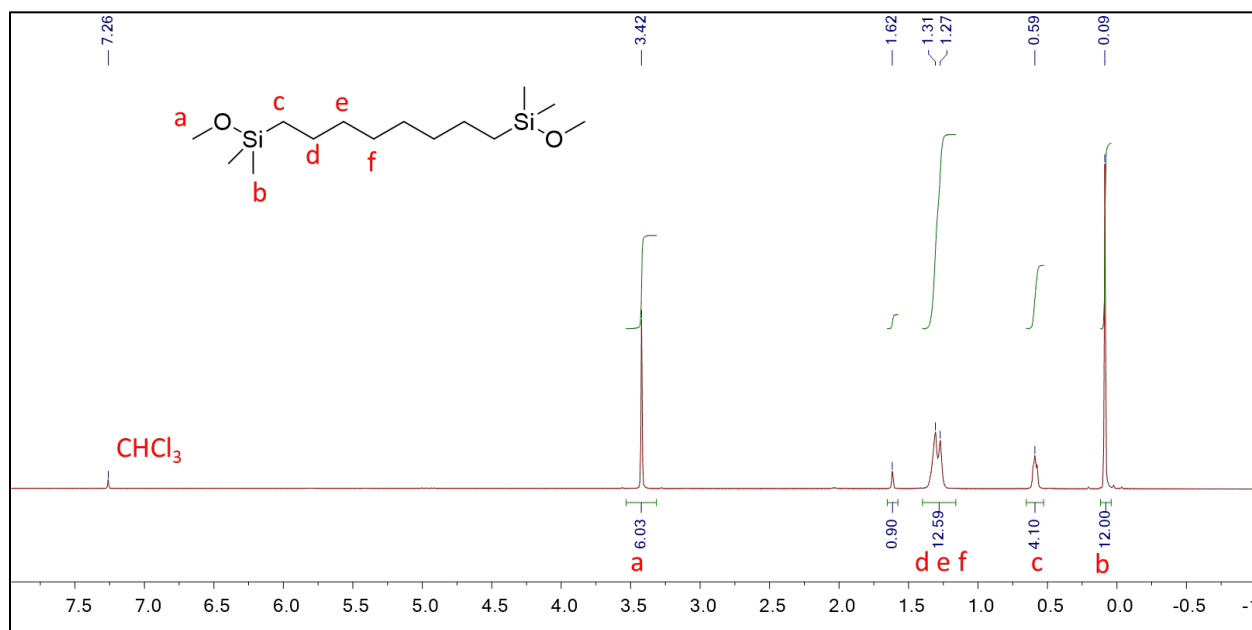


**Figure S11.**  $^1\text{H}$  NMR (500 MHz,  $\text{CDCl}_3$ , 298 K) spectrum of **1,8-bis(methoxydimethylsilyl)octane**

## Vitrimer preparation and studies

Into a flame-dried test tube, 3 g of PE-OTMS (6 mol% silyl ether) was added, sealed with a septum, and flushed with N<sub>2</sub>. Anhydrous toluene (15 mL) was added via syringe and heated to 75 °C until dissolved. Separately, a stock solution of CSA catalyst was prepared in anhydrous toluene. To the dissolved PE-OTMS, CSA (2 mol% relative to silyl ether, 0.123 mmol, 28.5 mg) was added and stirred to homogenize. The bis-silyl ether cross-linker (3 mol% relative to silyl ether motif on polymer, 0.184 mmol, 53.5 mg) was then added dropwise while vigorously mixing. The temperature was maintained at 75 °C, and the viscosity increased over the course of 10 minutes until the solution became completely gelled. After 30 minutes the gel was removed from the test tube, moved to a PTFE dish, and placed in a N<sub>2</sub>-flushed vacuum oven heated at 90 °C to slowly dry for 4 hours. High vacuum was then pulled for 6 hours to remove residual solvent.

The cross-linked network was then cut into small pieces and compression molded with a Specac West 6100+ High Temperature Hot Press. The cut pieces were placed into preheated PTFE molds at 150 °C and pressurized to 2 tons (~400 psi) for 20 minutes followed by a 30-minute cooldown to room temperature. Samples were then annealed at 150 °C for 4 hours under gentle pressure prior to testing to ensure full sintering of cut pieces. For reprocessing, the samples were cut into small pieces (approximately 1 mm<sup>3</sup>) with a razor and compression molded as previously described.



### ***Gel fraction testing***

To test the gel fraction, samples were cut into approximately 30 mg pieces and suspended in excess solvent (dry toluene, 20 mL). The pieces were then swollen by heating to 70 °C for 16 hours. This allowed for un-crosslinked polymer chains to diffuse into the excess solvent, leaving the cross-linked network in the swollen state. The swollen samples were then removed from solvent and dried in a heated vacuum chamber to remove any residual solvent. The weight before and after testing was recorded and the weight fractions are listed in Table 1.

**Table S1.** Gel fraction data for reprocessed vitrimer samples

Reprocessing	Before	After	Insoluble fraction (%)
Processed x1	28.9 mg	18.2 mg	63.0%
Processed x2	31.6 mg	19.5 mg	61.7%
Processed x3	36.3 mg	23.2 mg	64.0 %

### ***Thermal characterization of PE-OTMS vitrimer.***

Differential Scanning Calorimetry (DSC) measurements were performed on PE-OTMS linear and vitrimer samples using ~10 mg of material in an aluminum non-hermetic pan (Figure S12 and S13). Samples were scanned against an empty reference pan from -50 °C to 150 °C at a ramp rate of 20 °C/min. PE-OTMS was found to have a broad melting range from 54 °C to 104 °C with the peak endotherm at 93 °C. To determine the degree of crystallinity of PE-OTMS, the area of the endotherm (94.5 J/g) is divided by the enthalpy of melting for crystalline LDPE<sup>1</sup> (293 J/g) to give a 32.3% crystalline content. DSC endotherms were calibrated to an indium standard reference.

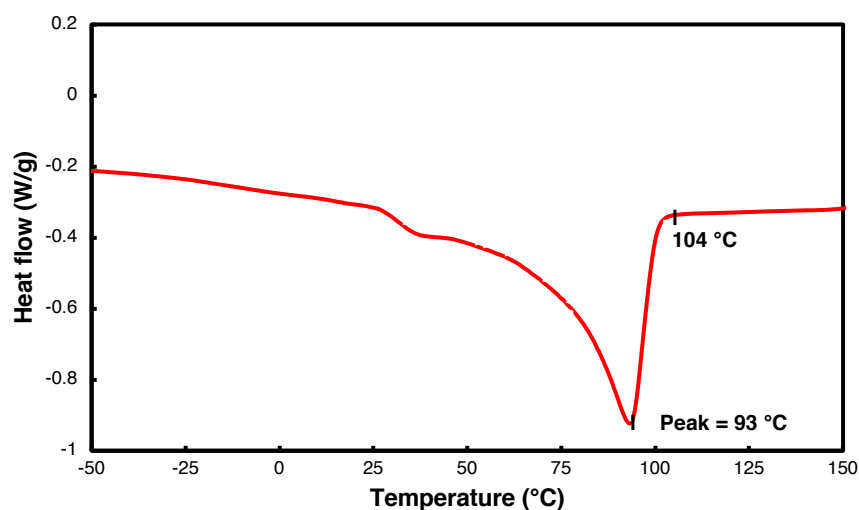


**Figure S12.** DSC thermogram of PE-OTMS vitrimer from -50 °C to 150 °C.

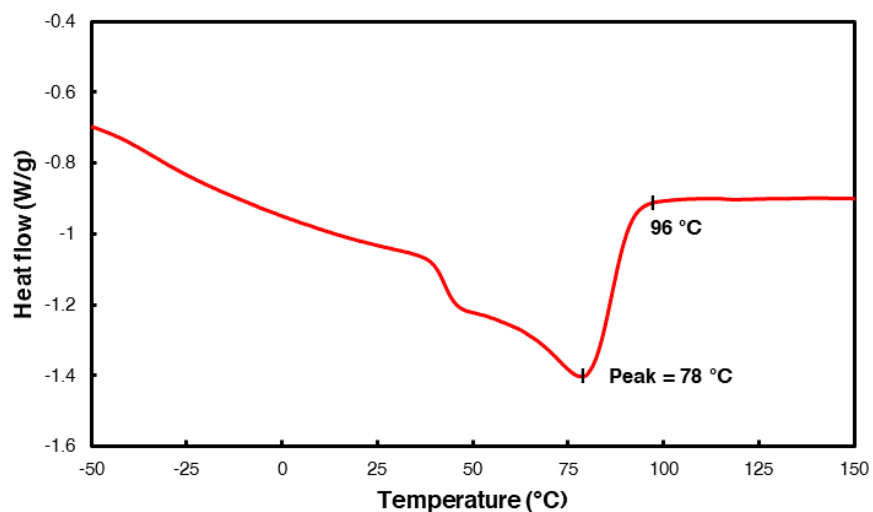


**Figure S13.** DSC thermogram of linear PE-OTMS from -50 °C to 150 °C.

Thermogravimetric analysis (TGA) was performed to determine polymer stability (Figure S14). The sample was placed in a platinum crucible under constant N<sub>2</sub> flow and heated to 850 °C at 20 °C/min. The sample had lost ~5% of its original mass at 427 °C and completely degraded at ~ 500 °C.

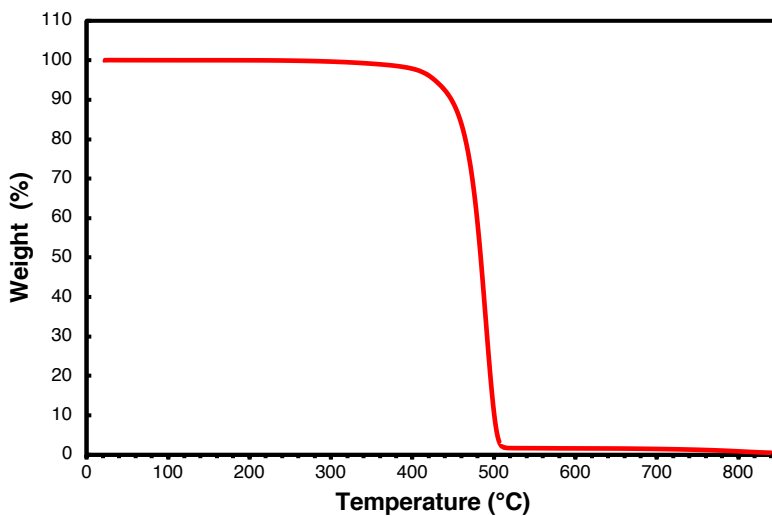


**Figure S14.** TGA thermogram of PE-OTMS vitrimer.

### ***Tensile testing of PE-OTMS vitrimer***

For tensile testing, the samples were compression molded as previously described and cut into approximately 3 mm x 2 mm x 25 mm strips. Tensile testing was performed at room temperature at a pull rate of 0.5 mm/mm/min. All samples broke cleanly between the clamps.

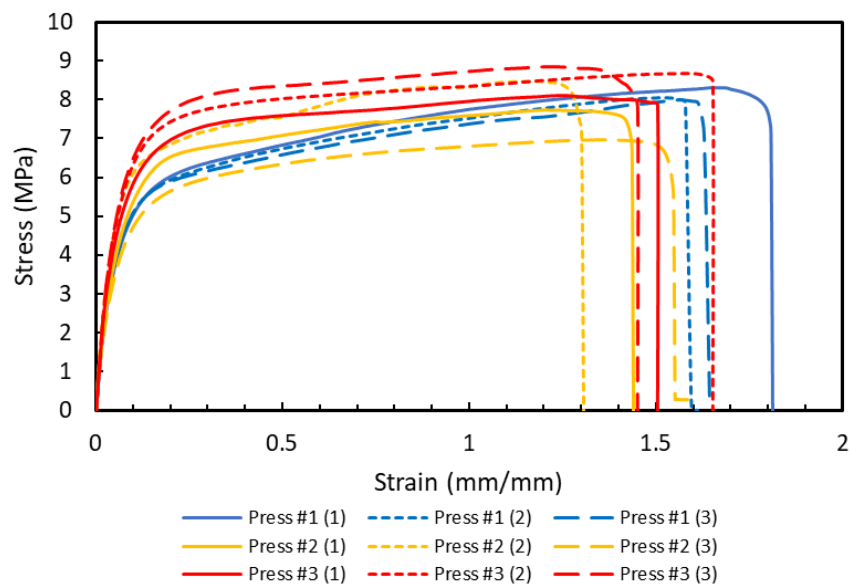


**Figure S15.** Tensile testing of PE-OTMS vitrimer over three iterations of reprocessing.

**Table S2.** Mechanical properties of repetitively reprocessed PE-OTMS vitrimer (triplicates).

	x1	x2	x3
Young's Modulus (MPa)	101 ± 19	132 ± 16	98 ± 3
Tensile Strength (MPa)	8.3 ± 0.2	7.7 ± 0.8	8.1 ± 0.4
Toughness (MJ/m <sup>3</sup> )	13.1 ± 3.0	10.0 ± 0.2	11.2 ± 1.0
Elongation (mm/mm)	1.8 ± 0.1	1.4 ± 0.1	1.5 ± 0.1

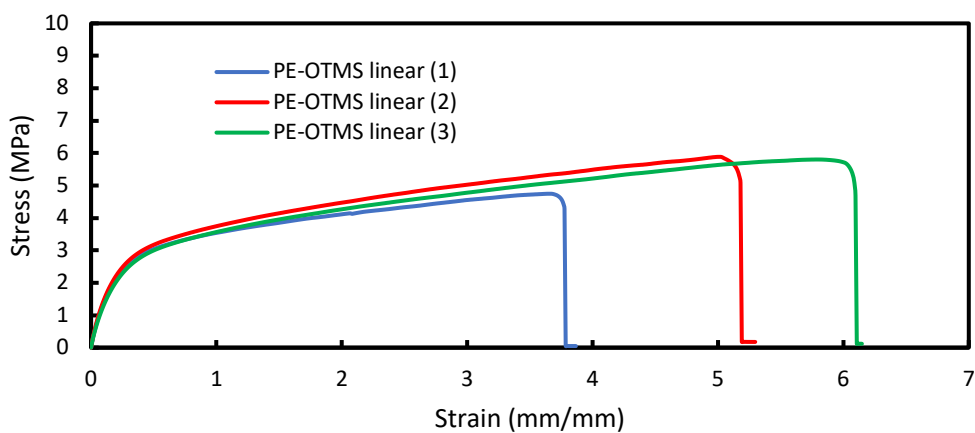


**Figure S16.** Tensile testing of linear PE-OTMS polymer.

**Table S3.** Mechanical properties of linear PE-OTMS polymer (triplicates).

	Linear PE-OTMS
Young's Modulus (MPa)	19.2 ± 1.13
Tensile Strength (MPa)	5.5 ± 0.6
Toughness (MJ/m <sup>3</sup> )	21.9 ± 6.8
Elongation (mm/mm)	5.1 ± 1.2

#### ***Dynamic Mechanical Thermal Analysis (DMTA) testing***

DMTA testing was performed on a DMA Q800 by cutting a sample into thin films approximately 2 mm x 1 mm x 15 mm and mounting to the clamp in tensile mode. The sample was heated at a constant rate of 3 °C/min while subjected to a 15 µm amplitude oscillation at 5 Hz. For the linear PE-OTMS (Figure 3A), the sample completely flowed above the  $T_m$ . However, the PE-OTMS vitrimer showed a rubber plateau and retained elasticity above the  $T_m$ . The storage modulus plateaued at approximately 0.95 MPa, which is indicative of the cross-linked network preventing the flow of material.

### ***Stress relaxation testing***

Stress relaxation experiments were performed on a DMA Q800 by cutting a sample into thin films approximately 2 mm x 1 mm x 15 mm and mounting to the clamp in tensile mode (Figure 4). Samples were pulled to 10% strain and held until the relaxation modulus crossed the relaxation time,  $\tau^*$ , which is defined from the Maxwell model of viscoelastic fluids as the time required for the relaxation modulus to fall to  $e^{-1}$  (~37%) from the initial relaxation modulus. The stress relaxation data underwent Arrhenius treatment to yield a straight light with a slope defined by equation (1):

$$\ln \tau^*(T) = 9.356 \cdot \frac{1000}{T} - 14.445 \quad (1)$$

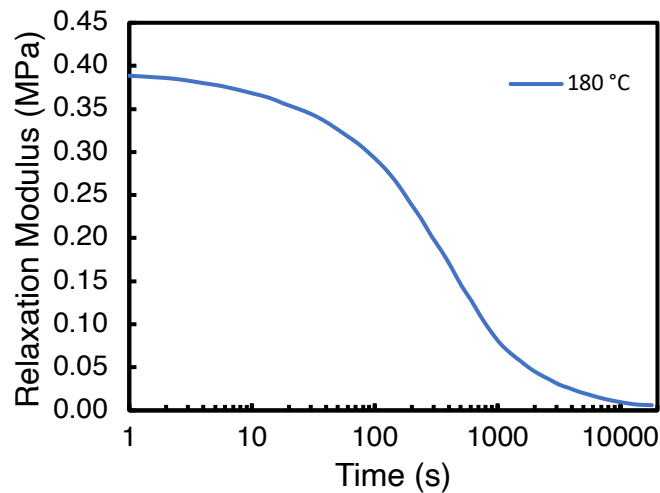


**Figure S17.** Stress relaxation of the PE-OTMS vitrimer at 180 °C with 10% strain.

### ***Creep testing***

Creep experiments were performed on a DMA Q800 by cutting a sample into thin films approximately 2 mm x 1 mm x 15 mm and mounting to the clamp in tensile mode. Samples were heated to their respective temperatures and exerted to a constant force of 0.1 MPa. After a brief elastic response, the samples begin to creep, following Arrhenius temperature-dependent behavior. After 30 minutes, the force was released and the samples could return to their relaxed state (Figure 3B). The samples at higher temperatures exhibited more creep and consequently did not return to the same position. Due to the melting range, the samples exhibit dramatically different behaviors below and above the  $T_m$ . While below the  $T_m$ , the network didn't exhibit as strong of an elastic response – most likely due to the crystalline domains limiting molecular motion. Above the  $T_m$ , the cross-linking stabilizes the material from completely melting.



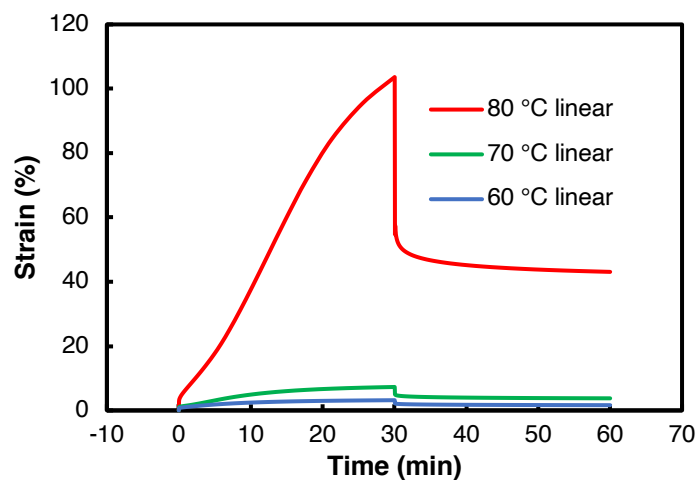


**Figure S18.** Creep-relaxation testing on linear PE-OTMS polymer. Samples had a 0.1 MPa force applied for 30 minutes followed by relaxation for 30 minutes.

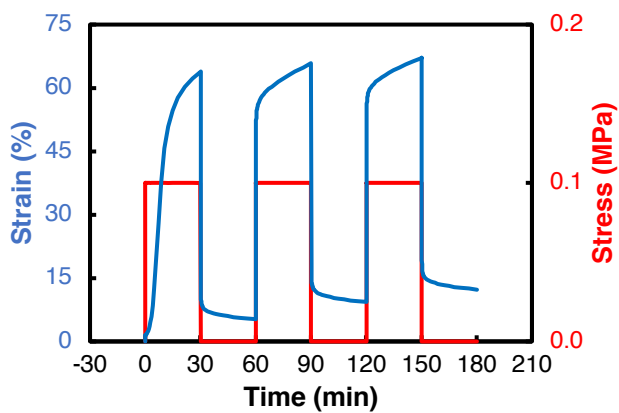


**Figure S19.** Creep relaxation test at 100 °C where PE-OTMS vitrimer was cycled three times without removing from the clamp.

### ***Network dissolution***

To show that cross-linking is not permanent, i.e. no new C-C bonds were formed, a 130 mg piece of a 3x reprocessed sample was placed in a combination of 90% toluene and 10% benzyl alcohol with 10 mg CSA. Benzyl alcohol can exchange with the silyl ether cross-linker to depolymerize the network, leaving only linear polymers behind. Photos were taken before and after heating overnight at 70 °C (Figure S20). As seen in Fig. S20b, the sample became fully un-crosslinked.

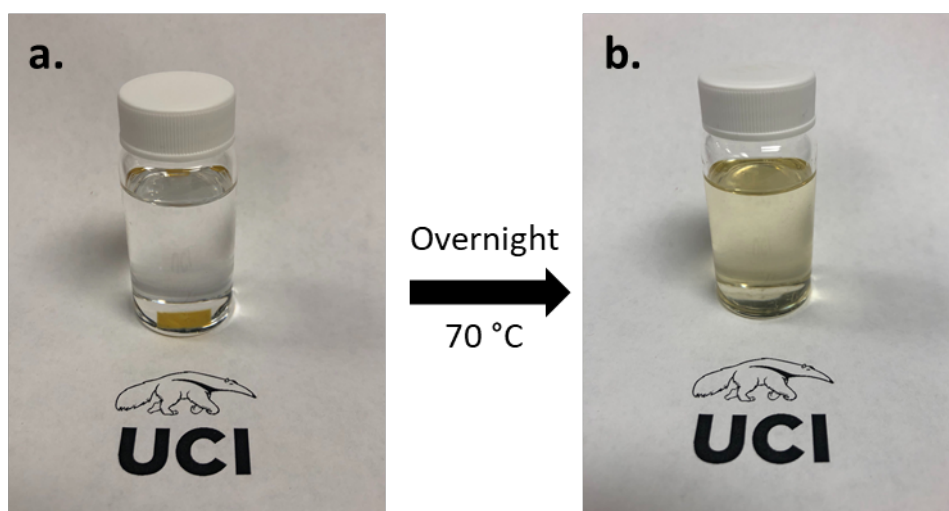


**Figure S20.** **a.** 130 mg piece of 3x reprocessed sample dissolved in 90% toluene and 10% benzyl alcohol. **b.** Fully un-crosslinked sample after heating overnight at 70 °C.

## Calculations

### *Determination of $T_v$*

The topology freezing temperature,  $T_v$ , is defined as the transition of a material from a viscoelastic solid to a viscoelastic liquid. This transition is generally considered to be when the viscosity reaches  $10^{12}$  Pa. The viscosity can be calculated from DMTA and stress relaxation experiments by using the Maxwell equation:<sup>2</sup>

$$\eta = G \cdot \tau^* = \frac{E'}{2(1+\nu)} \cdot \tau^* \quad (2)$$

Where:

G = shear modulus

$\tau^*$  = relaxation time

E' = storage modulus

$\nu$  = Poisson's ratio

By inputting the known Poisson's ratio for LDPE (0.43)<sup>3,4</sup> into equation (2), it is simplified to:

$$\eta = 0.350 \cdot E' \cdot \tau^* \quad (3)$$

Using DMTA analysis of the PE-OTMS vitrimer, the storage modulus at rubber plateau (Figure 3A) was found to be approximately 0.94 MPa for the range of 110–150 °C. The values  $E' = 0.94$  MPa and  $\eta = 10^{12}$  Pa were inserted into equation (3) to give an extrapolated

relaxation time  $\tau^* = 3,039,513$  s for the calculated  $T_v$ . By plugging the extrapolated  $\tau^*$  back into equation (1) from stress relaxation, it was found that  $T_v = 45$  °C.

### ***Determination of $M_c$***

Calculation of the molecular weight between cross-links ( $M_c$ ) can be performed using the equation:<sup>5</sup>

$$M_c = 2(1 + \nu) \frac{pRT}{E'} \quad (4)$$

Where:

$\nu$  = Poisson's ratio (0.43)

$p$  = density (0.92 g/cm<sup>3</sup> or 920 kg/m<sup>3</sup>)<sup>6</sup>

$R$  = universal gas constant (8.314 m<sup>3</sup>·Pa/K·mol)

$T$  = temperature (413 K)

$E'$  = storage modulus (0.94 MPa at 140 °C (413 K))

The  $M_c$  value for the PE-OTMS network at 140 °C ( $E' = 0.94$  MPa) is found to be 9.61 kDa.

## References:

- (1) Morawiec, J.; Pawlak, A.; Slouf, M.; Galeski, A.; Piorkowska, E.; Krasnikowa, N. Preparation and Properties of Compatibilized LDPE/Organo-Modified Montmorillonite Nanocomposites. *Eur. Polym. J.* **2005**, *41* (5), 1115–1122.
- (2) Capelot, M.; Unterlass, M. M.; Tournilhac, F.; Leibler, L. Catalytic Control of the Vitrimer Glass Transition. *ACS Macro Lett.* **2012**, *1* (7), 789–792.
- (3) Sound Velocity in Polyethylene. *J. Polym. Sci.* **1959**, *36* (130), 475–483.
- (4) Psomiadou, E.; Arvanitoyannis, I.; Biliaderis, C. G.; Ogawa, H.; Kawasaki, N. Biodegradable Films Made from Low Density Polyethylene (LDPE), Wheat Starch and Soluble Starch for Food Packaging Applications. Part 2. *Carbohydr. Polym.* **1997**, *33* (4), 227-242.
- (5) Platzner, N. Encyclopedia of Polymer Science and Engineering, H. F. Mark, N. M. Bikales, C. G. Overberger, and G. Menges, Wiley-Interscience, New York, 1985, 720 Pp. *J. Polym. Sci. Part C Polym. Lett.* **1986**, *24* (7), 359–360.
- (6) Zoller, P. The Pressure–Volume–Temperature Properties of Three Well-Characterized Low-Density Polyethylenes. *J. Appl. Polym. Sci.* **1979**, *23* (4), 1051–1056.

## Chapter 4: Siloxane Exchange Chemistry for High-Stability Vitrimer

### Designs

#### 4.1 Introduction

Due to global pressure for a reduction in plastic waste, concentrated effort has been put forth to find materials that have the capacity to meet the rigorous mechanical requirements of crosslinked thermosets while still maintaining reprocessability.<sup>1,2</sup> Vitrimers are a relatively new family of polymeric materials containing dynamic crosslinks that exchange under heat and stress. Vitrimers use associative exchange to maintain a fixed crosslink density and prevent network integrity loss at elevated temperatures.<sup>3,4</sup> For this reason, vitrimers are advantageous in applications requiring dimensional stability, increased temperatures, and solvent resistance.<sup>5</sup> Several vitrimer motifs have been explored including transamination of vinylogous urethanes,<sup>6-10</sup> boronic ester or boroxine exchange,<sup>11-16</sup> imine exchange,<sup>17-20</sup> transition metal-catalyzed transesterification,<sup>21-24</sup> olefin metathesis,<sup>25</sup> triazolium trans-alkylation,<sup>26</sup> acetal exchange,<sup>27,28</sup> siloxane exchange,<sup>29,30</sup> and thiol conjugate addition-elimination.<sup>31</sup> Many of these dynamic chemistries have limitations such as oxidative, thermal, and hydrolytic stability, or difficulty in synthesis which severely limits their application in commercial operation.

Recent work with silyl ether exchange<sup>29,30,32</sup> was demonstrated to have exceptional thermal and oxidative stability, however there was a potential challenge of hydrolytic stability. When exposed to excess moisture and heat, silyl ethers can be hydrolyzed to dimethylsilanol and volatilize during processing.<sup>33</sup> To address this challenge, we have worked towards making use of the analogous siloxane linkage, which is thermally,

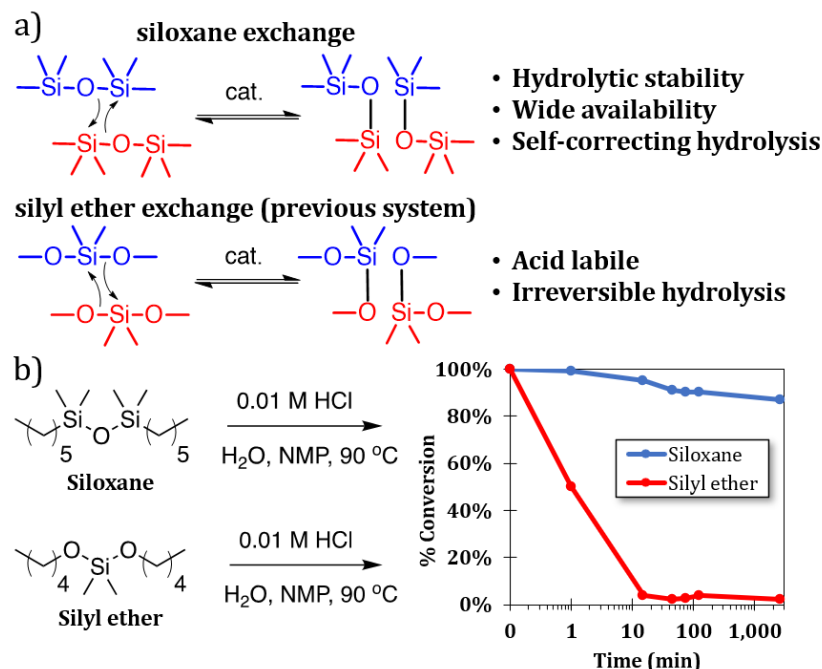


**Figure 4.1.** Reversible siloxane exchange. (a) Comparison between the current siloxane exchange and previous silyl ether exchange. (b) Comparison between siloxane and silyl ether model compounds in the presence of a dilute acid and water.

oxidatively, and hydrolytically stable as well as commercially available in a variety of analogues (Figure 4.1a).<sup>34</sup> To give a brief comparison between the stability of silyl ether and siloxane motifs, model compounds were synthesized and exposed to 0.01 M HCl at 90 °C (Figure 4.1b). By monitoring the reaction progress via GC-MS it was found that under dilute acidic conditions, the silyl ether model compound was cleaved within 10 minutes while the siloxane retained much of its integrity over the course of 40+ hours. While it is possible for the siloxane model compound to be hydrolyzed, the resulting silanol can easily condense to re-form the siloxane linkage at high temperatures.<sup>34,35</sup> By moving towards siloxane groups as the crosslinkers in vitrimers, we can gain a large degree of hydrolytic resistance while retaining oxidative and thermal stability.

## 4.2 Results and Discussion

While the Si-O bond is inert to a wide variety of functional groups, it was found that both Brønsted and Lewis acids can promote Si-O exchange in silyl ether model studies.<sup>30</sup> We aimed to determine if these catalysts had similar reactivity towards siloxanes. Model compound studies explored the exchange of dihexyldisiloxane and dinonyldisiloxane alkoxy groups in the presence of 2 mol% catalyst. Under exchange, a new compound consisting of the combination of the two emerges in a statistical 1:2:1 distribution (Figure 4.2a,b). For both camphorsulfonic acid and Sc(III)OTf<sub>3</sub> (Figure 4.2c,d), relatively rapid exchange occurred above 160 °C indicated they would be a viable candidates for vitrimer exchange studies. The mild Lewis acid catalyst Zn(II)OTf<sub>2</sub> was also found to facilitate exchange, albeit at a slower rate, suggesting that a wider variety of transition metal catalysts might also promote siloxane exchange – each with different levels of catalytic activity. Unfortunately, many transition metal catalysts have poor solubility in nonpolar matrices and unwanted side reactions with sensitive functional groups which limit the scope of their application.

For these reasons, we began searching for a more selective catalyst for siloxane exchange. Turning our focus towards motifs that interact strongly with silicon, we began exploring fluoride-containing compounds as a possible reaction catalyst. Fluoride has a strong affinity to silicon such that the Si-F bond in SiF<sub>4</sub> has the highest BDE of any single bond.<sup>36</sup> Despite the high BDE, the Si-F bond is very ionic – in fact, the difference in electronegativity of Si-F is higher than that of Na-Cl.<sup>37</sup> As such, it has been shown that fluoride can participate in the reorganization of POSS cages without forming irreversible linkages.<sup>38-</sup>  
<sup>40</sup> We envision that while strong, the Si-F bond can also be transient, moving from silicon to



silicon and modifying the reactivity of the siloxane linkage. To this end, several potential catalysts were explored to facilitate siloxane exchange. Fluoride sources included tetrabutylammonium fluoride (TBAF), tetramethylammonium fluoride (TMAF), tetrabutylammonium triphenyldifluorosilicate (TBAT), potassium fluoride (KF), potassium fluoride coordinated to dibenzo-18-crown-6 ether (KF:DB18-c-6), cesium fluoride, sodium monofluorophosphate, XtalFluor-E, XtalFluor-M, and potassium tetrafluoroborate.

The naked fluoride anion, TBAF and TMAF, offered extremely fast reaction rates at low temperatures. Unfortunately, above 100 °C the solution browned, and subsequent additions of siloxane starting material did not change the composition – indicating the catalyst had degraded during the initial heating. TBAT (Figure 4.2e) offers an interesting alternative to TBAF in that the fluoride is already bound to a silicon atom. TBAT offered rapid exchange rates, however also degraded at temperatures above 100 °C, albeit at a slower than TBAF. Several other catalysts were screened that did not have sufficient solubility such as NaF, sodium monofluorophosphate, KF, and CsF. Electrophilic fluorine sources such as Xtalfluor-E/M also had no effect on the exchange rate. To increase the solubility and nucleophilicity of the alkali metal fluoride, dibenzo-18-crown-6 ether and KF were prepared in a 1:1 ratio to coordinate to the potassium ion and increase solubility (Figure 4.2f). When added to the model siloxanes exchange occurred rapidly with a strong temperature dependence. The stabilization of the potassium ion appears to have a significant impact on the ability of the fluoride to participate in siloxane exchange. The KF:DB-18-c-6 species

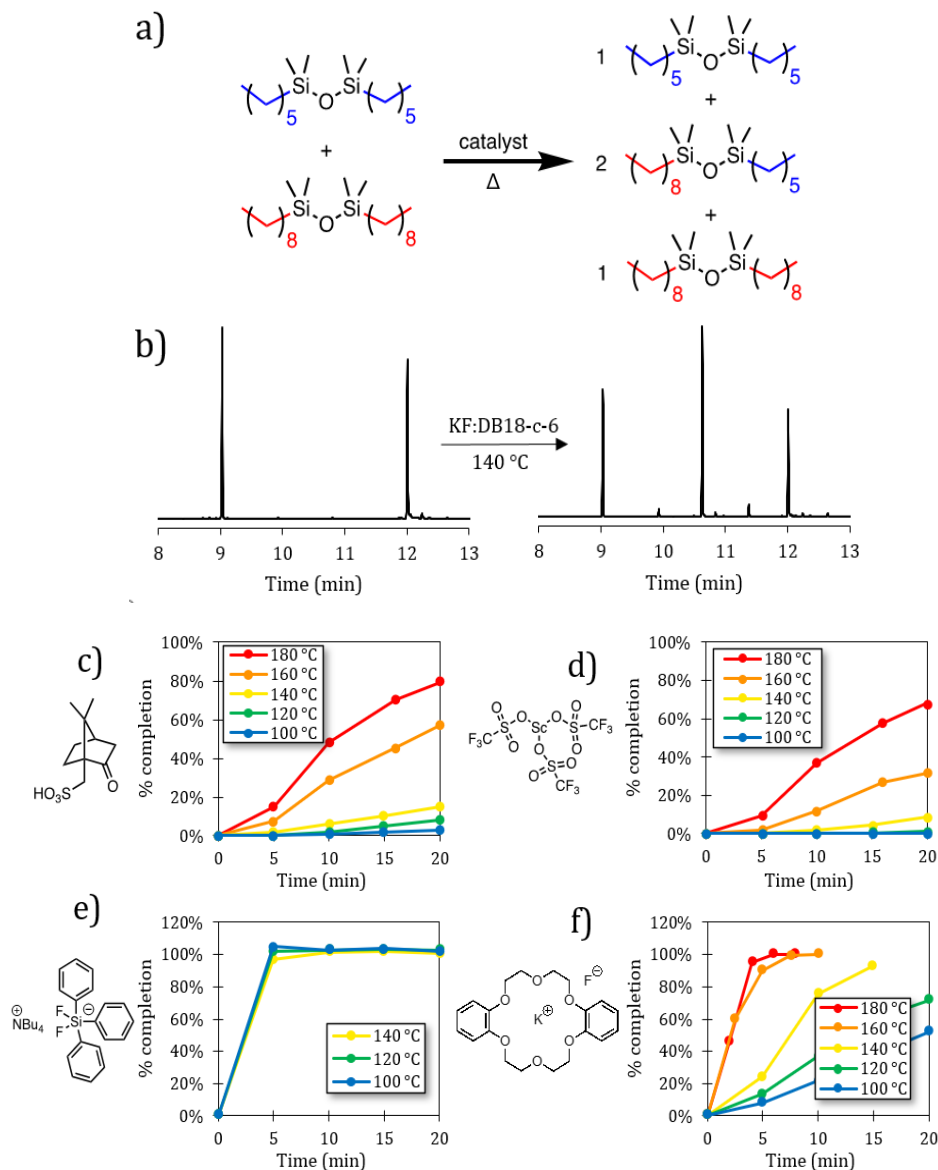


**Figure 4.2.** Catalyzed siloxane exchange. (a) Dihexyltetramethyldisiloxane and dinonyltetramethyldisiloxane converted to a statistical distribution of products. (b) Gas Chromatography-Mass Spectrometry (GC-MS) chromatogram of siloxane model compound exchange. Percent completion for the siloxane scrambling reaction (33% w/v) catalyzed at different temperatures by (c) 2 mol% camphorsulfonic acid, (d) 2 mol% scandium (III) triflate (e) 2 mol% *N*-tetrabutyl ammonium difluoro-triphenylsilicate (TBAT), (f) 2 mol% potassium fluoride:dibenzo 18-crown-6 ether (KF:DB18-c-6).

reached ~95% conversion within 5 minutes at 160 °C and was thermally stable for all tested conditions. The solubility and/or dispersibility of the catalyst is a critical requirement for use in solvent-free applications such as bulk polymer crosslink exchange.

Following small molecule studies, we aimed to probe the fluoride catalyst behavior in polymeric materials. The most common siloxane-containing materials to explore are polydimethylsiloxane (PDMS) elastomers, which contain only Si-O bonds throughout the backbone. PDMS elastomers are normally tough and resistant to creep, however upon the addition of fluoride catalyst became malleable at high temperatures (Figure 4.3). The catalyst KF:DB-18-c-6 was dispersed into a 2-part PDMS elastomer kit (Dow® Sylgard 184) at 0.1 mmol per gram polymer under high-speed mechanical mixing. The PDMS was cured at room temperature and punched into disks. Using stress relaxation measurements to monitor the network malleability, the PDMS with catalyst was able to quickly dissipate stress above 160 °C owing to the embedded fluoride. The comparable un-catalyzed PDMS elastomer retained its integrity and was slow to dissipate the applied stress. The apparent  $E_a$  for the catalyzed

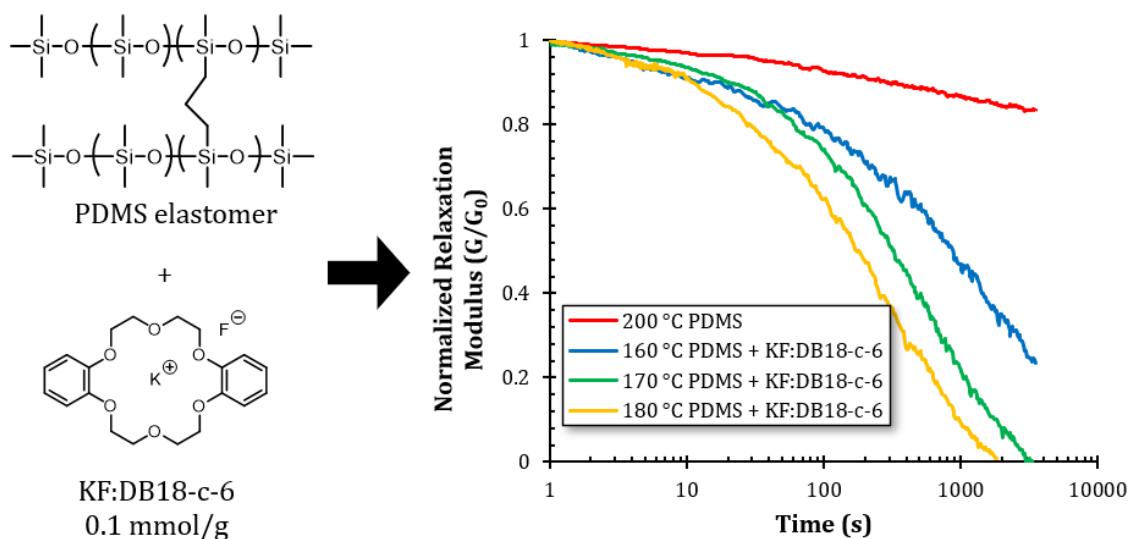


**Figure 4.3.** KF:DB18-c-6 incorporation at 0.1 mmol/g into PDMS elastomer induces malleability when monitored by stress relaxation experiments. At higher temperatures, the the catalyzed PDMS relaxes stress faster. PDMS without catalyst at 200 °C only shows a slight dissipation of stress.

PDMS exchange was  $\sim 138$  kJ/mol and relaxation behavior followed an Arrhenius temperature dependence, which is indicative of associative exchange chemistries.

With evidence that fluoride is an efficient catalyst for siloxane exchange, we aimed to prepare polymer networks bearing siloxane crosslinks that can undergo exchange and retain malleability. There has been little attention towards the incorporation of vitrimer chemistries into commodity plastics despite the dramatic improvements they could provide. As such, we aimed to broaden the scope of siloxane exchange from PDMS elastomers into high-volume commercial polymers using reactive extrusion. With a generalizable preparation process in mind, we aimed to generate vitrimers using siloxane linkages for high density polyethylene (HDPE-v) and polymethylmethacrylate (PMMA-v). We use the high shear rate and high temperatures of a compounding twin-screw extruder to add functionality to polymer backbones in a scalable manner through either trans amination or radical grafting.

PMMA was easily functionalized by the commercially available 1,3-bis(3-aminopropyl)tetramethyldisiloxane through melt blending in the presence of KF:DB-18-c-6 catalyst (Figure 4.4a). The primary amines in 1,3-bis(3-aminopropyl)tetramethyldisiloxane react via transamidation with the methyl ester in the PMMA side chains, generating siloxane bridges that can undergo exchange in the presence of fluoride catalyst. Our compounding extruder has a recirculating channel that allows for extended run times to more accurately mimic large-scale extruders. As such, the reaction progress can be monitored through the viscosity evolution over the course of the run. As transamination occurs, the polymers first undergo chain extension followed by crosslinking into a dense network. Owing to rapid

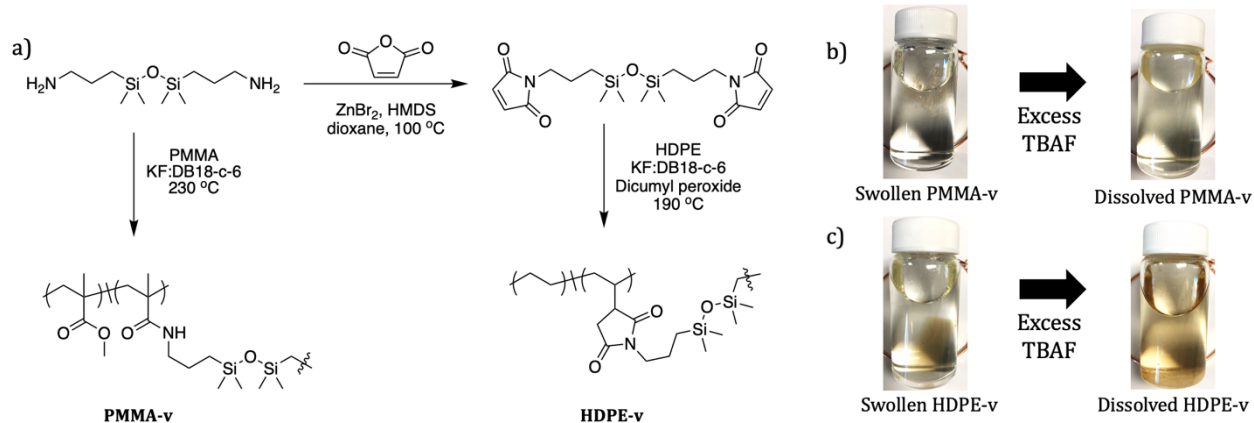


**Figure 4.4.** Preparation of siloxane-bearing vitrimers. (a) Synthesis of crosslinker, preparation of PMMA-v, and preparation of HDPE-v. (b, c) Images of PMMA-v and HDPE-v before and after addition of excess TBAF, indicating that crosslinking is formed through siloxane bridges only.

fluoride-catalyzed exchange, the crosslinked networks are not destroyed by the high shear of the extruder and instead reach a steady exchange rate that is observed by a plateau in viscosity after all available amine has been consumed (Figure 4.5a). At 190 °C the viscosity reaches plateau after approximately 13 minutes, however at 230 °C the viscosity reaches plateau after only 3 minutes of mixing. The difference in the time to reach plateau is caused by the faster rate of amine consumption at the higher temperatures. When an analogous C<sub>8</sub>-diamine without the siloxane bridge was used, the extruder torque never plateaued and continued to climb until the 14-minute mark where the extruder pressure limit was reached – indicating the dynamic crosslinks play an integral role in the homogenous mixing and processing of crosslinked vitrimers. After removal from the barrel, the C<sub>8</sub>-diamine crosslinked PMMA was not moldable at any temperature and was insoluble in good solvents. After swelling, the PMMA-v would completely dissolve upon the addition of excess TBAF (Figure 4.4b), while the C<sub>8</sub>-diamine crosslinked network remained an insoluble gel.

**Table 4.1.** PMMA-v crosslinking conditions.

<b>Temp.</b>	<b>Crosslinker wt%</b>	<b>Max viscosity</b>	<b>Insoluble %</b>
190 °C	5 wt%	13 minutes	82.3% ± 6.1%
190 °C	2 wt% C <sub>8</sub> -diamine	13 minutes	93.7% ± 6.4%
230 °C	5 wt%	3 minutes	84.7% ± 2.1%
230 °C	4 wt%	3 minutes	84.5% ± 1.4%
230 °C	3.5 wt%	3 minutes	80.2% ± 0.4%
230 °C	2 wt%	4 minutes	70.2% ± 1.8%
230 °C	1 wt%	5 minutes	40.7% ± 4.0%

To explore the influence of the fluoride catalyst on the exchange reaction, the molar ratio of catalyst in PMMA-v was varied at 1, 5, and 10 mol% relative to diaminosiloxane crosslinker. The viscosity quickly increased after complete addition of the mixture into the feed hopper and plateaued at ~5 minutes (Figure 4.5a). The melt viscosity at plateau was comparable for all samples, indicating all samples were at full conversion. Despite similar viscosity during extrusion, stress relaxation experiments of the sample with 10 mol% catalyst showed faster relaxation than the 5 and 1.25 mol% (Figure 4.5b). This also indicates the relaxation behavior is directly related to the fluoride-catalyzed siloxane exchange, and the exchange rate can be tuned by the addition of catalyst.

A radical graft-to process was utilized to produce HDPE-v. For the radical crosslinker, 1,3-bis(3-aminopropyl)tetramethyldisiloxane was converted to a bis-maleimide through a ring-opening and closing of maleic anhydride (Figure 4.4a). The maleimide is a good radical acceptor and grafting agent for polyolefin functionalization. The bis-maleimidotetramethyldisiloxane was blended with HDPE (MFI = 2.2 g/10min), dicumyl peroxide, and KF:DB-18-c-6 catalyst. The blend was vigorously mixed, and melt blended at

190 °C for five minutes until the peroxide initiator had been sufficiently consumed. After extrusion, the samples were compression molded for mechanical testing. Molded samples had a constant gel fraction of ~45% regardless of the number of reprocessing cycles. To test if HDPE-v had been crosslinked with only siloxane crosslinks, a small piece was swollen in hot xylene. A large excess of TBAF was added to the swollen sample and the insoluble gel completely dissolved as the siloxane bonds were cleaved (Figure 4.4c).

To show the reprocessability of HDPE-v, the samples were ground and fed back into the extruder. As measured by tensile testing (Figure 4.5c), HDPE-v maintained its integrity over the course of each reprocessing and preserved its mechanical properties. For comparison, unmodified HDPE was also tested and showed a slightly higher Young's modulus and yield point, but was found to have a similar elongation at break to HDPE-v. The decrease in Young's modulus for HDPE-v is attributed to a slight reduction in crystallinity, which was verified by DSC measurements where the unmodified HDPE was approximately 69% crystalline while HDPE-v was around 55% crystalline (Figures S14, S15). HDPE-v was molded into flat coupons and punched into disks for stress relaxation testing on a parallel plate rheometer (Figure 4.5d). HDPE-v stress relaxation shows Arrhenius temperature dependence above the  $T_m$  for HDPE and an apparent  $E_a$  of 49 kJ/mol. DMTA temperature sweeps showed a plateau of the storage and loss modulus above the  $T_m$ , indicating the HDPE-v was indeed crosslinked, while the unmodified HDPE melted at ~150 °C and lost all mechanical integrity.

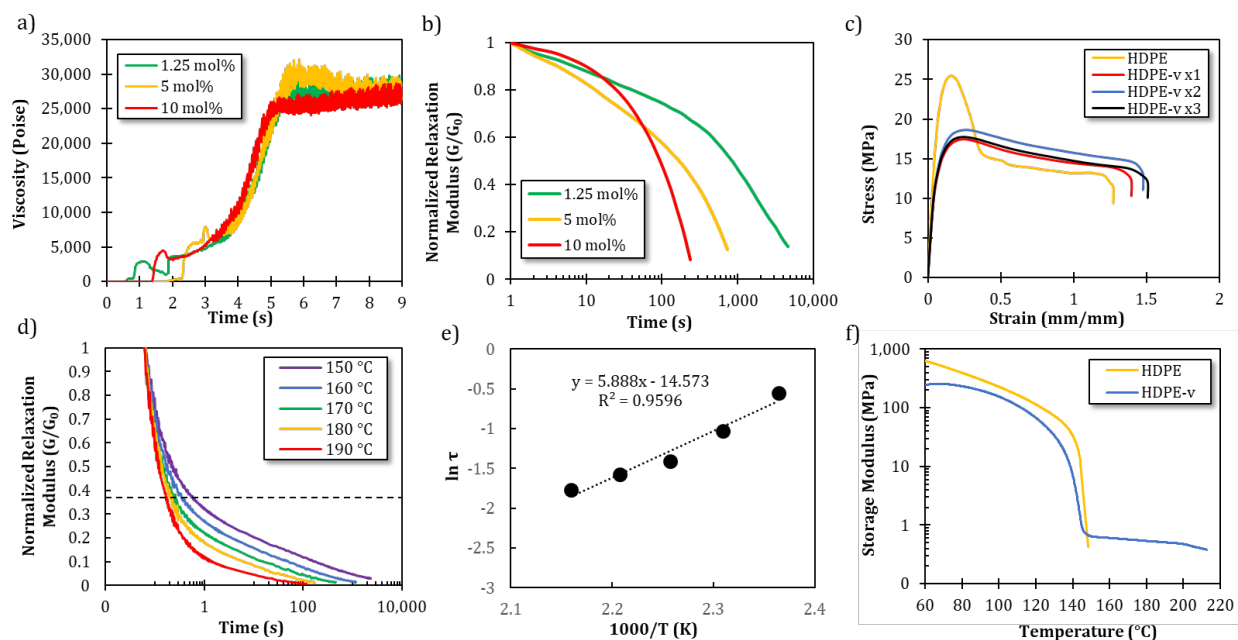


**Figure 4.5.** Physical testing of PMMA-v and HDPE-v. (a) Viscosity evolution during extrusion of PMMA-v with 4 wt% diaminosiloxane crosslinker at 230 °C. (b) Stress relaxation of PMMA-v with 4% diamine crosslinker at 180 °C and 1% strain using different catalyst concentrations. (c) Tensile testing of unmodified HDPE and HDPE-v over three reprocessing cycles. (d) Stress relaxation of HDPE-v at different temperatures. (e) Arrhenius treatment of HDPE-v stress relaxation. (f) DMTA temperature sweep of unmodified HDPE and HDPE-v showing plateau of modulus above the  $T_m$ .

One of the major benefits of using vitrimer chemistry in traditional applications is their inherent resistance to creep. Linear polymers tend to creep above their  $T_g$  in response to stress, while vitrimers prepared from analogous polymer backbones resist flow due to the embedded crosslinks. Owing to the associative exchange mechanism of the dynamic crosslinks, flow is restricted until two exchangeable motifs come into sufficient contact with each other. The exchange rate has a temperature dependence, thus making vitrimers a desired material for high-temperature applications. In Figure 4.6a, the creep resistance of HDPE-v was compared to unmodified HDPE at temperatures above the  $T_m$ . Unmodified HDPE has a low melt viscosity and flows easily while HDPE-v strongly resists creep – even well above the  $T_m$ . Dramatic creep resistance was also observed for PMMA-v (Figure 4.6b) at 190



°C. More practically, we tested the creep resistance for HDPE and HDPE-v at room temperature under very large stresses of 10 MPa (Figure 4.6c,d). HDPE-v had approximately 2.5x the creep resistance compared to HDPE and much less initial strain. The incorporation of crosslinks limited the initial extension under heavy load and limited the amount of creep in the amorphous phase.

An interesting consideration on vitrimers prepared from reactive extrusion is the mechanism for the retention in network integrity during the high-shear environment. Under non-dynamic circumstances, highly crosslinked materials are sheared until they reach a sufficient domain size to pass through the internal gaps between the screws and barrel. In the case of dynamic materials however, there appears to be a dramatic shear-dependent

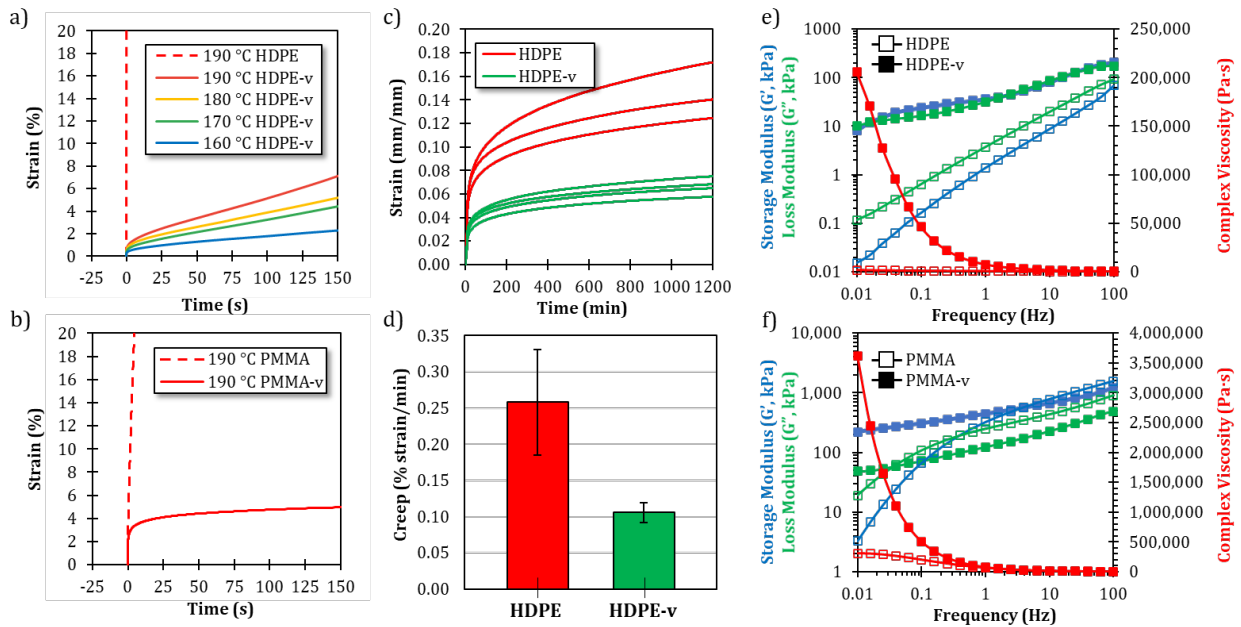


**Figure 4.6.** Creep and rheological testing of HDPE-v and PMMA-v. (a) Creep testing of HDPE and HDPE-v at various temperatures under 1 kPa force. (b) Creep resistance of PMMA-v as compared to PMMA under 10 kPa force. (c) Creep resistance of HDPE and HDPE-v under heavy force (10 MPa) at room temperature and the (d) statistical analysis. Frequency sweep of (e) HDPE and HDPE-v and (f) PMMA and PMMA-v from 0.01 to 100 Hz at 190 °C measuring  $G'$ ,  $G''$ , and complex viscosity.

viscosity decrease at frequencies above 1 Hz (Figure 4.6e,f). Samples were punched into disks and heated to 190 °C in a parallel plate rheometer where the frequency was swept from 0.01–100 Hz. At low shear rates the viscosity of HDPE-v and PMMA-v were significantly higher than the analogous unmodified polymers. This large difference in viscosity is demonstrated by the vitrimers' creep resistance at high temperatures where the strain rate is low. However, a marked viscosity drop occurs as the shear rate increases above 1 Hz and the complex viscosity of the vitrimer begins to merge with that of the unmodified polymer. At low shear rates, polymer chains are crosslinked by the siloxane linkages as well as physically entanglement. At high shear rates, the rapid siloxane exchange allows for polymer chains to disentangle and align along the direction of shear, leading to less molecular interaction and a dramatic decrease in viscosity. Although these dynamic networks are densely crosslinked, they were easily processed on common polymer processing equipment at elevated temperature and shear. Shear thinning of vitrimers has been experimentally observed by other labs in the use of injection molding instruments to prepare samples for mechanical testing.<sup>14</sup> If static crosslinks were used instead of dynamic crosslinks, samples would not be processable in the same manner as evidenced from the C<sub>8</sub> diamine PMMA crosslinking. This behavior provides some insight into the preservation of crosslinks during the extrusion process.

### **4.3. Conclusion**

In conclusion, we have discovered fluoride-catalyzed siloxane exchange as a new dynamic exchange motif. Siloxane linkages are highly stable to heat and oxidation while also being commercially relevant. Several catalysts were screened to promote the siloxane exchange and KF:DB18-c-6 was both stable over a wide temperature range and promoted the selective exchange of siloxane linkages. When incorporated into polymer networks such as PDMS, crosslinked HDPE, and crosslinked PMMA, fluoride-catalyzed siloxane exchange provided a robust method for preventing sample creep and maintaining network integrity at high processing conditions. Using rheology frequency sweeps, we elucidated the shear thinning behavior of PMMA and HPDE vitrimers to provide rationale for the retention of crosslinks through the reactive extrusion process. We envision that fluoride-catalyzed siloxane exchange chemistry can be used to broaden the adoption of vitrimer chemistry.

#### 4.4 References

- (1) Imbernon, L.; Norvez, S. From Landfilling to Vitrimer Chemistry in Rubber Life Cycle. *European Polymer Journal* **2016**, *82*, 347–376. <https://doi.org/10.1016/j.eurpolymj.2016.03.016>.
- (2) The Future of Plastic. *Nat Commun* **2018**, *9* (1), 2157. <https://doi.org/10.1038/s41467-018-04565-2>.
- (3) Denissen, W.; Winne, J. M.; Du Prez, F. E. Vitrimers: Permanent Organic Networks with Glass-like Fluidity. *Chem Sci* **2016**, *7* (1), 30–38. <https://doi.org/10.1039/c5sc02223a>.
- (4) Van Zee, N. J.; Nicolaÿ, R. Vitrimers: Permanently Crosslinked Polymers with Dynamic Network Topology. *Progress in Polymer Science* **2020**, *104*, 101233. <https://doi.org/10.1016/j.progpolymsci.2020.101233>.
- (5) Alabiso, W.; Schlögl, S. The Impact of Vitrimers on the Industry of the Future: Chemistry, Properties and Sustainable Forward-Looking Applications. *Polymers (Basel)* **2020**, *12* (8), 1660. <https://doi.org/10.3390/polym12081660>.
- (6) Denissen, W.; Droesbeke, M.; Nicolaÿ, R.; Leibler, L.; Winne, J. M.; Du Prez, F. E. Chemical Control of the Viscoelastic Properties of Vinylogous Urethane Vitrimers. *Nature Communications* **2017**, *8*, 14857. <https://doi.org/10.1038/ncomms14857>.
- (7) Denissen, W.; Rivero, G.; Nicolaÿ, R.; Leibler, L.; Winne, J. M.; Prez, F. E. D. Vinylogous Urethane Vitrimers. *Advanced Functional Materials* **2015**, *25* (16), 2451–2457. <https://doi.org/10.1002/adfm.201404553>.
- (8) Tellers, J.; Pinalli, R.; Soliman, M.; Vachon, J.; Dalcanale, E. Reprocessable Vinylogous Urethane Cross-Linked Polyethylene via Reactive Extrusion. *Polymer Chemistry* **2019**, *10* (40), 5534–5542. <https://doi.org/10.1039/C9PY01194C>.
- (9) Lessard, J. J.; Garcia, L. F.; Easterling, C. P.; Sims, M. B.; Bentz, K. C.; Arencibia, S.; Savin, D. A.; Sumerlin, B. S. Catalyst-Free Vitrimers from Vinyl Polymers. *Macromolecules* **2019**, *52* (5), 2105–2111. <https://doi.org/10.1021/acs.macromol.8b02477>.
- (10) Taplan, C.; Guerre, M.; M. Winne, J.; Prez, F. E. D. Fast Processing of Highly Crosslinked, Low-Viscosity Vitrimers. *Materials Horizons* **2020**, *7* (1), 104–110. <https://doi.org/10.1039/C9MH01062A>.
- (11) Cash, J. J.; Kubo, T.; Bapat, A. P.; Sumerlin, B. S. Room-Temperature Self-Healing Polymers Based on Dynamic-Covalent Boronic Esters. *Macromolecules* **2015**, *48* (7), 2098–2106. <https://doi.org/10.1021/acs.macromol.5b00210>.
- (12) Cromwell, O. R.; Chung, J.; Guan, Z. Malleable and Self-Healing Covalent Polymer Networks through Tunable Dynamic Boronic Ester Bonds. *J. Am. Chem. Soc.* **2015**, *137* (20), 6492–6495. <https://doi.org/10.1021/jacs.5b03551>.

- (13) Ogden, W. A.; Guan, Z. Recyclable, Strong, and Highly Malleable Thermosets Based on Boroxine Networks. *J. Am. Chem. Soc.* **2018**, *140* (20), 6217–6220. <https://doi.org/10.1021/jacs.8b03257>.
- (14) Röttger, M.; Domenech, T.; Weegen, R. van der; Breuillac, A.; Nicolaÿ, R.; Leibler, L. High-Performance Vitrimers from Commodity Thermoplastics through Dioxaborolane Metathesis. *Science* **2017**, *356* (6333), 62–65. <https://doi.org/10.1126/science.aah5281>.
- (15) Bao, C.; Jiang, Y.-J.; Zhang, H.; Lu, X.; Sun, J. Room-Temperature Self-Healing and Recyclable Tough Polymer Composites Using Nitrogen-Coordinated Boroxines. *Advanced Functional Materials* **2018**, *28* (23), 1800560. <https://doi.org/10.1002/adfm.201800560>.
- (16) P. Bapat, A.; S. Sumerlin, B.; Sutti, A. Bulk Network Polymers with Dynamic B–O Bonds: Healable and Reprocessable Materials. *Materials Horizons* **2020**, *7* (3), 694–714. <https://doi.org/10.1039/C9MH01223K>.
- (17) Taynton, P.; Yu, K.; Shoemaker, R. K.; Jin, Y.; Qi, H. J.; Zhang, W. Heat- or Water-Driven Malleability in a Highly Recyclable Covalent Network Polymer. *Advanced Materials* **2014**, *26* (23), 3938–3942. <https://doi.org/10.1002/adma.201400317>.
- (18) Hajj, R.; Duval, A.; Dhers, S.; Avérous, L. Network Design to Control Polyimine Vitriimer Properties: Physical Versus Chemical Approach. *Macromolecules* **2020**, *53* (10), 3796–3805. <https://doi.org/10.1021/acs.macromol.0c00453>.
- (19) L. Snyder, R.; L. Lidston, C. A.; Hoe, G. X. D.; S. Parvulescu, M. J.; A. Hillmyer, M.; W. Coates, G. Mechanically Robust and Reprocessable Imine Exchange Networks from Modular Polyester Pre-Polymers. *Polymer Chemistry* **2020**, *11* (33), 5346–5355. <https://doi.org/10.1039/C9PY01957J>.
- (20) Liu, Y.; Tang, Z.; Chen, J.; Xiong, J.; Wang, D.; Wang, S.; Wu, S.; Guo, B. Tuning the Mechanical and Dynamic Properties of Imine Bond Crosslinked Elastomeric Vitrimers by Manipulating the Crosslinking Degree. *Polymer Chemistry* **2020**, *11* (7), 1348–1355. <https://doi.org/10.1039/C9PY01826C>.
- (21) Liu, T.; Zhao, B.; Zhang, J. Recent Development of Repairable, Malleable and Recyclable Thermosetting Polymers through Dynamic Transesterification. *Polymer* **2020**, *194*, 122392. <https://doi.org/10.1016/j.polymer.2020.122392>.
- (22) Montarnal, D.; Capelot, M.; Tournilhac, F.; Leibler, L. Silica-Like Malleable Materials from Permanent Organic Networks. *Science* **2011**, *334* (6058), 965–968. <https://doi.org/10.1126/science.1212648>.
- (23) Brutman, J. P.; Delgado, P. A.; Hillmyer, M. A. Polylactide Vitrimers. *ACS Macro Lett.* **2014**, *3* (7), 607–610. <https://doi.org/10.1021/mz500269w>.
- (24) Yang, Y.; Zhang, S.; Zhang, X.; Gao, L.; Wei, Y.; Ji, Y. Detecting Topology Freezing Transition Temperature of Vitrimers by AIE Luminogens. *Nat Commun* **2019**, *10* (1), 3165. <https://doi.org/10.1038/s41467-019-11144-6>.

- (25) Lu, Y.-X.; Tournilhac, F.; Leibler, L.; Guan, Z. Making Insoluble Polymer Networks Malleable via Olefin Metathesis. *J. Am. Chem. Soc.* **2012**, *134* (20), 8424–8427. <https://doi.org/10.1021/ja303356z>.
- (26) Obadia, M. M.; Mudraboyina, B. P.; Serghei, A.; Montarnal, D.; Drockenmuller, E. Reprocessing and Recycling of Highly Cross-Linked Ion-Conducting Networks through Transalkylation Exchanges of C–N Bonds. *J. Am. Chem. Soc.* **2015**, *137* (18), 6078–6083. <https://doi.org/10.1021/jacs.5b02653>.
- (27) Li, Q.; Ma, S.; Wang, S.; Yuan, W.; Xu, X.; Wang, B.; Huang, K.; Zhu, J. Facile Catalyst-Free Synthesis, Exchanging, and Hydrolysis of an Acetal Motif for Dynamic Covalent Networks. *Journal of Materials Chemistry A* **2019**, *7*, 18039–18049. <https://doi.org/10.1039/C9TA04073K>.
- (28) Li, Q.; Ma, S.; Wang, S.; Liu, Y.; Taher, M. A.; Wang, B.; Huang, K.; Xu, X.; Han, Y.; Zhu, J. Green and Facile Preparation of Readily Dual-Recyclable Thermosetting Polymers with Superior Stability Based on Asymmetric Acetal. *Macromolecules* **2020**, *53* (4), 1474–1485. <https://doi.org/10.1021/acs.macromol.9b02386>.
- (29) Nishimura, Y.; Chung, J.; Muradyan, H.; Guan, Z. Silyl Ether as a Robust and Thermally Stable Dynamic Covalent Motif for Malleable Polymer Design. *J. Am. Chem. Soc.* **2017**, *139* (42), 14881–14884. <https://doi.org/10.1021/jacs.7b08826>.
- (30) Tretbar, C. A.; Neal, J. A.; Guan, Z. Direct Silyl Ether Metathesis for Vitrimers with Exceptional Thermal Stability. *J. Am. Chem. Soc.* **2019**, *141* (42), 16595–16599. <https://doi.org/10.1021/jacs.9b08876>.
- (31) El-Zaatari, B. M.; Ishibashi, J. S. A.; Kalow, J. A. Cross-Linker Control of Vitrimer Flow. *Polym. Chem.* **2020**, *11*, 5339–5345. <https://doi.org/10.1039/D0PY00233J>.
- (32) Zych, A.; Pinalli, R.; Soliman, M.; Vachon, J.; Dalcanale, E. Polyethylene Vitrimers via Silyl Ether Exchange Reaction. *Polymer* **2020**, *199*, 122567. <https://doi.org/10.1016/j.polymer.2020.122567>.
- (33) Parrott, M. C.; Luft, J. C.; Byrne, J. D.; Fain, J. H.; Napier, M. E.; DeSimone, J. M. Tunable Bifunctional Silyl Ether Cross-Linkers for the Design of Acid-Sensitive Biomaterials. *J. Am. Chem. Soc.* **2010**, *132* (50), 17928–17932. <https://doi.org/10.1021/ja108568g>.
- (34) Shit, S. C.; Shah, P. A Review on Silicone Rubber. *Natl. Acad. Sci. Lett.* **2013**, *36* (4), 355–365. <https://doi.org/10.1007/s40009-013-0150-2>.
- (35) Kuan, H.-C.; Kuan, J.-F.; Ma, C.-C. M.; Huang, J.-M. Thermal and Mechanical Properties of Silane-Grafted Water Crosslinked Polyethylene. *Journal of Applied Polymer Science* **2005**, *96* (6), 2383–2391. <https://doi.org/10.1002/app.21694>.
- (36) Walsh, R. Bond Dissociation Energy Values in Silicon-Containing Compounds and Some of Their Implications. *Acc. Chem. Res.* **1981**, *14* (8), 246–252. <https://doi.org/10.1021/ar00068a004>.
- (37) Haynes, W. M. *CRC Handbook of Chemistry and Physics, 93rd Edition*; CRC Press, 2012.

- (38) Bassindale, A. R.; Pourny, M.; Taylor, P. G.; Hursthouse, M. B.; Light, M. E. Fluoride-Ion Encapsulation within a Silsesquioxane Cage. *Angewandte Chemie* **2003**, *115* (30), 3612–3614. <https://doi.org/10.1002/ange.200351249>.
- (39) Asuncion, M. Z.; Laine, R. M. Fluoride Rearrangement Reactions of Polyphenyl- and Polyvinylsilsesquioxanes as a Facile Route to Mixed Functional Phenyl, Vinyl T10 and T12 Silsesquioxanes. *J. Am. Chem. Soc.* **2010**, *132* (11), 3723–3736. <https://doi.org/10.1021/ja9087743>.
- (40) C. Furgal, J.; Iii, T. G.; M. Laine, R. D 5h [PhSiO 1.5 ] 10 Synthesis via F – Catalyzed Rearrangement of [PhSiO 1.5 ] n . An Experimental/Computational Analysis of Likely Reaction Pathways. *Dalton Transactions* **2016**, *45* (3), 1025–1039. <https://doi.org/10.1039/C5DT04182A>.
- (41) Brandrup, J.; Immergut, E. H. *Polymer Handbook*, 3rd ed.; John Wiley & Sons, 1989.

## 4.5 Experimental

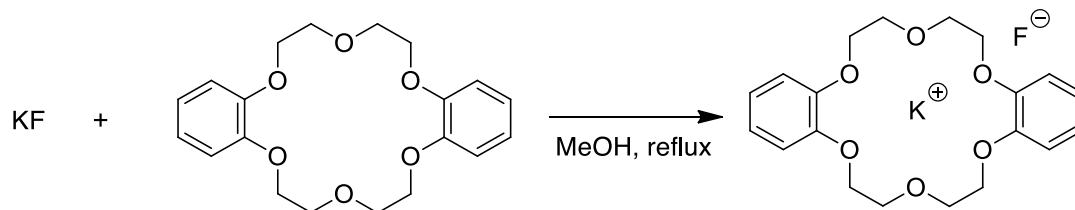
### General Experimental Information

Unless otherwise noted, reactions were carried out with dry solvents using a magnetic stir bar. Commercial reagents were used as received with no further purification, unless otherwise noted.  $^1\text{H}$  NMR spectra were recorded at 500 MHz on a Bruker DRX500 spectrometer.  $^{13}\text{C}$  NMR spectra were recorded at 125.2 MHz using a Bruker AVANCE600 with a BBFO cryoprobe. NMR spectra peaks are reported as  $\delta$  values in ppm relative to TMS or residual solvent:  $\text{CDCl}_3$  ( $^1\text{H}$  = 7.26 ppm;  $^{13}\text{C}$  = 77.0 ppm),  $\text{C}_6\text{D}_6$  ( $^1\text{H}$  = 7.16 ppm,  $^{13}\text{C}$  = 128.06 ppm).  $^1\text{H}$  NMR data are reported as follows: chemical shift in ppm, multiplicity (s = singlet, d = doublet, t = triplet), coupling constants in Hz, and relative integration of the number of protons. Multiplets (m) are reported over the range of chemical shifts at which they appear. For  $^{13}\text{C}$  NMR, only chemical shift values are reported. Tensile tests were performed on an Instron 3365 mechanical tester. Differential Scanning Calorimetry (DSC) thermograms were evaluated using a TA Instruments DSC2500. Thermogravimetric Analysis (TGA) thermograms were evaluated using a TA Instruments Q500. Dynamic Mechanical Thermal Analysis (DMTA) analysis was evaluated using a TA Instruments Q800. Rheology was evaluated using a TA Instruments DHR-2 Rheometer. Gas chromatography-mass spectrometry experiments (GC-MS) were taken using a Thermo Scientific ISQ GC Ultra. Extrusion was performed on a Thermo Haake Minilab II conical twin screw extruder with 7  $\text{cm}^3$  volume under nitrogen flow.



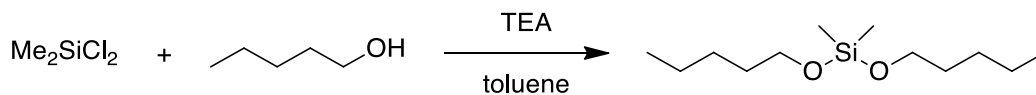
## Synthesis and vitrimer preparation

**Scheme S1.** Preparation of *KF:DB18-c-6*.



Potassium fluoride (1 equiv., 1.721 mmol, 100.0 mg) and dibenzo-18-crown-6 (1 equiv., 1.721 mmol, 620.3 mg) were added to 300 mL of methanol in a round bottom flask with a magnetic stir bar. The solution was brought to reflux for 1 hour and subsequently cooled to room temperature. The solvent was removed *in vacuo* to yield dry white flakes. The flakes were then ground to a fine powder using a mortar and pestle.

**Scheme S2.** *Synthesis of dipentoxysilyl ether.*



To a flame-dried and nitrogen-purged 3-necked flask fitted with a condenser and magnetic stir bar, anhydrous toluene (30 mL), anhydrous pentanol (3 equiv., 60 mmol, 6.498 mL), and anhydrous triethyl amine (3 equiv., 60 mmol, 8.362 mL) were added and the mixture lowered to 0 °C. Dichlorodimethylsilane (1 equiv., 20 mmol, 2.412 mL) was added dropwise through a syringe. After 1 hour of stirring at 0 °C, the reaction was slowly brought to reflux and held for 4 hours. The flask was then cooled to room temperature and the solvent was removed *in vacuo*. The slurry was dissolved in diethyl ether and filtered through a zeolite plug. The diethyl ether was removed, and the crude product was purified through fractional distillation at 78 °C/0.50 mmHg. Yield: 3.2368 g (70%).

**Dipentoxysilyl ether.**  $^1\text{H}$  NMR (500 MHz,  $\text{CDCl}_3$ , 298 K)  $\delta$  3.66 (t,  $J = 6.6$  Hz, 4H), 1.63-1.48 (m, 4H), 1.36-1.26 (m, 8H), 0.90 (t,  $J = 6.3$  Hz, 6H), 0.11 (s, 6H).  $^{13}\text{C}$  NMR (125 MHz,  $\text{CDCl}_3$ , 298 K)  $\delta$  62.62, 32.36, 28.05, 22.54, 14.10, 3.15.

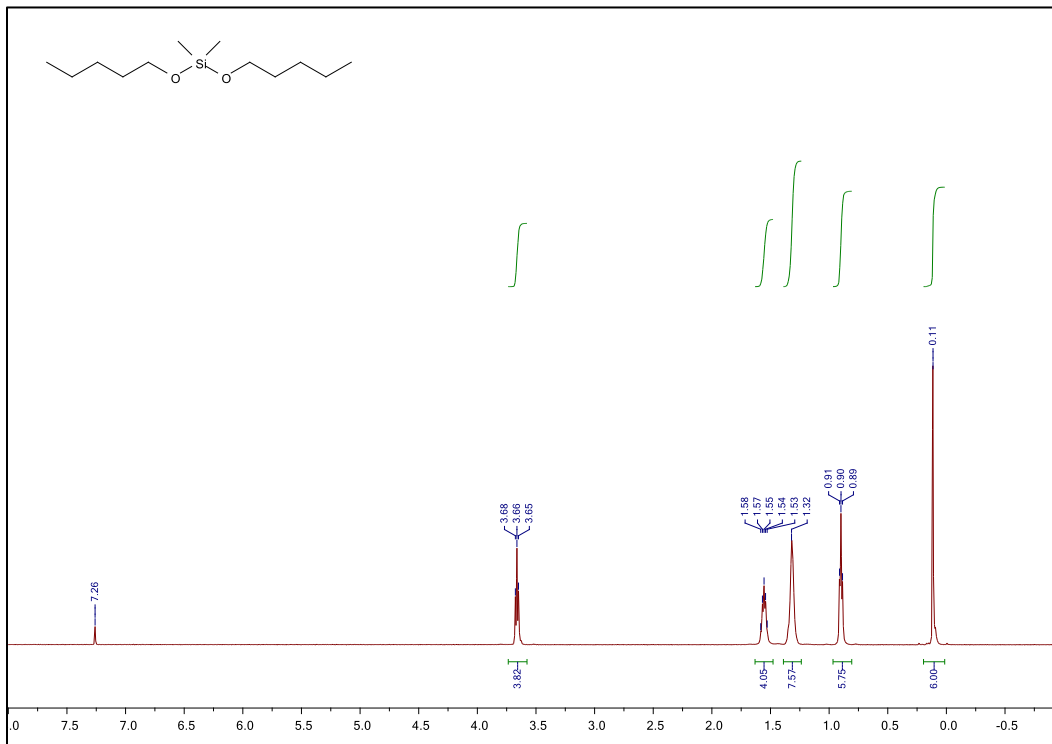


**Figure S1.**  $^1\text{H}$  NMR (500 MHz,  $\text{CDCl}_3$ , 298 K) spectrum for **dipentoxysilyl ether**.

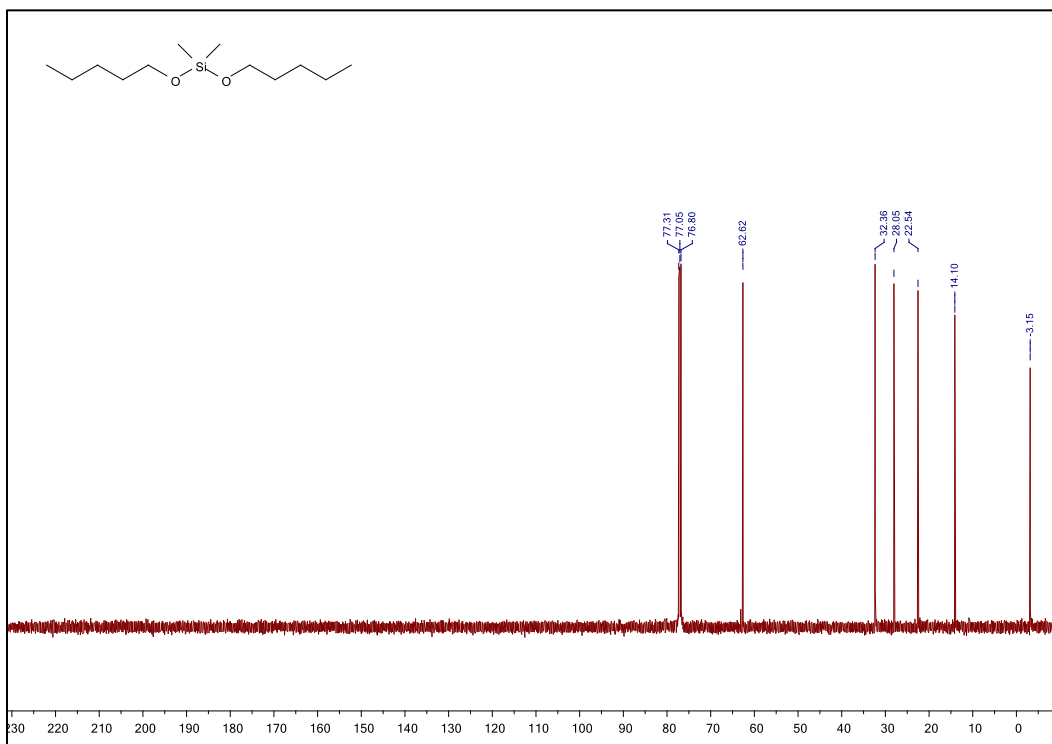
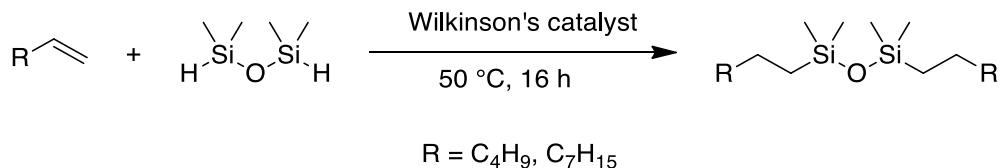


**Figure S2.**  $^{13}\text{C}$  NMR (125 MHz,  $\text{CDCl}_3$ , 298 K) spectrum for **dipentoxysilyl ether**.

**Scheme S3.** *Synthesis of dihexyltetramethyldisiloxane & dinonyltetramethyldisiloxane*



Into a round bottom flask with a magnetic stir bar, Wilkinson's catalyst (0.0005 equiv., 12.7  $\mu$ mol, 11.7 mg), alkene (2.5 equiv., 63.37 mmol), and 1,1,3,3-tetramethyldisiloxane (1 equiv., 23.35 mmol, 3.405 g) were added without solvent. The mixture was heated to 50 °C overnight followed by purification by fractional distillation (125 °C/0.350 mmHg for R=C<sub>4</sub>H<sub>9</sub> and 166 °C/0.168 mmHg for R=C<sub>7</sub>H<sub>15</sub>) twice to yield a colorless oil.

R=C<sub>4</sub>H<sub>9</sub>: 4.3166 g (37.5% yield)

R=C<sub>7</sub>H<sub>15</sub>: 7.5082 g (76.6% yield)

**Dihexyltetramethyldisiloxane.** <sup>1</sup>H NMR (500 MHz, CDCl<sub>3</sub>, 298 K)  $\delta$  1.35-1.2 (m, 16H), 0.89 (t, J=6.3 Hz, 6H), 0.50 (t, J=5.4 Hz, 4H), 0.03 (s, 12H). <sup>13</sup>C NMR (125 MHz, CDCl<sub>3</sub>, 298 K)  $\delta$  33.17, 31.70, 23.30, 22.66, 18.48, 14.19, 0.42.

**Dinonyltetramethyldisiloxane.** <sup>1</sup>H NMR (500 MHz, CDCl<sub>3</sub>, 298 K)  $\delta$  1.35-1.20 (m, 28H), 0.88 (t, J=6.9 Hz, 6H), 0.50 (t, J=7.2 Hz, 4H), 0.03 (s, 12H). <sup>13</sup>C NMR (125 MHz, CDCl<sub>3</sub>, 298 K)  $\delta$  33.50, 31.98, 29.63, 29.47, 29.45, 23.34, 22.74, 18.47, 14.16, 0.43.

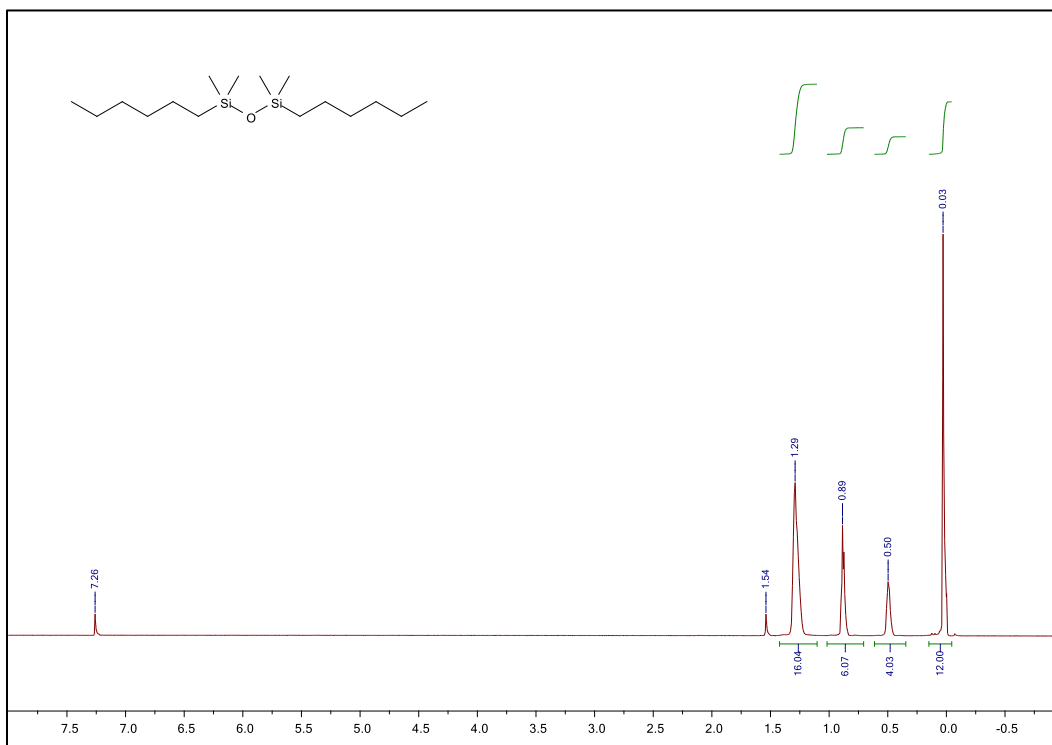


**Figure S3.**  $^1\text{H}$  NMR (500 MHz,  $\text{CDCl}_3$ , 298 K) spectrum for **dihexyltetramethyldisiloxane**.

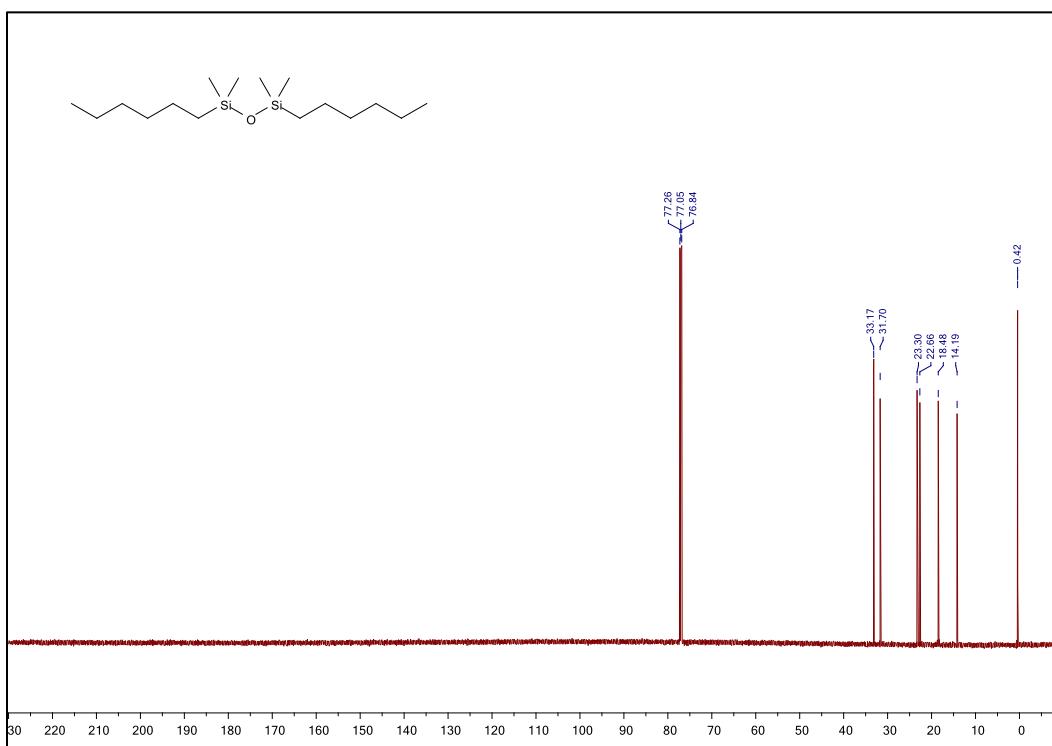


**Figure S4.**  $^{13}\text{C}$  NMR (125 MHz,  $\text{CDCl}_3$ , 298 K) spectrum for **dihexyltetramethyldisiloxane**

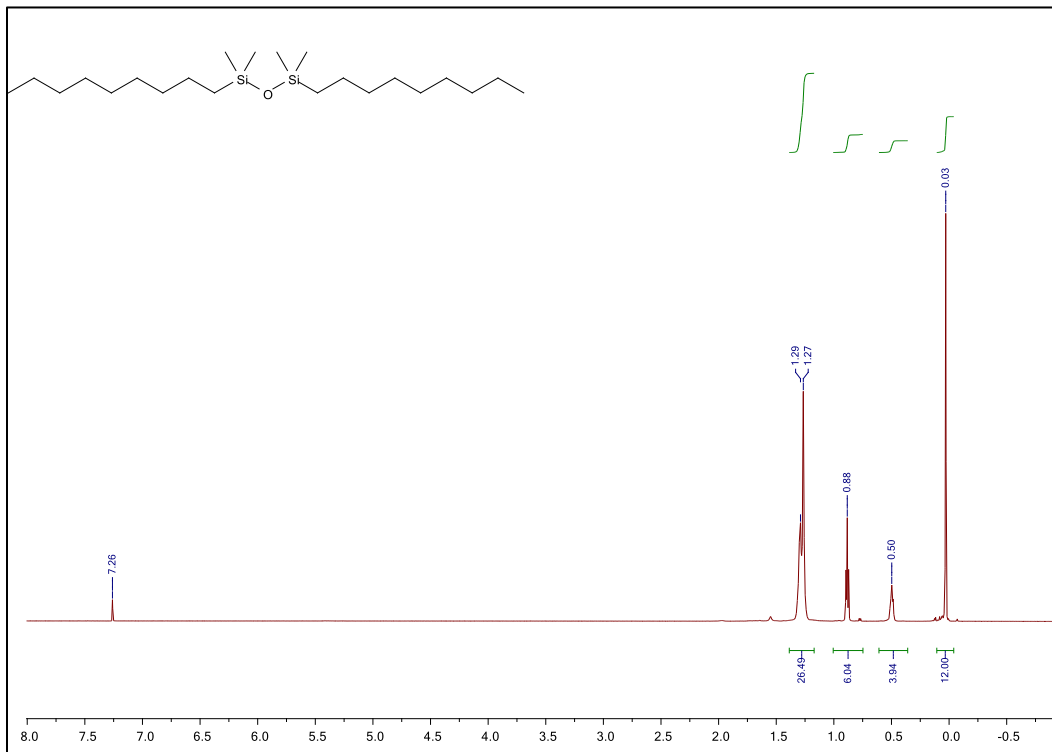


**Figure S5.**  $^1\text{H}$  NMR (500 MHz,  $\text{CDCl}_3$ , 298 K) spectrum for **dinonyltetramethyldisiloxane**.

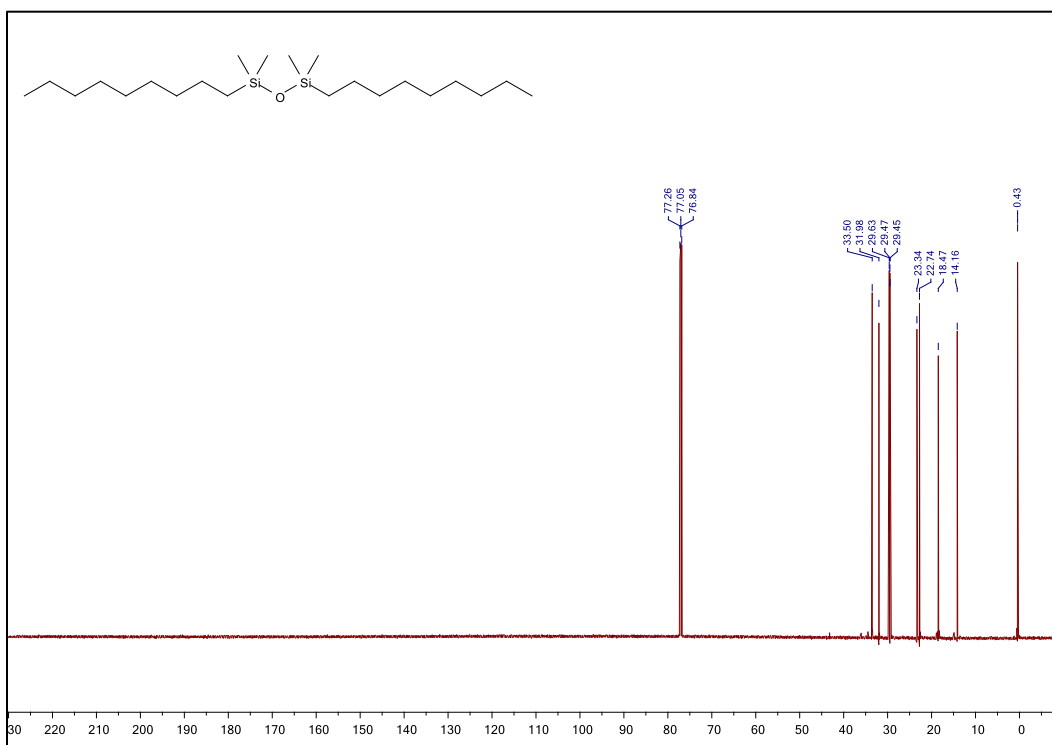
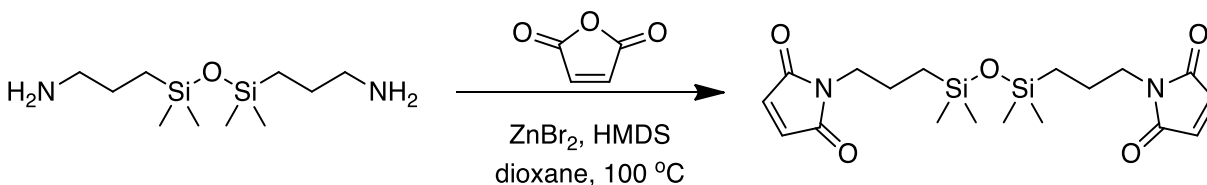


**Figure S6.**  $^{13}\text{C}$  NMR (125 MHz,  $\text{CDCl}_3$ , 298 K) spectrum for **dinonyltetramethyldisiloxane**.

**Scheme S4.** *Synthesis of bismaleimidotetramethyldisiloxane.*



Maleic anhydride (2 equiv., 32.19 mmol, 3.157 g) was added to a dried 3-necked round bottom flask and dissolved with 30 mL dry dichloromethane followed by the dropwise addition of 1,3-bis(aminopropyl)tetramethyldisiloxane (1 equiv., 16.10 mmol, 4.000 g). After 1 hour of stirring at room temperature, the solvent was removed *in vacuo* and the brown oil was re-dissolved in 1,4-dioxane (30 mL). To the solution, zinc bromide (2 equiv., 32.19 mmol, 7.249 g) and hexamethyldisilazane (3 equiv., 48.29 mmol, 7.778 g) were added and the slurry was brought to 100 °C. After 30 minutes, the mixture was brought back to room temperature and the solvent was removed *in vacuo*. The crude powder was purified through solid loading flash chromatography (Teledyne Isco® CombiFlash+) with 30:70 ethyl acetate to hexanes. Yield: 1.9567 g (30%).

**Bismaleimidotetramethyldisiloxane:** <sup>1</sup>H NMR (500 MHz, CDCl<sub>3</sub>, 298 K) δ 6.68 (s, 4H), 3.48 (t, J = 7.3 Hz, 4H), 1.62-1.50f (m, 4H), 0.53-0.38 (m, 4H), 0.03 (s, 12H). <sup>13</sup>C NMR (125 MHz, CDCl<sub>3</sub>, 298 K) δ 170.96, 134.06, 40.77, 22.60, 15.36, 0.27.

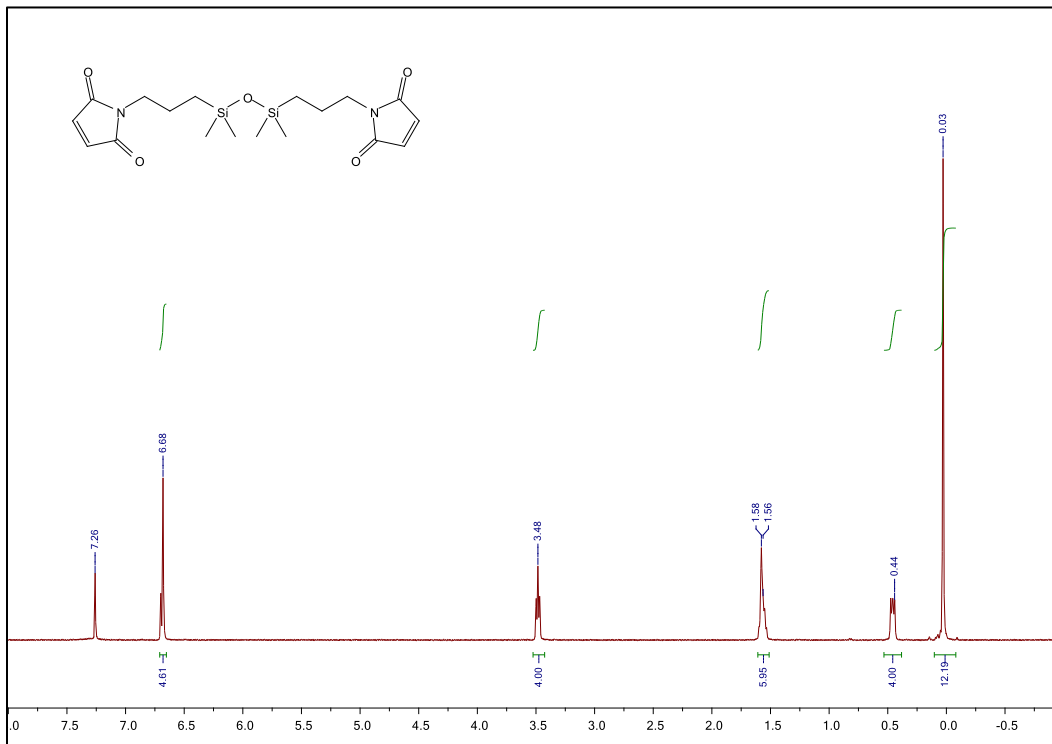


**Figure S7.**  $^1\text{H}$  NMR (500 MHz,  $\text{CDCl}_3$ , 298 K) bismaleimidotetramethyldisiloxane

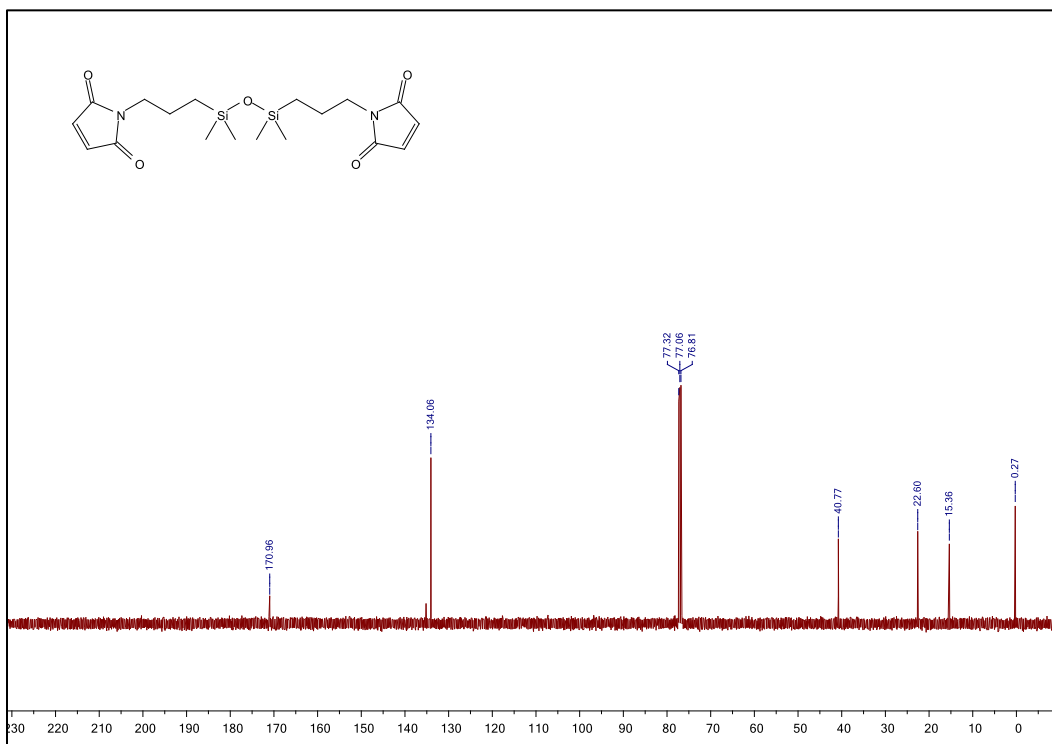


**Figure S8.**  $^{13}\text{C}$  NMR (125 MHz,  $\text{CDCl}_3$ , 298 K) bismaleimidotetramethyldisiloxane



***Procedure for model compound hydrolysis study.***

The model compound of interest (dipentoxysilyl ether or dihexyltetramethyldisiloxane, 0.50 mmol) was added to a one-dram vial with a magnetic stir bar and dissolved with 0.350 mL N-methyl-2-pyrrolidone and 0.005 mL of 1 M HCl. The vial was capped and heated to 90 °C and aliquots were taken at different time intervals for analysis via GC-MS. The disappearance of starting material was used to calculate percent conversion.

***Representative procedure for siloxane exchange model compound study***

First, a stock solution of the required catalyst was prepared by dissolving the catalyst (77.4  $\mu\text{mol}$ ) in 1,2,4-trichlorobenzene to bring the total volume to 4.00 mL. For the exchange study, dihexyltetramethyldisiloxane (43.9 mg, 145.1  $\mu\text{mol}$ ) and dinonyltetramethyldisiloxane (56.1 mg, 145.1  $\mu\text{mol}$ ) were added to a one-dram vial and dissolved with the stock catalyst solution (300  $\mu\text{L}$ , 5.8  $\mu\text{mol}$  catalyst) to yield a 2 mol% catalyst solution. The vial was capped and heated in an oil bath to the required temperature. Aliquots were taken at various time points and analyzed through GC-MS.

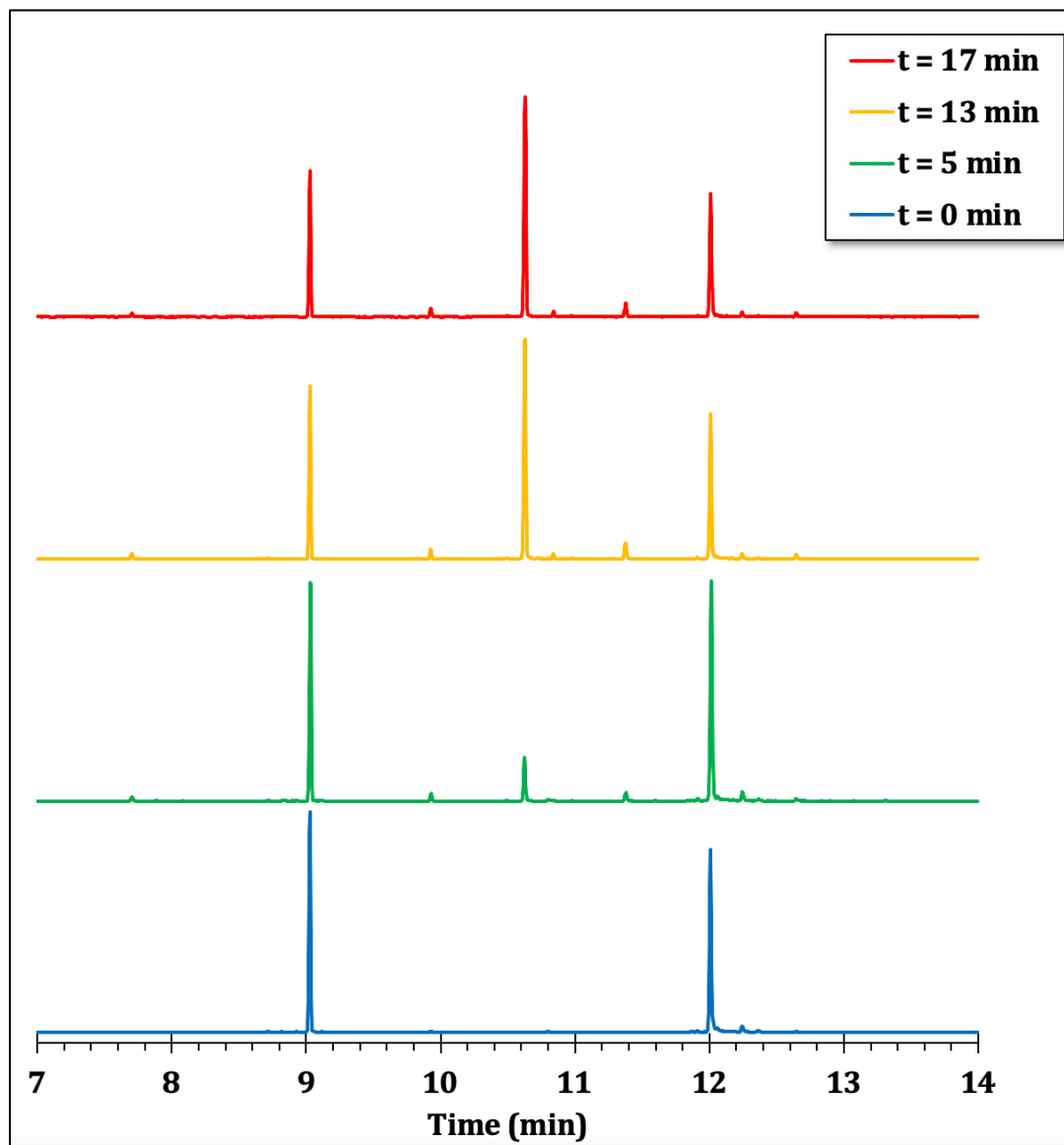


**Figure S9.** Representative GC-MS chromatogram of the exchange between dihexyltetramethyldisiloxane (RT: 9.017 min) and dinonyltetramethyldisiloxane (RT: 11.997 min) in the presence of 2 mol% KF:DB18-c-6 at 140 °C to yield the mixed product (RT:10.612 min). The small peaks at RT 9.926 min, 11.375 min, and 12.646 min are 1,5-bisdihexylhexamethyltrisiloxane, 1,5-bishexylnonylhexamethyltrisiloxane, and 1,5-bisnonylhexamethyltrisiloxane, respectively. The small peak at 12.242 min is an isomer of 1,5-dinonyltetramethyldisiloxane that could not be removed with distillation.

***Determining the energy of activation from small molecule kinetics.***

The chemical equation to represent the model siloxane exchange is



AA = dihexyltetramethyldisiloxane

AB = 1-hexyl-3-nonyltetramethyldisiloxane

BB = dinonyltetramethyldisiloxane

By using the initial time points at 100 °C (373 K), AB\* had reached 8.22% conversion in 5 (300 s) minutes, therefore:

$$t_{0 \text{ min}} = 0.362 M_{AA} + 0.362 M_{BB} \rightarrow 0 M_{AA^*} + 0 M_{AB^*} + 0 M_{BB^*}$$

$$t_{5 \text{ min}} = 0.332 M_{AA} + 0.332 M_{BB} \rightarrow 0.015 M_{AA^*} + 0.030 M_{AB^*} + 0.015 M_{BB^*}$$

Using the rate equation:

$$rate = -\frac{d[AA]}{dt} = k[AA][BB] \quad (1)$$

$$k_1 = 8.986 \times 10^{-4} \text{ s}^{-1}\text{M}^{-1}$$

By using the initial time points at 120 °C (393 K), AB\* had reached 13.76% conversion in 5 minutes (300 s), therefore:

$$t_{0 \text{ min}} = 0.362 M_{AA} + 0.362 M_{BB} \rightarrow 0 M_{AA^*} + 0 M_{AB^*} + 0 M_{BB^*},$$

$$t_{5 \text{ min}} = 0.312 M_{AA} + 0.312 M_{BB} \rightarrow 0.025 M_{AA^*} + 0.050 M_{AB^*} + 0.025 M_{BB^*}$$

By using equation 1:  $k_2 = 1.704 \times 10^{-3} \text{ s}^{-1}\text{M}^{-1}$

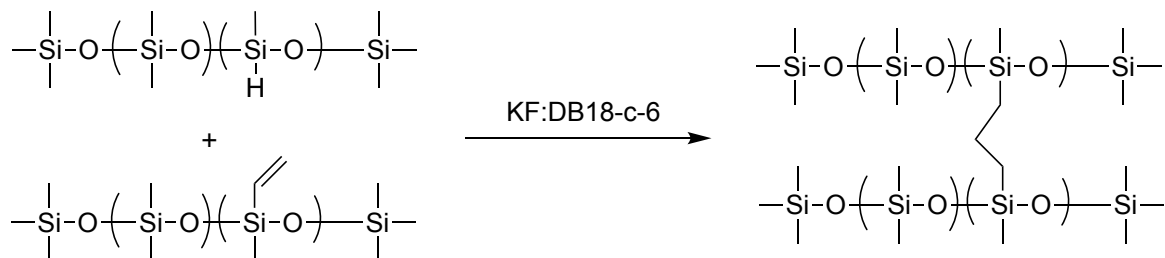
Inputting the above values into the Arrhenius equation:

$$\ln\left(\frac{k_1}{k_2}\right) = \left(\frac{1}{T_2} - \frac{1}{T_1}\right) \frac{E_a}{R} \quad (2)$$

Yields an  $E_a$  of 38.98 kJ/mol

### ***Preparation of the PDMS elastomer with embedded catalyst***

**Scheme S5.** *Synthesis of PDMS elastomer with embedded catalyst.*



The commercially available Dow<sup>®</sup> Sylgard 184 2-part elastomer kit was used to prepare the PDMS samples. The PDMS base (5.0228 g) was added to a 6 dram vial followed by the addition of 250 mg KF:DB18-c-6 fluoride catalyst. The base and catalyst were vigorously mixed with a mechanical stirrer and gentle heating to disperse the catalyst throughout the base. The curing agent (0.5020 g) was then vigorously mixed into the base and catalyst without heat. The mixture was poured into flat-bottom culture dishes and bubbles were removed at room temperature under low vacuum (260 mmHg) for 30 minutes followed by high vacuum (0.3 mmHg) for 30 minutes. A PDMS elastomer without catalyst was prepared in the same manner. After curing at room temperature for 3 days, the elastomer was punched into 20 mm disks for use on a parallel plate rheometer. Stress relaxation measurements were taken at 1% strain, which was within the linear response range.

### ***PMMA-v preparation***

Poly(methyl methacrylate) (Acros Organics,  $M_n = 35,000$ ) beads of approximately 0.5 mm were dried under heat and vacuum at 60 °C and 0.3 mmHg for two hours prior to use. The PMMA beads (5.000 g), 1,3-bisaminopropyltetramethyldisiloxane (4 wt%, 200 mg), and KF:DB18-c-6 (5 mol%, 16.8 mg) were added to a Nalgene tube and vigorously mixed for five

minutes. The mixture was fed into an extruder and melt blended at 230 °C and 60 RPM for 10 minutes under nitrogen. After flushing the extrudate through the strand die, the strands were compression molded at 180 °C for physical testing.

### ***HDPE-v preparation***

HDPE pellets with MFI = 2.2 g/10 minutes (190 °C/2.16 kg) were milled into a fine powder using a Fritsch Pulverisette rotary mill fitted with a 0.5 mm sieve cassette and dried at under heat and vacuum at 60 °C and 0.3 mmHg for two hours prior to use. HDPE powder (5.000 g), bismaleimidotetramethyldisiloxane (4 wt%, 200 mg), powdered dicumyl peroxide (0.25 wt%, 12.5 mg), and KF:DB18-c-6 (10 mol% fluoride, 20.5 mg blend) were added to a Nalgene tube and vigorously mixed for five minutes. The blend was fed into the extruder at 190 °C and 60 RPM for 5 minutes under a blanket of nitrogen. After flushing the extrudate, the strands were compression molded at 180 °C for physical testing. For recycling demonstrations, the HDPE-v was cut into ~4 mm pieces, coated with a small amount of BHT antioxidant (~2000 ppm) and fed back into the extruder at 190 °C running at 60 RPM.

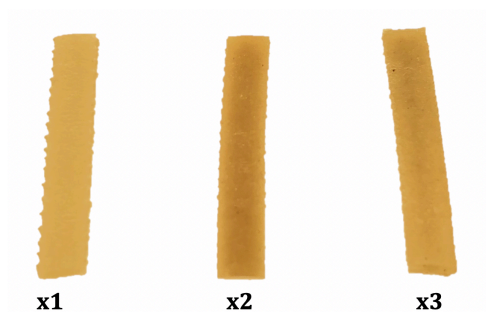


**Figure S10.** Photograph of HDPE-v extrudate after three consecutive cycles of recycling.

## Physical characterization and testing

### *Insoluble content testing*

Approximately 75 mg portions of crosslinked material were swollen in 20 mL of dried solvents (PMMA-v = 22 °C chloroform and HDPE-v = 120 °C xylenes) for 24 hours. The swollen gel was then physically removed and dried under high vacuum until the weight became constant. The gel fraction is based on the weight after swelling and drying divided by the weight before swelling.

**Table S1.** Gel content of HDPE-v over three reprocessing cycles.

		<b>Piece 1</b>	<b>Piece 2</b>	<b>Piece 3</b>	<b>Average</b>
<b>Round 1</b>	<b>Before</b>	52.1 mg	64.5 mg	75.0 mg	
	<b>After</b>	26.3 mg	33.1 mg	34.3 mg	
	<b>Gel %</b>	50.5%	51.3%	45.7%	49.2% ± 3.0%
<b>Round 2</b>	<b>Before</b>	62.7 mg	77.1 mg	74.5 mg	
	<b>After</b>	32.6 mg	35.1 mg	34.0 mg	
	<b>Gel %</b>	52.0%	47.1 %	45.6 %	48.2% ± 3.3%
<b>Round 3</b>	<b>Before</b>	76.6 mg	73.4 mg	72.4 mg	
	<b>After</b>	36.3 mg	34.5 mg	33.7 mg	
	<b>Gel%</b>	47.4 %	47.0%	46.5%	47.0% ± 3.3%

**Table S2.** Gel content of PMMA-v at different catalyst loading concentrations.

<b>Catalyst Loading</b>		<b>Piece 1</b>	<b>Piece 2</b>	<b>Piece 3</b>	<b>Average</b>
<b>10 mol%</b>	<b>Before</b>	120.9 mg	106.8 mg	95.0 mg	
	<b>After</b>	104.3 mg	89.4 mg	79.5 mg	
	<b>Gel %</b>	86.2%	83.7%	83.7 %	84.5% ± 1.4%
<b>5 mol%</b>	<b>Before</b>	160 mg	132.4 mg	83.7 mg	
	<b>After</b>	119.6 mg	99.0 mg	65.4 mg	
	<b>Gel %</b>	74.8%	74.8%	78.1%	75.9% ± 1.9%
<b>1.25 mol%</b>	<b>Before</b>	85.7 mg	222.6 mg	60.3 mg	
	<b>After</b>	66.2 mg	173.7 mg	46.6 mg	
	<b>Gel%</b>	77.2%	78.0%	77.3%	77.5% ± 0.4%

### ***TBAF dissolution***

Approximately 75 mg portions of crosslinked network were swollen in 20 mL of good solvents (PMMA-v = chloroform, HDPE-v = 120 °C xylenes) for 24 hours. Approximately 10 mg of tetrabutylammonium fluoride hydrate was added in three portions over the course of 3 hours due to the rapid degradation of TBAF in hot solvent. After the final addition of excess fluoride, the samples had totally dissolved, and no gel remained.



**Figure S11.** Photographs of swollen PMMA-v before and after the addition of excess TBAF.



**Figure S12.** Photographs of swollen HDPE-v before and after the addition of excess TBAF.



### ***Creep tests***

At room temperature, creep tests were performed on a Instron 3365 mechanical tester fitted with pneumatic grips. Dog bone shaped samples (1.5 mm x 3.5 mm x 15 mm) were exerted to 10 MPa force for 20 minutes. The average creep rate was taken from 100-1200 seconds to remove the initial elastic response of the sample. At elevated temperatures, creep testing was performed on a TA Instruments DHR-2 rheometer equipped with a 12 mm parallel plate. A constant normal force of 10 Newtons was applied for vitrimer samples to maintain good contact.

### ***Stress relaxation***

For HDPE-v, stress relaxation experiments were performed on a TA Instruments DHR-2 rheometer equipped with a 12 mm parallel plate. HDPE-v samples were first compression molded into coupons and then punched into 12 mm disks for testing. A strain of 3% was applied using a strain rise time of 0.1 seconds. For PMMA-v, stress relaxation was performed on a TA Instruments DMA Q800 in film mode using 1% strain. A constant normal force of 10 Newtons was applied for vitrimer samples to maintain good contact.

### ***Dynamic mechanical thermal analysis (DMTA)***

DMTA temperature sweeps of PMMA, PMMA-v, HDPE, and HDPE-v were characterized on a TA Instruments DMA Q800 in film mode. The oscillation frequency was set to 3 Hz, the oscillatory strain to 0.1%, and the temperature ramp was set to 3 °C/min.

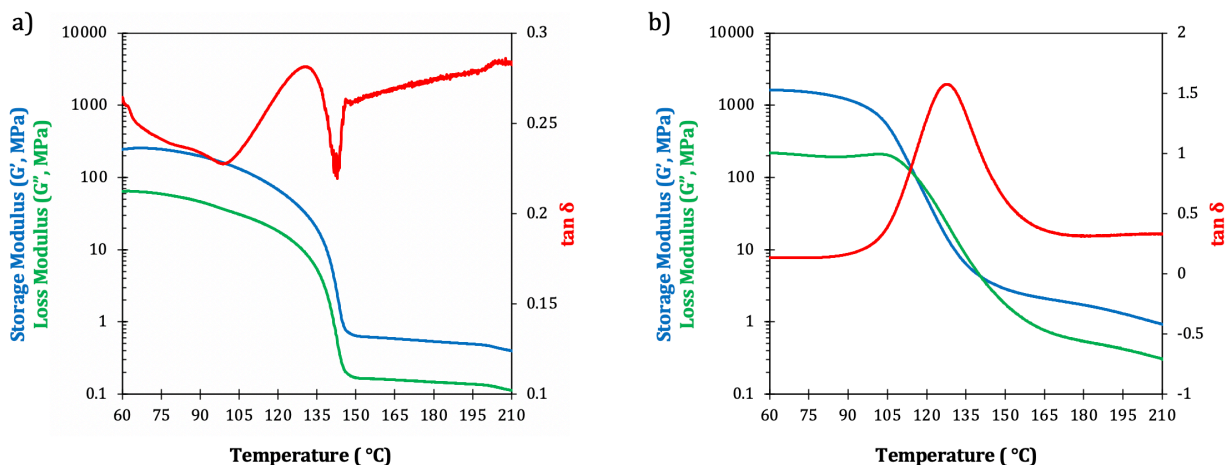


**Figure S13.** DMTA temperature sweeps (a) HDPE-v and (b) PMMA-v.

### ***Frequency sweeps***

Frequency sweeps were performed on a TA Instruments DHR-2 rheometer equipped with a 12 mm parallel plate. The oscillatory strain was set to 0.5% and the frequency was swept from 0.01–100 Hz at 190 °C.

### ***DSC measurements***

DSC measurements were performed on a TA Instruments DSC2500 under an inert nitrogen atmosphere. Approximately 10 mg of sample was sealed in a hermetic pan and subjected to a heat-cool-heat cycle where the sample was heated at 20 °C/min and cooled at 10 °C/min from -90 °C to 200 °C.

*Unmodified HDPE:* Enthalpy of 2<sup>nd</sup> melting heat: 200.95 J/g = 68.6% crystalline.

*HDPE-v:* Enthalpy of 2<sup>nd</sup> melting heat: 159.89 J/g = 54.6% crystalline.

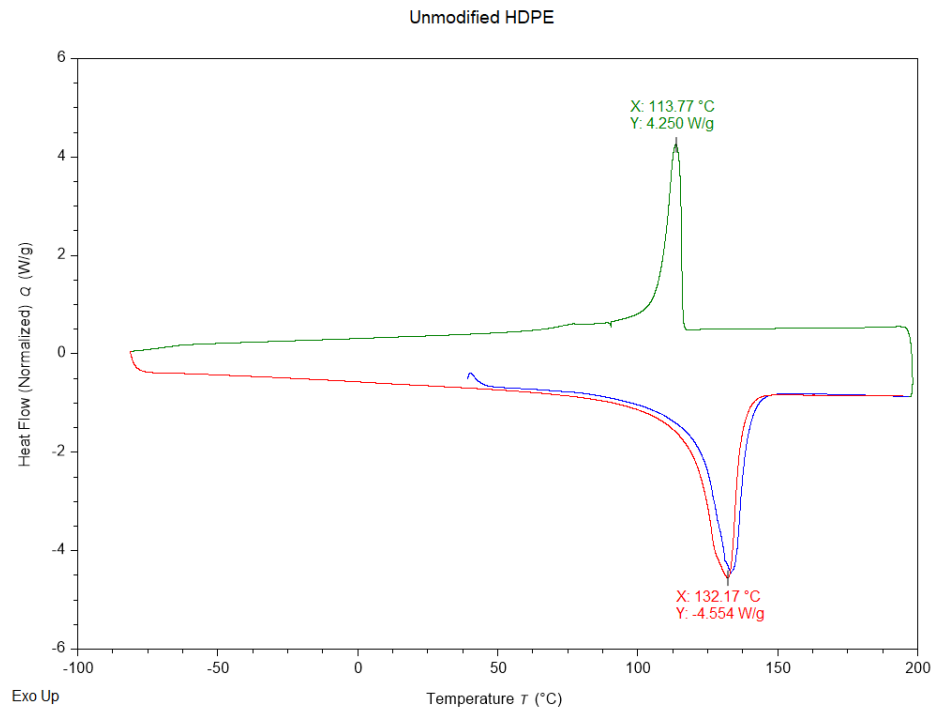


**Figure S14.** DSC thermogram of unmodified HDPE.

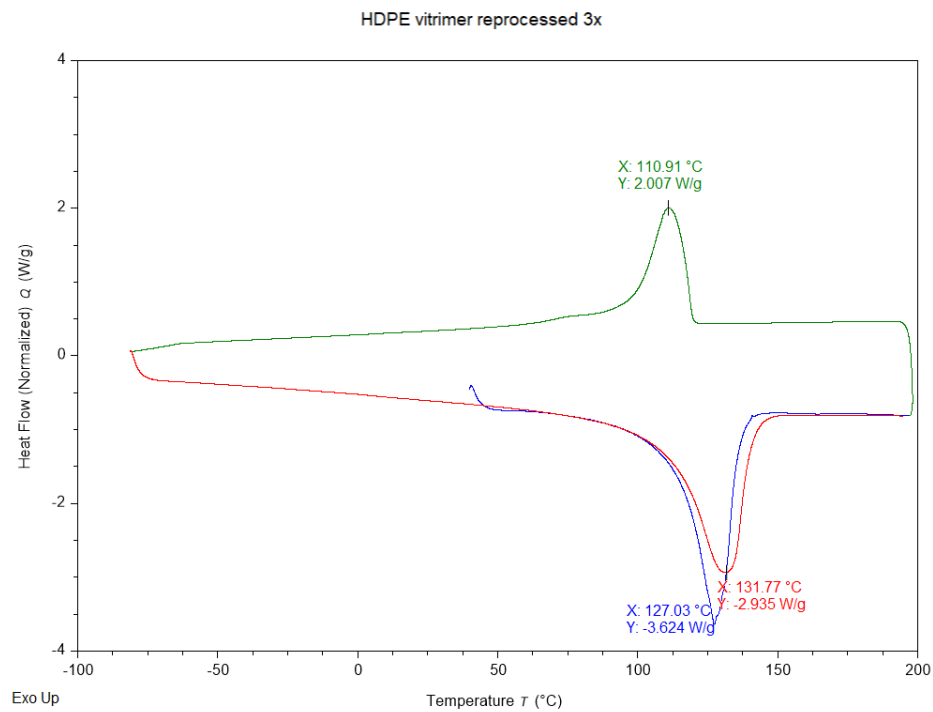


**Figure S15.** DSC thermogram of HDPE-v after three reprocessing cycles.

### ***TGA measurements***

TGA measurements were performed on a TA Instruments Q500 under nitrogen atmosphere. Approximately 15 mg of sample was placed on a platinum crucible and heated at a rate of 20 °C/min from ambient temperature to 850 °C.

*Unmodified HDPE*: 5% weight loss at 456 °C

*HDPE-v*: 5% weight loss at 414 °C

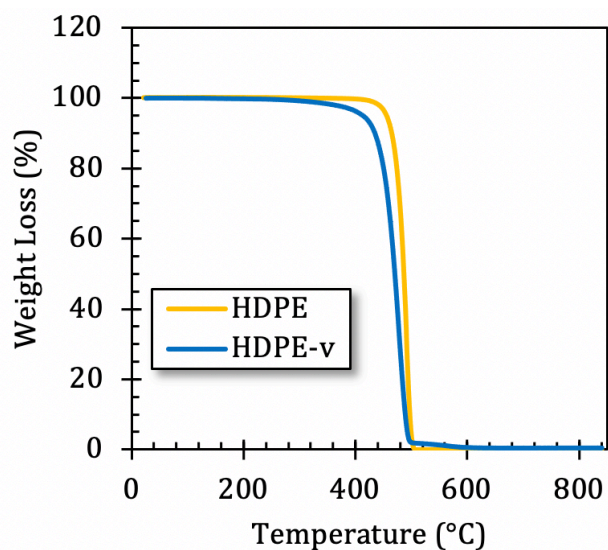


**Figure S16.** TGA thermogram of unmodified HDPE and HDPE-v.

### Tensile testing

Tensile testing was performed on a Instron 3365 mechanical tester fitted with pneumatic grips. Samples were compression molded into dog bone shapes (1.5 mm x 3.5 mm x 15 mm) and exerted to a strain rate of 1 mm/mm/min (100% of the initial measured length per minute).

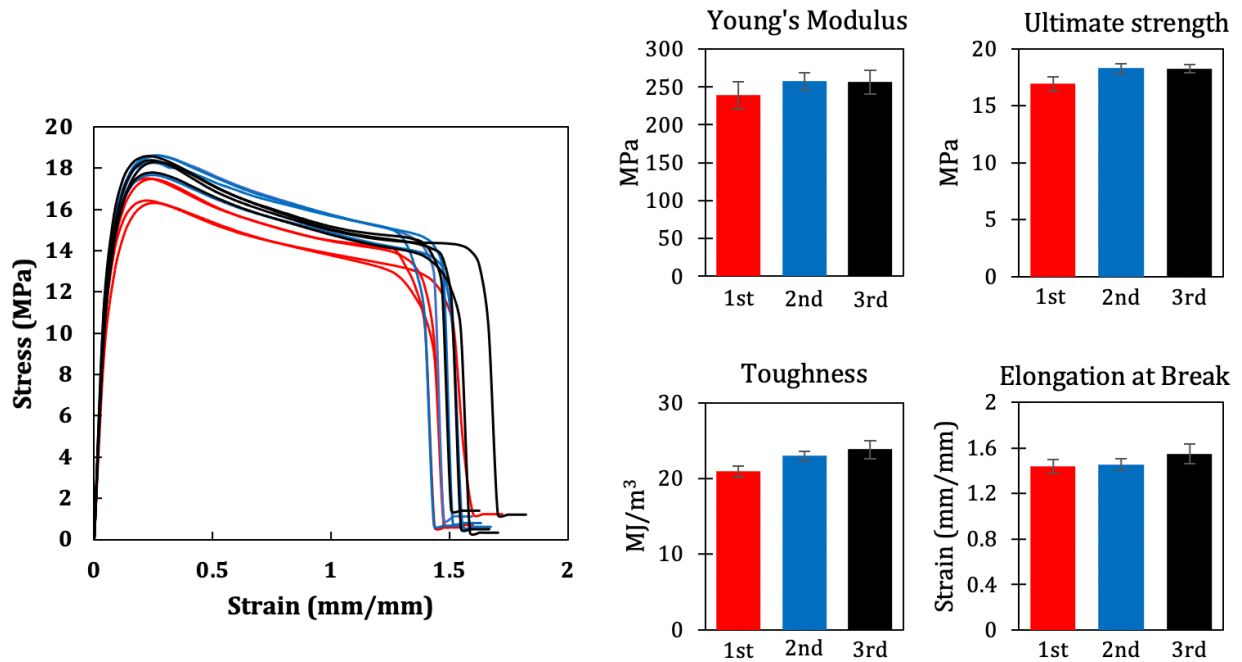


**Figure S17.** Tensile testing of HDPE-v for x1 (red), x2 (blue), and x3 (black) reprocessing in triplicates.

## Determination of the topology freezing temperature ( $T_v$ )

The topology freezing temperature was determined as previously reported.<sup>1</sup>

Using the Maxwell equation for viscosity

$$\eta = G \cdot \tau^* = \frac{E'}{2(1+\nu)} \cdot \tau^* \quad (1)$$

and inputting the Poisson's ratio ( $\nu$ ) for HDPE (0.46),<sup>2</sup> Equation S1 is simplified to:

$$\eta = 0.342 \times E' \times \tau^* \quad (2)$$

From DMTA measurements, the storage modulus  $E'$  is approximately 0.60 MPa at 160 °C. The viscosity at the topology freezing temperature is approximated to  $\eta = 10^{12}$  Pa, therefore  $\tau^* = 4,863,518$  s. By inserting  $\tau^*$  into the equation for the line of best fit from the stress relaxation Arrhenius treatment of HDPE-v:

$$\ln \tau^*(T) = 5.888 \times \frac{1000}{T} - 14.573 \quad (3)$$

we can extrapolate to the temperature at which the siloxane exchange has been arrested. It was found that the  $T_v$  for HDPE-v is 196 K (-76 °C).

## 4.6 References:

- (1) Tretbar, C. A.; Neal, J. A.; Guan, Z. Direct Silyl Ether Metathesis for Vitrimers with Exceptional Thermal Stability. *J. Am. Chem. Soc.* **2019**, 141 (42), 16595–16599. <https://doi.org/10.1021/jacs.9b08876>.
- (2) Brandrup, J.; Immergut, E. H. *Polymer Handbook*, 3rd ed.; John Wiley & Sons, 1989.

# Chapter 5: Progress Towards a General Strategy for Polymer Compatibilization

## 5.1 Introduction and current state of compatibilizers

Despite the seemingly limitless combination of polymers, relatively few are miscible.<sup>1,2</sup> Most polymer blends have a positive free energy of mixing ( $\Delta G_m > 0$ ) since  $\Delta G_m$  is largely determined by the enthalpic contribution of mixing high molecular weight polymers. Macromolecules have a low entropy of mixing, therefore the entropic contribution to  $\Delta G_m$  is low.<sup>3</sup> The blending of immiscible polymers results in a phase segregated material with poor physical properties, coarse morphology, and weak adhesion between domains.<sup>4</sup> Since polymers derive their strength from chain entanglement, a discontinuity of entanglement at the phase-separated interface dramatically weakens polymer blends.<sup>5,6</sup> To improve performance, the interface between domains can be strengthened by the addition of a compatibilizer.<sup>1</sup>

Compatibilizers work to reduce interfacial tension and act as emulsifiers between the phases. When compatibilizers are added, the mechanical strength is dramatically increased due to the formation of covalent bonds across the interface.<sup>1</sup> Compatibilizers can be grouped into two major categories that work through: *i*) addition of a pre-made compatibilizer such as block copolymers,<sup>7,8</sup> random copolymers,<sup>9,10</sup> and mutually miscible homopolymers,<sup>1</sup> and *ii*) reactive compatibilization which generates linkages between immiscible polymers *in situ* such as the direct reactive compatibilization of homopolymers<sup>11,12</sup> and preparation of graft-from homopolymers.<sup>13,14</sup> Neither method of compatibilization is a general solution and each method remains limited in application scope. In the case of pre-made compatibilizers, the

compatibilizer structure needs to be tailored for the individually immiscible polymers, and in the case of reactive compatibilization, the immiscible polymers must have complementary reactive motifs. Due to the expansive variety of polymer backbones, a generalized compatibilizer has not been developed to date. Such a development would be of great importance for combining unknown types and compositions of immiscible blends.

## 5.2 Our design for a general polymer compatibilizer

We propose that immiscible blends can be kinetically trapped by the addition of a covalent adaptive network (CAN) which will dissociate under high temperature and stress and would quickly reform once shear and heat are removed. Mechanically trapping the immiscible polymers from phase segregating provides a novel route for compatibilization that is distinctly different than previously reported approaches. This method of freezing the topology would be independent of the polymer composition since it doesn't rely on the specific chemistry of the polymers in the blends. To achieve rapid and stable trapping, the dynamic motif must *i)* utilize dissociative exchange *ii)* have thermal stability under processing conditions, and *iii)* have chemical stability towards the functionalities observed in most polymers.

A well-studied dissociative exchange motif that fits the above criteria is the Diels-Alder (DA) adduct, which has been studied extensively due to the wide variety of available diene and dienophiles.<sup>15</sup> By changing the DA constituents, the temperature window of cycloaddition and retro-Diels Alder (r-DA) can be tuned to match the specific application. Herein, we report progress towards the development of DA-based compatibilizers (Figure 5.1). Specifically, we aim to prepare DA-functional polymers and melt blend them into a



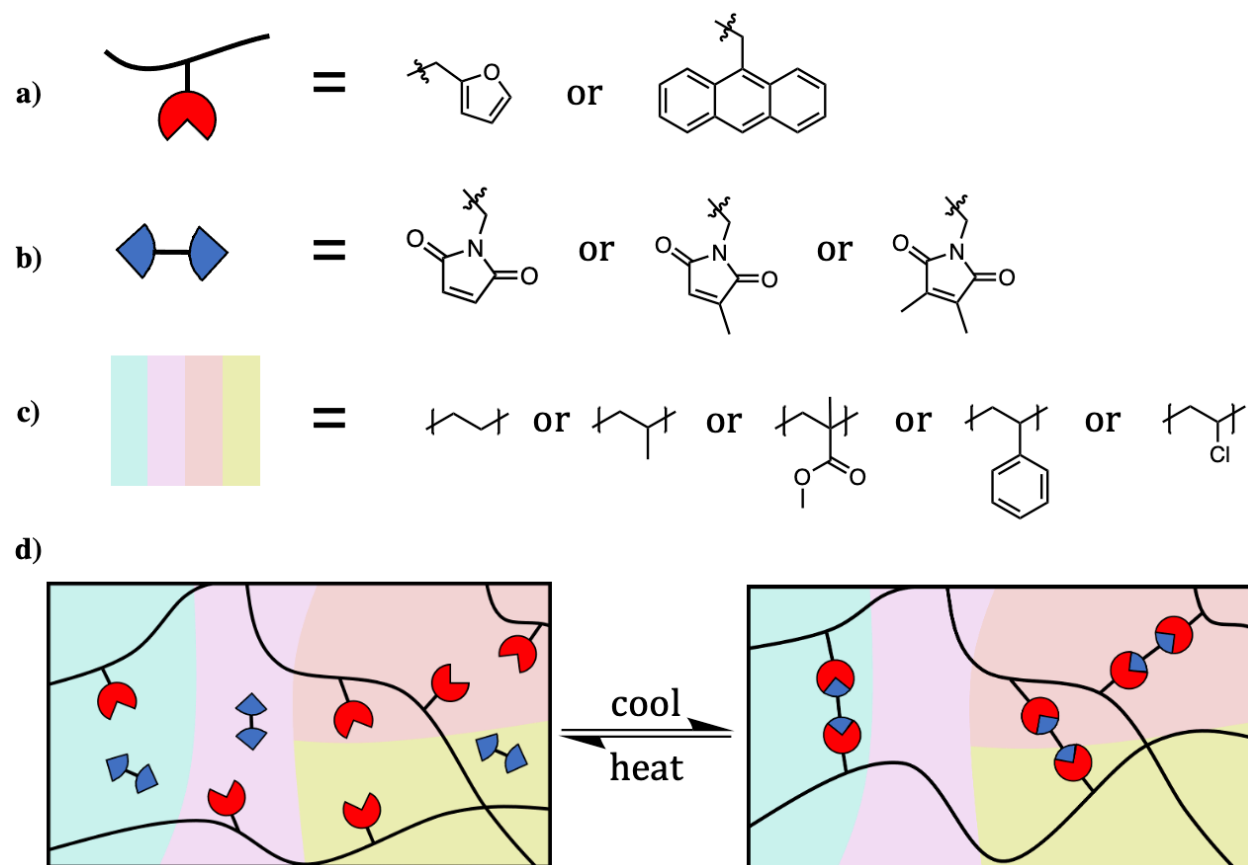


**Figure 5.1.** Design concept for generalized compatibilizer. By mixing a polymer-grafted diene (a) and dienophile (b) in a blend of polymers (c), the topology can be arrested with cooling (d) prior to phase segregation of the mixture. The network can be reprocessed with further heat and mixing.

several immiscible polymer blends. Upon cooling, the DA adducts will form crosslinks that trap the blend from phase separating.

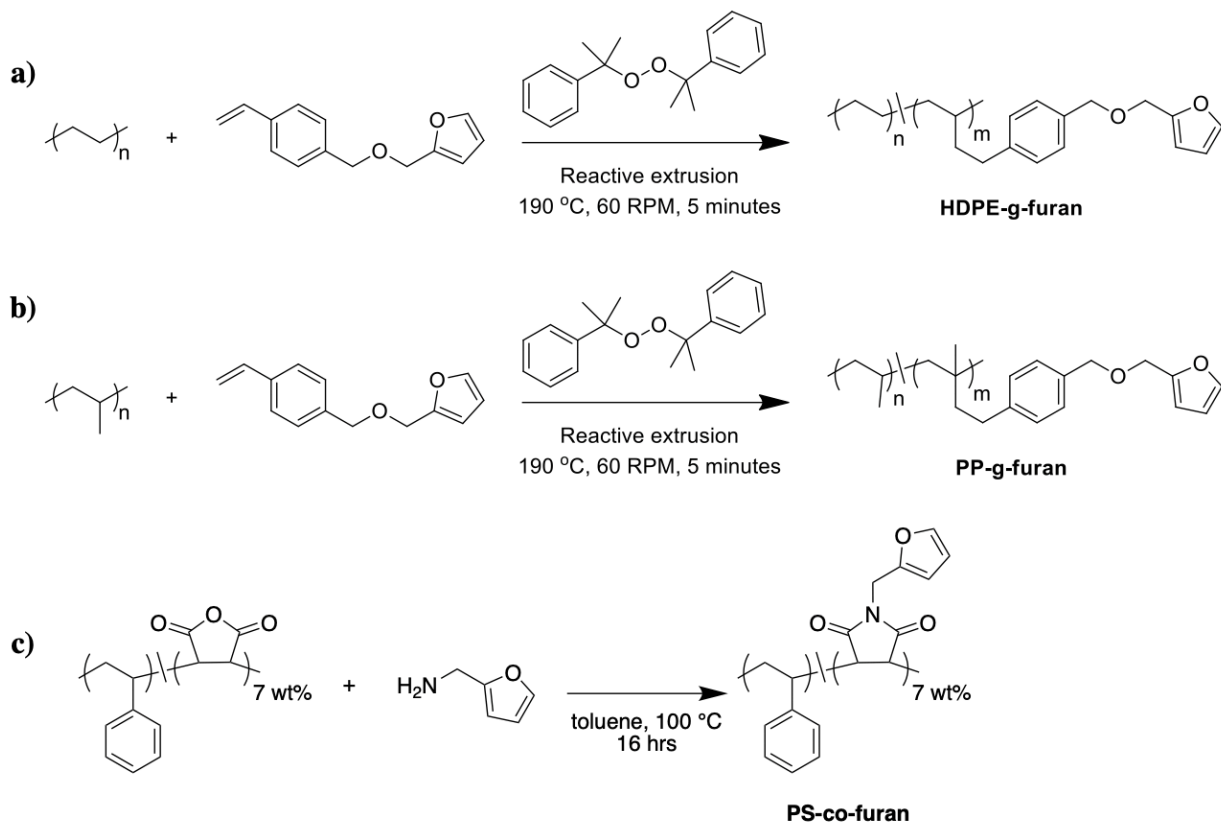
## 5.3 Results and Discussion

### 5.3.1 Initial efforts with furan and maleimide DA adducts

Furan-maleimide DA adducts are thermally stable, insensitive to common functional groups, and have been well studied in literature for their high efficiency and mild temperature window for DA/r-DA.<sup>16</sup> At approximately 100 °C the r-DA begins to dominate,

and below 80 °C the adduct begins to form. This temperature window was initially targeted as it meant that we could anneal the freshly mixed blend at room temperature without further processing. To synthesize the compatibilizer (Scheme 5.1), the monomer 2-(((4-vinylbenzyl)oxy)methyl)furan was synthesized and radically grafted to both high density polyethylene (HDPE, MFI = 2.2 g/10min) and isotactic polypropylene (PP,  $M_n = 97,000$  g/mol) using dicumyl peroxide (DCP). The radical grafting was achieved using a benchtop twin screw extruder heated to 190 °C and operating at 60 RPM for five minutes. The extruder has a recirculating valve that allows for extended residence time to mimic large-scale production extruders. The material was ejected and residual monomer was removed through precipitation from heated xylene into methanol. Through  $^1\text{H-NMR}$  it was found that

**Scheme 5.1.** Synthesis of furan-functionalized polymers.



the HDPE-*g*-furan had an average ratio of 1:238 furan to ethylene repeat units while the PP-*g*-furan had an average of 1:243 furan to propylene repeat units. Higher degrees of functionality were not achievable under this process due to observed side-reactions. Other monomers such as 2-(nitrovinyl)furan, furan-2-ylmethyl acrylate, and furan-2-ylmethyl methacrylate were attempted, however the grafting yield to HDPE was low while no grafting was achieved with PP. Separately, polystyrene-co-furan was prepared from the imidation of poly(styrene-co-maleic anhydride) (Scheme 5.1c). These three compatibilizer backbones provide different levels of miscibility with the bulk polymer blend. The maleimides used were BMI-358 and BMI-1500, which are commercially available bifunctional maleimides of 4,4'-methylenedianiline and a low molecular weight fatty imide-extended oligomer. The number following BMI represents the molecular weight of the bismaleimide.

After preparing the three types of furan-grafted polymers, they were screened against several commodity polymer blends using maleimide as the dienophile. Different levels of compatibilized material were melt blended using a twin-screw extruder heated to 190 °C operating at 60 RPM. After extrusion, the samples were flushed from the extruder and immediately annealed at 70 °C for 2 hours under vacuum to promote Diels-Alder formation. After annealing, samples were characterized by SEM, DSC, DMTA, and FTIR. Scanning electron microscopy (SEM) micrographs were taken of the fractured interface to observe compatibility. If compatibilized, the phases should have stronger adhesion and resist breakage. This can be tested by looking at the fractured surface for stretched polymer strands as the compatibilized interface resists separation. It has also been observed that compatibilization promotes smaller droplet size for the minor phase, however it is unknown if our kinetic trapping design will have similar behavior to literature. If there is no

compatibilization, the interface should have clean separation as the phases are cleanly de-bonded.

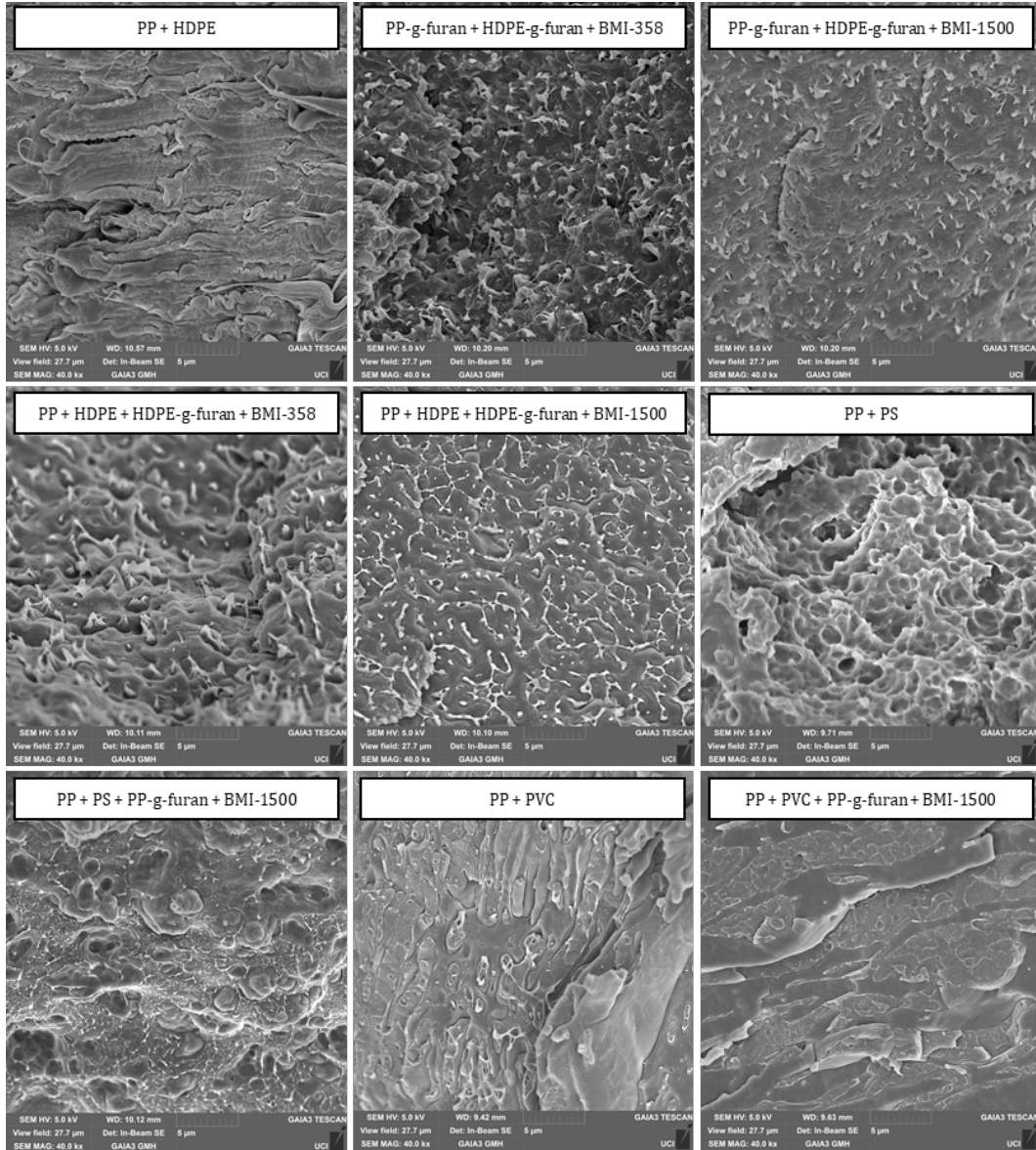


**Figure 5.2.** Representative SEM micrographs of immiscible polymer blends. (*top left*) 50% iPP + 50% HDPE (*top center*) 50% PP-g-furan + 50% HDPE-g-furan + 1 equiv. BMI-358 (*top right*) 50% PP-g-furan + 50% HDPE-g-furan + 1 equiv. BMI-1500 (*middle left*) 50% iPP + 40% HDPE + 10% PP-g-furan + 1 equiv. BMI-358 (*middle center*) 50% iPP + 40% HDPE + 10% PP-g-furan + 1 equiv. BMI-1500 (*middle right*) 50% iPP + 50% polystyrene (*lower left*) 50% iPP + 40% polystyrene + 10% PP-g-furan + 1 equiv. BMI-1500 (*lower center*) 50% iPP + 50% polyvinyl chloride (*lower right*) 50% iPP + 40% polyvinyl chloride + 10% PP-g-furan + 1 equiv. BMI-1500.

The SEM micrographs in Figure 5.2, show low levels of compatibilization for a several blends. The *iPP + HDPE control (top left)* showed large scale tearing and relatively large dispersions. Upon the addition of our compatibilizer to *PP + HDPE* blends, smaller features begin to emerge, and hair-like strands can be observed as the blend resists the shearing force. In the case of the *PP + PS control* and the *PP + PS + compatibilizer*, the change is less dramatic. Pitting can be observed where one of the phases cleanly de-bonds from the other and leaves craters, indicating challenges in compatibilizing PP and PS. For *PP + PVC control* and *PP + PVC + compatibilizer*, the change is more dramatic. The *PP + PVC control* has clear dark lines surrounding the domains which indicates clean de-bonding of the phases, however upon the addition of a compatibilizer the separation lines disappear, and the blend becomes more homogenous. The difference in compatibilization in the blends is likely to arise from the dispersion ability of PP-g-furan and BMI-1500 in the molten state. Both DA polymers must have similar miscibility to find each other and form the adducts upon cooling. If there is a large difference in miscibility, then the DA polymers will likely not find each other, and phase separation will continue to occur. This observation prompts a proposed design change to where both diene and dienophile are bound to the same polymer backbones to ensure mutual miscibility, which will be covered in Section 5.4 Troubleshooting and Future Directions.

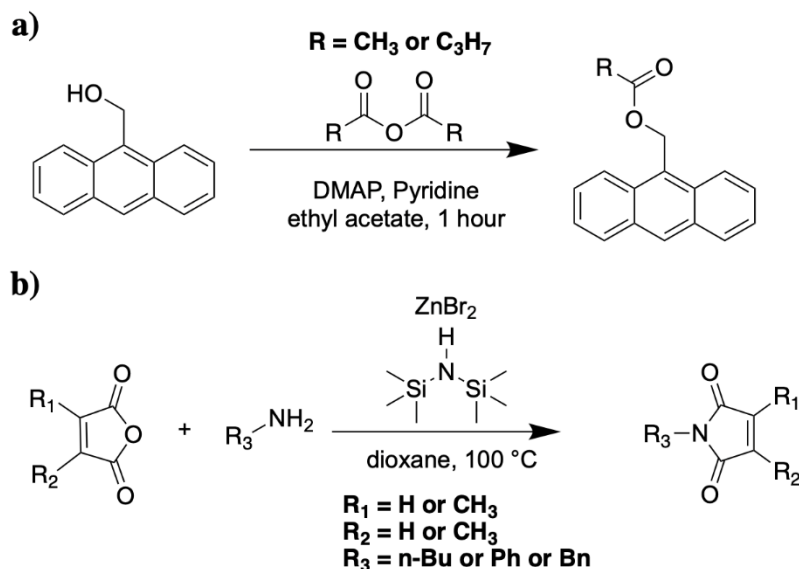
Other methods of characterization such as DSC, DMTA, and FT-IR provided no evidence for compatibilization. The Flory-Fox equation predicts that in miscible polymer blend a new  $T_g$  will form between the two  $T_g$ s of the main constituents.<sup>17</sup> We were hoping to observe the  $T_g$  using DSC or DMTA measurements, however no  $T_g$  was observed for any of the compatibilized blends (data not shown). Our rationale is that the DA adduct-bearing

polymers are not totally miscible with either of the main components and may instead reside at the interface. As such, the kinetic trapping will only occur at the thin interface between phases. Such behavior would be difficult to detect through DSC and DMTA measurements as they don't have the sensitivity to detect such small glass transitions. In FT-IR measurements, the furan and maleimide signals could not be observed despite their observation in  $^1\text{H-NMR}$ . We attribute this to the low abundance of furan and maleimide due to the low grafting efficiency from the reactive extrusion process. Alternatives to the grafting process are proposed in Section 5.4. Separately, an additional screen of polymer blend compatibilization was attempted using the polystyrene-based furan (Scheme 5.1c). We hoped that a modification to the backbone would promote better mixing with the main blend components, however little compatibilization was observed (data not shown). The positive results from SEM imaging in Figure 5.2 indicate there is some compatibilization effect we are observing, however without further characterization data it is problematic to draw conclusion from our limited observations.

### **5.3.2 Current efforts towards anthracene-maleimide DA adducts**

The results from the furan-maleimide DA adducts suggest that we need faster cycloaddition between the diene and dienophile as well as an increase in the thermal window for the DA/r-DA. With these new targets, the trapping process can occur more quickly post-extrusion which will give the immiscible phases less chance to phase separate. After searching for compatible DA adducts, we settled on anthracene as the diene and alkyl-substituted maleimide as the dienophile. Anthracene-maleimide DA adducts are extremely stable and have been well studied in literature, however the DA reaction only occurs above

**Scheme 5.2.** Synthesis of substituted anthracenes and maleimides.



180 °C and the r-DA at temperatures >250 °C. While this temperature window is too high for our applications, the window can be tuned by the addition of alkyl substituents to the maleimide (Scheme 5.2b). The alkyl substituents introduce steric hinderance to the adduct and lower the DA/retro-DA window down into our extrusion temperature zone.

To determine the DA/r-DA temperatures for methyl-substituted maleimides, a model compound screen of anthracene and maleimide were performed. For anthracene and unsubstituted maleimide (Figure 5.3a), the adduct did not form until temperatures reached 180 °C, however the reaction was practically irreversible as the adduct decomposed at 250 °C before any retro-DA was observed. Dimethyl maleimide (Figure 5.3c) was on the opposite end of the reactivity spectrum in that no DA adduct was observed at when held at 25 °C, 160 °C, and 200 °C. In the apparent Goldilocks zone, the monomethyl maleimide was found to start forming the DA adduct above 160 °C and the retro-DA was observed at temperatures above 200 °C (Scheme S4, Figure S1). This thermal window is better suited for the processing

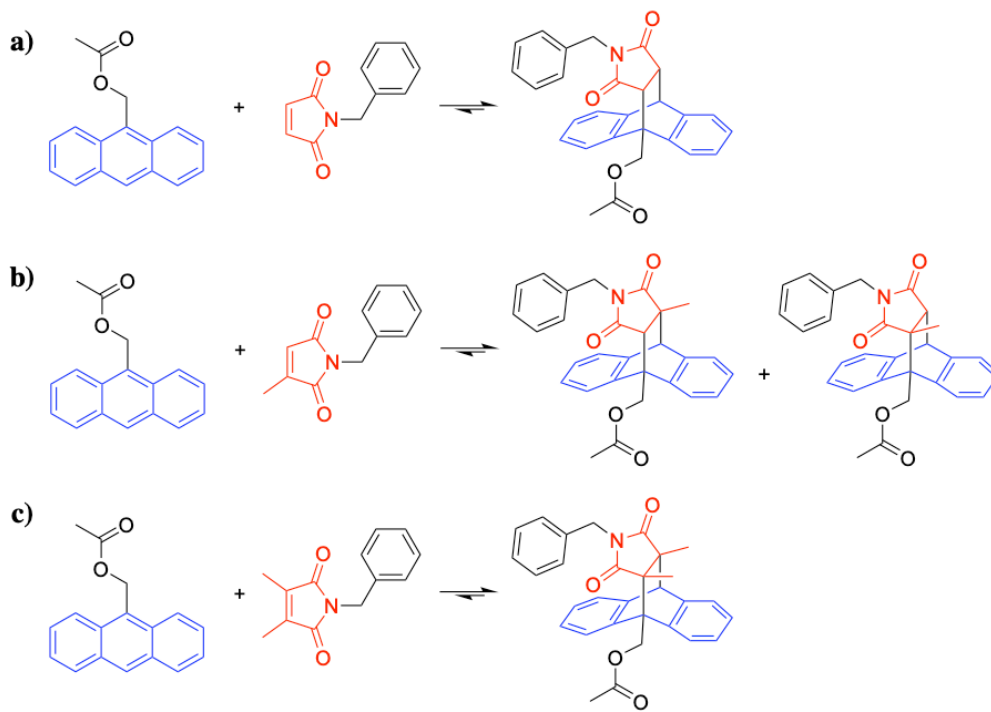


**Figure 5.3.** Model reactions of substituted anthracene and maleimides (a) Equilibrium between acetylated anthracene and unsubstituted maleimide. (b) Equilibrium between acetylated anthracene and monosubstituted maleimide. Two isomers are available for the product resulting from the asymmetric adduct formation. (c) Equilibrium between acetylated anthracene and the disubstituted maleimide.

conditions of the extruder since most plastics are processed in the temperature range of 180-230 °C.

To further investigate the thermal window of DA/retro-DA equilibrium for the monomethylmalide adduct, thermal sweeps using DSC were utilized to measure the endothermic and exothermic transitions. The adduct formation is an exothermic process while the retro-DA is an endothermic process. Butyric anthracene and monomethylmaleimide (Figure 5.4a) were added in a 1:1 ratio in 1,2,4-trichlorobenzene and heated to 180 °C for 1 hour. The solution was then precipitated into methanol and filtered and dried to yield the isolated DA adduct. On the first heating cycle in DSC (Figure 5.4b), an exothermic peak



can be observed at 91 °C indicating some further DA adduct formation is occurring. Immediately following, two endothermic peaks at 140 °C and 161 °C indicate a retro-DA process is occurring. The first peak is likely the *cis* isomer and the second peak is likely the *trans* isomer in reference to the monomethyl peak's relationship to the alkyl substituent on anthracene. The two isomers were likely caused by the rapid cooling of the initial DA adduct formation. The heat-cool was repeated several times and the more gradual cooling process

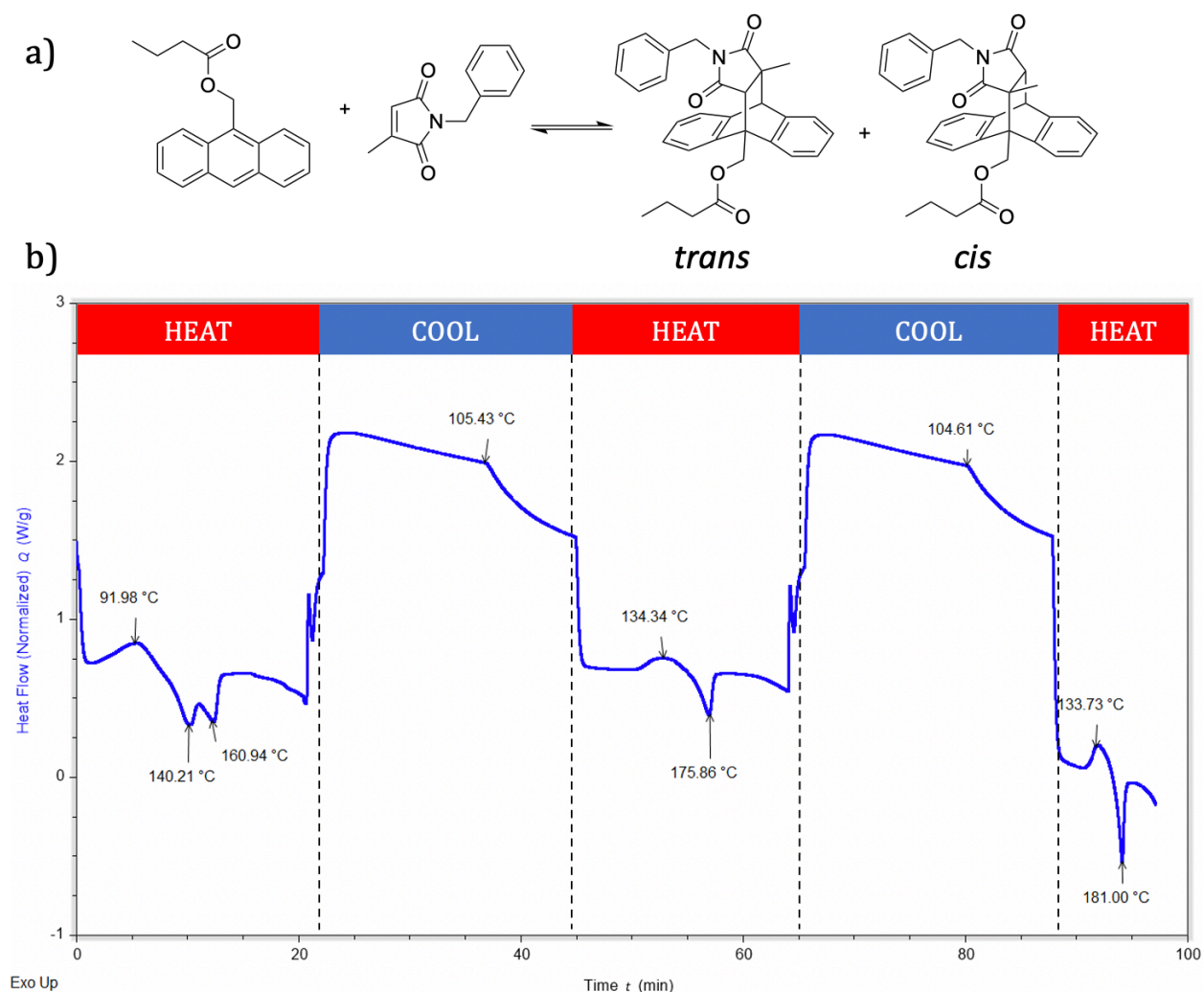


**Figure 5.4.** DSC thermogram of the anthracene-monomethylmaleimide DA equilibrium. (a) Equilibrium between the butyric anthracene and monomethylmaleimide. With rapid cooling, both *cis* and *trans* conformations can be detected. (b) DSC heat-cool thermograms indicating adduct formation and reversion at different temperatures.

seems to promote the formation of the more thermodynamically favored *trans* product. The DA chemistry has good reversibility and should translate well to the compatibilizer system where it may experience several reprocessing cycles.

#### 5.4 Troubleshooting and future directions

The furan-maleimide DA adducts showed some promise, however no other characterization methods were able to detect compatibilization. By moving to the more thermally stable anthracene-maleimide adduct, we hope to observe better compatibilization effects that are detectable by more methods of characterization.

Some issues of grafting efficiency were encountered during the grafting process of furan onto HDPE and iPP. It became very difficult to graft more than approximately 0.4 mol% furan relative to repeat units. Increasing the grafting efficiency through radical grafting is unlikely due to side reactions, so we must turn towards different chemistries to prepare DA-active polymers. We envision that post-polymerization modification of a different commercially available polyolefin copolymer through more traditional chemistries such as transesterification and transamination will allow for higher degrees of functionality. One such polymer is poly(ethylene-co-methyl methacrylate), which can be purchased in several grades of acrylate content. Transesterification of 9-methoxyanthracene onto the backbone would provide an excellent method for increasing the available anthracene to promote kinetic trapping.

In addition to increasing the DA adduct concentration, it would be conceptually more elegant to design a single polymer backbone that contained both diene and dienophile. Such a polymer would reduce the number of variables in the melt and ensure that diene and

dienophile are in close proximity at all times. Initial work was put forth to develop a single polymer backbone bearing both the furan and maleimide groups through copolymerization of furan and maleimide monomers. Unfortunately, premature gelation prevented this route to be explored further. With the more recent discovery of maleimide-anthracene adducts, the gelation would be suppressed until the temperature was raised above ~70 °C and the adducts had sufficient energy to form. Alternatively, the adducts can be copolymerized at much lower temperatures using photo-initiated radical polymerizations.

## 5.5 References:

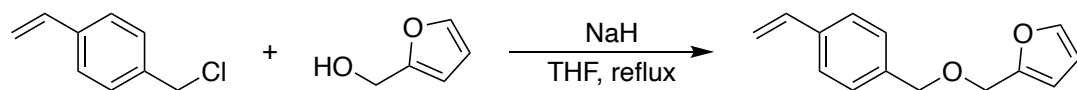
- (1) Utracki, L. A. *Polymer Blends Handbook*; Kluwer Academic Pub, 2002.
- (2) Barlow, J. W.; Paul, D. R. Polymer Blends and Alloys—a Review of Selected Considerations. *Polym. Eng. Sci.* **1981**, *21* (15), 985–996. <https://doi.org/10.1002/pen.760211502>.
- (3) Bates, F. S. Polymer-Polymer Phase Behavior. *Science* **1991**, *251* (4996), 898–905. <https://doi.org/10.1126/science.251.4996.898>.
- (4) Luciani, A.; Jarrin, J. Morphology Development in Immiscible Polymer Blends. *Polym. Eng. Sci.* **1996**, *36* (12), 1619–1626. <https://doi.org/10.1002/pen.10558>.
- (5) Porter, R. S.; Johnson, J. F. The Entanglement Concept in Polymer Systems. *Chem. Rev.* **1966**, *66* (1), 1–27. <https://doi.org/10.1021/cr60239a001>.
- (6) Kinloch, A. J. *Fracture Behaviour of Polymers*; Springer Science & Business Media, 2013.
- (7) Eagan, J. M.; Xu, J.; Girolamo, R. D.; Thurber, C. M.; Macosko, C. W.; LaPointe, A. M.; Bates, F. S.; Coates, G. W. Combining Polyethylene and Polypropylene: Enhanced Performance with PE/IPP Multiblock Polymers. *Science* **2017**, *355* (6327), 814–816. <https://doi.org/10.1126/science.aah5744>.
- (8) Xu, Y.; Thurber, C. M.; Macosko, C. W.; Lodge, T. P.; Hillmyer, M. A. Poly(Methyl Methacrylate)-Block-Polyethylene-Block-Poly(Methyl Methacrylate) Triblock Copolymers as Compatibilizers for Polyethylene/Poly(Methyl Methacrylate) Blends. *Ind. Eng. Chem. Res.* **2014**, *53* (12), 4718–4725. <https://doi.org/10.1021/ie4043196>.

- (9) Rigby, D.; Lin, J. L.; Roe, R. J. Compatibilizing Effect of Random or Block Copolymer Added to Binary Mixture of Homopolymers. *Macromolecules* **1985**, *18* (11), 2269–2273. <https://doi.org/10.1021/ma00153a036>.
- (10) Blom, H. P.; Teh, J. W.; Rudin, A. I-PP/HDPE Blends. III. Characterization and Compatibilization at Lower i-PP Contents. *J. Appl. Polym. Sci.* **1996**, *61* (6), 959–968. [https://doi.org/10.1002/\(SICI\)1097-4628\(19960808\)61:6<959::AID-APP10>3.0.CO;2-Q](https://doi.org/10.1002/(SICI)1097-4628(19960808)61:6<959::AID-APP10>3.0.CO;2-Q).
- (11) Sun, Y.-J.; Hu, G.-H.; Lambla, M.; Kotlar, H. K. In Situ Compatibilization of Polypropylene and Poly(Butylene Terephthalate) Polymer Blends by One-Step Reactive Extrusion. *Polymer* **1996**, *37* (18), 4119–4127. [https://doi.org/10.1016/0032-3861\(96\)00229-7](https://doi.org/10.1016/0032-3861(96)00229-7).
- (12) Wei, B.; Lin, Q.; Zheng, X.; Gu, X.; Zhao, L.; Li, J.; Li, Y. Reactive Splicing Compatibilization of Immiscible Polymer Blends: Compatibilizer Synthesis in the Melt State and Compatibilizer Architecture Effects. *Polymer* **2019**, *185*, 121952. <https://doi.org/10.1016/j.polymer.2019.121952>.
- (13) Jannasch, P.; Wesslén, B. Poly(Styrene-Graft-Ethylene Oxide) as a Compatibilizer in Polystyrene/Polyamide Blends. *J. Appl. Polym. Sci.* **1995**, *58* (4), 753–770. <https://doi.org/10.1002/app.1995.070580408>.
- (14) Xu, Y.; Thurber, C. M.; Lodge, T. P.; Hillmyer, M. A. Synthesis and Remarkable Efficacy of Model Polyethylene-Graft-Poly(Methyl Methacrylate) Copolymers as Compatibilizers in Polyethylene/Poly(Methyl Methacrylate) Blends. *Macromolecules* **2012**, *45* (24), 9604–9610. <https://doi.org/10.1021/ma302187b>.
- (15) Brieger, G.; Bennett, J. N. The Intramolecular Diels-Alder Reaction. *Chem. Rev.* **1980**, *80* (1), 63–97. <https://doi.org/10.1021/cr60323a004>.
- (16) Gandini, A. The Furan/Maleimide Diels–Alder Reaction: A Versatile Click–Unclick Tool in Macromolecular Synthesis. *Prog. Polym. Sci.* **2013**, *38* (1), 1–29. <https://doi.org/10.1016/j.progpolymsci.2012.04.002>.
- (17) Aubin, M.; Prud’homme, R. E. Analysis of the Glass Transition Temperature of Miscible Polymer Blends. *Macromolecules* **1988**, *21* (10), 2945–2949. <https://doi.org/10.1021/ma00188a010>.
- (18) Geyer, R.; Jambeck, J. R.; Law, K. L. Production, Use, and Fate of All Plastics Ever Made. *Sci. Adv.* **2017**, *3* (7), e1700782. <https://doi.org/10.1126/sciadv.1700782>.

## 5.6 Experimental

Unless otherwise noted, reactions were carried out with dry solvents using a magnetic stir bar. Commercial reagents were used as received with no further purification unless otherwise noted.  $^1\text{H}$  NMR spectra were recorded at either 500 MHz on a Bruker DRX500 spectrometer or at 600 MHz on a Bruker AVANCE600 spectrometer. NMR spectra peaks are reported as  $\delta$  values in ppm relative to TMS or residual solvent:  $\text{CDCl}_3$  ( $^1\text{H}$  = 7.26 ppm),  $\text{C}_7\text{D}_8$  ( $^1\text{H}$  = 7.10-7.20, 2.34 ppm). Differential Scanning Calorimetry (DSC) thermograms were evaluated using a TA Instruments DSC2500. Thermogravimetric Analysis (TGA) thermograms were evaluated using a TA Instruments Q500. Dynamic Mechanical Thermal Analysis (DMTA) analysis was evaluated using a TA Instruments Q800. Gas chromatography-mass spectrometry experiments (GC-MS) were taken using a Thermo Scientific ISQ GC Ultra. Scanning electron microscopy (SEM) micrographs were taken on a Tescan GAIA-3 XMG FIB by first sputter coating samples with carbon. SEM acceleration voltage was set to 5.0 kV and both backscattering and secondary electron detectors were used.

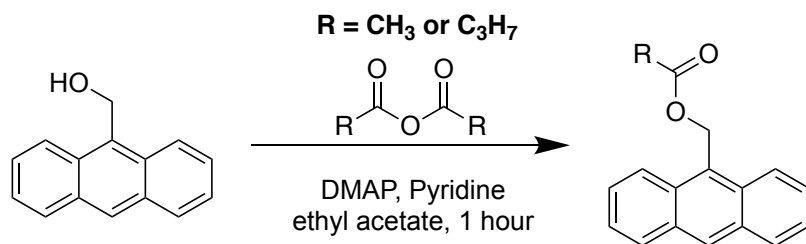
### Scheme S1. Synthesis of styryl furan



To prepare the styryl furan monomer, furfuryl alcohol (2.5 equiv., 65.5 mmol, 6.43 g) was dissolved in 15 mL anhydrous THF and added to a flame dried, nitrogen flushed, 3-necked round bottom fitted with a condenser and stir bar. The solution was cooled to 0 °C. Sodium hydride (60% in mineral oil, 1.1 equiv., 28.8 mmol, 1.15 g) was dissolved in 20 mL anhydrous THF to form a suspension. The suspension slowly to the round bottom, turning the solution from light yellow to pale orange. After bubbling ceased, 1-(chloromethyl)-4-vinylbenzene (1 equiv., 26.2 mmol, 4.00 g) dissolved in 15 mL anhydrous THF was added dropwise. The solution was slowly brought to reflux where the color changed to a transparent brown. The reaction progress was monitored by TLC in 100% hexanes. After completion, the sodium hydride was quenched with 25 mL saturated ammonium chloride and the mixture was transferred to a 250 mL separatory funnel. The crude product was extracted with dichloromethane (50 mL x 3), dried over magnesium sulfate, and purified by column chromatography (1:10 ethyl acetate:hexane). The diluted product was reduced in vacuo to yield 4.12 g (73.4%).

$^1\text{H}$  NMR (500 MHz,  $\text{CDCl}_3$ )  $\delta$  7.43 (s, 1H), 7.40 (d,  $J$  = 7.9 Hz, 2H), 7.31 (d,  $J$  = 7.8 Hz, 2H), 6.72 (dd,  $J$  = 17.2, 10.5 Hz, 1H), 6.35 (s, 1H), 6.33 (s, 1H), 5.75 (d,  $J$  = 17.7 Hz, 1H), 5.24 (d,  $J$  = 10.9 Hz, 1H), 4.54 (s, 2H), 4.48 (s, 2H). Low resolution MS (ESI+):  $m/z$  calcd. for  $\text{C}_{14}\text{H}_{14}\text{NaO}_2$  [M+Na]: 237.1; found 237.6.

## Scheme S2. Representative synthesis of acetylated anthracene

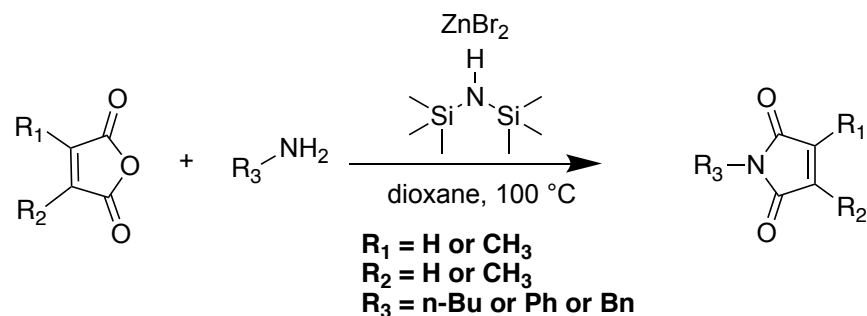


Substituted anthracenes were prepared according to literature procedure.<sup>1</sup> Into a nitrogen-flushed round bottom flask, 9-methoxyanthracene (1 equiv., 14.41 mmol, 3.000 g) was dissolved in anhydrous dichloromethane (50 mL) and cooled to 0 °C. Once cooled, pyridine (5 equiv., 72.03 mmol, 5.80 mL), acetic anhydride (3 equiv., 4.412 g, 4.09 mL), and dimethyl aminopyridine (0.1 equiv., 176 mg, 1.44 mmol) were added and stirred for 1 hour. The solvent was then evaporated in vacuo and the crude mixture was dissolved in 300 mL ethyl acetate. The organic layer was washed with saturated copper sulfate (3 x 100 mL) to remove residual amines. The organic layer was then washed with brine (2 x 100 mL) and dried with magnesium sulfate. The solvent was removed and the product was purified with flash chromatography (80:20 hexanes:ethyl acetate) to afford acetylated anthracene (3.4032 g, 94.4% yield).

**R = CH<sub>3</sub>:** <sup>1</sup>H NMR (500 MHz, CDCl<sub>3</sub>) δ 8.52 (s, 1H), 8.34 (d, *J* = 8.9 Hz, 2H), 8.04 (d, *J* = 8.4 Hz, 2H), 7.54 (dt, *J* = 14.9, 6.9 Hz, 4H), 6.16 (s, 2H), 2.09 (s, 3H). <sup>13</sup>C NMR (125 MHz, CDCl<sub>3</sub>) δ 171.39, 131.45, 131.10, 129.26, 129.18, 126.72, 126.25, 125.17, 123.97, 58.88, 21.07.

**R = C<sub>3</sub>H<sub>7</sub>:** <sup>1</sup>H NMR (500 MHz, CDCl<sub>3</sub>) δ 8.55 (s, 1H), 8.40 (d, *J* = 8.9 Hz, 2H), 8.08 (d, *J* = 8.4 Hz, 2H), 7.64 (t, *J* = 7.4 Hz, 2H), 7.56 (t, *J* = 7.5 Hz, 2H), 6.22 (s, 2H), 2.39 (t, *J* = 7.4 Hz, 2H), 1.77 – 1.67 (m, 2H), 0.98 (t, *J* = 7.4 Hz, 3H). <sup>13</sup>C NMR (125 MHz, CDCl<sub>3</sub>) δ 174.01, 131.45, 131.10, 129.16, 126.66, 126.46, 125.15, 124.01, 58.69, 36.25, 18.55, 13.70.

### Scheme S3. Representative synthesis of maleimide synthesis



Substituted maleimides were prepared according to similar literature procedure.<sup>2</sup> Into a dried round bottom flask, citraconic anhydride (1.05 equiv, 21.53 mmol, 1.94 mL) was dissolved in anhydrous dioxanes (50 mL). *n*-Butyl amine (1 equiv., 20.51 mL, 2.00 mL) was added dropwise and the mixture was brought to 100 °C and heated for 1 hour. The reaction was brought to room temperature and ZnBr<sub>2</sub> (1.05 equiv., 21.53 mmol, 4.849 g) and hexamethyl disilazane (1.5 equiv., 30.76 mmol, 6.4 mL) were added. The suspension was then heated to 100 °C for 1 hour and progress monitored by TLC. The solvent was removed in vacuo and the slurry resuspended in ether. The suspension was filtered through a cellulose filter to remove ZnBr<sub>2</sub>. The ether was removed in vacuo and the crude product was purified through flash chromatography (80:20 hexanes:ethyl acetate) to yield *N*-butyl monomethylmaleimide (1.208 g, 43% yield).

**R<sub>1</sub> = H, R<sub>2</sub> = H, R<sub>3</sub> = Ph:** Yield = 46%, <sup>1</sup>H NMR (500 MHz, CDCl<sub>3</sub>) δ 7.53 – 7.29 (m, 5H), 6.86 (s, 2H). <sup>13</sup>C NMR (125 MHz, CDCl<sub>3</sub>) δ 169.6, 134.3, 131.3, 129.2, 128.0, 126.1

**R<sub>1</sub> = CH<sub>3</sub>, R<sub>2</sub> = H, R<sub>3</sub> = Bn:** Yield = 43%, <sup>1</sup>H NMR (500 MHz, CDCl<sub>3</sub>) δ 7.43 – 7.16 (m, 5H), 6.32 (s, 1H), 4.65 (s, 2H), 2.08 (s, 3H). <sup>13</sup>C NMR (125 MHz, CDCl<sub>3</sub>) δ 171.6, 170.5, 145.8, 136.5, 128.7, 128.4, 127.8, 127.5, 41.5, 11.0



**R<sub>1</sub> = CH<sub>3</sub>, R<sub>2</sub> = CH<sub>3</sub>, R<sub>3</sub> = Bn:** Yield = 59%, <sup>1</sup>H NMR (500 MHz, CDCl<sub>3</sub>) δ 7.40 – 7.19 (m, 5H), 4.64 (s, 2H), 1.95 (s, 6H). <sup>13</sup>C NMR (125 MHz, CDCl<sub>3</sub>) δ 171.9, 137.3, 136.8, 128.6, 128.4, 127.7, 41.5, 8.8.

### **Isotactic polypropylene grafting procedure**

Isotactic polypropylene pellets (iPP, M<sub>n</sub> = 97,000, 3 mm diameter) were cryogenically milled using a Fritsch rotary mill through a 2.0 mm sieve cassette to produce a fine powder. The powder was dried at 80 °C for 4 hours prior to grafting. Into a mixing tube, iPP powder (8.00 grams), styryl furan (8 wt%, 640 mg), and dicumyl peroxide (0.5 wt%, 40 mg) were added and vigorously mixed for 10 minutes. The mixture was split into two portions and were fed into a twin-screw extruder heated to 180 °C with nitrogen flushing. The speed was set to 60 RPM and the molten polymer was cycled for 10 minutes before expelling and pelletizing. The PP-*g*-furan was dissolved in refluxing xylenes and precipitated into vigorously mechanically stirred methanol to remove residual un-grafted monomer. The powder was dried and used for compatibilization experiments without further purification. <sup>1</sup>H-NMR spectra can be found in Section 5.7.

### **High density polyethylene grafting procedure**

High density polyethylene pellets (HDPE, MFI = 2.2 g/10 minutes (190 °C/2.16 kg), 3 mm diameter) were cryogenically milled using a Fritsch rotary mill through a 0.5 mm sieve cassette to produce a fine powder. The powder was dried at 80 °C for 4 hours prior to grafting. Into a mixing tube, HDPE powder (8.00 grams), styryl furan (8 wt%, 640 mg), and dicumyl peroxide (0.5 wt%, 40 mg) were added and vigorously mixed for 10 minutes. The

mixture was split into two portions and were fed into a twin-screw extruder heated to 190 °C with nitrogen flushing. The speed was set to 60 RPM and the molten polymer was cycled for 10 minutes before expelling and pelletizing. The HDPE-*g*-furan was dissolved in refluxing xylenes and precipitated into vigorously mechanically stirred methanol to remove residual un-grafted monomer. The powder was dried and used for compatibilization experiments without further purification. <sup>1</sup>H-NMR spectra can be found in Section 5.7.

### **Preparation of poly(styrene-co-furan)**

Poly(styrene-co-maleic anhydride) (7 wt% maleic anhydride) pellets of approximately 3 mm diameter were dried in a PTFE dish in a vacuum oven at 175 °C for one hour. After drying, 10.00 grams of pellets and a stir bar were added to a nitrogen-flushed round bottom. Approximately 100 mL of dry toluene was added to the flask and the mixture was heated to 90 °C. After pellets had dissolved, furfuryl amine (3 equiv., 1.89 mL) was added and the flask was wrapped in aluminum foil. The mixture was stirred for 16 hours followed by precipitation into cold methanol. The precipitate was concentrated through centrifugation, filtered, and dried under vacuum at 175 °C. Conversion was determined to be 98% via <sup>1</sup>H-NMR. <sup>1</sup>H-NMR spectra can be found in Section 5.7.

### **Representative compatibilized polymer blending procedure**

Into a mixing tube 5 mg BHT inhibitor and the necessary amounts of ground polymer pellets were added. The pellets were vigorously shaken for 5 minutes to sufficiently coat the surface with BHT to prevent unwanted oxidation. The mixture was extruded at 190 °C at 60 RPM with nitrogen flushing for 5 minutes before expelling. Extruded strands were then

annealed for 2 hours at 70 °C. For SEM measurements, the strands were submerged into liquid nitrogen for 5 minutes and then snapped by hand. The fractured surface was then sputter coated with carbon filament and characterized using SEM.

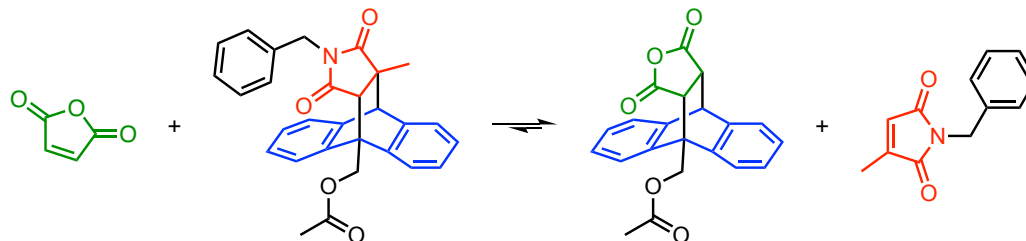
### **DSC measurements on the DA/r-DA for anthracene-monomethylmaleimide adducts**

The anthracene-monomethylmaleimide DA adduct was first prepared by adding acetylated anthracene (anthracene-9-ylmethyl butyrate, 1.00 equiv., 83.4 mg) and monomethyl maleimide (1-benzyl-3-methyl-1H-pyrrole-2,5-dione, 1.00 equiv., 60.3 mg) in 2 mL tetraglyme and heating to 200 °C for 20 minutes. The solution was cooled to room temperature and precipitated into cold methanol, filtered, and dried to yield a white powder. Approximately 10 mg of powder was placed in a hermetically sealed DSC pan and ramped at 20 °C/min and cooled at 10 °C/min between 50 °C and 250 °C in a heat/cool/heat/cool/heat cycle (Figure 5.4).

### **<sup>1</sup>H-NMR studies of r-DA temperatures using trapping reagent**

At high temperatures, observation of the r-DA reaction temperature for anthracene-monomethylmaleimide adducts become experimentally challenging due to rapid adduct formation during cooling back to room temperature for standard chemical characterization. As such, we proposed a trapping method to find the initial r-DA temperature by adding a trapping agent, maleic anhydride, that would preferentially react with the anthracene after its dissociation from the maleimide. By monitoring for the appearance of maleimide, we can determine the initial r-DA temperature.

**Scheme S4.** Scheme for the dissociation of the anthracene-monomethylmaleimide adduct and trapping of anthracene with maleic anhydride.



First, an anthracene-monomethylmaleimide DA adduct was prepared by adding acetylated anthracene (anthracene-9-ylmethyl acetate, 1.00 equiv., 75.0 mg) and monomethyl maleimide (1-benzyl-3-methyl-1H-pyrrole-2,5-dione, 1.00 equiv., 60.3 mg) in 2 mL of tetraglyme and heating to 200 °C for 20 minutes. The solution was cooled to room temperature, precipitated into cold methanol, filtered, and dried under vacuum to yield a white powder. An oil bath was preheated to 135 °C, and anthracene-monomethylmaleimide DA adduct (1 equiv., 43.7 mg, 0.1 mmol) was added to a vial containing 1.00 mL of 1,2,4-trichlorobenzene and a magnetic stir bar. Maleic anhydride (10 equiv., 98.0 mg, 1.0 mmol) was added to the vial and dissolved. The vial was sealed and placed in the oil bath for 10 minutes. After 10 minutes, an aliquot was taken and diluted in CDCl<sub>3</sub> for <sup>1</sup>H-NMR analysis. This procedure was repeated at 190 °C and 210 °C.

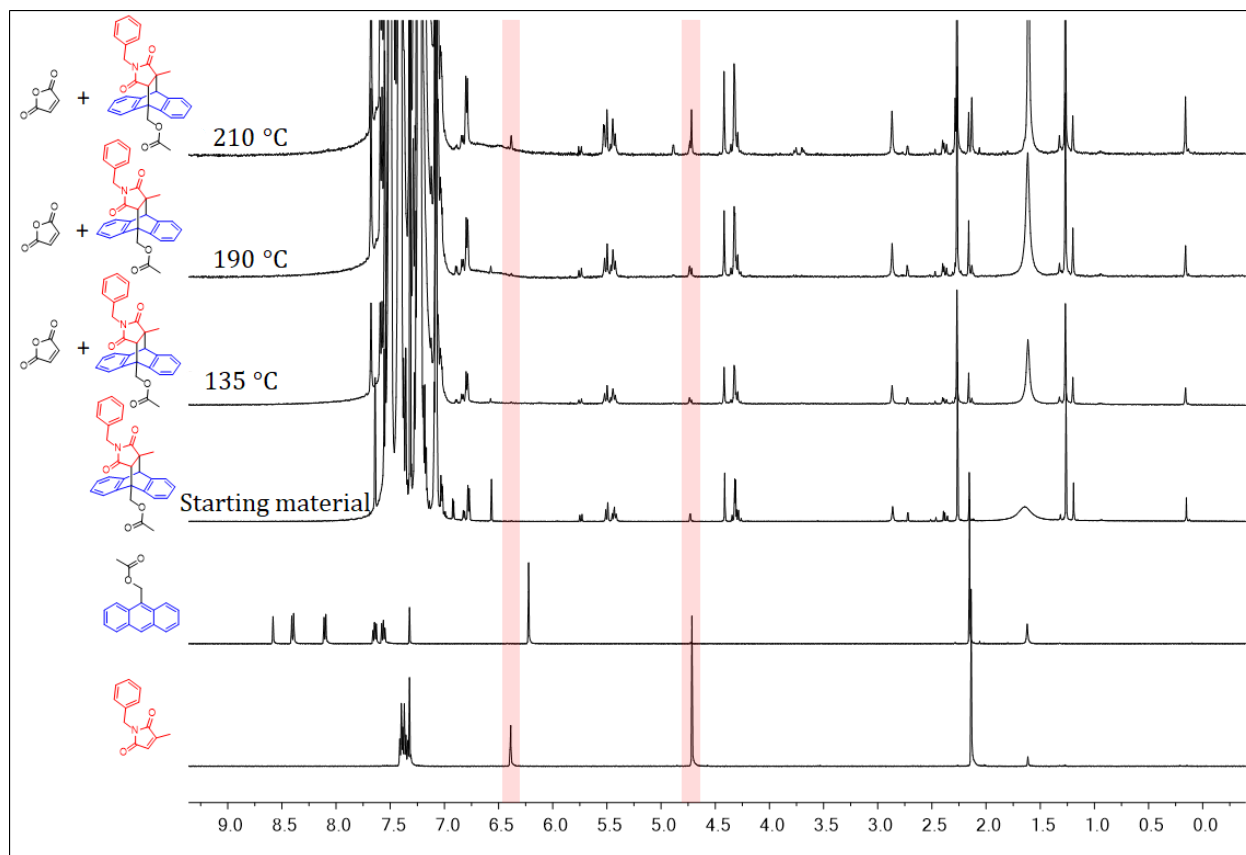
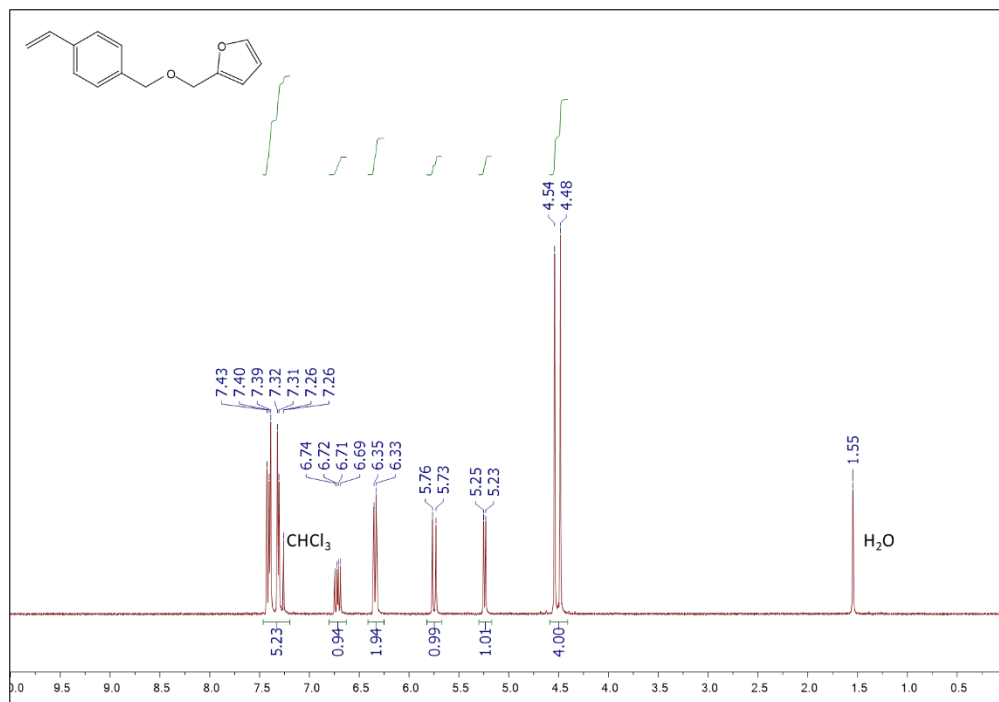
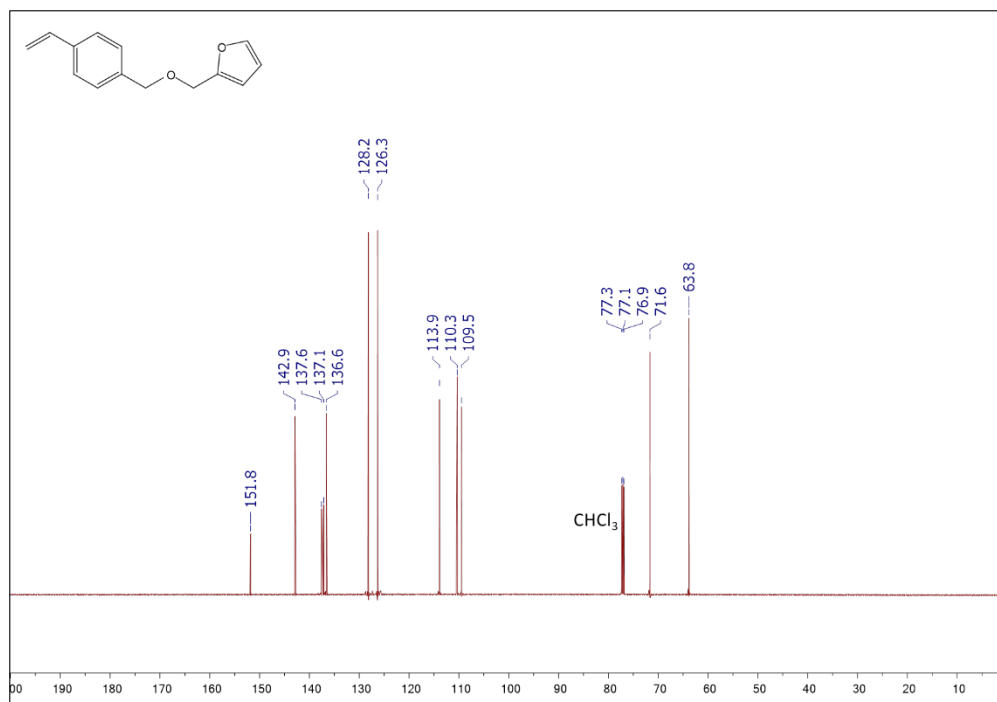


**Figure S1.** <sup>1</sup>H-NMR studies of r-DA temperatures using trapping reagent at 135 °C, 190 °C and 210 °C.

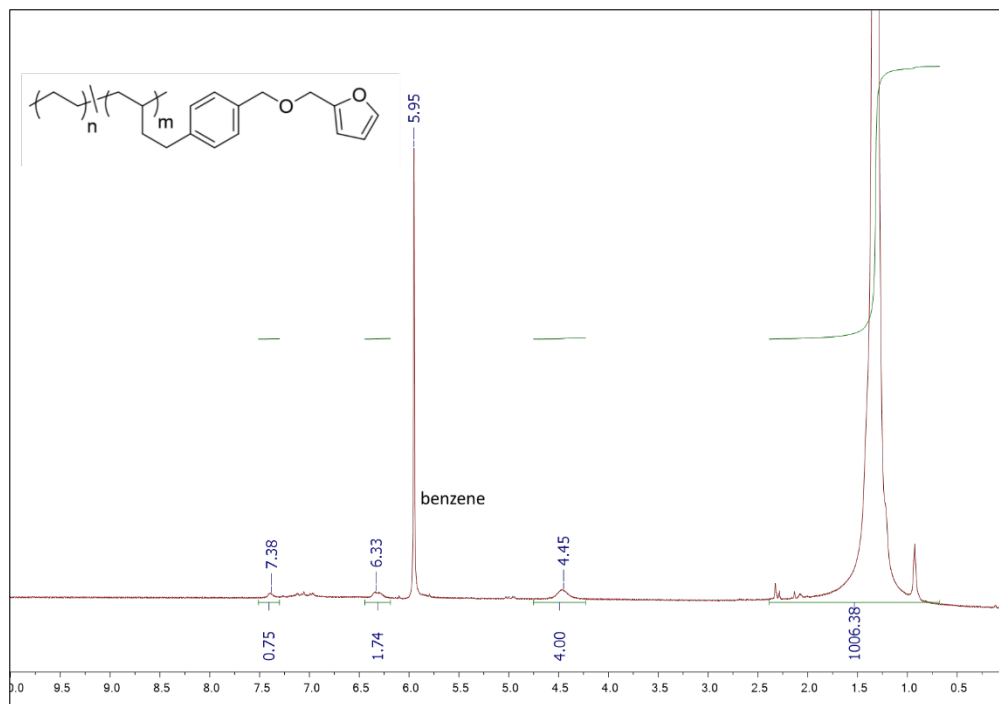
## 5.7 Spectra



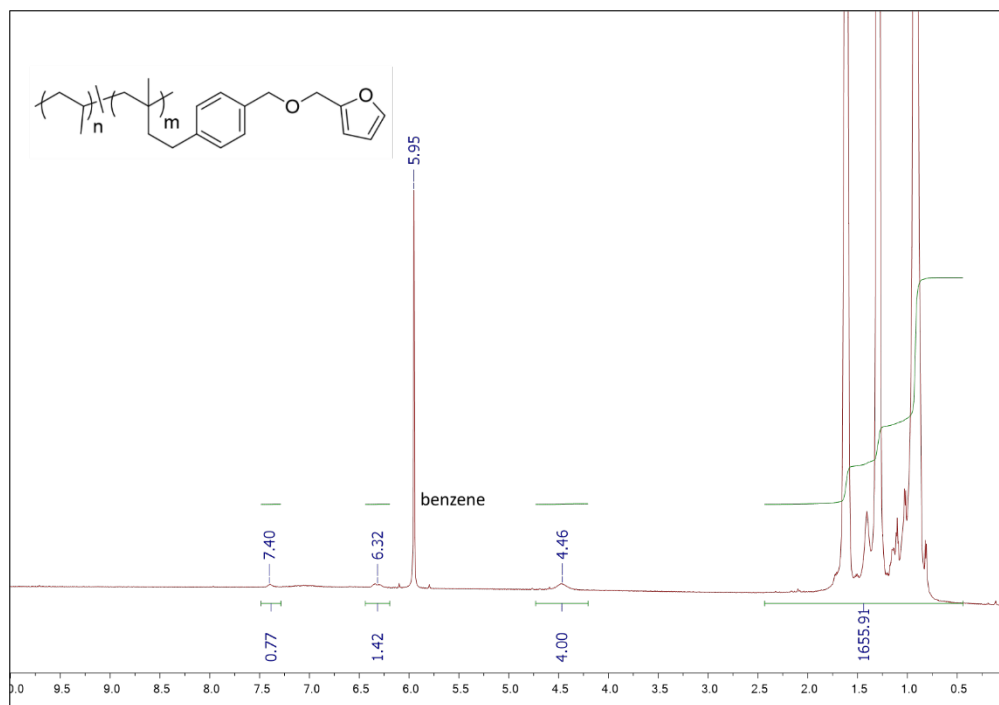
Styryl furan. <sup>1</sup>H NMR (500 MHz, CDCl<sub>3</sub>, 298K)



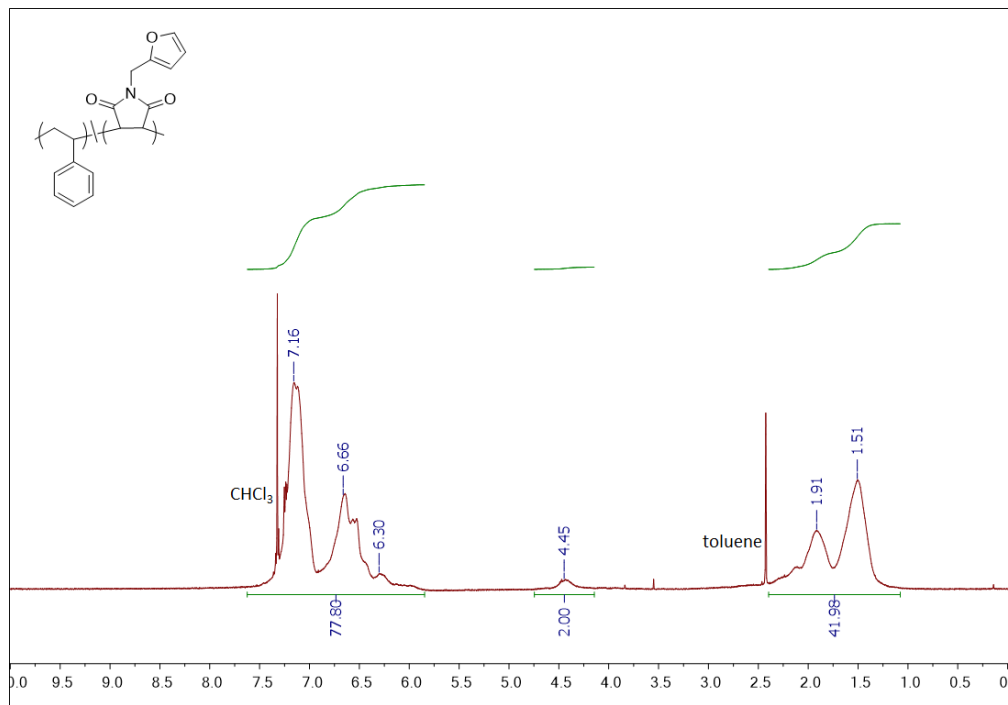
Styryl furan. <sup>13</sup>C NMR (125 MHz, CDCl<sub>3</sub>, 298K)



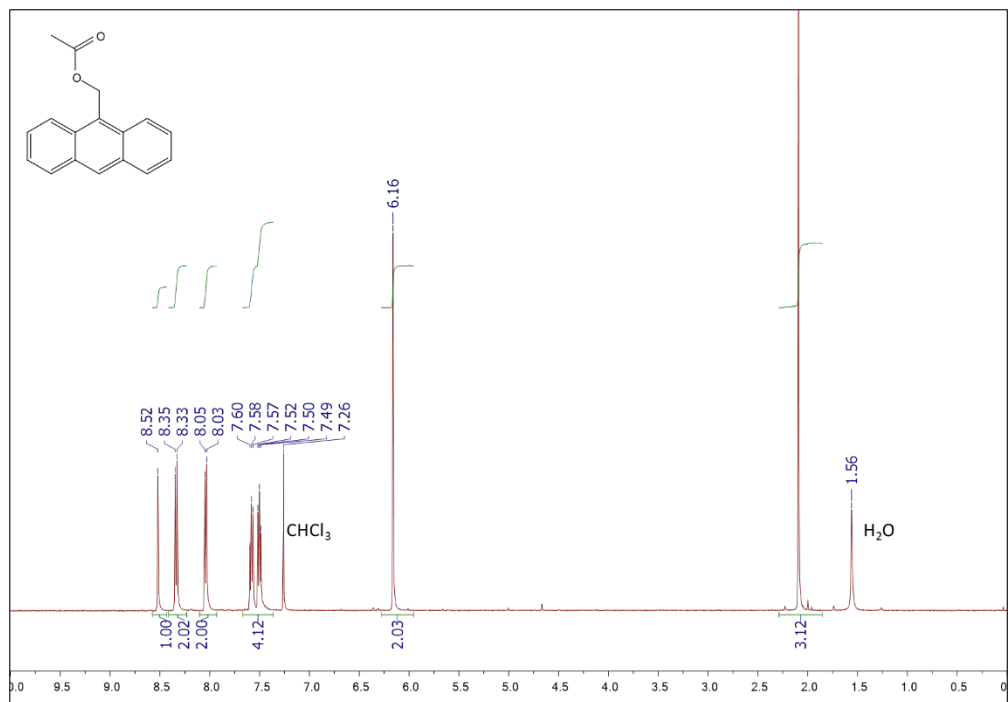
**HDPE-g-furan.**  $^1\text{H}$  NMR (500 MHz,  $\text{C}_6\text{D}_6$ , 298K)



**PP-g-furan.**  $^1\text{H}$  NMR (500 MHz,  $\text{C}_6\text{D}_6$ , 298K)

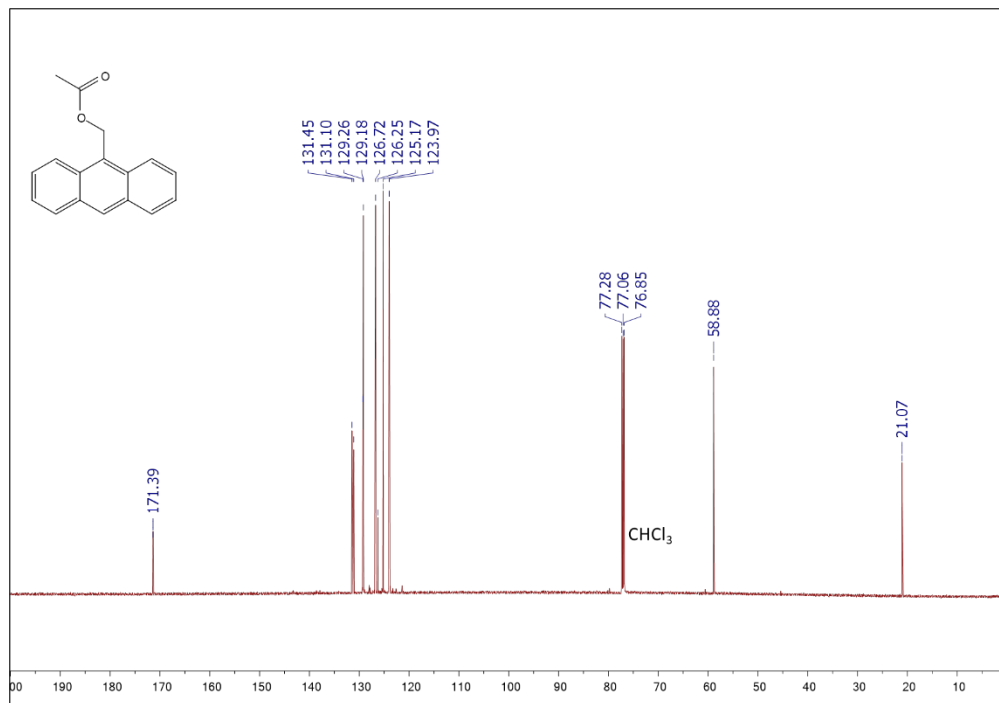


**Poly(styrene-co-furan).**  $^1\text{H}$  NMR (500 MHz,  $\text{CDCl}_3$ , 298K)

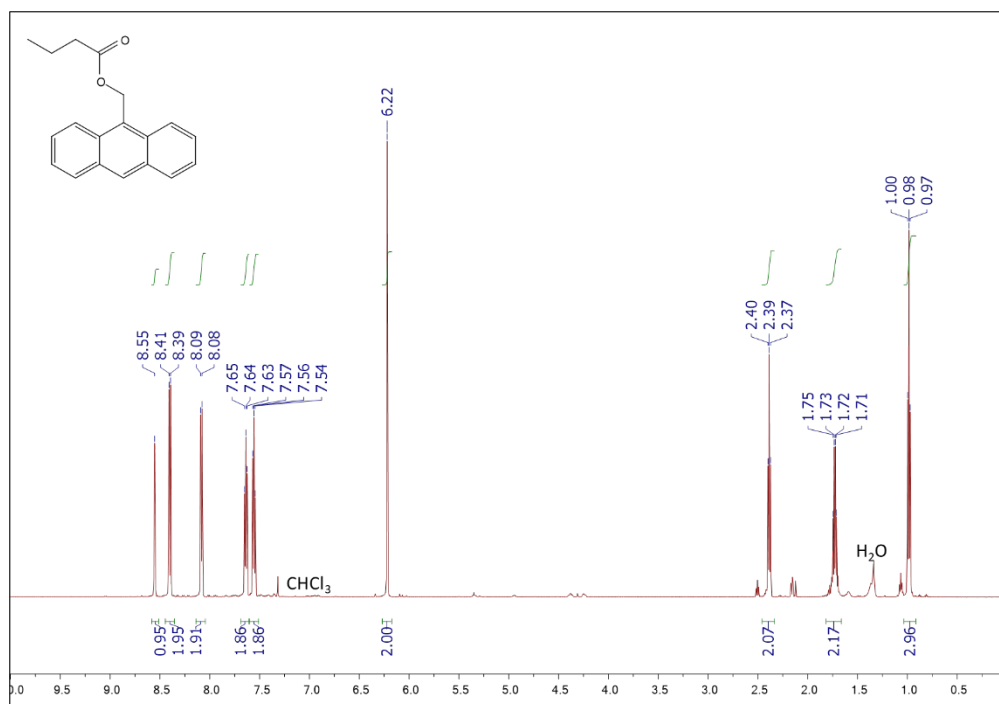


**Acetylated anthracene.**  $^1\text{H}$  NMR (500 MHz,  $\text{CDCl}_3$ , 298K)

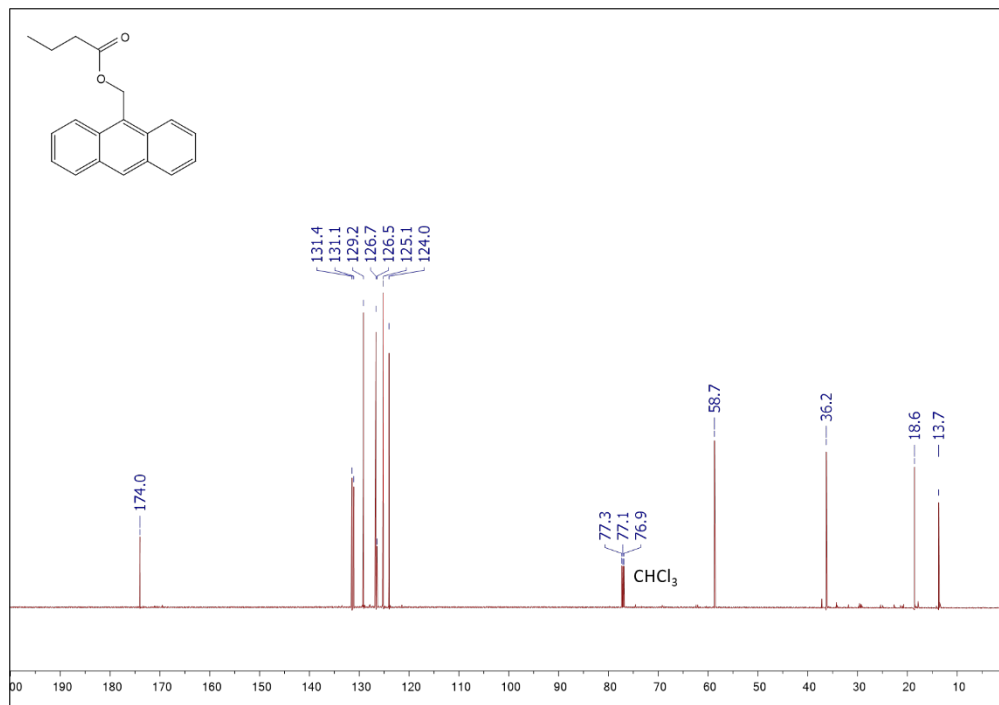




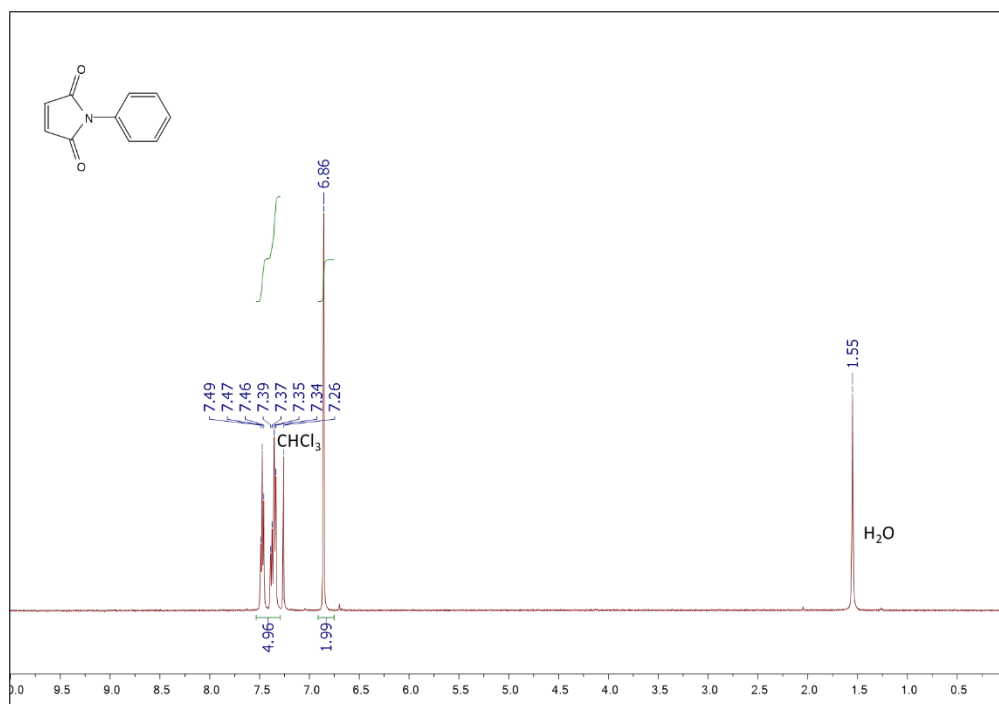
Acetylated anthracene.  $^{13}\text{C}$  NMR (125 MHz,  $\text{CDCl}_3$ , 298K)



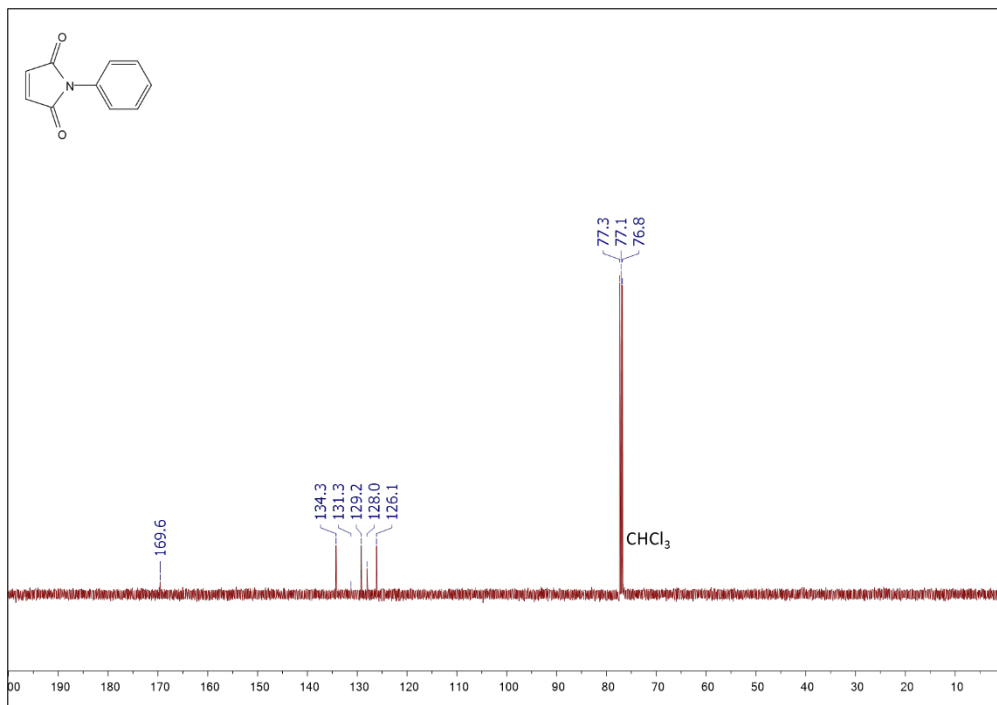
Butylated anthracene.  $^1\text{H}$  NMR (500 MHz,  $\text{CDCl}_3$ , 298K)



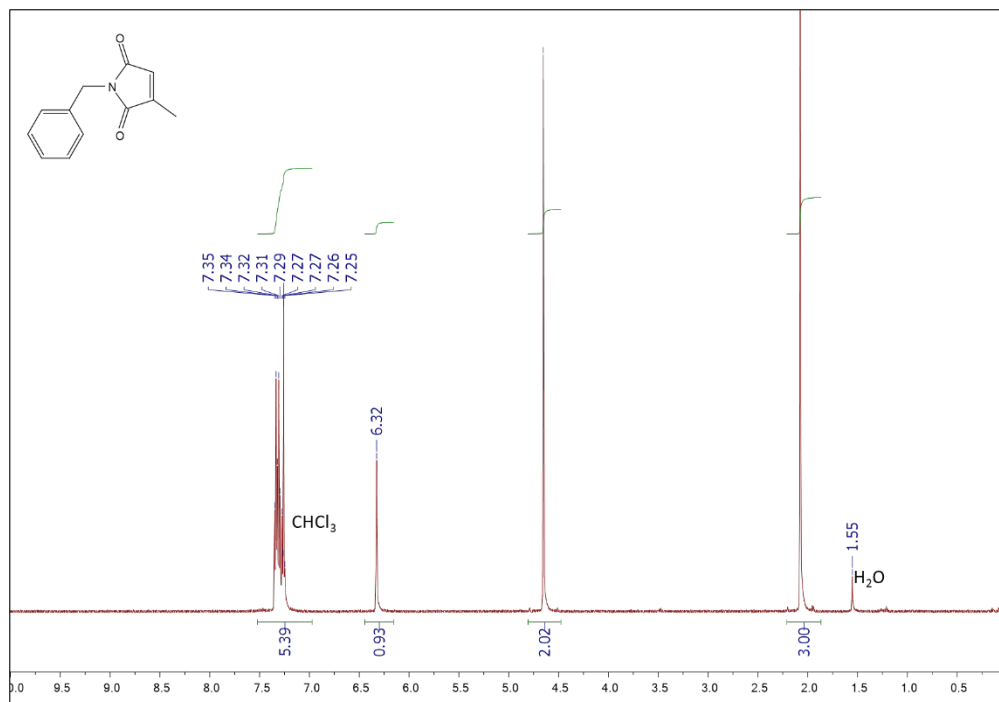
**Butylated anthracene.**  $^{13}\text{C}$  NMR (125 MHz, CDCl<sub>3</sub>, 298K)



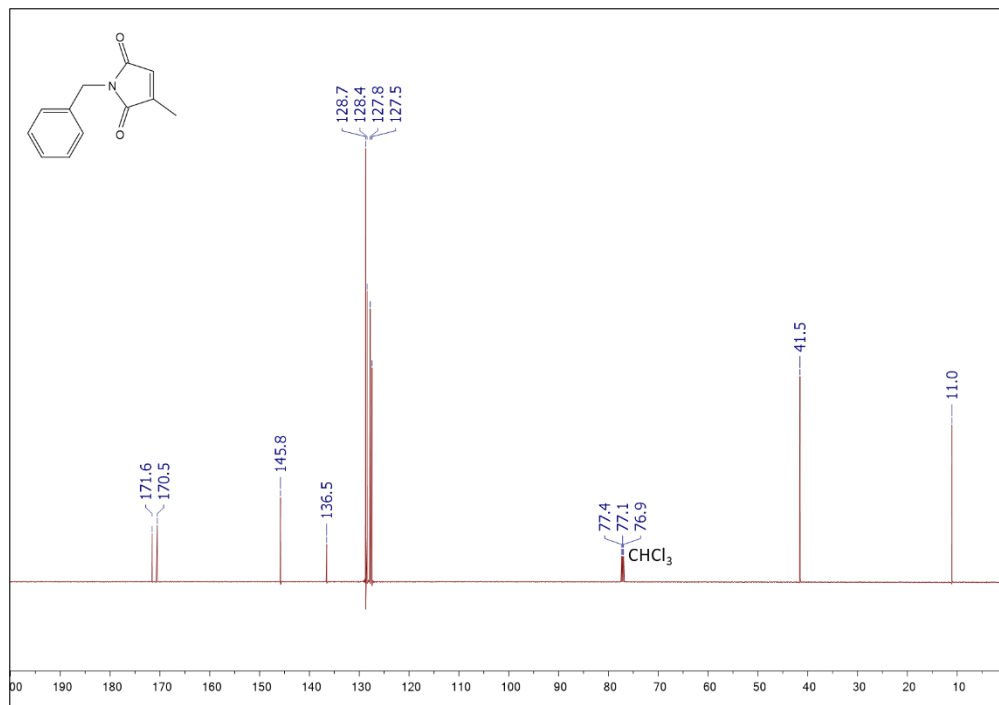
**N-phenyl monomethylmaleimide.**  $^1\text{H}$  NMR (500 MHz, CDCl<sub>3</sub>, 298K)



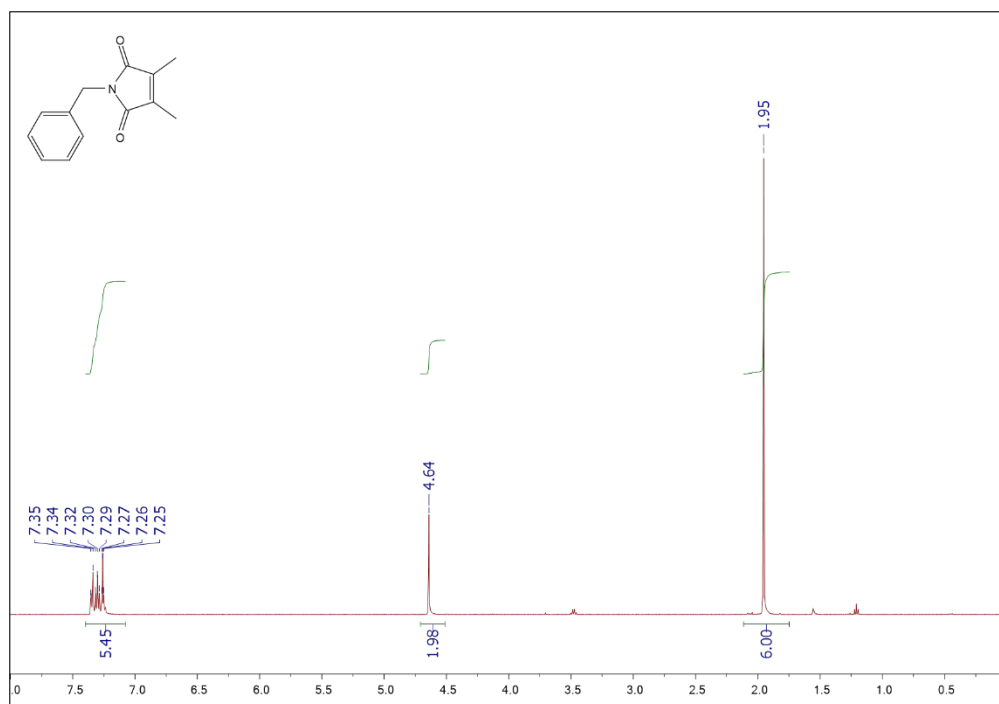
**N-phenyl monomethylmaleimide.**  $^{13}\text{C}$  NMR (125 MHz,  $\text{CDCl}_3$ , 298K)



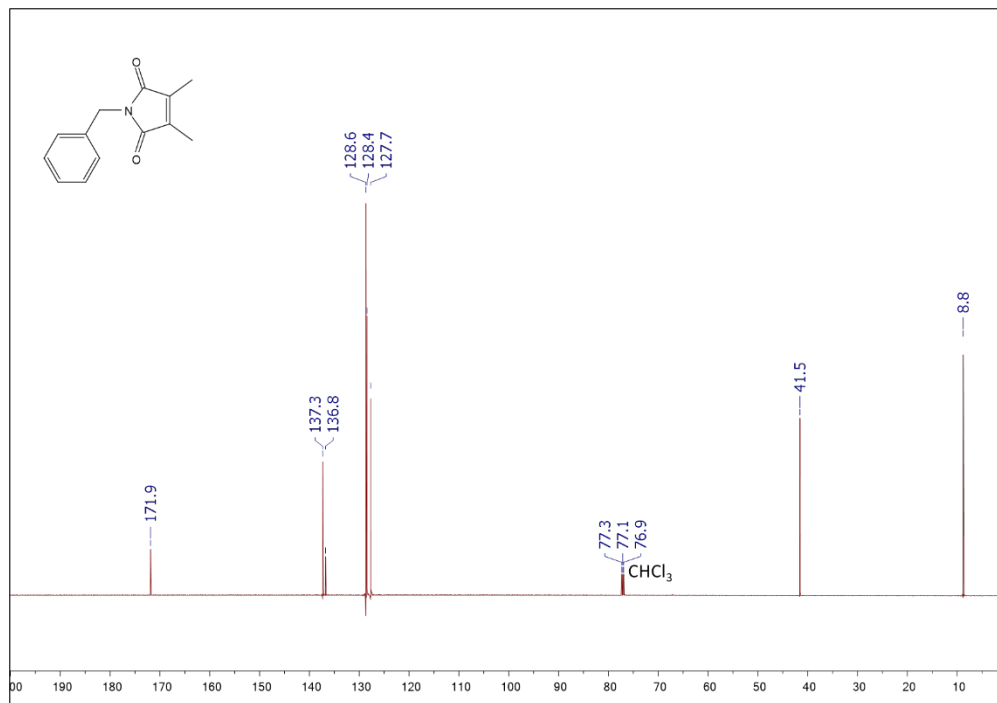
**N-benzyl monomethylmaleimide.**  $^1\text{H}$  NMR (500 MHz,  $\text{CDCl}_3$ , 298K)



**N-benzyl monomethylmaleimide.**  $^{13}\text{C}$  NMR (125 MHz,  $\text{CDCl}_3$ , 298K)



**N-benzyl dimethylmaleimide.**  $^1\text{H}$  NMR (500 MHz,  $\text{CDCl}_3$ , 298K)



**N-benzyl dimethylmaleimide.** <sup>13</sup>C NMR (125 MHz, CDCl<sub>3</sub>, 298K)

### 5.8 References:

- (1) A.; Joullie, M.; Spanevello, R.; Suarez, A. Microwave-Assisted Regioselective Cycloaddition Reactions between 9-Substituted Anthracenes and Levoglucosenone. *Org. Lett.* **2006**, 8, 24, 5561–5564. <https://doi.org/10.1021/ol062254g>.
- (2) Reddy, P.; Kondo, S.; Toru, T.; Ueno, Y.; Lewis Acid and Hexamethyldisilazane-Promoted Efficient Synthesis of *N*-Alkyl- and *N*-Arylimide Derivatives. *J. Org. Chem.* **1997**, 62(8), 2652-2654. <https://doi.org/10.1021/jo962202c>.